

Designing a safe dendronised polymeric nanocarrier for hydrophobic drugs or gene delivery in cancer therapy

Aisha Roshan Mohamed Wali BSc

A thesis submitted in partial fulfilment of the requirements of the
University of Wolverhampton for the degree of Doctor of Philosophy



Faculty of Science and Engineering
University of Wolverhampton

National Engineering Research Centre for Biomaterials
Sichuan University

November 2018

DECLARATION OF ORIGINALITY

This work or any part hereafter has not previously been presented in any form to the University or to any other body whether for the purposes of assessment, publication or for any other purpose (unless otherwise stated). Save for any express acknowledgements, reference and/or bibliographies cited in the work; I can confirm that the intellectual content of the work is the result of my own efforts and no other person.

The right of Aisha Wali to be identified as an author of this work is asserted in accordance with ss.77 and 78 of the Copyright, Designs and Patents Act 1988.
At this date copyright is owned by the author.

Aisha Wali

Date

DEDICATION

I dedicate this work to my beloved Father who has given me the greatest gift “Education” because he believed in me.

This work is also dedicated to my Mum, my Grandmother, my Uncle, my Aunty, my Brothers, my beloved sister and family & friends who gave me full prayers and support to make this possible.

Lastly, I would like to dedicate to all those African/Asian girls who have not been able to take further education because of family restrictions or affordability.

ABSTRACT

The hardship of cancer is continuously increasing and is rapidly spreading globally. At present, almost one-third of newly discovered potential therapeutics have poor pharmacokinetics and biopharmaceutical properties. Chemotherapeutic agents known to be the most effective treatment, lack tumour specificity and suffers from poor solubility. The lack of specificity results in severe side effects in off-target tissues, whereas poor soluble drugs exhibit short half-life in the bloodstream and high overall clearance rate. Amphiphilic block copolymers based on hydrophobic dendrons have shown to be a promising strategy to enhance the solubility of hydrophobic drugs, prolong circulation time, minimise non-specific uptake, and allow for specific tumour-targeting through the EPR effect. Herein, we have proposed the development of a new safe and more specific non-viral vector system based on peptide dendronised polymeric micelles to enhance the delivery of hydrophobic drugs into liver cancer cells. G3(PLLA and OGPLLL) arginine dendron of third generation bearing eight peripheral hydrophobic or cationic groups (PBF and BOC or guanidine groups) were synthesised in high yield, identified and tested for purity using NMR, MS and TLC. A series of three amphiphilic system characterised by different hydrophilic pullulan derivatives segments were then synthesised using Huisgen azide-alkyne 1,3-dipolar cycloaddition between pullulan (P), lactosylated pullulan (P(Lac)) and pullulan bearing disulphide linkage (PSS) with the G3 dendron to lead amphiphilic block copolymers P-PLLA, P(Lac)-PLLA and PSS-PLLA, respectively. Hydrophilic pullulan and lactobionic acid were selected for amphiphilic modification, aiming at specific asialoglycoprotein receptors recognition onto hepatocytes cells in the liver.

Macromolecular structures of amphiphilic P-PLLA, P(Lac)-PLLA and PSS-PLLA were able to self-assemble spontaneously into spherical nanoarchitectures of sizes less than 90nm with low polydispersity in the aqueous media, which was confirmed by CAC, DLS and TEM. Furthermore, the polyaromatic anticancer drug Doxorubicin (Dox) was selectively encapsulated in the hydrophobic core through multiple interactions with the dendron, including π - π interactions, hydrogen bonding and hydrophobic interactions. Such multiple interactions had the merits of enhanced drug loading capacity (>16%), excellent stability against dilution, and excellent sustained release property. Results showed that a high number of hydrophobic segments within a micellar core enhance higher loading efficiency of hydrophobic drugs, whereas, an increase of surface hydrophilicity or an increase in the length of the hydrophobic segment, both have an effect in reducing the micellar size and CAC value. The disulfide-containing PSS-PLLA micelles were able to co-encapsulate both hydrophobic drugs Dox and Curcumin (Cur) which could simultaneously be co-released in high rate from the carrier (>80wt% in 60hours) in response to the high redox potential environment. Most importantly, the release of Dox from the carrier at pH 5 enhanced the release of curcumin, whereas curcumin, in turn, would improve the efficiency of Dox anticancer activity by overcoming Dox MDR. Such a delivery system provides a promising approach for combination therapy in cancer. The cell viability assay presented that the blank micelles had excellent biocompatibility both in the normal and tumour cells. Moreover, loaded drugs nanoparticles could be effectively internalised into the hepatoma carcinoma cells, and Dox-Cur-PSS-PLLA dramatically inhibited cell proliferation. Also, cationic dendron conjugated pullulan (P-OGPLLL) could efficiently condense DNA with excellent hemocompatibility and high gene transfection in Hela and

Hek293T cells. Thus, this work offers an effective strategy of designing a non-viral system and the P-PLLA, P(Lac)-PLLA, PSS-PLLA and P-OGPLLL nanocarriers serve as a reliable drug/gene delivery nanoplatform to enable the improvement of the bioavailability, targetability, efficacy and overcome MDR of therapeutic agents.

ABSTRACT GRAPHIC

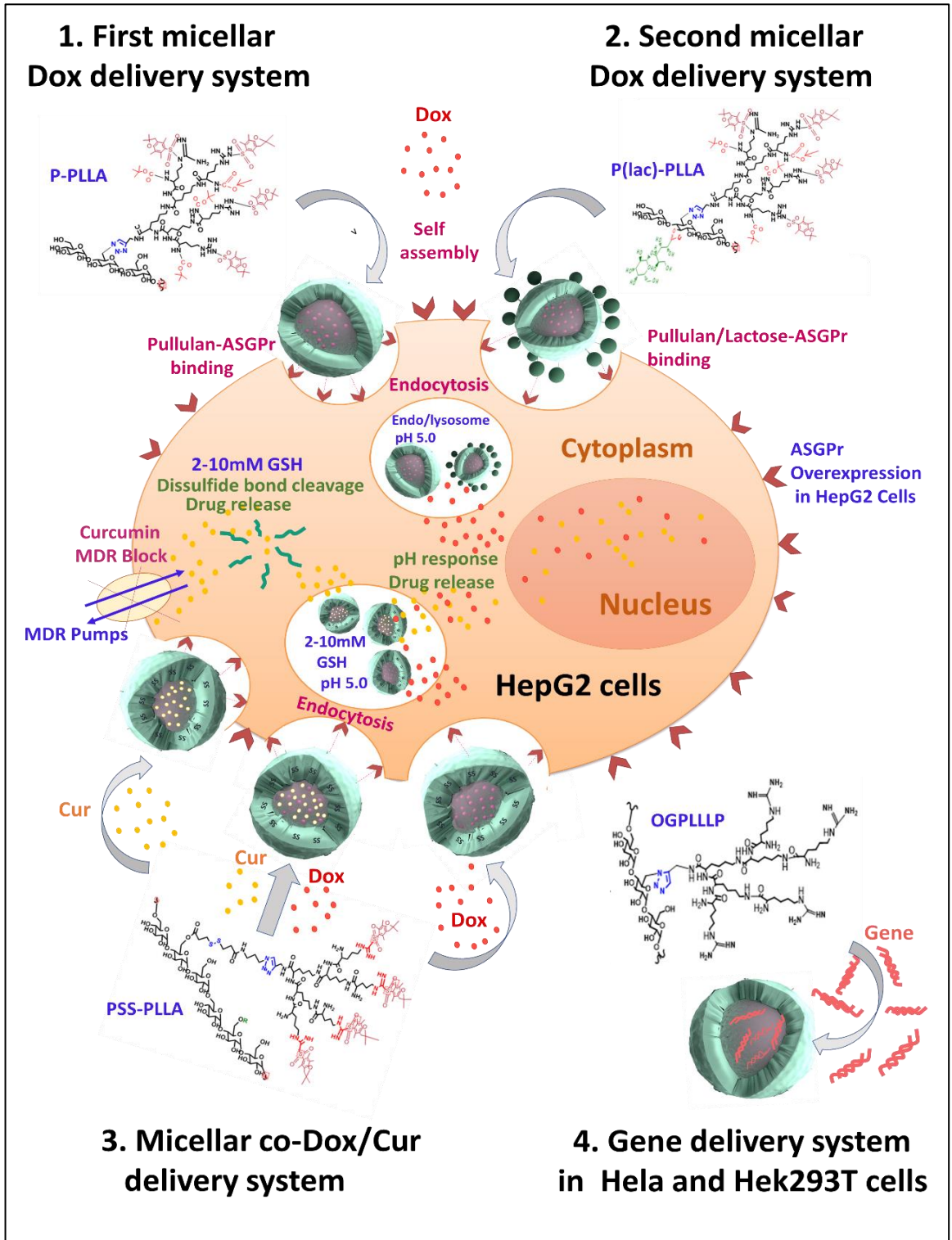


TABLE OF CONTENTS

DECLARATION OF ORIGINALITY	i
DEDICATION	ii
ABSTRACT	iii
ABSTRACT GRAPHIC	vi
TABLE OF CONTENTS	vii
LIST OF TABLES	xv
LIST OF FIGURES	xvi
ABBREVIATIONS	xxii
ACKNOWLEDGEMENTS	xxvii
CHAPTER 1. INTRODUCTION	1
1.1.Causes and formation of Cancer.....	1
1.2.Cancer therapy.....	2
1.2.1.Surgery.....	2
1.2.2.Radiotherapy (RT)	3
1.2.3.Photodynamic therapy (PDT).....	3
1.2.4.Ultrasonic therapy	4
1.2.5.Chemotherapy	5
1.2.6.Gene therapy	6
1.2.7.Immunotherapy	6
1.3.The drawback of existing therapy.....	7
1.4.New approaches to improve cancer therapies: delivery systems.....	10
1.4.1.Viral delivery system.	11
1.4.2. Non-Viral Delivery System	12
1.4.2.1. Nanotechnology	122
1.4.2.2. Importance of size, surface charge and composition of carriers to overcome extracellular barriers in the bloodstream	14
1.4.2.3. Targeted delivery system accumulation in tumours	16
1.4.2.3.1. Passive targeting: pathophysiology and anatomy of tumour vasculature enhancing the enhanced permeation and retention (EPR) effect.....	17
1.4.2.3.2. Active targeting	20

1.4.2.4. Intracellular barriers and the internalisation of carriers (vectors) by endocytosis: the chemotherapeutic agent release point.....	22
1.4.2.4.1. The cytosolic entrance of carriers	23
1.4.2.4.2. Physical targeting.....	24
a.pH-responsive drug release	24
b.Release via endosomes lysis.....	25
c.Redox-responsive drug release	25
d.External stimuli-responsive drug release	26
1.4.2.5. The nuclear entrance of therapeutic agents.....	27
1.4.2.6. Tumour Resistance.....	28
1.5.The anthracycline background: Doxorubicin (Dox).....	30
1.5.1.Doxorubicin structure	31
1.5.2.Antitumor activity of doxorubicin	32
1.5.3.Doxorubicin side effects	33
1.6.Targeting delivery Systems for the improvement of Doxorubicin therapy	34
1.6.1.Liposomes.....	34
1.6.2.Albumin-based carriers	38
1.6.3.Amphiphilic block copolymer/ Polymeric based nanocarriers/micelles.....	39
1.6.4.Dendron based nanocarriers / Dendronised polymers.....	41
1.6.5.Co-delivery system	44
1.7.Aim and Objective.....	46
CHAPTER 2. MATERIALS AND METHODS	48
2.1. Materials.....	48
2.1.1.Materials for chemical synthesis and characterisation	48
2.1.1.1.Glassware and equipment for synthesis	48
2.1.1.2.Chemicals for synthesis	50
2.1.2.Materials for in vitro cell studies.....	52
2.1.2.1.Glassware and Equipment for cells studies	52
2.1.2.2.Chemicals and reagents for cell studies.....	53
2.1.3.Cell lines	54
2.1.4 Buffers and solutions	55
2.2.Methods.....	56

2.2.1. Peptide dendron detection by thin layer chromatography	56
2.2.2. Peptides dendron purification.....	57
2.2.2.1. Acid and basic extraction to remove impurities	57
2.2.2.2. Column Chromatography	58
2.2.3. Characterisation of dendrons modified pullulan and conjugated product .	58
2.2.3.1. Mass spectrometry (MS)	58
2.2.3.2. Fourier transform infrared spectrometry (FTIR)	60
2.2.3.3. Elemental analysis (EA)	61
2.2.3.4. Proton nuclear magnetic resonance (¹ H NMR)	61
2.2.4. Micelles formation by diafiltration	62
2.2.4.1. Preparation of blank P-PLLA, P(lac)-PLLA and PSS- PLLA micelles ...	63
2.2.4.2. Drug loading into micelles	63
2.2.4.2.1. Preparation of hydrophobic doxorubicin by the removal of HCl	63
2.2.4.2.2. Doxorubicin loading into P-PLLA, P(lac)-PLLA and PSS-PLLA.....	64
micelles.....	64
2.2.4.2.3. Curcumin and Cur-dox loading into PSS-PLLA.....	64
2.2.5. Nanoparticle characterisation regarding size, polydispersity index and	
morphology	65
2.2.5.1. Dynamic light scattering	65
2.2.5.2. Scanning electron microscopy (SEM)	66
2.2.5.3. Transmission electron microscopy (TEM)	66
2.2.6. Stability studies	67
2.2.6.1. CAC studies	67
2.2.6.2. Blank and loaded nanoparticle stability studies.....	67
2.2.7. Drug release studies	68
2.2.7.1. Doxorubicin release from P-PLLA, P(lac)-PLLA and PSS- PLLA.....	68
2.2.7.2. Curcumin release from PSS-PLLA.....	68
2.2.8. Cell culture	69
2.2.8.1. Recovering cell lines from liquid nitrogen storage.....	69
2.2.8.2. Sub-culturing (splitting or passaging of adherent cells).....	70
2.2.8.2.1. Trypsinization of adherent cells.....	70
2.2.8.2.2. Counting cells in a haemocytometer	70
2.2.8.2.3. Seeding into tissue culture T25 and T75 vented flasks or 6 well and	
96 well plates.....	70

2.2.9. Freezing cells	71
2.2.10. In vitro cytotoxicity	71
2.2.10.1. Cell viability by cell counting kit-8 (CCK8) assay	71
2.2.10.2. Cell viability by sulforhodamine B (SRB) assay	73
2.2.11. Flow cytometry	74
2.2.11.1. Cellular uptake by flow cytometry	74
2.2.11.2. Apoptosis	75
2.2.12. Cellular uptake by confocal studies	76
2.2.13. Statistical tests	77
CHAPTER 3. DESIGN AND SYNTHESIS OF ALKYNATED PEPTIDE	
DENDRONS	
3.1. Introduction	78
3.1.1. Schematic overview of the synthesis of arginine-based dendrons	80
3.1.2. The process of dendron synthesis by peptide bond formation via the condensation of acid and amine	81
3.2. Aims and objective	86
3.3. Methodology	86
3.3.1. Synthesis of the lysine- dendron of generation 1 (PL)	86
3.3.2. Synthesis of the lysine-dendron of Generation 2 (PLL)	87
3.3.2.1. Removal of BOC from G1 dendron	87
3.3.2.2. Synthesis reaction of PLL	88
3.3.3. Synthesis of the dendron of generation 3 (PLLA and PLLL)	88
3.3.3.1. Removal of BOC from G2 Dendron	88
3.3.3.2. Synthesis of arginine dendron of generation 3 (PLLA)	88
3.3.3.3. Synthesis of lysine dendron of generation 3 (PLLL)	84
3.3.4. Characterisation of Dendrons	90
3.4. Results	91
3.4.1. Characterisation of lysine generation 1 dendron (PL)	91
3.4.2. Characterisation of lysine generation 2 dendron (PLL)	95
3.4.3. Characterisation of arginine dendron of generation 3 (PLLA (BOC/PBF)	98
3.4.4. Characterisation of the lysine generation 3 dendron (PLLL+)	100
3.5. Discussion	102

CHAPTER 4. MICELLAR DENDRONS FOR THE DELIVERY OF DOXORUBICIN IN VITRO CELL MODELS	105
4.1.Introduction.....	105
4.2.Aims and objective.....	107
4.3.Methodology.....	109
4.3.1.Synthesis of the arginine dendron of generation 3 (PLLA).....	109
4.3.2.Pullulan azidation (PN3)	109
4.3.3.Click reaction between azidated pullulan and PLLA dendron	110
4.3.4.Characterisation.....	110
4.4.Results.....	111
4.4.1.Characterisation of the azidated pullulan	111
4.4.2.Characterisation of clicked PG3(BOC/PBF) product.....	112
4.4.3.The self-assembly of P-PLLA.....	115
4.4.4.CAC and Stability studies of PG3(BOC/PBF) micelles	115
4.4.5.Drug loading into P-PLLA (P-PLLA-Dox)	116
4.4.6.In vitro drug Release studies of P-PLLA-Dox NPs	118
4.4.7.Stability of blank and Dox-loaded PG3 micelles.....	119
4.4.8.Cytotoxicity of Dox.HCl, blank and loaded Dox-P-PLLA	120
4.4.9.Cellular internalisation by Flow cytometry and confocal studies	124
4.4.10.Apoptosis studies	129
4.5.Discussion.....	130
4.6.Conclusions.....	134
CHAPTER 5. MODIFIED MICELLAR DENDRON FOR TARGETED Dox DELIVERY IN VITRO	136
5.1.Introduction.....	136
5.2.Aim and objective.....	138
5.3.Methodology.....	139
5.3.1.Dendron synthesis and pullulan azidation.....	139
5.3.2.Conjugation of lactose to azidated Pullulan (P(lactose)N3)	139
5.3.3.Click reaction between pullulan bearing lactose and PLLA.....	140
5.3.4.Characterisation.....	141
5.4. Results.....	141

5.4.1.Characterisation of the lactose conjugated pullulan.....	141
5.4.2.Characterisation of the clicked product P(Lac)G3.....	143
5.4.3.The self-assembly of P(Lac)G3.....	144
5.4.4.CAC and Stability studies of P(Lac)G3 micelles	145
5.4.5.Drug loading in P(Lac)G3.....	146
5.4.6.In vitro drug release studies of Dox-P(lac)G3 nanoparticles	148
5.4.7.Stability of blank and Dox-loaded P(Lac)G3 micelles	149
5.4.8.Cytotoxicity of Dox.HCl, blank and loaded Dox-P(Lac)G3	150
5.4.9.Cellular internalisation by Flow cytometry and confocal studies	154
5.4.10.Apoptosis studies.....	157
5.5.Discussion.....	158
5.6. Conclusions.....	161
CHAPTER 6. CO-DELIVERY OF DOXORUBICIN AND CURCUMIN USING	
 REDOX-BASED MICELLAR DENDRONS.....	163
6.1.Introduction.....	164
6.2.Aims and objective.....	167
6.3.Methodology.....	168
6.3.1.Dendron synthesis	168
6.3.2.Addition of disulphide bond to Pullulan (P-SS-COOH).....	168
6.3.3.Azidation of disulphide modified pullulan (PSS-N ₃).....	169
6.3.4.Click reaction between PSSN ₃ and PLLAG3 dendron	170
6.3.5.Characterisation.....	170
6.4.Results.....	170
6.4.1.Characterisation of the PSS-COOH and P-SS-N ₃ conjugates.....	170
6.4.2.The self-assembly of PSSG3 and their stability studies	172
6.4.3.Drug loading into PSSG3 nanocarriers	174
6.4.4.In vitro drug Release studies of PSSG3-Dox (or cur or cur/Dox) NPs...	179
6.4.5.Cytotoxicity.....	182
6.4.6.Cellular uptake by confocal studies.....	184
6.5.Discussion.....	186
CHAPTER 7. GUANIDINYLATED DENDRON GRAFTED PULLULAN	
 TOWARD GENE DELIVERY	191
7.1.Introduction.....	191

7.2.Aim and Objective.....	192
7.3.Methodology.....	193
7.3.1.Synthesis of Lysine dendron of generation 3 (PLLL+) and Pullulan azidation.....	193
7.3.2.Click reaction between PLLL+ dendron and azidated pullulan.....	193
7.3.3.Guanidinylation of generation 3 (PLLL) dendrons.....	194
7.3.4.Characterisation.....	195
7.3.5.DNA Complexes Assembly.....	195
7.3.6.Agarose Gel Retardation Assay.....	195
7.3.7.Particle Size characterisation.....	194
7.4.Results.....	195
7.4.1.Synthesis and characterisation of clicked Pullulan- PLLL(Boc) (G3P) and OGG3P.....	195
7.4.2.Characterisation of DNA Complexes.....	197
7.5.Discussion.....	200
7.6.Conclusion.....	202
CHAPTER 8. GENERAL DISCUSSION AND FUTURE STUDIES.....	204
8.1.General Discussion.....	204
8.1.1.General chemical structure of the micellar carriers synthesised.....	204
8.1.2.The general effect of the hydrophobic/hydrophilic segment in the micellar self-assembly process.....	207
8.1.3.The general loading efficiency of hydrophobic drugs into the carriers and their effect on their sizes.....	210
8.1.4.The general effect on the release rate of encapsulated drugs.....	211
8.1.5.Effect on the addition of lactose to enhance pullulan targeting on HepG2 cells.....	214
8.2.Final conclusions and future studies.....	218
CHAPTER 9. APPENDIX.....	219
9.1. The Standard method of Removal of BOC and PBF from PLLA to yield PLLA+.....	219
9.2. Characterisation of deprotected PLLA products.....	220
9.3. Guanidinylation of G2 Dendron for gene compaction.....	222

9.4. Method for the Removal of Lysine or arginine from lysine-dendron of generation 2 and Arginine-dendron of generation 3.....	224
9.5. Growth curve of HepG2 and U251 cells.....	225
9.6. Investigation for the best parameters to carry out esterification reaction..	226
REFERENCES	229

LIST OF TABLES

Table 1-1. Biochemical classification of chemotherapy drugs.....	5
Table 1-2. The three main ATP-binding cassette (ABC) efflux transporters, their chemotherapeutic drug substrates and chemosensitizers.	30
Table 2-1. Preparation of pH 5, 6.8 and 7.4 PBS buffers.....	55
Table 4-1. Determination of the substitution degree of azidated pullulan by elemental analysis.	111
Table 4-2. Drug loading content (LC) and encapsulation efficiency (EE) of P-PLLA.....	117
Table 4-3. Calculated IC ₅₀ values of free Dox.Hcl and PG3-Dox in HepG2, U251, Hek293 and NIH3T3 cell lines at a varying time.....	122
Table 5-1. Drug loading content (LC) and encapsulation efficiency (EE) of P(Lac)G3	146
Table 5-2. Calculated IC ₅₀ values of free Dox.HCl and Dox-P(Lac)G3 in HepG2, Hek293 and NIH3T3 cell lines at a varying time by CCK8 and SRB assays.....	153
Table 6-1. Drug loading content (LC) and encapsulation efficiency (EE) of Dox and Cur in PSSG3 nanocarriers.....	176
Table 6-2. IC ₅₀ determined by SRB assay in the HepG2, NIH3T3 and Hek293 cells after 72h of incubation with blank PSSG3, PSSG3-Dox, PSSG3-Cur and PSSG3-Dox/Cur.....	182
Table 7-1 Determination of the substitution degree by elemental analysis	198
Table 8-1. Overall physical and chemical characteristics of the PG3, P(Lac)G3 and PSSG3 amphiphilic micellar nanocarriers	212

LIST OF FIGURES

Figure 1-1. Routes of administration: summary of the routes of exposure commonly used for nanomaterial administration, including their main advantages and challenges	14
Figure 1-2. Schematic representation of nanoparticles accumulation within tumour by passive targeting.....	19
Figure 1-3. Schematic representation of nanoparticles accumulation within a tumour by active targeting.....	22
Figure 1-4. Summary of the extra- and intracellular barriers faced by non-viral gene therapies following systematic delivery	26
Figure 1-5. Mechanisms of anticancer drug resistance mediated by transmembrane transporters of the ATP-binding cassette (ABC) superfamily: p-gp, BCRP and MRP1 enhanced ATP energy-dependent efflux of various hydrophobic anticancer drugs	29
Figure 1-6. Chemical structure of Doxorubicin	32
Figure 1-7. Advantages and disadvantages of the existing delivery system	35
Figure 1-8. Different types of organic delivery system including their advantages and disadvantages.....	37
Figure 1-9. Schematic view of diverse types of polymeric carriers.....	40
Figure 1-10. Schematic overview of dendrons and dendrimers	42
Figure 2-1. Schematic of the basic components of a mass spectrometer	59
Figure 2-2. The formula for determining the degree of azidation	61
Figure 2-3. Formula for determining the percentage of lactose conjugated into pullulan	62
Figure 2-4. The schematic reaction of the conversion of hydrophilic doxorubicin (Dox.HCl) into hydrophobic doxorubicin (Dox) by the removal of HCl with NaOH	63
Figure 2-5. Cell viability detection mechanism with CCK-8.....	72
Figure 2-6. Gating of cells undergoing apoptosis and necrosis using flow cytometry.	76
Figure 3-1. Schematic structure of the dendron synthesis method.	78
Figure 3-2. Schematic synthesis of generation 1,2 and 3 dendrons.....	80
Figure 3-3. General chemical equations of peptide bond formation.....	81
Figure 3-4. Commonly used carbodiimides and their resulting urea product obtained depending on the coupling agents used	83

Figure 3-5. The synthesis of lysine dendron of generation 1 by the coupling of propargylamine and BOC-Lys(BOC)-OH in the presence of EDC.HCl, HOBT and DIPEA.....	84
Figure 3-6. The synthesis of lysine dendron of generation 2 by the coupling of lysine dendron of generation 1 or lysine of G2 and BOC-Lys(BOC)-OH or BOC(Arg)PBF in the presence of HBTU, HOBT and DIPEA.....	85
Figure 3-7. Synthesis equation of G1 dendron (PL).....	86
Figure-3.8. Synthesis equation of G2 dendron (PLL).....	87
Figure 3-9. Synthesis equation of dendron of generation 3 (PLLA)	89
Figure 3-10. Synthesis equation of dendron of generation 3 (PLLL).....	89
Figure 3-11. Mass spectra of the PL Dendron of generation 1.	91
Figure 3-12. H1NMR spectrum of Dendron PL	92
Figure 3-13. TLC of PL obtained after reaction	94
Figure 3-14. ESI-MS of the deprotected PL G1 dendron	94
Figure 3-15. Mass spectra of the PLL Dendron of generation 2	95
Figure 3-16. H ¹ NMR spectrum of Dendron PLL.....	96
Figure 3-17. TLC of PLL dendrons obtained at different stages of purification	97
Figure 3-18. The ESI-MS of the deprotected PLL G2 dendron	97
Figure 3-19. H ¹ NMR spectrum of dendron PLLA	99
Figure 3-20. TLC of PLLA dendrons	99
Figure 3-21. ESI-MS of PLLA dendron	100
Figure 3-22. ESI-MS of PLLL dendron.....	101
Figure 3-23. H1NMR spectrum of dendron PLLL	101
Figure 3-24. The ESI-MS of the deprotected PLLL G3 dendron	102
Figure 4-1. Synthesis equation of the azidated pullulan PN3.....	109
Figure 4-2. Synthesis equation of Pullulan clicked PLLA (PG3 or P-PLLA)	110
Figure 4-3. IR spectrum of Pullulan and Azido-Pullulan.....	112
Figure 4-4. FTIR spectrum of the azidated Pullulan, dendron of generation 3 PLLA and clicked product PG3 BOC/PBF.	113
Figure 4-5. ¹ HNMR of clicked PG3	114
Figure 4-6. Size distribution and morphology studies of blank of PG3.....	115
Figure 4-7. Critical association concentration of PG3 measured using the fluorescent dye pyrene.....	116
Figure 4-8. A standard curve of Doxorubicin determined at 480nm	117
Figure 4-9. Size distribution of Dox-loaded PG3 micelles	118

Figure 4-10. pH sensitive release of Dox from PG3 (BOC/PBF) micelles.....	119
Figure 4-11. Images and size distribution of blank PG3 and loaded Dox-PG3 micelles.....	120
Figure 4-12. Biocompatibility assay of HepG2, U251, Hek293 and NIH3T3 cells against blank PG3 nanoparticles for 72h and Image of the PG3 micelles suspension in DMEM containing 10% (V/V) FBS.....	121
Figure 4-13. The in vitro cytotoxicity of Dox.HCl and PG3-Dox after 24, 48, 72 and 96 hours of incubation against HepG2 cells, U251 cells, NIH3T3 cells and Hek293 cells	Error! Bookmark not defined.
Figure 4-14. Image of the PG3-Dox micelles suspension In DMEM containing 10% (V/V) FBS.....	122
Figure 4-15. Flow cytometry plots of HepG2 control HepG2 cells treated with 5µg/mL of DOX.HCl at various time.....	124
Figure 4-16. The cellular uptake by Flow cytometry against HepG2 cells treated with Dox.HCl and PG3-Dox nanoparticles for 0.5, 1 and 6 hours.	125
Figure 4-17. The cellular uptake by Flow cytometry results against U251 cells treated with Dox.HCl and PG3-Dox nanoparticles for 0.5, 1 and 6 hours. ..	Error! Bookmark not defined.
Figure 4-18. The cellular uptake by confocal laser scanning microscopy against HepG2 cells treated with Dox.HCl and PG3-Dox nanoparticles for 0.5, 1 and 6 hours.....	130
Figure 4-19. The cellular uptake by confocal laser scanning microscopy against U251 cells treated with Dox.HCl and PG3-Dox nanoparticles for 0.5, 1 and 6 hours.....	129
Figure 4-20. The effect of free Dox.HCl and Dox -loaded PG3 on the induction of apoptosis in HepG2 and U251 cells.....	130
Figure 5-1. The synthesis equation of the azidated pullulan modified lactose	139
Figure 5-2. The synthesis equation of pullulan bearing G3 clicked PLLA (P(Lac)G3	140
Figure 5-3. IR spectrum of Pullulan, lactobionic acid and lactose conjugated azidated pullulan (P(Lac)N3).....	141
Figure 5-4. ¹ H-NMR of pullulan and P(Lac) N3.....	142
Figure 5-5. FTIR spectrum of azidated lactose bearing pullulan, Dendron of generation 3 PLLA and clicked product P(Lac)G3	143
Figure 5-6. Chemical structure of P(Lac)G3, and ¹ HNMR of pullulan, P(lac)N3 and P(Lac)G3.....	144
Figure 5-7. Size distribution and morphology studies of blank of P(Lac)G3....	145
Figure 5-8. Critical association concentration of P(Lac)G3 measured using the fluorescent dye pyrene.....	146

Figure 5-9. Size distribution of Dox -loaded P(Lac)G3 micelles	147
Figure 5-10. The pH-sensitive release of Dox from P(Lac)G3 micelles	148
Figure 5-11. DLS results of Dox -P(Lac)G3 nanoparticles	149
Figure 5-12. Biocompatibility assay of HepG2, Hek293 and NIH3T3 cells against blank P(Lac)G3 nanoparticles for 24h by the SRB assay and CCK8 assay.	150
Figure 5-13. Dose-dependent cytotoxicity of HepG2 and NIH3T3 cells against Dox-P(Lac)G3 nanoparticles and free Dox.HCl solutions for 24 h.....	151
Figure 5-14. The in vitro cytotoxicity by SRB assay of Dox.HCl and Dox - P(Lac)G3 after 24, 48, 72 and 96 hours of incubation against NIH3T3 cells; Hek293 cells and HepG2 cells	152
Figure 5-15. The cellular uptake against HepG2 cells treated with Dox.HCl and Dox-P(Lac)G3 nanoparticles for 0.5, 1 and 6 hours using Confocal microscopy	157
Figure 5-16. The cellular uptake against HepG2 cells treated with Dox.HCl and Dox-P(Lac)G3 nanoparticles for 0.5, 1 and 6 hours using Flow cytometry.	158
Figure 5-17. The effect of free Dox.HCl and Dox -P(Lac)G3 on the induction of apoptosis in HepG2 cells.....	157
Figure 6-1. Chemical structure of curcumin	166
Figure 6-2. Synthesis equation of disulfide linked pullulan PSS-COOH.....	168
Figure 6-3. Synthesis equation of azidated disulfide linked Pullulan (PSSN3)	169
Figure 6-4. Synthesis equation of disulphide pullulan modified G3 bearing a disulphide linkage (PSSG3).....	170
Figure 6-5. FTIR spectrum of pure pullulan, pullulan-SS-COOH and Pullulan-SS-N3 conjugates	171
Figure 6-6. ¹ H-NMR spectrum of pullulan and Pullulan-SS-COOH conjugate	172
Figure 6-7. Size distribution and morphology studies of the blank PSSG3.	173
Figure 6-8. Critical association concentration of PG3 measured using the fluorescent dye pyrene.....	174
Figure 6-9. A standard curve of curcumin determined at 425nm	175
Figure 6-10. Size distribution and morphology studies of PSSG3-Dox.	177
Figure 6-11. Size distribution and morphology studies of PSSG3-Cur.....	178
Figure 6-12. Size distribution and morphology studies of PSSG3-Dox/Cur. ...	179
Figure 6-13. Cumulative release profiles of Dox from PSSG3-Dox and PSSG3-Dox/Cur at pH 7.4 (with and without 10mM DTT) and pH 5.0 in a period of 65hours.....	180

Figure 6-14. Cumulative release profiles of curcumin from PSSG3-Cur and PSSG3- Dox /Cur at pH 7.4 (with and without 10mM DTT) and pH 5.0 in a period of 60.5hour.....	181
Figure 6-15. Cytotoxicity of blank PSSG3, PSSG3-Dox, PSSG3-Cur and PSSG3-Dox/Cur against HepG2 cells, NIH3T3 cells and Hek293 cells after the 72h incubation period.....	183
Figure 6-16. Confocal scanning electron micrographs of HepG2 cells after 6h incubation with Dox.HCl, Curcumin, PSSG3-Dox, PSSG3-Cur and after 6 and 10h incubation with PSSG3-Dox/Cur.	185
Figure 7-1. Synthesis equation of clicked PLLL dendron into pullulan.....	193
Figure 7-2. Synthesis equation of guanidinylated pullulan-PLLL	194
Figure 7-3. The ¹ H-NMR spectra of pullulan, pullulan-PLLL(G3P) and the pullulan-octa-guanidine functionalized generation 3 lysine dendrons (OGG3P) in D2O	197
Figure 7-4. Gel retardation assay for OGG3P and G3P complexes prepared at varying weight ratios and Zeta potential of OGG3P complexes prepared at different OGG3P to DNA weight ratios.....	199
Figure 7-5. Size distribution,TEM images and Zeta potential of OGG3P complexes and G3P complexes at the weight ratio of 8	200
Figure 8-1. The cellular uptake of PG3-Dox and P(Lac)Dox nanoparticles by HepG2 cells after 1h treatment with confocal laser.....	215
Figure 8-2. The Cellular uptake of Dox.HCl, PG3-Dox and P(Lac)Dox nanoparticles by HepG2 cells after 0.5,1 and 6h treatment by flow cytometry histogram	216
Figure 9.1. Synthesis equation of dendron of generation 3 (PLLA) deprotonation into PLLA+	219
Figure 9.2. ESI-MS of first deprotected PLLA dendron product	220
Figure 9.3. ESI-MS of second deprotected PLLA dendron product	220
Figure 9.4. ESI-MS of third deprotected PLLA dendron product.....	221
Figure 9.5. ESI-MS of fourth deprotected PLLA dendron product.....	221
Figure 9.6. Agarose gel electrophoresis retardation assay of PG3/pDNA and PEI/pDNA complexes at various N/P ratios	222
Figure 9.7. Synthesis equation of Pullulan-PLL	223
Figure 9.8. Synthesis equation of Pullulan-PLLG.....	223
Figure 9.9. FTIR spectrum of Pullulan, PN3 and P-PLL.....	223
Figure 9.10. Agarose gel electrophoresis retardation assay of PG2/pDNA, PG2G/pDNA and PEI/pDNA complexes at various N/P ratios	224

Figure 9-11. HepG2 and U251 growth curve (conditions: cells were seeded at 100000 cells, HepG2 cells and U251 cells under a light microscope.....	225
Figure 9-12. Synthesis equation of disulfide linked pullulan PSS-COOH.....	226
Figure 9-13. ¹ HNMR of each pullulan derivatives obtained after different experimental condition.	227

ABBREVIATIONS

ASGPr	Asialoglycoprotein Receptor
BBB	Blood-Brain Barrier
BCSFB	Blood Cerebrospinal Fluid Barrier
BM	Basement membrane
BMB	Blood-Meningeal Barrier
BOC	Tert-Butyloxycarbonyl
bp	base pair
CAC	Critical Aggregation Concentration
CBr₄	Tetrabromomethane
CCK8	Cell Counting Kit-8
CCV	Clathrin-Coated Vesicles
CDCL3	Chloroform
CNS	Central Nervous System
CSF	Cerebrospinal Fluid
Cur	Curcumin
DCU	Dicyclohexylurea
DCC	Dicyclohexyl-carbodiimide
DCM	Dichloromethane
DIPEA	Diisopropylethylamine
DLS	Dynamic light Scattering
DMAP	4-Dimethylaminopyridine
DMEM	Dulbecco's Modified Eagles Medium
DMSO	Dimethyl Sulfoxide
Dox	Doxorubicin
Dox.HCl	Doxorubicin Hydrochloride
DS	Degree of Substitution
DSs	Delivery systems
DTDPA	3, 3'-dithiodipropionic acid
DTS	DNA targeting sequences
EA	Elemental Analysis
ECM	Extracellular matrix
EDC	1- [3-dimethylaminopropyl]-3-ethylcarbodiimide

EDTA	Ethylenediamine tetraacetic acid
EPR	Enhanced Permeability and Retention
FBS	Foetal Bovine Serum
FTIR	Fourier-Transform Infrared Spectroscopy
G1,2,3,3,...	Generation 1,2,3,...dendron
GSH	Glutathione
PPLLL	Pullulan-propargylamine-lysine third generation
H.Cl	Hydrochloride
HBTU	Hexafluorophosphate Benzotriazole Tetramethyl Uronium
HCC	Hepatocellular carcinoma
HOBT	1-Hydroxybenzotriazole
ISS	Interstitial system
ISF	Interstitial fluids
IV	Intravenous
MDR	Multiple Drug Resistance
Mg	Milligram
Min	Minute
mL	Millilitre
MPs	Mononuclear Phagocytic System
MS	Mass Spectrometry
MTS	3-(4,5-dimethylthiazol-2-yl)-5-(3-carboxymethoxyphenyl)-2-(4-sulfophenyl)-2H-tetrazolium
MTT	3-(4,5-dimethylthiazol-2-yl)-2,5-diphenyl-2Htetrazolium Bromide
N₂	Nitrogen
NaHCO₃	Sodium bicarbonate
NaOH	Sodium hydroxide
NH₂	Amine ends
NHS	N-hydroxysuccinimide
NLS	Nuclear Localisation
NMR	Nuclear Magnetic Resonance
NPs	Nanoparticles
OGG3P	Octa-guanidine functionalized generation 3 lysine dendrons -graft-pullulan

OGPLLL	Octa-guanidine functionalized generation 3 lysine dendrons
P	Pullulan
P(Lac)	Lactosylated-Pullan
P(Lac)G3-Dox	Dox loaded Generation 3 arginine (PLLLA) dendrons-graft-lactosylated pullulan
PANAM	Polyamidoamine
PBF	2,2,4,6,7-pentamethyldihydrobenzofuran-5-sulfonyl group
PBS	Phosphate Saline Buffer
PDT	Photodynamic Therapy
PG3	Generation 3 arginine (PLLLA) dendrons-graft-pullulan
PG3-Dox	Dox loaded in pullulan conjugated PLLA nanocarrier
PH₃P	Triphenylphosphine
PL	Propargylamine-lysine dendron of generation 1
PLL	Propargylamine-lysine-lysine dendron of generation 2
PLLA	Hydrophobic-propargylamine-lysine-lysine-Arginine (BOC/PBF) dendron of generation 3
PLLL	Hydrophobic-propargylamine-lysine-lysine-lysine (BOC) dendron of generation 3
PLLL+	Hydrophilic-propargylamine-lysine-lysine-lysine(amine) dendron of generation 3
PN3	Azidated pullulan
PSs	Photosensitizers
PSS	Pullulan bearing disulphide linkage
PSSG3-Cur	Cur loaded in pullulan bearing disulphide modified G3 carrier
PSSG3-Dox	Dox loaded in pullulan bearing disulphide modified G3 carrier
PSSG3-Dox/Cur	Dox and Cur loaded in pullulan bearing disulphide modified G3 carrier
RES	Reticuloendothelial System
ROS	Reactive Oxygen species
RT	Room Temperature
RT	Radiotherapy
SEM	Scanning Electron Microscope

SIONPs	Superparamagnetic Iron Oxide Nanoparticles
SMANCS	poly (styrene-co-maleic acid half-butylate) linked to neocarzinostatin
SRB	Sulforhodamine B assay
TEM	Transmission Electron Microscopy
TCA	Trichloroacetic acid
TFA	Trifluoroacetic acid
TLC	Thin-Layer Chromatography
WHO	World Health Organisation
XTT	2,3-bis-(2-methoxy-4-nitro-5-sulfophenyl)-2H-tetrazolium-5-carboxanilide
μL	Microlitre
°C	Degrees Celsius

ACKNOWLEDGEMENTS

All praises due to the Lord of the worlds, the Most Beneficent, the Most Merciful for keeping me alive and healthy and for giving me the strength to complete this work.

I would like to express my deepest gratitude to my supervisor, Professor James Tang for his excellent guidance and supervision throughout my PhD studies. Being only a bachelor's degree holder, thank you for believing in me by not only allowing me to do my PhD with you but also for selecting me as an Early-Stage researcher for the ongoing FP7-IRSES-HEPTAG EXCHANGE project program to China.

This research would not have been possible without the support of Professor Zhongwei GU, Dr Yiyang He, Jie Zhou and Shengnan Ma at Sichuan University. Working collaboratively with them for a year has given me enormous opportunities in learning new techniques and new culture. I am indebted to Dr.Yiyang He whose encouragement and valuable advice helped me with the understanding and the development of the subject and most importantly for taking such good care of me during my stay in China and my appendix operation and recovery time.

I would also like to acknowledge Dr Tracy war, Dr Rowther Farjana and Dr Eagles Lawrence for their guidance with the in vitro cell experiments, the technical staff Dr. Jones Keith, Clare Murcott for their guidance with SEM and confocal training, as well as to my colleagues Inas, Rose, Asma, Fakhra, Fatima, Husseiny, Karu and Sajid.

Finally, I would like to thank you Papa for all your support and belief in me. I thank with all my heart to my grandma, uncle, aunty, brother and especially my

little sister for standing by my side, for loving, encouraging and supporting me. Thank you to all my close friends, close family and work friends. At last, I am eternally grateful to my only and only one “Mum” for her love, support and prayers.

CHAPTER 1. INTRODUCTION

Cancer is one of the most significant disease that affects the world population. GLOBOCAN estimates that in 2012, there were 14.1 million new cancer cases, 8.2 million cancer deaths and 32.6 million people living with cancer within five years of diagnosis (IARC.FR-Globocan, 2017). An increase to 19.3 million new cancer cases per year by 2025 has been predicted. According to WHO, the most commonly diagnosed cancers worldwide are those of the lung (1.8 million, 13.0% of the total), breast (1.7 million, 11.9%) and colorectum (1.4 million, 9.7%) whereas the most common causes of cancer death were cancers of the lung (1.6 million, 19.4% of the total), liver (0.8 million, 9.1%), and stomach (0.7 million, 8.8%) (IARC.FR-WHO, 2017).

1.1. Causes and formation of Cancer

The cause of cancer is a series of successive mutation in genes changing the function of a cell. Chemical compounds can easily cause a gene mutation; also, smoking contains some carcinogenic chemicals that can lead to lung cancer (Aizawa et al., 2016, Poon et al., 2014; Antwi et al., 2015). Viruses, bacteria and radiation are other carcinogenesis factors (Parkin, 2006). In 2011, Hanahan and Weinberg reported the six biological capabilities that enable tumour growth and metastatic dissemination. These include sustaining proliferative signalling, evading growth suppressors, resisting cell death, enabling replicative immortality, inducing angiogenesis, and activating invasion and metastasis (Hanahan and Weinberg, 2011). Cancer cells proliferate abnormally resulting into a tumour which can either remain confined to its site of origin (a benign tumour) or invade surrounding healthy tissue and metastasise throughout the body via the circulatory or lymphatic systems forming a malignant tumour (the

one referred adequately as cancer). Cancers can be divided in 3 categories: carcinomas consisting of 90% of cancers (malignancies of epithelial cells), sarcomas (tumors of connective tissue such as muscle, bone cartilage and fibrous tissue), and leukemias or lymphomas consisting of 8% of cancers (arising from blood-forming cells and cells of the immune system) (Cooper and Hausman, 2000).

1.2. Cancer therapy

Cancer treatment mainly consists of surgery, radiotherapy and systemic therapy (hormonal therapy, targeted therapy and chemotherapy). The procedures are sometimes combined for an effective cure (Mokhtari et al., 2017). They all work in different ways by either killing the tumour cells directly or stopping their increase or by stimulating factors inside the body that can kill cells or reduce proliferation. Here, we briefly present the main advanced types of treatment used in cancer therapy.

1.2.1. Surgery

Surgery has been used as a treatment for cancer since 3000 B.C (Wyld, Audisio and Poston, 2015). After the invention of anaesthesia, surgeons, Bilioth, Handley and Halsted became famous because of their first contributions to the science of cancer surgery (Kapur, 2014). In the 1970s, advances in technology such as the development of sonography, computed tomography (CT scans), magnetic resonance imaging (MRI scans) and positron emission tomography (PET scans) have improved surgery techniques (Sudhakar, 2009). Moreover, the introduction of cryosurgery in the 18th century consisting of freezing cells and killing cancer cells has shown to be less invasive with lower morbidity compared to surgical resection (Yiu et al., 2007).

1.2.2. Radiotherapy (RT)

X-rays were discovered in 1895 by Wilhelm Conrad Röntgen from Germany (Panchbhai, 2015). The year 2011 was designated as the year of radiation therapy in the UK after a century of advances in the field. It has been reported that 50% of all cancer patients will receive radiotherapy which contributes to around 40% towards curative treatment (Delaney et al., 2005; Begg, Stewart and Vens, 2011; Barnett et al., 2009; Baskar et al., 2012). Radiotherapy consists of a physical agent (ionising radiation) which destroy cancer cells by forming electrically charged particles or by depositing high energy that can damage the genetic material in the cells of tissue it passes through, therefore resulting in cell death (Jackson and Bartek, 2009). Ionising radiation rapidly induces water radiolysis products inside cells mitochondria, which trigger ROS production such as hydroxyl radicals which then causes DNA damages (Azzam, Jay-Gerin and Pain, 2012).

1.2.3. Photodynamic therapy (PDT)

PDT has only been developed in the last century and is being clinically tested for the treatment of the head, neck, brain, lung, pancreas intraperitoneal cavity, breast, prostate and skin (Dolmans, Fukumura, and Jain, 2003). The therapy consists of the administration of photosensitizers (PSs) followed by illumination on the tumour with a localised energy source to activate the specific PSs which produce cytotoxic singlet oxygen that results in damage to cell membrane structure and destroys biological tissues (Huang et al., 2012). Examples of photosensitizers used in PDT include haematoporphyrin derivative (Myers et al., 1989), Photofrin (Gollnick and Brackett, 2009), phthalocyanines (Rosenthal, 1991), benzoporphyrins, purpurins and chlorines (Kadish, Smith and Guillard,

2010). PDT has shown extreme valuable approach for cancer treatment since it can directly kill tumour cells, damage tumour vasculature, inhibit angiogenesis by disrupting the supply of oxygen and nutrients to the tumour cells, thus inhibiting tumour growth and also, activate the body's immune response against tumours (Castano, Mroz and Hamblin, 2006; Gollnick and Brackett, 2009; Bhuvaneswari et al., 2009).

1.2.4. Ultrasonic therapy

Low power ultrasound has been applied since the 1950s for physical therapy. By the 1970s, this technique was used for physiotherapy, Parkinson's disease and cancer (Wells, 1977; Kremkau, 1979; Miller et al., 2012). The therapy consists of the exposure to heat, mechanical effects and acoustic cavitation. Studies have shown that low-intensity ultrasound could suppress cell proliferation and clone formation, improve the impact of anti-cancer chemicals and deactivate cells via indirect mechanisms (Lejbkowicz and Salzberg, 1997; Yu, 2004). Similarly, to PDT, sonodynamic therapy (SDT) is a technique that can activate some chemicals known as sonosensitizers to generate free radicals such as hydrogen, hydrogen peroxidase, singlet oxygen and superoxide ions that are produced by the breakdown of water molecules (Kardos and Luche, 2001; Yu, 2004). FDA has approved a number of devices for therapeutic applications by ultrasound based on their thermal use (physical therapy, hyperthermia and high intensity focussed ultrasound: HIFU) and non-thermal use (extracorporeal shock wave lithotripsy, intracorporeal lithotripsy and lower power kilohertz frequency ultrasound devices) (Miller et al., 2012).

1.2.5. Chemotherapy

Chemotherapy was first introduced in the 1940s (Brighton, 2005), it was noticed that during the first and second World War, soldiers exposed to mustard gas presented low levels of leucocytes, from this in 1943, Gilman developed the first chemotherapy agent (nitrogen mustard) to treat lymphomas (Smith, 2017).

In the following years, more classes of drugs were designed for different tumour treatment. The drugs exert their effects on cancer cells by interfering with the processes involved in cell division in many ways. They cause cell apoptosis by either directly interfering with DNA or by targeting the proteins involved in cell division (Caley and Jones, 2012). The table-1 shows the classification of chemotherapy drugs and their mode of action with corresponding examples of drugs reported by Caley and Jones in 2012.

Table 1-1. Biochemical classification of chemotherapy drugs (Caley and Jones, 2012)

Drug class	Mechanism of action	Examples
Alkylating agents	Impair cell function by forming covalent bonds on essential molecules in proteins, DNA and RNA. Classified by their chemical structure and mechanism of covalent bonding.	Cisplatin, carboplatin, chlorambucil, cyclophosphamide, ifosfamide.
Anti-metabolites	Structural analogues of naturally occurring metabolites involved in DNA and RNA synthesis. They either substitute for a metabolite that is usually incorporated into DNA or RNA or compete for the catalytic site of a key enzyme.	5-Fluorouracil, methotrexate (1948), pemetrexed, mercaptopurine, gemcitabine.
Anti-tumour antibiotics	Intercalate DNA at specific sequences, creating free radicals which cause strand breakage. Anthracyclines are products of the fungus <i>Streptomyces</i> , also have a mechanism of action of topoisomerase I and II, required for the uncoiling of DNA during replication.	Bleomycin, anthracyclines (doxorubicin, epirubicin)
Topoisomerase inhibitors	Topoisomerases are enzymes that control the 3-D structure of DNA. Topoisomerase I and Topoisomerase II are enzymes responsible for the uncoiling of DNA during replication	Topoisomerase I: irinotecan, topotecan Topoisomerase II: etoposide
Tubulin-binding drugs	Vinca alkaloids bind to tubulin and prevent the formation of the microtubule, which is essential during mitosis, but also for cell shape, intracellular transport and axonal function. Taxoids prevent the disassembly of the microtubules, thereby inhibit normal function.	Vinca alkaloids: vincristine, vinorelbine Taxoids: docetaxel, paclitaxel

1.2.6. Gene therapy

Gene therapy was first proposed in the 1960s, it can be used to express a gene that induces apoptosis (examples include TNF-related apoptosis-inducing ligand: TRAIL (Griffith et al., 2009); Melanoma differentiation-associated gene-7: *mda-7* or Interleukin-24: IL-24 (Fisher, 2005)), to increase the efficiency of conventional drug or radiation therapy, to replace a defective or missing tumour suppressor gene by a functional healthy copy of the same gene (examples include p53 (Matlashewski et al., 1984), retinoblastoma gene *Rb* (Wiman, 1993), p16INK/CDKN2, PTEN, E1A, Fhit, Fus1 and BiKDD (Shanker et al., 2011)) and to block the expression of oncogene by using an antisense (RNA/DNA) approach, also, to enhance the immunogenicity of tumour (Friedmann, 1992).

1.2.7. Immunotherapy

Immunotherapy is currently the treatment of choice for several illnesses including allergies (Larenas-Linnemann et al., 2017), autoimmune (Di Sabatino et al., 2018), infectious diseases (Naran et al., 2018) and macular degeneration (Kosmidou et al., 2018). It incorporates the use of antibodies, cytokines and dendritic cells and presents much more specificity, higher efficacy, directed therapy, less toxicity, lower secondary effects and better tolerance. The objective of this technique is to help the immune system to recognise and attack cancer cells. There has been many FDA approved product and monoclonal antibodies for the treatment of metastatic melanoma. Example includes Ipilimumab for colorectal cancer and kidney cancer, Pembrolizumab for urothelial cancer, Nivolumab for lung cancer and Kidney cancer, Trastuzumab for breast cancer and gastric cancer, Rituximab for non-Hodgkin lymphoma and

chronic lymphocytic leukaemia and Cetuximab for bowel cancer) (Sharma and Allison, 2015; Farkona, Diamandis and Blasutig, 2016; Meiliana, Dewi and Wijaya, 2016).

1.3. The drawback of existing therapy

All the existing therapies have shown to kill cancer cells successfully, but at the same time, affect other healthy cells lacking tumour targeting and thus resulting in severe side effects in off-target tissues and organs. Also, the development of therapy-resistance has contributed to the failure of some treatments. Despite the new advancements, treatment by surgery can be very risky and inconvenient for patients. During operation, there could be risks of cutting through lymphatics or manipulation of a tumour can occur, resulting in tumour spread (Saltzstein, Levin and Sharp, 1957). Moreover, after surgery, there are chances of patients death due to recurrences. For example, it has been reported that 30-50% of non-small cell lung cancer (NSCLC) patients develop recurrence and die (Al-Kattan, 1997; Uramoto and Tanaka, 2014). Also, severe trauma scars and injury of soft tissues during surgery (breast cancer, for example) can cause acute and chronic pain (Fassoulaki et al., 2005).

Radiotherapy is limited due to its unacceptable normal tissue toxicity, radiation sensitivity, and resistance in tumour lesions. For example, the technique has shown complications and mortality among elderly patients over 75 years with rectal cancer (Maas et al., 2013). Also, radiotherapy faces challenges in tumour repair since malignant cells can repair radiation-induced DNA damage leading the tumour to become insensitive to radiotherapy owing to intrinsic resistance, or recur after treatment because of acquired resistance (Wang et al., 2010; Morrison et al., 2011). Radiotherapy, therefore, still needs improvement.

For the photodynamic therapy, the PSs are activated by visible light at the wavelength range of 630-690nm. However, light can only penetrate in tissue by 2-4mm depth, therefore long wavelength light sources are needed, this, can come as a tradeoff with excitation losses due to poor overlap with absorption spectra (Kalka, Merk and Mukhtar, 2000; Prasad, 2003; Ran et al., 2011; Xu, Gao and Wei, 2016). Xu and his colleagues reported in 2016, the side effects of the different categories of PSs used in photodynamic therapy including first, second and third generation PSs. The first-generation PSs have been reported that they induce cutaneous phototoxicity and increased risk of sunburns and may be less effective. An example is that of photofrin which has showed phototoxicity effects to 20-40% patients after treatment and also have shown to be less useful to tumours larger than 10 mm in diameter with a fall in response rate from 98% to 43% (Dougherty, Cooper and Mang, 1990; Furuse et al., 1993). The other generation of PSs has also been reported to present severe drawbacks in the fact that they can be overactive even in dim light (60-watt bulb) and can lead to severe skin photosensitivity (Allison et al., 2004). Although there have been regulatory-approved PSs, PDT is limited due to its inability to deliver adequate light doses to the target, unavailability of suitable PSs, high toxicity, slow pharmacokinetics and high skin photosensitivity (Allison, 2014).

Ultrasounds also present adverse effects since it can suppress the mitosis of cancer cells but at the same time could trigger the proliferation of malignant tissues, thus favouring cancer metastasis (Yu, 2004). The ultrasonic therapy uses irradiation that can create damage to the biological milieu, for example, it has been reported that ultrasound-induced shear forces, can disrupt cellular membranes and activate gas in the body and inertial cavitation which can result

in cell lysis (Miller, Miller and Brayman, 1996). Side effects can also occur from ultrasound as when affecting tumour cells, healthy cells morphology can also be affected either by DNA strand breakage, chromosome breakage, sister chromatid aberrations, cell transformation, calcium uptake or by mutations (Liebeskind et al., 1979; Miller, Reese and Frazier, 1989; Macintosh and Davey, 1970; Mortimer and Dyson, 1988; Kaufman, 1985; Miller, Miller and Brayman, 1996; Rosenthal, 2004).

Treatment by immunotherapy also faces various challenges. Although immunotherapy helps the immune system attack tumour cells, it has, at the same time, been reported to promote tumour development or growth. For example, CD4⁺T cells are known to be protective in a murine model of human papillomavirus (HPV)-induced cervical carcinoma whereas in (HPV)-induced skin carcinogenesis, both CD4⁺T and B cells enhance tumor growth (Daniel et al., 2005; De Visser, Korets and Coussens, 2005; Daniel et al., 2003). Tumours and their microenvironment can become so used to the therapy that they can potentially grow in the inflamed environment becoming immune-resistant. Moreover, tumour cells tend to have this ingenious capability of entirely transforming the immune system. The cells can achieve this by either producing substances such as cytokines and chemokines, which deactivates dendritic cells. This can happen by either displaying losses of tumour antigens (losses of HLA class I, for example, can result in NK cell lysis) or by inducing lymphocyte cell death through the triggering of Fas pathway (Bottino, Moretta and Moretta, 2006; Rescigno, Avogadri and Curigliano, 2007; Zitvogel, Tesniere and Kroemer, 2006).

Gene therapy and Chemotherapy are the other most dangerous treatments that cause severe side effects as they do not discriminate between tumour and

healthy cells. Moreover, traditional chemotherapeutic agents do not achieve satisfactory therapeutic results due to their low solubility, poor stability, rapid metabolism, non-targeted body distribution and multi-drug-resistance. Also, both therapies face various challenges before reaching their targets. In the systemic circulation, naked DNA has been used successfully either by direct injection or DNA vaccines (Cohen et al., 2018). However naked DNA can be degraded rapidly by nucleases, and monocular-phagocyte system, a specially when DNA is injected directly into tissue drains, the lymphatic system and endonucleases in the extracellular space can degrade naked DNA within 30 minutes (Schmidt-Wolf and Schmidt-Wolf, 2003). Similarly, before reaching the tumour site, chemotherapeutic drugs can be cleared by the immune system, which then reduces the amount necessary to achieve tumour cell killing.

To improve the therapeutic potential of cancer immunotherapy, PDT, SDT, gene therapy and most importantly cancer chemotherapy, new approaches have been developed for better long-term prognosis, improved targeted therapy with reduced side effects, improved drug solubility and to overcome therapy resistance. These approaches are illustrated in the following part of the introduction.

1.4. New approaches to improve cancer therapies: delivery systems

The new approach is based on the fact that drugs, DNA, sonosensitizers, photosensitizers, antibodies, cytokines or other single cancer therapeutic agents can be encapsulated in a safe (protect from blood/renal clearance) carrier (vehicle or cargo) that can deliver them specifically to the target tumour depending on the route of administration. Two or more therapeutic agents can

also be incorporated at the same time in one carrier, forming a combinational therapy. The whole idea of being able to deliver therapeutic agents came from the mechanism of how viruses carry their gene into cells. There are two types of carriers: biological and non-biological carriers (viral and non-viral). The approach here is to incorporate a therapeutic agent into a vector or a chemically synthesised carrier, then introduce the vector into the body, and the cells are expected to uptake the carrier similarly as viruses.

1.4.1. Viral delivery system.

Biological carrier involves the use of viral vectors derived from natural viruses that can deliver genetic materials into host cells. Viruses are known to be able to efficiently gain access to host cells and exploit the cellular machinery to facilitate their replication (Thomas, Ehrhardt and Kay, 2003).

In the early 1990s, a retrovirus-vector was the first successful therapeutic application used to deliver the gene encoding adenosine deaminase (ADA) into T-cells of two children suffering from severe combined immunodeficiency (SCID) (Blaese et al., 1995; Bordignon et al., 1995; Herzog and Srivastava, 2010). More viruses such as adenovirus (AdV), lentivirus (LV), herpes simplex virus (HSV), adeno-associated virus (AAV), baculoviral and pox virus have been modified in the laboratory to eliminate their toxicity and maintain their high gene transfer capability (Kay, Glorioso and Naldini, 2001; Thomas, Ehrhardt and Kay, 2003; El-Aneed, 2004). Although many viral vectors have been developed for gene delivery, their use has been limited due to their immunogenic response, insertional mutagenesis and cytotoxicity (Nayak and Herzog, 2009). In the recent years, a decline in the use of retroviral vectors and adenoviruses has been observed (Thomas, Ehrhardt and Kay, 2003). For example, the case of a

clinical trial patient who died four days after receiving adenoviral therapy for the treatment of ornithine transcarbamylase deficiency (Marshall, 1999). Researchers have, therefore focussed on non-viral systems as an alternative to viral vectors. There have been over 1500 approved clinical trials using viral and non-viral systems since 1990 for various cell types and diseases (Herzog and Srivastava, 2010).

1.4.2. Non-Viral Delivery System

Over the past few decades, many drug and gene delivery systems have been developed in different structures and sizes (nm or μm); made of polymers (polymeric carriers, micelles or dendrimers), lipids (liposomes), solid lipid carriers, gold carriers, nanotubes and magnetic carriers (Cho et al., 2008). The use of nanotechnology for the non-viral delivery system and its extreme advantage over the other types of a delivery system is illustrated here.

1.4.2.1. Nanotechnology

Nanotechnology is defined as the branch of technology that creates functional material, devices and systems through control of matter at dimensions between 1 and 100nm where unique phenomena enable novel properties (physical, chemical, biological, mechanical, electrical) and novel application (Hulla, Sahu and Hayes, 2015; www.nano.gov). Nanotechnology is the most recently arrived therapeutic alternative for controlled drug delivery, combining imaging and treatment, applying hyperthermia and providing directed target therapy (Arruebo et al., 2011). As delivery systems, various nanoparticles (NPs) have been formulated to improve chemotherapeutic agents delivery in several ways: by controlling their release and distribution, by enhancing drug absorption, by

protecting their degradation, by delivering agents specifically in tumours via the enhanced permeation and retention (EPR) effect (Talekar et al., 2011; Hillaireau and Couvreur, 2009; Fumagalli et al., 2016), by increasing drug concentration in tumour tissues (loading efficiency), by improving drug solubility (Fang et al., 2015) and by overcoming drug resistance. In addition to that, nanoparticles present optimal size and surface characteristics to increase their circulation time in the bloodstream (Fumagalli et al., 2016). Moreover, non-viral systems can be easily produced on a large scale at a reduced cost (McCrudden and McCarthy, 2013). Although nanoparticles have shown increased benefits, some obstacles exist in their implementation for therapeutic purposes.

In the following part, the biological and chemical fundamental concept in the design of targeted drug delivery systems will be reviewed. Generally, a nanocarrier must be designed in a way that it overcomes all biological strategies (Figure 1-4) in vitro and in vivo environments which may limit their efficacies. This is dependent on the carrier physical and chemical properties such as structure, shape, size, surface charge and composition as well as the site of the target to be delivered. The overall carrier should be biodegradable, stable, nonimmunogenic, easy to fabricate, cost-effective, and able to release the chemotherapeutic agents only at the target site.

Delivery systems including NPs, can be administrated intravenously, intramuscularly, ocularly, and by nasal airways. Figure 1-1. shows the advantages and disadvantages related to the different route of nanocarriers administration.

It is reported that intravenously delivered therapies have the potential to target almost all tissues in the body, therefore, we will be focussing more on systematic delivery systems (McCrudden and McCarthy, 2013; Miyata, Nishiyama and Kataoka, 2012). In fact, oral administration can easily degrade carriers in the digestive tract (Varde and Pack, 2004).

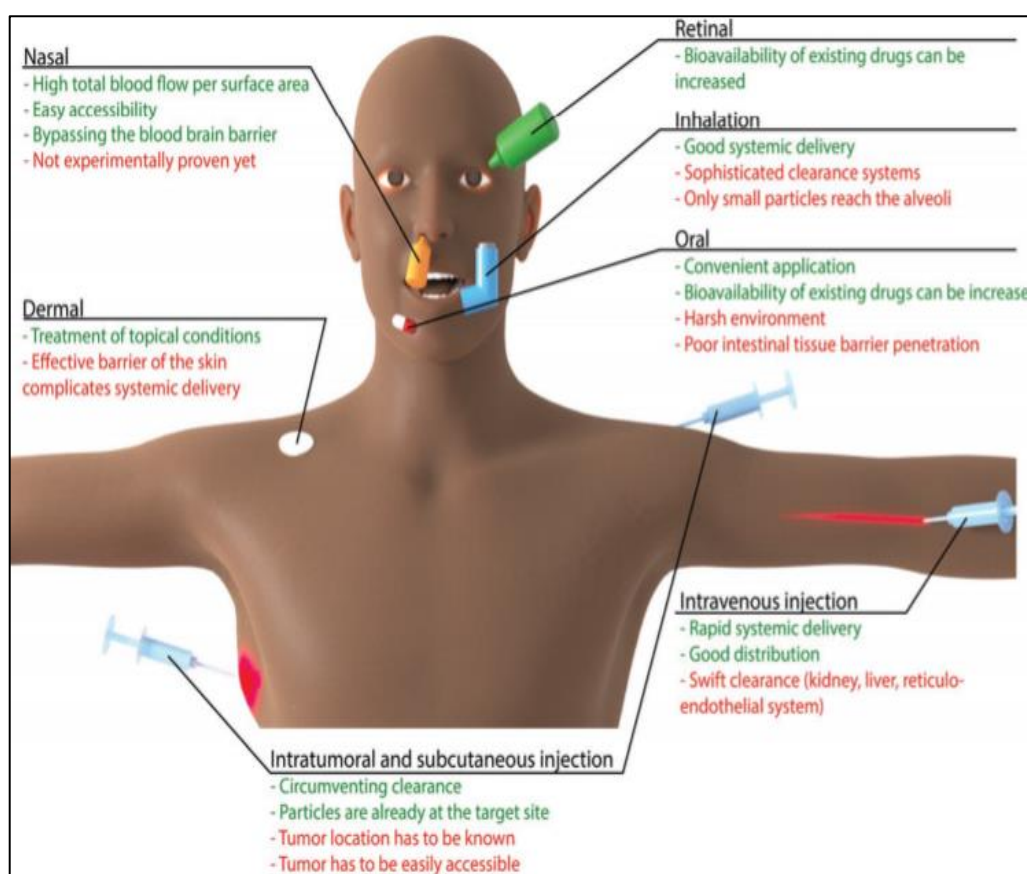


Figure 1-1. Routes of administration: summary of the routes of exposure commonly used for nanomaterial administration, including their main advantages (green) and challenges (red) (Bourquin et al., 2018).

1.4.2.2. Importance of size, surface charge and composition of carriers to overcome extracellular barriers in the bloodstream

When administrated intravenously or intramuscularly, the agents get straight access to the bloodstream; the first clearance chances are that nucleases can easily destroy therapeutic agents whereas nasally or ocularly-administrated

carriers may not face nucleases clearance (Bitko et al., 2004; Dawson et al., 2004; McCrudden and McCarthy, 2013). The body can excrete unwanted materials from the body through renal (urine) and hepatic (bile or faeces) pathways. Since the blood consists of proteins and low molecular weight solutes (plasma), non-viral agents with overall positive charge may interact with negatively charged proteins resulting in non-specific binding forming aggregation or dissociation of non-viral carriers. Aggregation of the nanoparticles for examples can cause embolisation of microvessels (Miyata, Nithe shiyama and Kataoka, 2012). Conventional non-stealth polymeric carriers can quickly bind with the opsonin protein present in blood serum, allowing their visibility to macrophages of the mononuclear phagocytic system (MPS) resulting in their elimination within seconds. Phagocytic cells such as monocytes, macrophages, dendritic cells and neutrophils all form a network or a reticulum in different organs contributing to a system known as the reticuloendothelial system (RES). It is reported that when using non-degradable polymers, they undergo readily phagocytic attack which accumulates the carriers into organs such as liver by Kupfer cells and spleen by spleen macrophages which can lead to severe toxicity and side effects (OwensIII and Peppas,2006). Also, larger particles of 500-5000nm have shown to be cleared faster than smaller sizes by the RES (Harashima, Ochi and Kiwada, 1994; Bourquin et al., 2018). For this reason, carriers need to have a so-called 'Stealth' property, which overcomes the challenges of nucleases attack, proteins interaction and opsonisation so that their stability in circulation is increased. To reduce opsonisation effect, for example, researchers have discovered that grafting shielding groups (non-ionic surfactant or neutral or negatively charged hydrophilic polymer such as polysaccharides, polyacrylamide, poly (vinyl

alcohol), poly(*N*-vinyl-2-pyrrolidone) and PEG) which can block the electrostatic and hydrophobic interactions in carriers surfaces can be helpful (Hidalgo-Alvarez, 2009). Also, nanoparticles of less than 100nm have been reported to have reduced hepatic filtration (Alexis et al., 2008). Renal excretion can also be done by glomerular filtration in kidneys, which can be influenced by the carrier size, charge and shape. It is reported that the filtration-size threshold of glomerular capillary walls is typically 6~8 nm for spherical particles (Yu and Zheng, 2015).

Furthermore, molecules with a molecular weight of around 5000 to 100,000 Daltons can easily be removed from the body by the renal system before reaching their target (OwensIII and Peppas,2006; Ostroff and Ernesto, 2016) whereas negatively charged nanoparticles and liposomes have shown faster uptake by the RES than that of neutral particles (Li and Huang, 2008). It is still important that delivery systems be appropriately designed to evade these clearance mechanisms enabling the systems to stay longer in the circulation.

1.4.2.3. Targeted delivery system accumulation in tumours

Once carriers bypass extracellular barrier, they then need to reach tumours without affecting healthy cells. Targeted delivery systems are the best approach for this; it consists of targeting specific sites or characteristics that only tumours environment present. Carriers can be designed to target tumours in 3 different ways: passive targeting, active targeting and physical targeting.

1.4.2.3.1. Passive targeting: pathophysiology and anatomy of tumour vasculature enhancing the enhanced permeation and retention (EPR) effect

The tumour microenvironment is characterised by abnormal vasculature, inefficient lymphatic network and disorganised endothelial cells compared with healthy tissues. Within the tumour microenvironment persists a neovasculature supplying an increased amount of nutrients and oxygen; this permits the cancer cells to proliferate rapidly near the vessels (Armulik, Genové and Betsholtz, 2011; Nakamura et al., 2016). As a tumour grows, new vessels that engulf existing blood vessels are recruited and reach 2-3mm, where angiogenesis is induced (Iyer et al., 2006). Normal capillaries are lined by tightly sealed endothelium supported by stellate-shaped pericytes which are further enveloped in a thin layer of basement membrane (BM) whereas the blood vessels in a tumour are irregular in shape and have incomplete endothelial lining permitting relative larger pores of 0.1-3 μm in diameter leading to higher vascular permeability and hydraulic conductivity (Nakamura et al., 2016). In addition to the space within epithelial cells in tumour vasculature, both pericytes and BM are loosely associated with endothelial cells and occasionally penetrate deep in the tumour parenchyma (Nakamura et al., 2016). The tumour anatomical defectiveness along with the disorganised epithelial cells with large fenestrations results in the extensive leakage of blood plasma components, such as macromolecules, nanoparticles and lipidic particles, into the tumour tissue (Iyer et al., 2006). Moreover, due to the poor lymphatic drainage, carriers that reach the tumour environment are less prone to immune clearance which means that carriers can retain in a tumour for an extended period (Danquah, Zhang and Mahato, 2011; Nakamura et al., 2016, Iyer et al., 2006). This

phenomenon of how delivery systems accumulate the tumours by passing across the fenestrated capillary endothelium and then get introduced into the interstitial space through tumour vasculature leakage is known as the enhanced permeability and retention (EPR) (Kobayashi, Watanabe and Choyke, 2014). In another term, it is the consequence of increased vasculature permeability and decreased lymphatic functions of a tumour (Sun et al., 2017, Hillaireau and Couvreur, 2009; Miyata, Nishiyama and Kataoka, 2012). Polymeric macromolecules larger than 40KDa including poly (styrene-co-maleic acid half-butylate) linked neocarzinostatin (SMANCS), the first macromolecular anticancer drug approved for use in clinical trials in 1993 have shown to be very highly accumulated in tumours via the EPR effect compared to healthy tissue (Maeda and Konno 1997; Fang, Nakamura and Maeda, 2011). Low-molecular-weight drugs do not apply the EPR effect due to their rapid diffusion into the circulating blood, followed by renal clearance (Iyer et al., 2006). Also, it has been reported that carriers of less than 200nm accumulate effectively into tumours (Miyata, Nishiyama and Kataoka, 2012). Since passive targeting of delivery systems is a progressive step, stability and solubility of the carriers in the plasma becomes essential to achieve the minimum time required in circulation for the EPR effect to occur (6h) (Matsumura and Maeda, 1986; McCrudden and McCarthy, 2013). The use of ionic or neutral particles would be ideal for increasing their plasma half-life. Also, the use of polymers to make drugs macromolecules would facilitate not only their EPR effect but would permit their diffusion across matrix gel (fibrin gel or stromal tissues) which surround tumour tissues (Fang, Nakamura and Maeda, 2011).

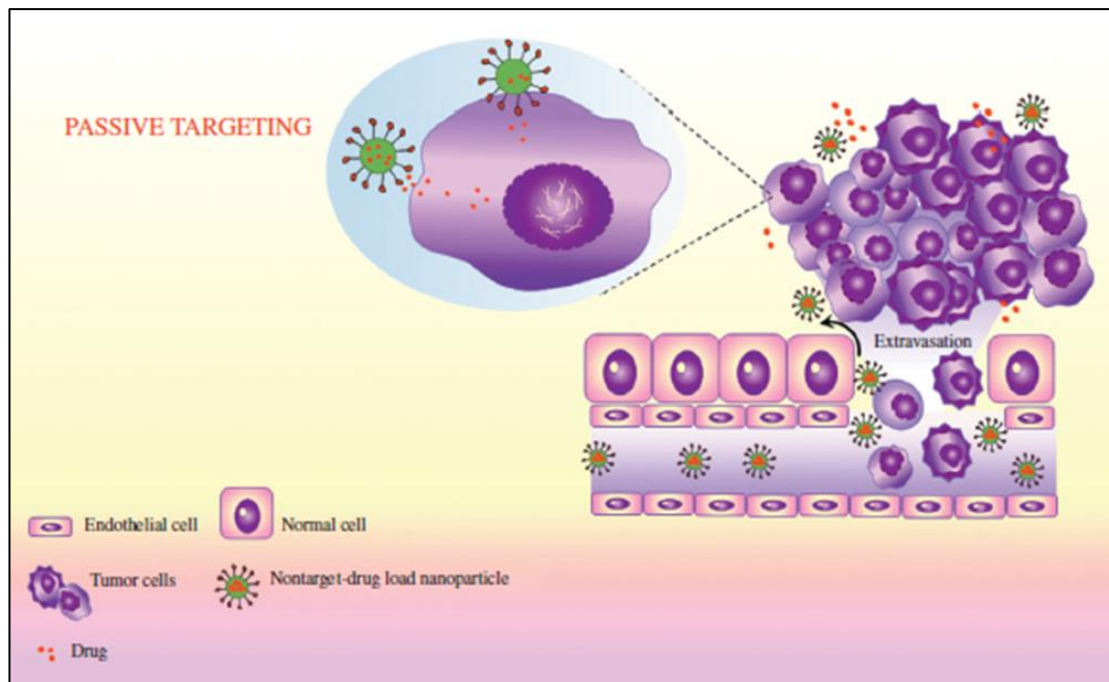


Figure 1-2. Schematic representation of nanoparticles accumulation within tumour by passive targeting (pelissari et al., 2018).

Although EPR facilitates the tumour targeting of carriers passively, more challenges can still limit their effect on tumour cells. The increased vessel permeability, hyperfusion, the poor lymphatic drainage, the hyperplasia around blood vessels and increased production of extracellular matrix components elevate the interstitial fluid pressure in tumours (from 0mmHg to 10-40mmHg) (Nakamura et al., 2016). This, in turn, creates hypoxic and acidic intratumoral conditions and at same time may prevent the penetration of carriers deep within the tumor therefore contributing to tumor progression, metastasis and therapy resistance (Jain, 1987; Carmeliet and Jain, 2000; Jain, 2005; Jacobetz et al., 2012; Nakamura et al., 2016). Also, other organs may present different tumour features, for example, the brain possesses the blood-brain barrier (BBB) which control tightly the movement of particles (more detailed will be explained in chapter 4).

1.4.2.3.2. Active targeting

Once carriers reach the tumour interstitium via the EPR effect, they need to find their way to enter the cell. For this reason, active targeting via receptor-mediated internalisation can be employed. The lipid bilayer of cells consists of proteins and saccharides of different shapes and sizes known as receptors which can be distributed evenly across the cell surface or localised within microdomains. These receptors can convey changes in the presence of external environments such as the presence of nutrients, toxins, attractants or foreign invaders (Kiessling, Gestwicki and Strong, 2000). Cancer cells overexpress specific antigens or surface receptors which can be targeted (Attarwala, 2010). Receptor targeting can be done by adding targeting moieties such as ligands or antibodies into the backbone of polymers. There have been some targeted cancer treatments that are FDA approved using antibodies (Gasser and Waaga-Gasser, 2016). However, the use of peptides as targeting moieties have been reported to be beneficial over antibodies because of the difficulties of conjugating antibodies into carriers and their high molecular weight of 160000 can affect their circulation time whereas peptides are smaller, simple, more stable and easier to produce (Aina et al., 2002; Yu et al., 2016). Since the 1980s, there has been 239 FDA approved therapeutic proteins and peptides in which 60 peptide drugs are already in the market (Fosgerau and Hoffmann, 2015; Usmani et al., 2017). Tumors have a developed lumen structure and secrete a variety of proangiogenic factors such as vascular endothelial growth factor (VEGF), platelet-derived growth factor (PDGF), basic fibroblast growth factor (bFGF), interleukin-8 (IL-8), angiogenin, angiotropin, platelet-derived endothelial cell growth factor (PD-ECGF), transforming growth factor- α (TGF- α), TGF- β , epidermal growth factor (EGF), and tumour necrosis factor- α (TNF- α))

(Folkman, 1996; Byrne, Betancourt and Brannon-Peppas, 2008). Targeting angiogenesis being the central phenomenon that influences tumour growth can also be achieved via Vascular endothelial growth factor VEGF receptors targeting in angiogenic endothelial cells. The tripeptide arginine-glycine-aspartic acid (RGD) was the first and most widely used peptide to target angiogenesis by binding specifically to the overexpressed integrins $\alpha_v\beta_3$ and $\alpha_v\beta_5$ (Yu et al., 2016). Targeting to specific cells of specific organs is also achieved by small ligand targeting molecules which are more beneficial than peptides as they do not exhibit immunogenicity. Examples include folic acid, a low molecular weight vitamin that selectively binds to folate receptors highly expressed by many primary and metastatic including breast and ovarian, endometrial, lung, kidney, breast, colon and nasopharyngeal cancers (Yoo and Park, 2004; Li et al., 2016).

Another example is the use of galactose residues for the targeting of the asialoglycoprotein receptor (ASGPr) in liver cancer (see chapter 4 and 5). Polymers such as Pullulan and Hyaluronic acid can also target overexpressed receptors such as ASGPr in liver and CD44 in leukaemia, breast, intestinal and colon cancers, respectively (Basakran,2015). However, receptors overexpressed in tumour cells are also present in healthy cells, which can affect the targeting of carriers into tumour cells only. Also, due to the tumour environment with a high level of proteases, transmembrane proteins expressed on cell surfaces can be cleaved or can be present in a variety of isoforms thus may affect the targeting recognition (Hayashida et al., 2010; Andreadis, 1987; Muro, 2012).

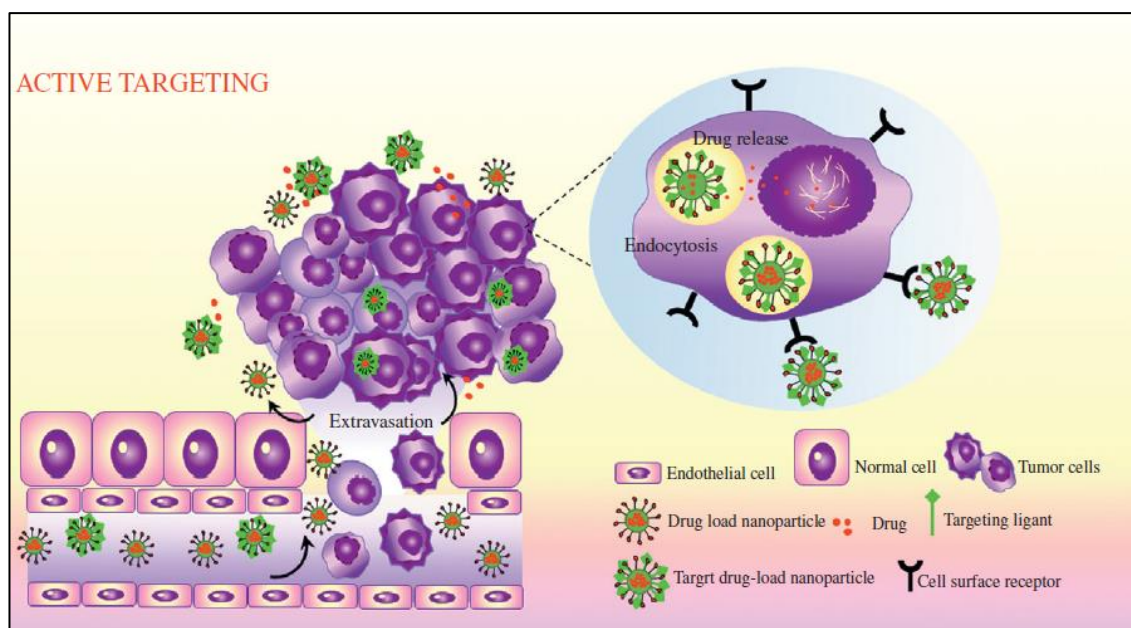


Figure 1-3. Schematic representation of nanoparticles accumulation within a tumour by active targeting (pelissari et al., 2018).

Furthermore, Yu et al. in 2010 report the potential of active targeting to suppress multidrug resistance (MDR) via bypassing of P-glycoprotein- mediated drug efflux (Gottesman, Fojo and Bates, 2002; Gu et al., 2007; Peer et al., 2007). Usually, the passive and active targeting are combined to increase the delivery efficiency on tumour cells, once the carrier has reached the tumour cells, they are often taken inside cells by a phenomenon known as endocytosis.

1.4.2.4. Intracellular barriers and the internalisation of carriers (vectors) by endocytosis: the chemotherapeutic agent release point

One of the major obstacles that non-viral carriers face is the loading capacity and the release rate of therapeutic agents encapsulated at the right time and in the right site of action. Carriers should be able to load sufficient amount of therapeutic agents to achieve a therapeutic effect, and they should be released at an optimal rate to the right site of action (3-10% per day) (Fang, Nakamura

and Maeda, 2011). The too slow or too rapid release rate can also affect the effectivity of the delivery system. A too slow release will result in an inefficient concentration of active drugs whereas rapid release will lead to a high concentration of free drug in circulation which will result to undesired systemic toxicity (Fang, Nakamura and Maeda, 2011). Most therapeutic agents undergo their mode of action to the tumour site; therefore it is essential for carriers to be able to release the agents to the main tumor site and achieve higher drug concentration in the vicinity of the tumor (Ratain and Plunkett, 2003).

1.4.2.4.1. The cytosolic entrance of carriers

In 2010, Ziello and his colleagues explained the mechanism of how materials are undertaken by cells. The cell membrane is permeable to materials less than 1KDa and can internalise them in a variety of different ways (Bareford and Swaan, 2007). The primary pathway that most viruses use to enter the cell is the endocytic route (Thorley, McKeating and Rappoport, 2010). Macromolecules present in the surrounding medium of cells can be taken up by cells, the material is internalised by an area of the plasma membrane which then engulfs the material inside the cell to form a vesicle containing the ingested material. The other pathway is by receptor-mediated endocytosis where the macromolecule present in surrounding of the cells interact with specific cell surface receptors present in the clathrin-coated pits (specific regions of the cell plasma membrane) which then internalise the material (~200nm) to form clathrin-coated vesicles (CCV) (Wang, Upponi and Torchilin, 2012). Endocytosis is also reported to be achieved via the caveolae present in the plasma membrane (for particles of~300nm) (Wang, Upponi and Torchilin, 2012). After macromolecules internalisation, endocytosis vesicles may fuse to

form acidic early, late endosomes and lysosomes (Anderson, 1998; Aniento, 1993; Ziello, 2010; Wang, Upponi and Torchilin, 2012).

1.4.2.4.2. Physical targeting

Apart this accumulation of materials by the endosomal system, materials contained in early endosomes (can be taken as quickly as in 5-10minutes) can be recycled and exocytosed or trafficked to other organelles such as Golgi and mitochondria (Steinman, 1983; Bareford and Swaan, 2007). Therapeutic agents should be released safely once they reach intracellular compartments to be able to achieve their role. It is therefore crucial that carriers escape the endosomes or avoid degradation through lysosomes trafficking. It is known that macromolecules (hydrophobic or charged) that undergo endocytosis depending on clathrin are destined for lysosome degradation whereas independent clathrin pathway leads to endosomal accumulation only (Bareford and Swaan, 2007).

a. pH-responsive drug release

The early endosomes possess some vacuolar ATPase which pumps in H^+ ions making an overall acidic environment in early endosomes to pH 6.0-6.5, late endosome to pH 5.5 and the lysosomes to pH nearly 4.5 (Bareford and Swaan, 2007; Li et al., 2018). Current strategies take benefits of this pH condition to escape endosomes by tailoring modified carriers such as pH-sensitive polyplexes, cell-penetrating peptides, and photosensitive molecules. pH-sensitive materials are either designed by incorporating a pH-responsive linkage within the material or by using building blocks which are pH-responsive. An example of this, is molecules (such as Doxorubicin) that switch from uncharged to charge and hydrophobic to hydrophilic when they are below their pKa (Kongkatigumjorn et al., 2018).

b. Release via endosomes lysis

When polymeric materials are used, the polymers absorb protons in the endosome (proton sponge effect) which lead to chloride ions influx resulting in an increased osmotic pressure of water flow into the endosome and therefore leading to endosome rupture. Very recently, Rangasamy and his colleagues have also reported in 2018 a new way to facilitate endosomes rupture that can permit the release of biologics using a K^+/H^+ ionophore (Rangasamy et al., 2018). Another strategy is that of materials such as fusogenic lipid DOPE and Haemagglutinin that interact with the membrane either by electrostatic interaction or by fusion in the lipid bilayer. The sub-physiological pH of the endosomes can cause the materials to undergo conformational changes from lipid bilayer which then can disrupt the endosomal membrane (Wiley and Skehel, 1987; Varkouhi et al., 2011; Wang, Upponi and Torchilin, 2012; McCrudden and McCarthy, 2013). Moreover, cationic amphiphilic peptides (AMPs) can also bind to lipid bilayers, which can lead to internal stress resulting in pores formation in the lipid membrane (Jenssen, Hamill and Hancock, 2006). Also, photosensitizers such as TPPS₄, TPPS_{2a}, AIPcS_{2a} and dendrimer-based photosensitiser are able to induce the formation of singlet oxygen in the presence of light which have the capability to destroy endo/lysosome membrane (Prasmickaite, Høgset and Berg, 2001; Nishiyama et al., 2006; Varkouhi et al., 2011).

c. Redox-responsive drug release

The primary reducing agent to cause redox response is the most abundant thiol species known as Glutathione (GSH) present in the cytoplasm (Espinosa-Diez et al., 2015). The extracellular concentration of GSH is two μ M, whereas a

higher concentration of 1-10 mM is seen in the intracellular compartment of the cell. Delivery systems can be designed in a way that they contain disulphide leakage which can be broken under high concentration of GSH inside the cytoplasm and most importantly is to note the advantage of using the redox-responsive delivery system to overcome drug resistance (Bar-Zeev, Livney and Assaraf, 2017). For example, Ma and colleagues in 2015 have demonstrated that the use of redox-responsive polyphosphoester-based micellar has the potential to overcome MDR and can successfully deliver the anticancer drug dox against drug-resistant breast cancer cells. Further details are explained in chapter 6.

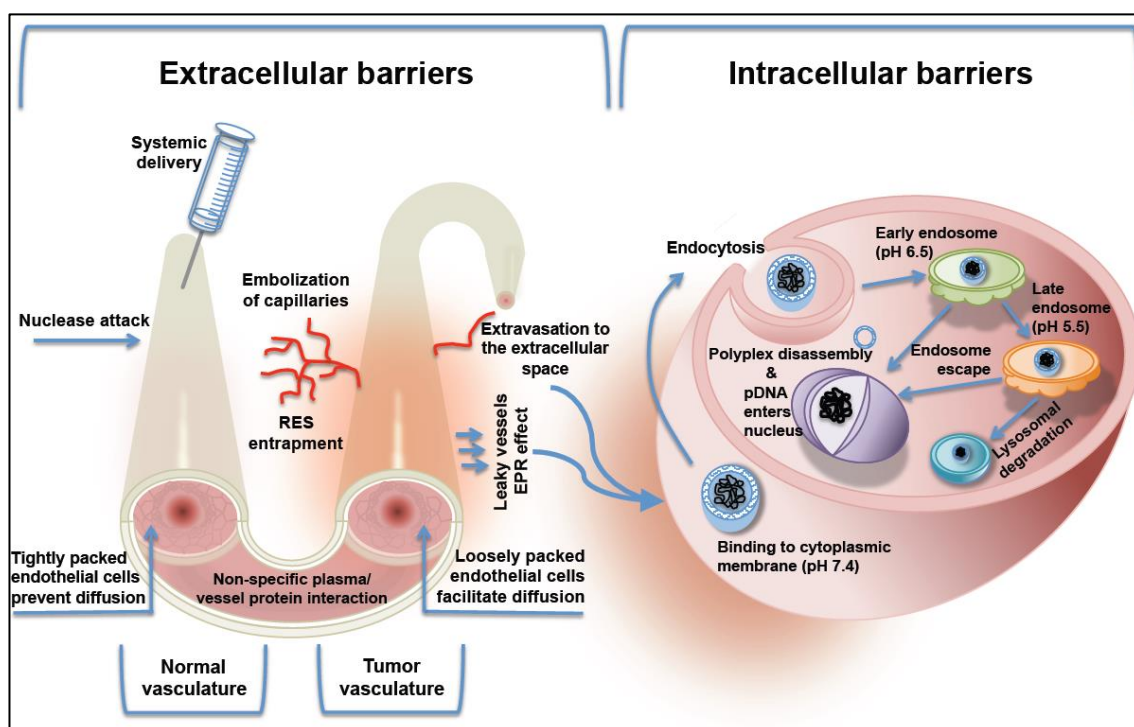


Figure 1-4. Summary of the extra- and intracellular barriers faced by non-viral gene therapies following systematic delivery (McCrudden and McCarthy, 2013; Miyata, Nishiyama and Kataoka, 2012).

d. External stimuli-responsive drug release

Release of therapeutic agents from carriers can also be released by the influence of external stimuli such as temperature, electromagnetic, ultrasound,

electric field or applied mechanical force (Zhang et al., 2016; Ge et al., 2011; Comes Franchini et al., 2010; Bar-Zeev, Livney and Assaraf, 2017). Carriers can be designed in a way that they are stable at 37 °C (normal physiological temperature) and at a higher temperature (40-42 °C which is the tumour temperature), the carrier undergoes a change resulting in drug release. A good example is that of ThermoDox, a temperature-sensitive doxorubicin-pegylated liposome developed for liver cancer, which has reached phase III trials (Pillai, 2014). In the condition of hyperthermia or radiofrequency ablation, the lipid components in the liposomes undergo a gel to liquid transition which facilitates the release of the drug (Pillai, 2014; Mura, Nicolas and Couvreur, 2013). Strategies using a magnetic field to release the drug from magnetic responsive carriers has also been developed. Superparamagnetic iron oxide nanoparticles (SIONPs) are the most famous nanoparticles used to achieve magnetic targeting. In 2009, Qin and colleagues developed SPEL ferrogel consisting of a pluronic F17 copolymer, SIONPS and hydrophobic drug in which under magnetic fields, iron oxide nanoparticles makes the systems attract each other and then get squeezed provoking drug release. Recently, a new study has also shown that ultrasound could destruct or degrade microparticles made of poly (lactic-co-glycolic acid) (PLGA) loaded and non-loaded with doxorubicin and therefore influencing controlled drug release of Dox (Jang et al., 2018).

1.4.2.5. The nuclear entrance of therapeutic agents

The final obstacle is crossing the nucleus for chemotherapeutic agents whose final target is inside the nucleus. Passive diffusion through the nucleus membrane could only happen for materials less than 50 kDa (~10 nm) whereas the nucleus penetration of macromolecules greater than 50 kDa can be

facilitated using nuclear localisation (NLS) peptides or DNA targeting sequences (DTS) (Barua and Mitragotri, 2014). The material around the nucleus periphery can also access entrance to the nucleus during mitotic division where the nuclear membrane's barrier is disrupted or via nuclear pore complex (NPC) (Khalil, 2006; McCrudden and McCarthy, 2013; Munsell, Ross and Sullivan, 2016). Non-NLS design strategies for effective nucleus entrance has also been developed. Sugar residues (for example lactose and mannose) are incorporated in carriers to induce nuclear localisation by interacting with sugar-binding proteins (lectins) as a shuttle between cytoplasm and nucleus (Munsell, Ross and Sullivan, 2016).

1.4.2.6. Tumour Resistance

Although successful delivery can be achieved using nanocarriers, treatment resistance still exists. The biggest challenge is the multi-drug resistance (MDR) to almost all anti-cancer agents due to the efflux of drugs by the p-glycoprotein. MDR is most commonly associated with the overexpression of pro-survival, anti-apoptotic protein and ATP-binding cassette (ABC) transporters genes (Mansoori et al., 2017). These transporters actively transport various drugs outside the cell through the plasma membrane, therefore, reducing the number of drugs inside cells (Figure 1-5.) (Bar-Zeev, Livney and Assaraf, 2017). Examples for chemotherapeutic drugs that face resistance are Doxorubicin, Cisplatin, Daunorubicin, Colchicine, Vincristine, Vinblastine, Vinorelbine, teniposide, irinotecan, topotecan, methotrexate and paclitaxel (Joshi, Vishwakarma and Bharate, 2017).

Various types of chemosensitizers have been developed to overcome MDR. These are compounds that include natural compounds derived from plants and marine compounds which specifically block MDR efflux transporters.

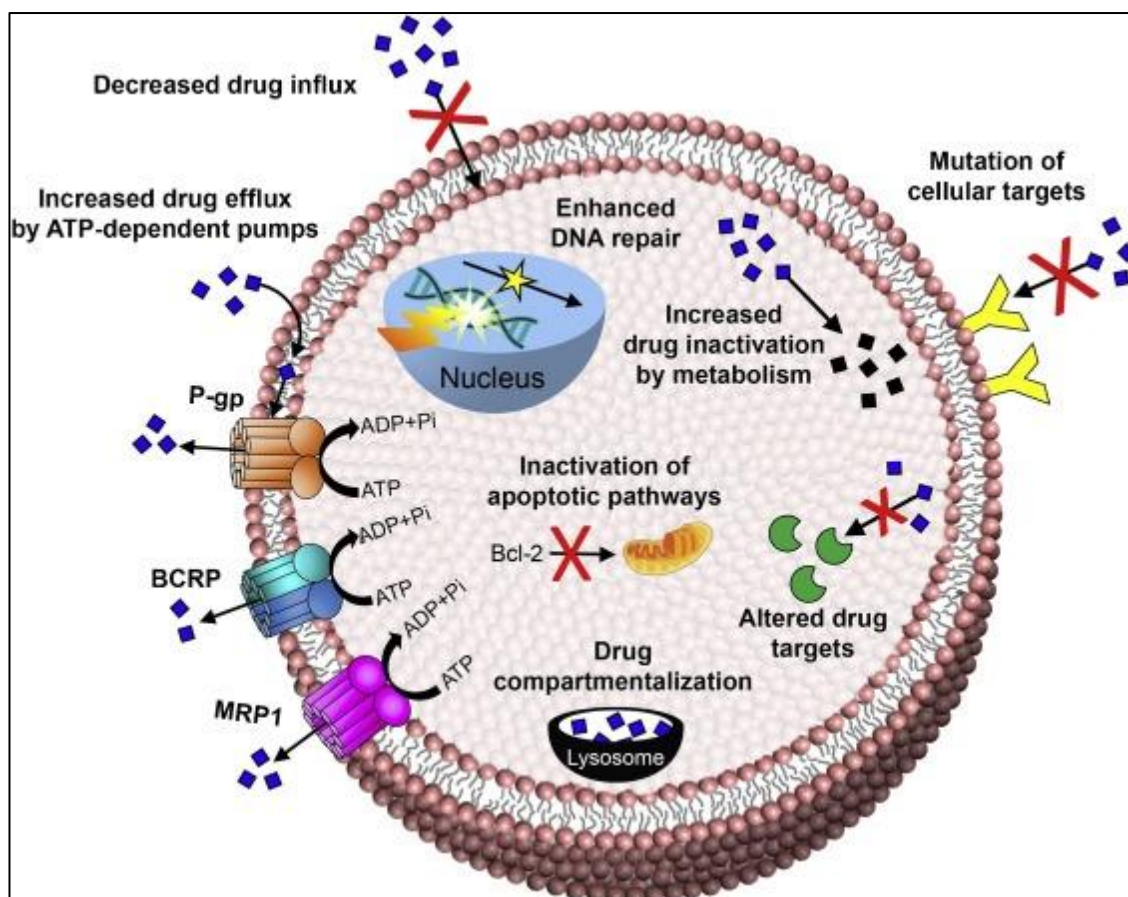


Figure 1-5. Mechanisms of anticancer drug resistance mediated by transmembrane transporters of the ATP-binding cassette (ABC) superfamily: p-gp, BCRP and MRP1 enhanced ATP energy-dependent efflux of various hydrophobic anticancer drugs (Bar-Zeev, Livney and Assaraf, 2017).

Table-2 (tabulated by Bar-Zeev and colleagues in 2017) shows the chemotherapeutics drugs that are associated with the resistant transporters and the correspondent chemosensitizers. As seen from the table, almost all-important ABC multidrug resistance-associated proteins involve the resistance of the lead compound of anthracycline: Doxorubicin. Doxorubicin being the most effective chemotherapeutic drug against various cancers, presents various cardiotoxicity effect but also presents continuous problems with MDR (Geisberg

and Sawyer, 2010). For this reason, many researchers focus on developing new strategies for improving Doxorubicin safety in cancer patients.

Table 1-2. The three main ATP-binding cassette (ABC) efflux transporters, their chemotherapeutic drug substrates and chemosensitizers (Bar-Zeev, Livney and Assaraf, 2017).

ABC efflux transporter	Abbreviation	Gene	Cytotoxic drug substrates	Inhibitors (Chemosensitizers)
P-glycoprotein	P-gp/ MDR1	ABCB1	Actinomycin D Anthracyclines (Daunorubicin, Doxorubicin) Anthracenediones (Mitoxantrone) Epipodophyllotoxins (Etoposide, Teniposide) Taxanes (Paclitaxel, Docetaxel) Vinca alkaloids (Vinblastine, Vincristine)	Borneol Chloroquine Curcumin Lapatinib Quercetin Sertraline (Zoloff®) Tariquidar Tetrandrine Verapamil Vitamin E
Breast cancer resistance protein	BCRP	ABCG2	Anthracyclines (Daunorubicin, Doxorubicin) Camptothecins (Irinotecan, SN-38) Mitoxantrone	Elacridar Hesperetin Ko143 Lapatinib
Multidrug resistance-associated protein 1	MRP1	ABCC1	Anthracyclines (Daunorubicin, Doxorubicin) Camptothecins (Irinotecan, SN-38) Cisplatin Mitoxantrone	MK571 Benzobromarone Quercetin Cyclosporin A

1.5. The anthracycline background: Doxorubicin (Dox)

Anthracyclines are the most widely used anticancer drugs from all the FDA approved drugs. The first two anthracyclines Doxorubicin and Daunorubicin were developed in the 1960s and originally isolated from the fungus *Streptomyces peucetius* (Rivankar,2014). In the 1950s, the bright red pigment isolated from the fungus was found to have good activity against mouse tumours and named daunorubicin (Rivankar,2014). However, by 1967s, the

compound was already determined to produce fatal cardiac toxicity (Shakir, 2009). It was then that some genetic modification to the fungus led to the production of Dox, which also presents severe toxicity (Rivankar, 2014). So much effort has been put in place to develop anthracyclines analogues (~2000 compounds) to overcome the severe side effects of first-generation anthracyclines such as acute toxicity, cardiomyopathy and congestive heart failure. However new analogues of which only a few have been clinically approved (epirubicin, aclarubicin, pirarubicin, mitoxantrone, idarubicin and valrubicin) have also failed to reduce these side effects, and none present stronger antitumor efficacy than the original two anthracyclines (Minotti et al., 2004; Kumar et al., 2014; Carvalho et al., 2009).

1.5.1. Doxorubicin structure

The antibiotic Doxorubicin is known in different names as adriamycin or hydroxydaunorubicin (Pérez-Arnaiz, Busto and García, 2014). Its structure consists of an aglyconic and daunosamine sugar moieties. The aglycone consists of a tetracyclic ring with adjacent quinone-hydroquinone groups in rings (the quinone and hydroquinone groups on adjacent rings permits the gain and loss of an electron by reaction mediated by cytochrome P450 reductase, NADH dehydrogenase, and xanthine oxidase), a methoxy substituent and a short side chain with a carbonyl group. The daunosamine sugar is attached via a glycosidic bond to one of the rings and consists of a 3-amino-2,3,6- trideoxyL-fucosyl moiety (Carvalho et al., 2009; Minotti et al., 2004).

For laboratory use, the drug is commercially available in salt form as Doxorubicin hydrochloride (Hydroxydaunorubicin hydrochloride; Dox.HCl; $C_{27}H_{29}NO_{11} \cdot HCl$; 579.98g/mol) giving it solubility in water, slightly in methanol

and practically insoluble in organic solvents including chloroform and ether (Arcamone et al., 1972, Kanwal et al., 2018).

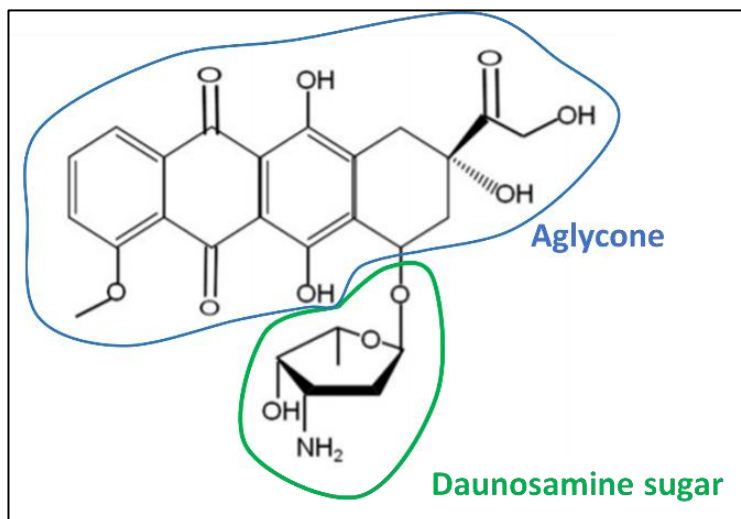


Figure 1-6. Chemical structure of Doxorubicin.

1.5.2. Antitumor activity of doxorubicin

Dox having a low molecular weight enter cancer cells via passive diffusion and then binds to the 20s proteasomal subunit in the cytoplasm to form a Dox-Proteasome complex which transports the drug into the nucleus via nuclear pores (Kiyomiya, Matsuo and Kurebe, 2001). The process is facilitated by the use of ATP. The drug then dissociates from the proteasome and binds to DNA to carry out its mode of action (Kiyomiya, Matsuo and Kurebe, 2001; Minotti et al., 2004). Anthracyclines including Dox have been reported to have the following mode of actions: intercalation between base pairs in DNA helix leading to inhibited replication and synthesis of proteins; generation of free radicals (superoxide anion ($O_2^{\cdot-}$) and hydrogen peroxide (H_2O_2)) resulting in cytotoxicity to cell membrane lipid peroxidation; DNA binding and alkylation; DNA cross-linking; interference with DNA unwinding or DNA strand separation and helicase activity; direct membrane effects; initiation of DNA damage via inhibition of topoisomerase II; and induction of apoptosis in response to topoisomerase II

inhibition (activation of p53-DNA binding) (Gewirtz, 1999; Minotti et al., 2004; Rivankar,2014).

Dox tend to interact with the cell compartment by electron transfer, which leads to the formation of toxic semiquinone radical intermediates that can react with oxygen to form reactive oxygen species (ROS). Moreover, Dox is among the most active chemotherapeutic agents and has become one of the leading 'first line' anticancer drugs. It is used for the treatment of a wide range of cancers including breast, lung, ovarian, neuroblastoma, acute lymphoblastic leukaemia, bile duct, prostate, uterus, ovary, oesophagus, stomach, childhood solid tumours, osteosarcomas, Kaposi's sarcoma, soft tissue sarcomas, acute myeloblastic and Wilms tumor (Kumar et al., 2014; Rivankar,2014). The drug is administrated intravenously (dose range of 10-50 mg/m²) as it can not be absorbed by the gastrointestinal tract since it is hugely irritating to tissues. After administration, Dox is very quickly distributed into the extravascular compartments and has a half-life of 12-18 hours (Kumar et al., 2014). It is reported that the binding of Dox to plasma protein is about 75% and does not cross the blood-brain barrier (Kumar et al., 2014). The drug is then metabolised in the liver into 13-OH-doxorubicinol by the enzyme aldo-ketoreductase and eliminated by metabolic conversion to a variety of aglycones and other inactive products which are then excreted through biliary and faecal excretion (Kumar et al., 2014).

1.5.3. Doxorubicin side effects

Doxorubicin having a low molecular weight quickly diffuse into all tissues in the body (heart, brain, liver and kidneys) thereby frequently causing toxicity leading to dose-related side effects. There are many common side effects associated

with Dox including acute nausea, stomatitis, gastrointestinal disturbances, alopecia, baldness, neurologic disturbances (hallucinations, vertigo, dizziness), acute or chronic cardiotoxicity and bone marrow aplasia (Li et al., 2017). The effect on bone marrow is accompanied by an increased incidence of microbial infection, gingival bleeding, anaemia, thrombocytopenia and neutropenia. Moreover, many other side effects have been reported such as cellulitis, vesication, thrombophlebitis, lymphangitis, painful induration, pheboscrosis and disruption of mitochondrial functions (Dox can bind to cardiolipin) (Hortobagyi, 1997; Maluf and Spriggs, 2002; Tokarska-Schlattner et al., 2007; Jung and Reszka, 2001; Julka et al., 2008; Carvalho et al., 2009; Li et al., 2017).

1.6. Targeting delivery Systems for the improvement of Doxorubicin therapy

Various carriers have been developed to assist the preferential distribution of Doxorubicin within tumours while not exposing healthy tissues to toxic levels of the drugs. Figure 1-7. gives an overview of the problems accounted with the delivery systems, whereas Figure 1-8. gives an overview of the types of organic delivery systems.

1.6.1.Liposomes

Liposomes were first discovered by Alec Bangham (Bangham, 1980; Samad, Sultana and Aqil, 2007). They are small vesicles of spherical shape produced from cholesterol, non-toxic surfactant, sphingolipids, glycolipids, long chain fatty acids or even membrane proteins. The use of liposomes to deliver compounds in the aqueous compartment started in the 1960s and developed for clinical potential in 1970s (Bozzuto and Molinari, 2015). Liposomes can

entrap both lipophilic (in the aqueous centre) and hydrophobic compounds (in the bilayer membrane).

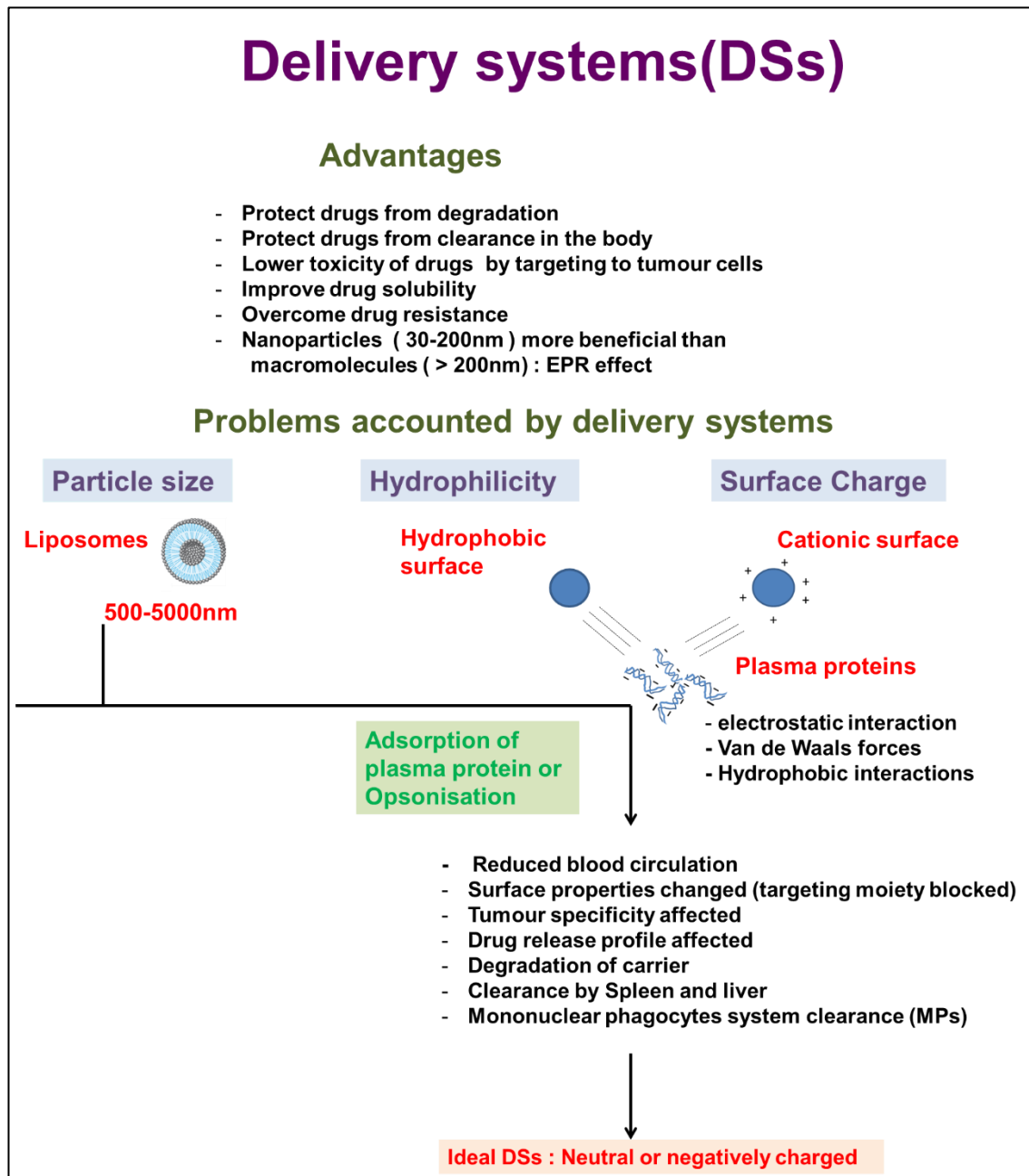


Figure 1-7. Advantages and disadvantages of the existing delivery system.

Conventional liposomal formulations were the first type of liposome to be developed, although they have shown strong enhancement for drug delivery in cancer cells, these systems have been prone to rapid elimination due to

opsonisation, RES, liver and spleen elimination. An example is that of the negatively charged medium-size oligolamellar liposomes containing Doxorubicin, which is referred as to OLV-Dox (200-500nm). The overall system has shown to be cleared by the RES and Dox situated in the bilayer of the liposome is easily released upon dilution and quickly eliminated (Hua and Wu, 2013; Sercombe et al., 2015; Gabizon et al., 1991; Amselem, Cohen and Barenholz, 1993; Barenholz, 2012). Another disadvantage on the use of these liposomes is their size being too large (400-2.5 μ m) which allows their extravasation in the extra-hepatic tissues and their uptake by RES effect (Maeda, Bharate and Daruwalla, 2009; Malam, Loizidou and Seifalian, 2009; Barenholz, 2012).

The reduced clearance, prolonged circulation and improved pharmacokinetics of conventional liposomes have been achieved by the addition of PEG and by the production of liposomes in nanoscales. There have been over 10 PEGylated drugs that have been FDA approved with over 20 drugs in clinical trials (Swierczewska, Lee and Lee, 2015). Doxil® (80-90nm) was the first FDA-approved PEGylated liposomal nano-Doxorubicin drug in 1995 for the treatment of ovarian cancer and AIDS-related Kaposi's sarcoma.

However, Although PEGylation in liposomes has shown prolonged circulation effect, there have also been shown to reduce the ability of liposome to interact with the intended targets (Sercombe et al., 2015).

More liposomes-based delivery system has been clinically approved not only in cancer therapy but also for other diseases such as fungal infections, vaccines against hepatitis and influenza, analgesic and photodynamic therapy.

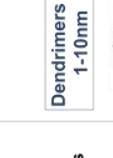
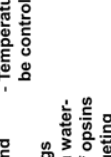
1960	2018
<p>Liposome (1965) 50-450nm</p>  <p>Advantages</p> <ul style="list-style-type: none"> - Phospholipid with large aqueous core - Best for water soluble encapsulation - Low toxicity (Immordino, Dosio and Cattel, 2006) <p>Disadvantages</p> <ul style="list-style-type: none"> - Opsonisation - Rapid clearance by MPS - Rapid release of encapsulated drugs - Hydrophobic drugs are rapidly released in presence of plasma proteins or cell membranes (Chowdhary, Shariff, and Dolphin, 2003 ; Allen and Cullis, 2004) <p>PEGylated or cholesterol added liposomes (1980)</p> <p>Advantages</p> <ul style="list-style-type: none"> - Increased solubility - Prevent adsorption and MPS clearance - Prolonged blood circulation - Cholesterol improve the stability of liposomes compared to PEG on its own <p>Disadvantages</p> <ul style="list-style-type: none"> - Delay carrier internalisation in tumour cells - Becomes cytotoxic due to internalisation delay (Hue et al., 2015) - Side effects : palmar-plantar erythrodysesthesia, stomatitis and mucositis (Ansari et al., 2017) <p>Doxil (1995) <100nm</p>  <p>Advantages</p> <ul style="list-style-type: none"> - Improved solubility - Prevent adsorption and MPS clearance - Prolonged blood circulation - Cholesterol improve the stability of liposomes compared to PEG on its own <p>Disadvantages</p> <ul style="list-style-type: none"> - Delay carrier internalisation in tumour cells - Becomes cytotoxic due to internalisation delay (Hue et al., 2015) - Side effects : palmar-plantar erythrodysesthesia, stomatitis and mucositis (Ansari et al., 2017) <p>Abraxane (2005) 130nm</p>  <p>Advantages</p> <ul style="list-style-type: none"> - Abraxane proved that the use of albumin is better than the use of PEG to avoid plasma protein adsorption, enhance blood circulation and suppress opsonisation - Abraxane have showed much lower toxicity compared to Doxil. 	<p>Polymeric system (1976)</p>  <p>Advantages</p> <ul style="list-style-type: none"> - Polysaccharides are biocompatible, non-immunogenic - Easily biodegradable into non-toxic products - Can undergo easily chemical modification - Smaller size can be obtained - Low cost compared to liposomes - Controlled release properties <p>Disadvantages</p> <ul style="list-style-type: none"> - Poor stability in aqueous environment - Rapid release may occur in vivo - Temperature may need to be controlled <p>Amphiphilic dendritic block copolymers (polymeric micelles) 10-200nm</p>  <p>Advantages</p> <ul style="list-style-type: none"> - protect drugs from degradation - controllable chemical composition (for higher loading and release properties) and size - Increased stability (at low CMC) and solubility - Solubilise poor water soluble drugs - Hydrophobic compartment form a water-bound barrier, blocks adhesion of opsins - Easy surface modification for targeting purpose <p>Disadvantages</p> <ul style="list-style-type: none"> - more expensive - Require many step for synthesis - Can be challenging for large-scale production (peer et al., 2007) <p>Dendrimers (1978) 1-10nm</p>  <p>Advantages</p> <ul style="list-style-type: none"> - New field - More spherical shape compared to irregular architecture of linear polymer - Precise nanostructure, water solubility, multivalence, high degree of branching, highly adaptable surface chemistry, controllable molecular size, low polydispersity - Easily conjugated into polymers - Can load both hydrophobic and hydrophilic agents <p>Disadvantages</p> <ul style="list-style-type: none"> - Dendron based polymeric amphiphilic system <p>Advantages</p> <ul style="list-style-type: none"> - Dendron with multiple surface properties - allow loading of multiple therapeutics into a single drug-delivery vehicle for concurrent delivery
<p>Targeted system (1980)</p>  <p>Advantages</p> <ul style="list-style-type: none"> - Targeting specific receptors overexpressed - Reduced side effects - Enhanced specific cellular uptake <p>Co-Delivery system (2006)</p>  <p>Advantages</p> <ul style="list-style-type: none"> - Combination therapy - Improved therapy efficiency - Overcome MDR of drug - Reduced concentration threshold for individual drugs - Inhibit cellular anti-apoptotic pathways - achieves synergic therapeutic effects <p>Disadvantages</p> <ul style="list-style-type: none"> - coordinating the pharmacokinetics and cellular uptake of combined therapeutic can be difficult 	<p>Targeted system (1980)</p>  <p>Advantages</p> <ul style="list-style-type: none"> - Targeting specific receptors overexpressed - Reduced side effects - Enhanced specific cellular uptake <p>Co-Delivery system (2006)</p>  <p>Advantages</p> <ul style="list-style-type: none"> - Combination therapy - Improved therapy efficiency - Overcome MDR of drug - Reduced concentration threshold for individual drugs - Inhibit cellular anti-apoptotic pathways - achieves synergic therapeutic effects <p>Disadvantages</p> <ul style="list-style-type: none"> - coordinating the pharmacokinetics and cellular uptake of combined therapeutic can be difficult

Figure 1-8. Different types of organic delivery system including their advantages and disadvantages (Immordino, Dosio and Cattel, 2006; Liu et al., 2017; peer et al., 2007).

Bulbake and colleagues in 2017 have reported 28 more products undergoing clinical in which 6 products are under clinical trial Phase III (Arikace, Stimuvax, T4N5 liposomal lotion, Liprostin, ThermoDox and Lipoplatin), 9 products in clinical Phase II (Aroplatin, Liposomal annamycin, SPI-077, OSI-211, S-CKD602, LE-SN38, LEP-ETU, Endotag-I and Atragen) and 13 products in clinical Phase I (LEM-ETU, Liposomal Grb-2, INX-0125, INX-0076, TKM-080301, Atu027, 2B3-101, MTL-CEBPA, ATI-1123, LiPlaCis, MCC-465, SGT-53, Alocrest). From all products, only two other Doxorubicin based liposomes are undergoing under clinical trials (Thermodox and MCC-465).

1.6.2. Albumin-based carriers

Albumin is an acidic and very soluble protein that is commercially obtained from egg white, bovine serum, human serum, soybeans, milk and grains (Arshady, 1989; Elzoghby, Samy and Elgindy, 2018). Albumin has been used as a drug carrier since it is biodegradable, non-toxic, easily prepared and reproducible (Elzoghby, Samy and Elgindy, 2018). The primary structure of albumin consists of charged amino acids, which can easily interact with charged molecules. It also has some hydrophobic binding domains which can interact with hydrophobic drugs (example of Abraxane® consisting of albumin and hydrophobic drug paclitaxel). Albumin-based nanoparticles are of smaller size (50 to 300nm), higher half-life in blood circulation (great solubility properties), better-controlled release properties, multiple ligand binding sites and high cellular interactions compared to liposomes (Khodabandehloo, Zahednasab and Ashrafi Hafez, 2016; Elzoghby, Samy and Elgindy, 2018). Aldoxorubicin (clinical trial phase I) is a prodrug of doxorubicin that contains an acid sensitive hydrazine moiety, a 6-carbon spacer and a thiol binding maleimide. The prodrug

is administrated intravenously, and when it reaches the bloodstream, the linker molecule binds covalently (within 5min) to the cysteine-34 amino acid of endogenous albumin. The bound albumin-doxorubicin then accumulates in tumour via EPR effect and the drug is released in the acidic environment of the tumour cells (Kratz et al., 2002; Mita et al., 2014).

1.6.3. Amphiphilic block copolymer/ Polymeric based nanocarriers/micelles

Polymeric carriers for the delivery of Doxorubicin have been studied. These consist of the use of natural or synthetic polysaccharide such as poly(d,l-*lactide*) (Margarida Cardoso et al., 2016), poly(lactic acid) PLA, poly(d,l-glycolide) PLG (Eisenbrey et al., 2010), poly(lactide-co-glycolide), PLGA (Tewes et al., 2007), and poly(cyanoacrylate) PCA, Pullulan (Lu et al., 2009), Hyaluronic acid (Cho et al., 2012), Heparin (She et al., 2013), alginic Acid (Cai, Ni and Zhang, 2012), Dextran, chitosan (Bisht and Maitra, 2009), sodium alginate (KITAZAWA et al., 1997) and other hydrophilic/biodegradable polymers. These polysaccharides have attracted the most attention because they are non-toxic, non-immunogenic, biocompatible, biodegradable and renewable (Akhlaghi et al., 2013; Hassani et al., 2012). Moreover, they have a wide range of molecular weight and a large number of reactive groups (-COOH, -NH₂, -OH,...) which permit their modification to various amphiphilic derivatives. The polysaccharide is usually considered as a backbone in which either a drug can be directly chemically linked by a simple ester or amide bond which can then be hydrolysed in VIVO. Alternatively, the hydrophilic polysaccharide can be modified by addition of hydrophobic complexes to form micelles that can load hydrophobic drugs. Current hydrophobic moieties involved in creating

amphiphilic polysaccharides derivatives that undergo self-assembly in aqueous solutions include linear molecules such as long-chain fatty acids (Nichifor et al., 2014; Pramod et al., 2012), poly(ϵ -caprolactone) (Chandel et al., 2016; Gu et al., 2014), cyclic molecules such as cholesterol (Kawasaki et al., 2016; Takahashi et al., 2011), bile acids (Li et al., 2012), doxorubicin (Cao et al., 2010; Xu et al., 2015), polyacrylate family such as Poly(methyl methacrylate) (Dupayage et al., 2011; Dupayage et al., 2008) and poly(isobutyl cyanoacrylate) (Bravo-Osuna et al., 2007; Wang et al., 2011). The stability and polarity of amphiphilic polysaccharides-based nanostructures are closely related to the structural characteristics of amphiphiles, such as hydrophobicity and intra/intermolecular interactions (Aschenbrenner et al., 2013). The overall polymeric carriers can be structured in many ways as seen in Figure 1-9.

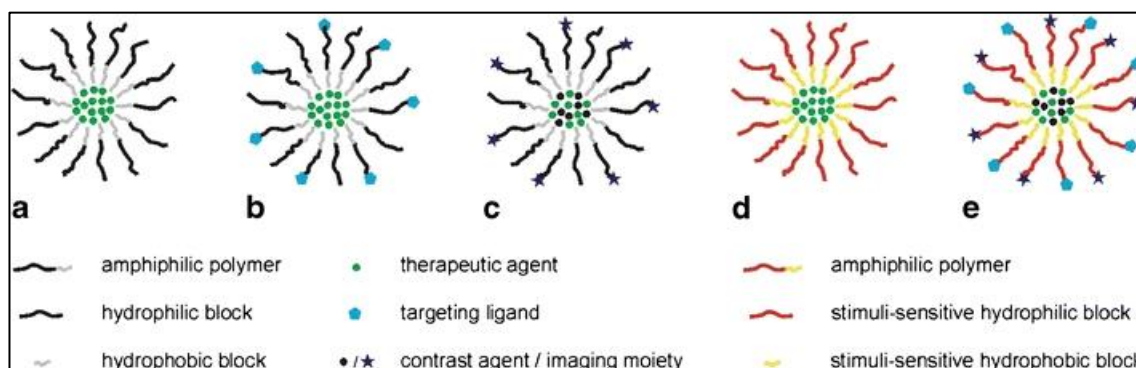


Figure 1-9. Schematic view of diverse types of polymeric carriers. Polymeric micelle (a). Micelle conjugated with a targeting ligand (b). A micelle containing an incorporated contrast agent or chelated imaging moieties (c). Micelle modified for triggered drug release (d). Either the hydrophilic or hydrophobic polymer can be rendered thermo/pH/light/ultrasound sensitive. Optimized micelle for anticancer therapy, bearing targeting ligands, contrast agents or imaging moieties, therapeutic drugs and polymers suitable for triggered, controlled release (e)(Oerlemans et al., 2010).

Bobo and colleagues reviewed in 2016 all the FDA approved nanomaterials. They reported 16 FDA approved polymeric based nanoparticles. Copaxone® (approved in 1996) and Neulasta® (approved in 2002) being the bestselling polymeric drugs in the USA are used for the treatment of multiple sclerosis and

chemotherapy-induced neutropenia, respectively. In 2014-2015, two new PEGylated drugs PLEGRIDY® and ADYNOVATE were approved for the treatment of relapsing multiple sclerosis and haemophilia A, respectively. Whereas only one FDA approved micelle (Estrasorb™) has been approved to date.

Overall, polymeric carriers have shown to be more effective compared to liposomes for the delivery of hydrophobic drugs since their size range is much smaller, they can be easily modified by the addition of hydrophobic blocks which increases the loading efficiency of hydrophobic drugs.

1.6.4. Dendron based nanocarriers / Dendronised polymers

Dendrimers are new macromolecules that are classed as polymeric materials. They present various advantages over traditional linear polymers. The name comes from the word Dendron which means tree. They behave with excellent amplification effects, precise nanostructure, water solubility, multivalency, high degree of branching, and highly adaptable surface chemistry, as well as controllable molecular size, mainly due to the unique radiate dendritic structures, low polydispersity and the amplification effect, which can be harnessed for providing large void space within the hydrophobic inner core. Generally, dendrimers involving well-defined molecular structures allow multivalency in a turnable way upon selecting the peripheral chemical groups and the generation properly (Majoinen et al., 2014; Roglin et al., 2011; Rosen et al., 2009; Nanjwade et al., 2009). Most importantly, compared to all others delivery systems, dendrimers are present in the smallest range of size (1-10nm) which is convenient when conjugated to polymers for example (Bhokare et al., 2016).

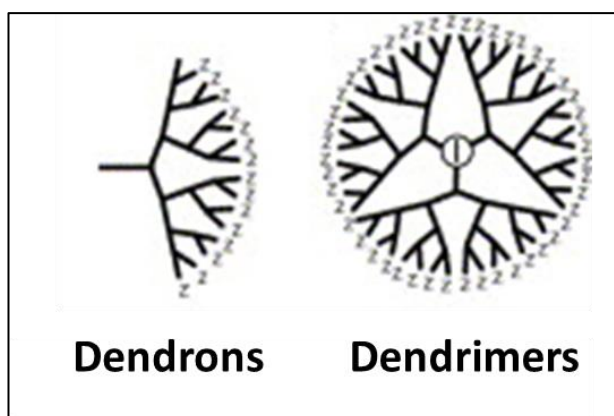


Figure 1-10. Schematic overview of dendrons and dendrimers.

Dendrimers are widely being studied as therapeutic agents for the drug, gene and vaccine delivery (Araújo et al., 2018). Dendrimers were first synthesised in the 1980s (Tomalia et al., 1985). Polyamidoamines (PANAMs) also called starburst dendrimers are the most widely used dendrimers (Malik, Evagorou and Duncan, 1999; Choudhary et al., 2017). It is known that higher generation dendrimers have higher loading capability due to more space available and surface groups to encapsulate hydrophobic drugs. Ammonia core PANAM of generations 3,4 and 5 are approximately the same size and shape as insulin (3 nm), cytochrome C (4 nm), and haemoglobin (5.5 nm), respectively (Svenson and Tomalia, 2012). PANAM dendrimers have been investigated for oral drug delivery; they have demonstrated to be able to permeate across epithelial barriers by a combination of transcellular and paracellular routes and can transiently open tight junctions (Jevprasesphant et al., 2004; Noriega-Luna et al.; 2014). Also, PANAM dendrimers have demonstrated to increase the aqueous solubility of poor drugs. For example, in 2004, D'Emanuele and colleagues have carried a study showing that PANAM dendrimers of third generation can increase the solubility of propranolol and bypass P-gp-mediated secretory efflux, thereby increasing its absorptive drug transport.

Moreover, PANAM of fifth generation has demonstrated to be able to prolong the delivery of the poor soluble non-steroidal anti-inflammatory drug “Ketoprofen” with a sustained release behaviour in vitro and in vivo (Na et al., 2006). PANAM have also been used to carry other drugs such as cisplatin, silver salts in which slow release was observed (Malik, Evagorou and Duncan, 1999; Balogh et al., 2001). Many other dendrimers have been studied and covalently conjugated into polymers to form supramolecular amphiphilic dendritic block copolymers that can self-assemble into various shape (micelles) for gene and drug anticancer therapy. Amphiphilic Poly (Lysine) Dendrons as an example have been synthesised for their use in several biomedical application and as carriers for drug and gene delivery. Janiszewska et al. in 2016 found that poly (Lysine) Dendrons can inhibit the proliferation of two glioblastoma cell lines by mitochondrial depolarization and reactive oxygen species production while being nontoxic to normal cells like neurons and glia. The incorporation of charged amino acids such arginine and lysine in PANAM dendrimers have been proposed by several articles to improve their interaction with genes (Choi et al., 2004; Kim et al., 2006; Márquez-Miranda et al., 2015). However, Choi et al. in 2004 report the better transfection efficiency of PANAM-Arginine compared to PANAM-Lysine.

Moreover, Padilla De Jesús and colleagues in 2002 demonstrated that Dox covalently bound via a hydrazone linkage to a high molecular weight 3-arm poly (ethylene oxide)-dendrimer hybrid is rapidly released at pH<6 into several cancer cell lines with significantly reduced cytotoxicity of doxorubicin (80–98%).

Although dendrons are great new carriers systems; they have still been reported to be toxic, similarly to other cationic macromolecules such as

liposomes and micelles, positively charged dendrimers are prone to destabilise cell membranes and cause cell lysis. PEGylation of dendrons have shown to reduce their cytotoxicity, for example, Bhadra and colleagues in 2013 reported that G4 PAMAM dendrimers with carboxymethyl PEG5000 surface chains could load reasonable amount of drug 5-fluorouracil with a reduced release rate and hemolytic toxicity compared to the non-PEGylated dendrimer.

In comparison, anionic dendrimers possessing carboxylate surface groups show neither haematotoxicity nor cytotoxicity at concentrations up to 2 mg/ml (Malik et al., 2000). To overcome the drawback of dendrimers, new modifications with neutral hydroxyl, acetyl or negatively charged carboxyl groups are being conducted. Also, the conjugation of the amine-based dendron into polymers can permit their self-assembly into nanoparticles where dendrons are hidden in the interior, and a safe polymer is on the surface.

1.6.5.Co-delivery system

Sometimes single treatment is not enough to achieve a therapeutic effect on cancer therapy (Mokhtari et al., 2017). Combinational cancer therapy, therefore, comes into place in which multiple anticancer drugs are simultaneously administered to enhance efficacy via synergistic effects, prevent adverse side effects and overcome drug resistance over monotherapy. Many types of research have shown that the co-delivery of 2 drugs (Qi et al., 2017) or drug/gene (Yang et al., 2015) or drug/other chemotherapeutic agents utilising nanocarriers is more efficient in cancer treatment compared to single chemotherapy (Mokhtari et al., 2017). In 2006, Yang's group first designed a co-delivery system to deliver an anticancer drug and a therapeutic gene to the same cells simultaneously for anticancer therapy. Co-delivery systems have

been developed for different strategies including overcoming the membrane transport protein related pump resistance (siRNA against genes encoding efflux pump proteins has been used to sensitize cells to chemotherapeutic drugs) (Fowers and Kopeček,2012), inhibiting the cellular anti-apoptotic pathways that can be activated to increase drug resistance (the use of BCL-2 protein family can inhibit the release of cytochrome C from the mitochondrion, which is required to trigger the caspase cascade during apoptosis) (Pakunlu et al., 2004) and lastly for synergetic therapeutic effect where 2 agents possessing different curative mechanisms are used for further therapeutic enhancement (Yang et al., 2015). However, many challenges have yet remained associated with the codelivery approaches including loading capacity, stability, release kinetics, biocompatibility and tumour targeting efficacy. Three formulations co-encapsulating dual chemotherapeutic drugs are being investigated in clinical trials for combination cancer treatment. One is the liposome co-loaded with cytarabine and daunorubicin (CPX-351 or Vyxeos) for the treatment of acute myeloid leukaemia in Phase III trials (Murphy and Yee, 2017). The other is the liposome co-loaded with irinotecan (CPT-11) and floxuridine (CPX-1) for the treatment of advanced colorectal cancer in Phase II trials (Chen et al., 2012). The third is a combination gene therapy using lipid nanoparticle-formulated small interfering RNAs (siRNAs) targeting vascular endothelial growth factor (VEGF) and kinesin spindle protein for the treatment of advanced cancers and liver metastases which demonstrated enhanced efficacy in Phase I trials (Shen et al., 2017).

1.7. Aim and Objective

The hardship of cancer is continuously increasing and is rapidly spreading globally. The anthracycline Doxorubicin is a potent chemotherapeutic drug which has been used to treat numerous cancers (Thorn et al., 2011). However, Dox present several side effects in major organs including acute cardiotoxicity and also develops drug resistance, which limits its dosage (Rahman, Yusuf and Ewer, 2007). This is a factor that makes Dox an essential subject to study and to improve its efficiency by developing a drug-loaded nanotechnological product. Doxorubicin.HCl was the first anticancer drug that was encapsulated into a carrier and received clinical approval against malignancies including solid tumours (Sercombe et al., 2015). Despite the existence of numerous studies focused on the encapsulation and controlled/targeted delivery of Dox by different nanocarriers, only a few have achieved to reduce the negative effects of the given devices (Malam, Loizidou and Seifalian, 2009; Vinothini et al., 2019). We propose here, different development of safer and more specific non-viral vector systems for the delivery of the Dox in liver cancer cells and brain tumour. The liver is the largest organ and plays major roles of the body function, therefore bears the most mutagenic phenomena which cause clinical disorders that have been attractive targets for liver-specific gene and drug therapy (Mishra et al., 2013). Hepatocytes are the principal parenchymal cells of the liver and mostly present errors of metabolism resulting in haemophilia and acquired diseases such as liver cancer and hepatitis. Therefore, targeting these cells with accuracy and precision without any side effects has been the goal of our research. Pullulan being a very neutral, natural polysaccharide, non-toxic, non-immunogenic, non-carcinogenic and most importantly a ligand for ASGPr (Farris, 2014; Yamaoka, Tabata and Ikada, 1993; Yamaoka, Tabata and Ikada,

1995; kaneo, 2001) is chosen as the shielding material in which arginine dendrons of hydrophobic and cationic surface chemistry are conjugated.

This work was therefore designed to meet the following objectives:

- ❖ To successfully synthesise and characterise four different drug delivery systems consisting of dendrons and pullulan with or without targeting ligand or with and without a responsive linkage:
 - Successfully synthesise hydrophobic and cationic peptide dendrons of the third generation
 - Successfully modify the polymer Pullulan
 - Successfully click dendrons into polymers
 - Successfully form micelles and load Doxorubicin or curcumin
 - Successfully characterise the micelles by size and morphology
- ❖ To examine the release studies of Doxorubicin or curcumin from each system
- ❖ To test the cytotoxic effect of each system in HepG2, U251, Hek293 or 3T3 cells
- ❖ To study the internalisation of these carriers into HepG2 cells

CHAPTER 2. MATERIALS AND METHOD

2.1. Materials

It is important to note that this work was carried out in different universities. Therefore, the chemicals and instruments were ordered from different locations: Sichuan University and the University of Wolverhampton, whereas other devices were obtained from the University of Birmingham.

2.1.1. Materials for chemical synthesis and characterisation

2.1.1.1. Glassware and equipment for synthesis

Beakers (100, 500, 1000 and 2000mL), a 250mL reagent bottle; 500, 1000 and 2000mL conical flasks; microscope slides; retort stands and clamps (Beijing Synthware Glass Co.Ltd, A3-806, Yingte Mansion, Xibahe, Chaoyang District, Beijing, Beijing, 100028, China).

150mm x 75mm crystallizing dish for the oil bath; glass desiccators with porcelain plates; 1000 and 2500mL vacuum filtering flasks with sidearm; 100, 500, 1000 and 2000mL measuring cylinders and 1000 and 2000mL separatory funnels (Sichuan Shubo (group) co. Ltd, no.125, South Shuzhu Road, Chongzhou City, Sichuan Province, 611230, China).

Rotary vacuum evaporator; high temperature drying oven; hot plate magnetic stirrer; lab 0.1mg analytical balance; UV viewing cabinet (Zhengzhou Nanbei Instrument Equipment Co. Ltd, no.72, Beihuan Road, Zhen, China).

100, 250 and 500 mL joint 24/40 round bottom single neck reaction flask with glass stopcock; 24/40 septum rubber stoppers; 12-60mm pivot ring, oval and micro stir bar set; 10, 15, 20cm spoons and spatulas; disposable syringes;

tweezers and needles; TLC spotting capillary tubes; 500 and 1000 mL-50mm chromatography columns with reservoirs and fitted disc; 40, 53 and 73mm Buchner funnel high vacuum pump; recirculating water vacuum pumps (Thomas Scientific, 1654, High Hill Road, Swedesboro, NJ 08085, USA).

MWCO 100-500, 1000 and 3500 Da regenerated cellulose dialysis membranes and clamps (Spectrum/Por, Spectrum Chromatography, 18211, Chisholm Tr Ste 300, Houston, TX 77060, USA).

Reagent grade column chromatography silica gel 200-300 mesh (Yucheng Chemical Co. Ltd, 3f/Building 5, No.3521, Chuanzhou Highway, Pudong District, 201319, Shanghai, China).

Silica quartz sand (CNPC Powder Group co. Ltd, Room 1211, No.8 Office building, Wanda Plaza, 58 He Xuan Road, 201803, Shanghai, China).

High-pressure nitrogen and argon gas cylinder (Shanghai Eternal Faith Industry Co., Ltd, No.6598, Hutai Road Baoshan, 201908, Shanghai, China).

Thermostatic shaking water bath (Biobase Biodustry Co., Ltd. No. 51 South Gongye Road, Jinan, 250101, Shandong, China).

Freeze dryer lyophilizer (Guangzhou Aolantec Commerce And Trade Co., Ltd., 702, Unit 2, Bldg. 5, Dingxiu Qingxi, Changping Dist., Beijing, China).

Christ Beta 1-8 -55 °C LSCbasic & 2-8 -85 °C LSCbasic 8kg freeze dryers (SciQuip LTD, Newtown, Wem, Shropshire, SY4 5NU UK).

NexION 2000 ICP mass spectrometer and Fourier transform infrared (3F, Tower 6, Huidu Headquarters Garden, No.5 Xixin Avenue, High-tech West District, 611730, Chengdu, China).

Fourier transform infrared (Perkin Elmer Life and Analytical Sciences, Wenlock Business Centre 50-52 Wharf Road, London N1 7EU, United Kingdom).

Tecnai G² F20 S-Twin HR (S) electron microscope with a voltage of 200kV (FEI Company, USA).

Malvern: Zetasizer Nano ZSP (Malvern Panalytical, a division of Spectris Instrumentation & Systems Shanghai Ltd, F909, Ruida Plaza, No. 74, Lu Gu Road, Shijingshan District, 100040, Beijing, China).

Advanced 400 nuclear magnetic resonance spectrometer (Bruker, 1711 Floor 17th, Tianyin Mansion, Zhongshan Road No. 437, Tianhe District, Guangzhou 510660, China).

Fluorescence spectrophotometer F-7100 (Hitachi High-Technologies Co., Ltd, 21F Hang Seng Bank Tower, 1000, Lujiazui Ring Road, Pudong New Area, Shanghai, China).

Zeiss® Evo 50 scanning electron microscope (Carl Zeiss AG Carl-Zeiss-strabe, 22, Oberkochen, 73447, Germany).

2.1.1.2. Chemicals for synthesis

Propargylamine, 55.08g/mol (J&K Scientific Ltd, 5/F, Building-A, TopBox, No.69 Bei Chen West Road, Chaoyang District Beijing, 100029, China).

Boc-L-Arg(Pbf)-OH, 526.65g/mol; Boc-L-Lys(Boc)-OH, 346.42g/mol; N-(3-dimethylaminopropyl)-N'-ethylcarbodiimidehydrochloride (EDC.HCl), 191.70g/mol; 1-hydroxybenzotriazole hydrate (HOBT), 135.12g/mol and O-Benzotriazole-N,N,N',N'-tetramethyl-uro-nium-hexafluorophosphate (HBTU),

379.24g/mol (GL Biochem Ltd, 519 Zi Yue Road, Shanghai, 200241, Shanghai, China).

Sodium azide (NaN_3), 65.01g/mol; triphenylphosphine (PPh_3), 262.29g/mol; tetrabromomethane (CBr_4), 331.63g/mol; 4-(Dimethylamino) pyridine (DMAP), 122.17g/mol; copper sulphate pentahydrate ($\text{CuSO}_4 \cdot 5\text{H}_2\text{O}$), 249.69g/mol; sodium ascorbate (SA), 198.11g/mol; pullulan (MW20,000Da), triethylamine (TEA), 101.19g/mol; ethylenediaminetetraacetic acid disodium salt ($\text{EDTA} \cdot 2\text{Na}$), 372.24g/mol and lactobionic acid, 358.30g/mol, Dicyclohexylcarbodiimide, 206.33g/mol (Shanghai Aladdin Bio-Chem Technology Co. Ltd, 5th Floor, Building 12, No 1001, North Qingzhou Road, Xuhui District, Shanghai, China).

Trifluoroacetic acid (TFA), 114.02g/mol; N,N-diisopropylethylamine (DIEA), 129.25g/mol; sodium chloride (NaCl), 58.4g/mol; hydrochloric acid (HCl), 36.46g/mol; anhydrous magnesium sulphate (MgSO_4), 120.37g/mol and sodium bicarbonate (NaHCO_3), 84.01g/mol (AstaTech BioPharmaceuticalcorp., 488, West Kelin Road, Wenjiang Dist, 611130, Chengdu, China).

Monopotassium phosphate, KH_2PO_4 , 136.086g/mol; Sodium phosphate dibasic dodecahydrate ($\text{Na}_2\text{HPO}_4 \cdot 12\text{H}_2\text{O}$), 358.14g/mol; ninhydrin, 178.14g/mol; 3,3'-Dithiodipropionic acid, 210.27g/mol; Pyrene, 202.25g/mol; 1H-Pyrazole-1-carboxamide hydrochloride, 146.58g/mol; DL-Dithiothreitol, 154.25g/mol and all solvents with the highest grade including ethanol, methyl sulfoxide, dimethylformamide, chloroform, acetone, petroleum, ethyl acetate, methanol (Sigma Aldrich Chemical GmbH, Sigma Aldrich Inc, 3050 Spruce Street, St Louis M063103, USA).

Curcumin, 368.39g/mol (Alfa Easer, Shore Road, Port of Heysham Industrial Park, Lancashire, LA3 2XY, Heysham, Lancashire, United Kingdom).

Doxorubicin hydrochloride (Dox.HCl), 579.98g/mol (Zhejiang Hisun Pharmaceutical co. Ltd, no 46, Waisha Road, Jiaojiang District, 318000, Taizhou, China).

Doxorubicin hydrochloride (Dox.HCl), 579.98g/mol (Alfa Easer, Shore Road, Port of Heysham Industrial Park, Lancashire, LA3 2XY, Heysham, Lancashire, United Kingdom).

2.1.2. Materials for in vitro cell studies

2.1.2.1. Glassware and Equipment for cells studies

Polystyrene tubes (10, 25, 50 and 100 mL), 6-well, 24 well and 96-well flat-bottom tissue culture plates with lids, tissue culture cell+ flasks with PE ventilation caps (T25, T75, T175), Filtropur V50.0.2 vacuum filter (500 mL), 1.5mL and 0.5mL Eppendorf tubes, sterile disposable pipettes (5mL, 10mL, 25mL) (Sarstedt Ltd., 68 Boston Rd, Leicestershire, LE4 1AW, Leicester, UK).

Micropipettes–Biopette™, autoclavable pipettes (Labnet International Inc., USA) and Pipetman™ autoclavable pipettes (Gilson Inc., 3b Humphrys Road, Woodside Estate, Dunstable LU5 4TP, Luton, UK).

Micropipette tip refill cartridges (1mL and 200µL) and nuclease-free filtered tips (1mL, 10µL, 40µL and 200µL) (Alpha Laboratories, 40 Parham Drive, Hampshire, SO50 4NU, Eastleigh, United Kingdom).

AmScope pre-cleaned microscope slides and square cover glass (22x22mm) (AmScope).

Hausser Scientific™ Phase Contrast Hemacytometer (Fisher Scientific, Bishop Meadow Road, Loughborough, LE11 5RG, UK).

Clean air laminar flow hood (Telstar, Netherlands).

Olympus Microscope CK2-TR (Olympus, KeyMed House, Stock Road, Southend-on-Sea, SS2 5QH, UK).

MSE Mistral 2000 centrifuge (DJB Labcare Ltd, 20 Howard Way, Interchange Business Park, Newport Pagnell, Buckinghamshire, MK16 9QS, England).

Panasonic Direct Heat CO2 incubator (Panasonic Healthcare Co. Ltd., 1-1-1 Sakata, Oizumi-Machi Ora-Gun, Gunma 370-0596 Japan).

Mettler Toledo™ FiveEasy™ Plus FP20 pH/mV meters (Fisher Scientific, Bishop Meadow Road, Loughborough, LE11 5RG, UK).

Zeiss LSM 880 Confocal Microscope (Carl Zeiss Ltd., 509 Coldhams Lane, Cambridge, Cambridgeshire, CB1 3JS, UK).

BD FACSCalibur™ Flow Cytometer, CellQuest™ Pro, Cell wash, FACS Clean, FACS Rinse, BD Falcon FACS tubes (Becton Dickinson (BD), The Danby Building, Edmund Halley Road, Oxford Science Park, Oxford OX4 4DQ, UK).

GloMax®-Multi Detection System (Promega GLO Reagents, 2800 Woods Hollow Road, Madison, WI 53711-5399, USA).

2.1.2.2. Chemicals and reagents for cell studies

Fetal bovine serum (FBS), F9665; Minimum Essential Medium Eagle (powder); M0268; Trypsin-EDTA solution, T4049; MEM non-essential amino acid solution (100×), M7145; antibiotic-antimycotic solution (100×), stabilised A5955;

Sulforhodamine B, 230162; Tris–Trizma base, T6066 – 1kg; trichloroacetic acid, T6399-1KG, phosphate buffered saline tablets, 79382, DAPI, D9542 (Sigma Aldrich Chemical GmbH, Sigma Aldrich Inc., 3050 Spruce Street, St Louis, M063103, USA).

Acetic Acid Glacial, 100% pure (GPR™ BDH laboratories supplies, Poole, BH15 1TD, England).

Dulbecco's modified Eagle's medium with high glucose (DMEM-HG) (Life Technologies Corporation, Gibco®, USA).

A cell-counting kit-8 (CCK-8) (Dojindo Laboratories, Asakawa Bldg, 7F Shibadaimon 2-1-17 Minato-ku, 105-0012, Tokyo, Japan).

FITC Annexin V Apoptosis Detection Kit II (Becton Dickinson (BD), The Danby Building, Edmund Halley Road, Oxford Science Park, Oxford OX4 4DQ, UK).

2.1.3. Cell lines

Human liver hepatocellular carcinoma cell line (HepG2), mouse embryonic fibroblast cell line (NIH3T3) (Shanghai Institute for Biological Sciences, 320 Yueyang Road, 200031, Shanghai, China).

Human glioblastoma cell line: U251MG and NIH3T3 (Dr Tracy Warr, BTUK neurooncology lab, University of Wolverhampton, UK).

Human liver hepatocellular carcinoma cell line (HepG2), 85011430-1VL (Sigma Aldrich, UK).

Human embryonic kidney cells (Hek293), (Sigma Aldrich, UK).

2.1.4. Buffers and solutions

All solutions and buffers were prepared in MilliQ ultrapure water and filtered (0.22 µm) before use.

❖ PBS buffer of pH 5, 6.8 and 7.4

1/15M of KH_2PO_4 and $\text{Na}_2\text{HPO}_4 \cdot 12\text{H}_2\text{O}$ Stock solutions: 9.07g of KH_2PO_4 in 1L water and 23.86g of $\text{Na}_2\text{HPO}_4 \cdot 12\text{H}_2\text{O}$ in 1L water.

Table 2-1. Preparation of pH 5, 6.8 and 7.4 PBS buffers

pH/ Vol [KH_2PO_4] or [$\text{Na}_2\text{HPO}_4 \cdot 12\text{H}_2\text{O}$]	1/15 M of KH_2PO_4	1/15 M of $\text{Na}_2\text{HPO}_4 \cdot 12\text{H}_2\text{O}$
pH 5	10 mL	990 mL
pH 6.8	50 mL	50 mL
pH 7.4	20 mL	80 mL

❖ **Ninhydrin solution:** 1g of ninhydrin powder in 200ml of ethanol (stored at RT).

❖ 1L of pH 7.4 Sterile culture media solution

Under stirring conditions in a 2000ml beaker:

- 9.5g of MEM powder was dissolved in 1000ml of autoclaved water giving a yellowish colour.

- 2.2.g of NaHCO_3 was then added to the mixture giving a red colour. pH adjusted to 7.2-7.3.

Under sterile conditions in a clean air laminar flow hood:

- The red solution was filtrated into 2x500mL Filtropur V50.0.2 vacuum filters.

- In each bottle, 1% of non-essential amino acids (5mL), 1% antibiotics (5mL) and 10% FBS were added (50mL).
- Stored for three months at 4 °C.
- ❖ **Sterile PBS for tissue culture:** 1 tablet of PBS dissolved in 200ml of water (stored at RT).
- ❖ **Cell freezing solution:** FBS+10%(v/v) DMSO (stored at 0 °C).
- ❖ **DAPI Dilution:** 5µ l dissolved in 995ul of water (stored at 0 °C).
- ❖ **1% Acetic acid solution :**10mL acetic acid in 1000mL of water.
- ❖ **0.4% SRB solution:** 2g of SRB powder in 500mL of 1% acetic acid.
- ❖ **10mM Tris solution:** 1.2114g of Tris powder in 1000mL of water.
- ❖ **500mL of 10% TCA:** 50g TCA in 500mL water (stored at 4 °C).

2.2. Methods

2.2.1. Peptide dendron detection by thin layer chromatography

To monitor the course of the reaction, for successful peptide isolations and purification the most widely used qualitative separation technique ‘thin layer chromatography’ was used. This technique is a relatively cheap, highly sensitive and fast method that can be applied to a wide range of samples (Touchstone, 1992). Silica gel was used as the stationary phase and suitable vapour solvents (~10ml of ethyl acetate/petroleum and dichloromethane/methanol) were used as the mobile phase whereas UV light was used to identify any spots of impurities observed (circled around their outline using a pencil). TLC plates were passed into a beaker containing ninhydrin solution and then dried with a strong drier which developed coloured spots.

The Rf value was calculated by dividing the distance travelled by the compound from the origin (point of compound application) by the distance travelled by the solvent from the origin:

$$R_f = \frac{\text{Distance moved by spot}}{\text{Distance migrated by solvent}}$$

2.2.2. Peptides dendron purification

2.2.2.1. Acid and basic extraction to remove impurities

This is a method usually used after chemical synthesis to extract mostly free neutral acidic and basic impurities from the product. The volume of the washing phase is often one-tenth to one half of the volume of the organic phase, and it is best to repeat the wash two or three times. First, the product is dissolved into a solvent (50-500mg of product into 25-100mL of solvent) that is easily removed by a rotary evaporator (e.g. ether and chloroform), whereas solvents such as ethyl acetate or DCM are difficult to evaporate and often form nasty emulsions. The product undergoes an acid wash (12-50mL of HCl 10 %, stirred for 1h30min) that removes the amines and a basic wash with 12-50mL of NaHCO₃, HCl (1M) or 10% NaOH stirred for 1hr to remove unwanted acids and then transferred into a separatory funnel. Finally, the product undergoes a brine wash (12-50mL of saturated NaCl solution, stirred for 20-30min) which helps to disrupt emulsion and dries the organic layer by extracting the water.

Moreover, a drying agent (MgSO₄ or Na₂SO₄) is also added and left overnight to remove all traces of water which binds to water-forming clumps when they react (enough drying agent is added until floating-crystals forms). The drying agents

are removed by a standard filtration method using a Büchner funnel and unfluted filter paper (or a fritted funnel) under mild vacuum (Hauenschild and Hinderberger, 2019). The product is then concentrated by evaporating the solvent and dried using a vacuum pump to obtain a solid white product.

2.2.2.2. Column Chromatography

For the isolation of the pure product, column chromatography was used to enable separation of the product from the mixture. The same stationary and mobile phase were used as for TLC. First, into a 2000mL beaker, silica gel (200-300 mesh) powder was mixed with petroleum (PE) until a thick pourable solution was obtained. The mixture was then transferred into a 1000mL chromatography column using a funnel and PE was allowed to drain out (a pressure vacuum was used to accelerate the process) into a beaker. More silica gel was added until a suitable amount of gel was present in the column. PE was left a very little over the gel (0.5cm) to avoid any dryness and the tap at the end of the column was closed. The mixture product was dissolved in DCM and then carefully added into the column. The rest of the PE was left to drain out taking along with it the product until the silica gel appeared and then the tap was closed again. More PE was added followed by quartz sand, and it was left again to drain out. The mobile phase was finally added and allowed to drain out in single drops. TLC was used to monitor the product.

2.2.3. Characterisation of dendrons modified pullulan and conjugated products

2.2.3.1. Mass spectrometry (MS)

The masses of dendrons of generations 1, 2 and 3 were confirmed by mass spectrometry. The method is a specific analytical technique used to identify and

quantitate molecules based on their mass-to-charge (m/z) ratio. The mass spectrometer consists of an ion source, a mass analyser and an ion detector.

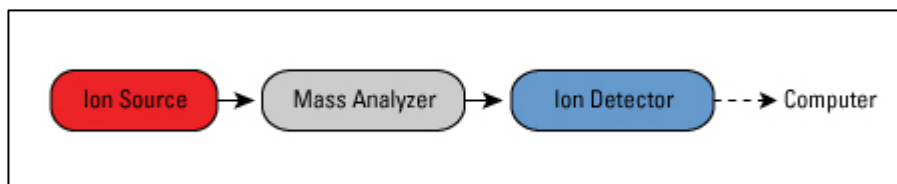


Figure 2-1. Schematic of the basic components of a mass spectrometer.

Each dendron products is loaded into the mass spectrometer in dried form (could also load in liquid or gas form). The product is evaporated and then leaked into the ionisation chamber where a beam of electrons bombards the samples which ionise the molecules (mainly positive ions are formed by the loss of valence electrons). A filament of the heated cathode produces the beam. The ions are then accelerated by an electrostatic of several hundred to thousands of volts before reaching the analyser. Ions separate in the mass analyser, and a magnetic field is applied perpendicular to the motional direction of the ions. The ions then move very quickly following a circular trajectory due to Lorentz acceleration, whose radius is determined by the mass/charge ratio of the ion and the strength of the magnetic field (Bagwell et al., 2017). The ions, therefore, hit the ion detector. A mass spectrum is obtained by a computer connected to the mass spectrometers with software that measures ion oscillation frequencies. The data analysis programs detections and produce a spectra whereby individual ions are presented according to their m/z values and relative abundance. For each dendron, databases of mass spectra were obtained, and the mass of each dendron molecule was confirmed based on its m/z value.

2.2.3.2. Fourier transform infrared spectrometry (FTIR)

FTIR is a technique that is used to analyse the absorption or emission of a solid, liquid or gas in the form of infrared spectrum. The analysis of individual spectra provides the identity of a chemical compound in the sample and was used here to confirm the structure of each product synthesised. A small amount of the sample was placed into the diamond stage of a Genesis II ATR FTIR (Attenuated Total Reflection Fourier Transform IR) instrument, and the probe was lowered down onto the sample. An infrared light passed through the sample, and the bonds between molecules in the sample get excited resulting in vibration due to electromagnetic radiation absorption ranging between 400cm^{-1} and 4000 cm^{-1} . The changes in vibrational energy in the IR region were recorded to generate spectral peaks. Normally, the infrared region of the electromagnetic spectrum ($10\text{--}14000\text{ cm}^{-1}$) is divided into three spectral sub-regions: near- ($4000\text{--}14000\text{ cm}^{-1}$), mid- ($400\text{--}4000\text{ cm}^{-1}$), and far-IR ($10\text{--}400\text{ cm}^{-1}$) (Türker-Kaya and Huck, 2017). The mid-IR region is the most common portion of the spectrum that has been used because characteristic absorbance frequencies and main molecular vibrations lie within this range. The bonds are, therefore, determined by the radiation wavelength absorbed (Witkowski and Koniorczyk, 2018; Watson, 2005; Larkin, 2011; Smith, 2011). Analysis of each sample was undertaken without the need for further sample preparations (Perkin Elmer Life and Analytical Sciences, 2005) and the spectrum was obtained using the WinFIRST software, which controls the FTIR spectrometer. The spectrum of each sample was then analysed by identifying the IR band positions, thereby confirming their chemical structure.

2.2.3.3. Elemental analysis (EA)

Elemental analysis is a simple technique that is used here to determine the degree of substitution of pullulan. This technique identifies and quantifies (typically in percentages) the elements present in a sample. The analytical method consists of complete and instantaneous oxidation of the sample by flash combustion which then converts all substances into combustion products. The samples experience a continuous flow of helium and are then dropped into a combustion reactor maintained at 900 °C. They are then separated and detected by a thermal conductivity detector which gives an output signal equivalent to the concentration of each elemental in the sample (Hemming, 2007; RSC.org, 2019). Analysis of carbon, hydrogen and nitrogen of the azidated product was carried out and the degree of azidation was determined by elemental analysis using the following formula:

$$DS = \frac{\frac{N(\%)}{3 \times 14}}{\frac{C(\%)}{6 \times 12}}$$

Figure 2-2. The formula for determining the degree of azidation.

2.2.3.4. Proton nuclear magnetic resonance (¹H NMR)

NMR is a powerful technique used together with FTIR to provide information about the molecular structure and purity of compounds. This technique was first used in 1946 (Webb, 2014; Becker, 1993) and its spectra have been in use within the field of organic chemistry since 1960. ¹H NMR is the most common NMR used because the proton nucleus is the most sensitive and usually yields

sharp signals (Zangger, 2015). Hydrogen nuclei can behave like a little magnet and spin when an external magnetic field is applied; energy is transferred to a higher level at a wavelength that correlates with radio frequencies whereas when the nucleus relaxes back, the energy is released at the same frequency (Callaghan, 1993). All the dendron structures (generation 1, 2 and 3 dendrons) were confirmed with ^1H NMR (400 MHz) using a Bruker avance 400 nuclear magnetic resonance spectrometer. Dried samples were dissolved in CDCl_3 before measurement. The use of NMR spectroscopy to characterise modified polysaccharides has also been widely used (Cheng and Neiss, 2012). All the clicked products and guanidilated products were confirmed using ^1H NMR spectrum analysis (samples were first dissolved in DMSO), and the percentage of lactose conjugated was determined using the following formula:

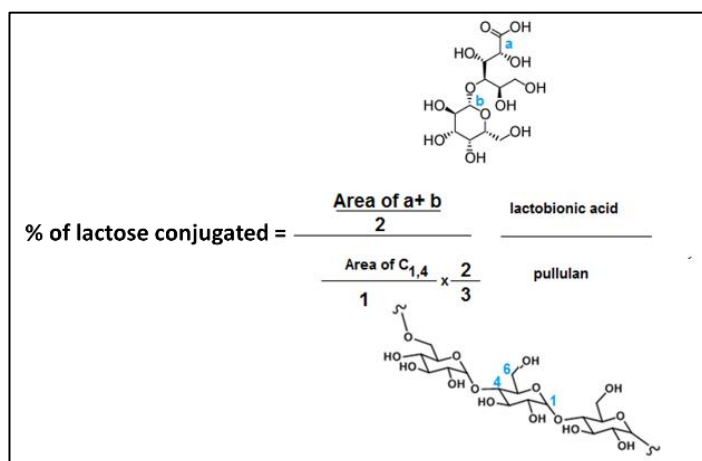


Figure 2-3. Formula for determining the percentage of lactose conjugated into pullulan.

2.2.4. Micelles formation by diafiltration

The formation of nanoparticles and drug loading was performed according to the method known as diafiltration (Ma et al., 2015).

2.2.4.1. Preparation of blank P-PLLA, P(lac)-PLLA and PSS-PLLA micelles

The blank nanoparticles of P-PLLA, P(Lac)-PLLA and PSS-PLLA were prepared by dissolving 5mg of each product in 1mL of DMSO and added dropwise into 5 mL of deionised water under vigorous stirring. The solution was stirred for 1hr and then transferred into a pre-swollen dialysis membrane (MWCO 3500 Da) and dialysed against deionised water at 4 °C for 12 hours. The outer water was replaced with fresh deionised water at 0.30, 1, 2, 3 ,5.30 hrs. The products were then analysed or freeze dried and stored at 4 °C.

2.2.4.2. Drug loading into micelles

2.2.4.2.1. Preparation of hydrophobic doxorubicin by the removal of HCl

2mg of Dox.HCl was first dissolved in 1ml of deionised water at 0 °C in the dark. Every 10 min, 50µl, 20µl, 10µl, 5 µl of 0.01M NaOH (200 µl prepared in total) was added to the stirring Dox.HCl solution. When 100µl was used, the sample was centrifuged at 2500 rpm for 20min and traces of solid Dox were observed with a darker reddish colour. The pellet was then collected and freeze dried to obtain a dry product.

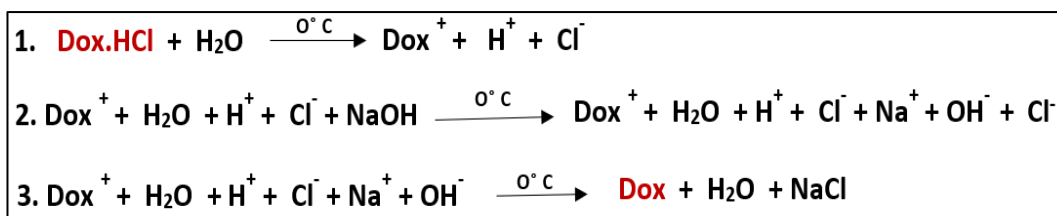


Figure 2-4. The schematic reaction of the conversion of hydrophilic doxorubicin (Dox.HCl) into hydrophobic doxorubicin (Dox) by the removal of HCl with NaOH.

2.2.4.2.2. Doxorubicin loading into P-PLLA, P(lac)-PLLA and PSS-PLLA micelles

For the preparation of drug-loaded nanoparticles, solutions of P-PLLA, P(lac)-PLLA and PSS-PLLA in DMSO (1.25, 0.5 and 0.25mg in 500 μ L) were separately mixed with 0.25mg hydrophobic doxorubicin in DMSO. The resulted mixture was then added dropwise into 5 mL of deionised water under stirring and then dialysed against water for 24 hrs at 4 $^{\circ}$ C in the dark to remove unloaded drug (6 changes of water/day). MWCO 3500 Da dialysis membrane was used, and the resultant solution was then freeze dried. The loading content of Dox was calculated by fluorescence measurement (F-7000, excitation at 480 nm) in DMSO according to the calibration curve obtained from Dox/DMSO solutions with different Dox concentrations (1,2,3,4,5 and 6 μ g/mL). Drug loading content (LC) and encapsulation efficiency (EE) were calculated using the following equations:

$$\text{LC (\%)} = (\text{weight of loaded drug/weight of drug-loaded micelle}) \times 100\%$$

$$\text{EE (\%)} = (\text{weight of loaded drug/weight of drug in feeding}) \times 100\%$$

2.2.4.2.3. Curcumin and Cur-Dox loading into PSS-PLLA

1mg of curcumin and 5mg of PSS-PLLA were dissolved in 1mL of acetone under sonication. The solution was then added dropwise into 9mL of deionised water and stirred for 4 hrs. The nanoparticles were collected by centrifuging the solution at 20000rpm for 1hr and then washed with ethanol to remove the unloaded curcumin. The nanoparticles were then lyophilised and stored at 4 $^{\circ}$ C (Kumari et al., 2017; Sanoj Rejinold et al., 2011). The wavelength of curcumin was determined using a wavescan of curcumin solution in ethanol by UV spectrometer (highest concentration was 0.0132mg/mL, whereas the lowest

concentration was 0.0005mg/mL). Similarly, to Dox, the loading content of curcumin was calculated by fluorescence measurement (F-7000, excitation at 438 nm) in DMSO according to the calibration curve obtained from Cur/DMSO solutions with different curcumin concentrations (0.4, 0.8, 1.7, 3.3, 6.6 and 13.2 µg/mL).

2.2.5. Nanoparticle characterisation regarding size, polydispersity index and morphology

2.2.5.1. Dynamic light scattering

The determination of nanoparticle sizes is very important when characterising nanoparticles. This is achieved using dynamic light scattering which is a technique that measures the intensity of laser light when scattered by molecules in solution. 1mg of P-PLLA, PSS-PLLA, P(lac)-PLLA, P-PLLL or OGPLLL were dissolved in 20µl of DMSO and then added dropwise under sonication into 980µl of deionised water (1mg/mL in triplicate). The samples were then filtered with a 5µm filter into cuvettes and characterised using the Malvern Zetasizer Nano ZS instrument (the parameters were set as material: polystyrene latex; refractive index: 1.590; absorption 0.010; viscosity: 0.8872; temperature: 25°C and equilibrium time: 120s). Different particles in suspension move in a random motion called Brownian motion and are illuminated by a laser beam which results in a variation of light scattering (Misono, 2019). It is the fluctuation rate of scattered light intensity which corresponds to the speed at which the particles move that is recorded. This provides information about the size of the particles. The results are expressed in a form of correlogram showing the scattered intensity as a function of time. The longer the time needed, the larger the

particles are, the steeper the curve, and the more monodisperse the sample is (Boyd, Pichaimuthu and Cuenat, 2011; Hiroi and Shibayama, 2017).

2.2.5.2. Scanning electron microscopy (SEM)

In early 1948, SEM was developed by Oatley (Collett, 2007). This technique employs a high energy electron beam which is scanned over the surface of a sample, and the backscattering of the electron beam is recorded (Bogner et al., 2007). Before the introduction to the microscope, the dried nanoparticle samples (0.1mg) were fixed on supports and pressure sprayed to dust off any debris. The particles were then gold coated in a high-vacuum evaporator to provide electrical conduction at the surface of the sample. The micrographs of the samples were produced and observed with a Zeiss® Evo 50 scanning electron microscope (Muscariello et al., 2005).

2.2.5.3. Transmission electron microscopy (TEM)

Ruska invented TEM in the 1930's (Harris, 2018). This technique uses more powerful electron beams and, therefore, provides higher resolution images compared to SEM which is more beneficial for nanoparticle analysis (Utsunomiya, and Ewing, 2003) The beam of electrons is transmitted through the sample and interacts with the sample as they pass through to produce an image (Reza et al., 2015). Magnetic condenser lenses are used to manipulate the beam path. TEM was performed on a Tecnai G2 F20 S-TWIN electron microscope at an accelerating voltage of 200 kV. An aqueous solution of each sample (1 mg/mL) that was measured by DLS was dropped onto a lacy carbon-coated copper grid and air-dried before morphology observation (Huseynov, Garibov and Mehdiyeva, 2016).

2.2.6. Stability studies

2.2.6.1. CAC studies

The critical micelle concentration was studied by fluorescence spectroscopy using pyrene as a hydrophobic fluorescence dye. Triplicate solutions of pyrene mixed with P-PLLA, P(Lac)-PLLA or PSSG3-PLLA nanoparticles of varying concentrations (1×10^{-5} to 0.1 mg/ml) were prepared, of which the concentration of pyrene in each sample solution was 6.0×10^{-7} M. Fluorescence emission spectra of pyrene were obtained by exciting samples at 390 nm and intensities at 337 nm and 334 nm were recorded. All fluorescence measurements were carried out at $25.0 \pm 0.1^\circ\text{C}$ in the absence of light. The CAC value was determined by plotting a curve of the intensity ratio (I_{337} / I_{334}) against the log of PG3 concentrations (mg/mL), where the corresponding CAC value is the crossover point when extrapolating the intensity ratio (I_{337} / I_{334}) at low and high concentration regions.

2.2.6.2. Blank and loaded nanoparticle stability studies

To investigate the stability of nanoparticles in different media and for different periods, Dox or Cur loaded and blank P-PLLA, P(LAC)-PLLA and P-SS-PLLA nanoparticles were stored in DI water at 4°C for 3 months and changes in sizes through DLS measurement was monitored. P(LAC)G3-Dox as required for publication purposes were incubated with DI water, 10% (V/V) FBS diluted with DI water, and DMEM containing 10% (V/V) FBS, respectively. Then the solutions were stored at 4°C for 5-day intervals followed by a daily measurement with DLS. Furthermore, the dilution stability of the loaded Dox

nanoparticles was studied in the above solvents in 1- to 500-fold dilutions at room temperature.

2.2.7. Drug release studies

2.2.7.1. Doxorubicin release from P-PLLA, P(lac)-PLLA and PSS- PLLA

In accordance with numerous empirical studies (Chen et al., 2010; Ma et al., 2015), in vitro drug release of the drug Dox from P-PLLA or P(lac)-PLLA or PSS-PLLA nanoparticles at different pH was carried out using a dialysis method. 1mg of Dox loaded nanoparticles dispersed in 1000 μ l of PBS solution (pH 5.0, 6.8, 7.4 and 7.4 with 10mM DTT for PSS-PLLA-Dox) was placed in a dialysis bag (MWCO=1,000 Da) and then dialysed against 25ml of corresponding buffer medium which was maintained at $37.0 \pm 0.5^{\circ}\text{C}$ in a shaking bed at 120rpm. The experiment was performed in triplicate. At predetermined time intervals, 1ml of the samples was taken out from the outer phase, and an equal amount of fresh corresponding buffer solution was replaced to maintain the original volume. The amount of released doxorubicin was quantified with a calibration curve using fluorescence measurement (F-7000), fluorescence was monitored at excitation 480nm and emissions were recorded in the interval of 500-700nm (3mm slit). The drug release experiments were repeated three times.

2.2.7.2. Curcumin release from PSS-PLLA

1mg of curcumin loaded PSS-PLLA was suspended in 10mL of PBS in triplicate (pH7.4 with and without 10mM DTT). The suspension was done in centrifuge tubes which were kept in a shaker at 37°C at 120rpm. At predetermined time

intervals, the suspension was centrifuged at 3000rpm for 10mins to obtain the curcumin released from the nanoparticles. The supernatant was collected re-dispersed in 5mL of PBS and then incubated for the next sampling, whereas the curcumin released present in the pellet was diluted in ethanol to be measured by fluorescence at excitation 438nm. Similarly, to Dox, the amount of released curcumin was determined by a calibration curve using a fluorescence measurement at 438nm (Khalil et al., 2013; Mohanty and Sahoo, 2010).

2.2.8. Cell culture

Purchased cells (HepG2, Hek293, U251 and NIH3T3 cells) were stored in liquid nitrogen until needed for the experiment. All cell culture experiments were carried under sterile conditions.

2.2.8.1. Recovering cell lines from liquid nitrogen storage

Cells were collected from liquid nitrogen storage and left to defrost for 1-2 mins at 37°C. The contents of the cryovial were then transferred into a vented T25 tissue culture flask containing 5mL of MEM medium supplemented with 10% (v/v) fetal bovine serum and 1% of antibiotics. The cells were then incubated at 37°C and allowed to attach and recover overnight. The media was then replaced by new media to remove dead, unattached cells and the DMSO used for cell freezing.

For each culture, media was replaced every other day and checked microscopically every day to ensure they are healthy (no contamination, few dead cells) and growing as expected.

2.2.8.2. Sub-culturing (splitting or passaging of adherent cells)

2.2.8.2.1. Trypsinization of adherent cells

When the cells reached 80% confluence (checked under a microscope), the media was removed, and the cells were gently washed 3 times with 2mL of PBS to remove the FBS which can inhibit trypsin. 1mL of trypsin was then added, the flask was swirled to cover all the surface and then incubated for a few minutes at 37°C until all the cells were detached. 3mL of media was added to inactivate trypsin and trypsinised cells were collected into pellets by centrifugation at 1500rpm for 5 mins and then re-suspended into 3-6mL of media.

2.2.8.2.2. Counting cells in a haemocytometer

After trypsinisation, 20 µL of trypsinized cells was pipetted out into 10µL of an isotonic solution (ISOTON® II Diluent, 20 L, Item No: 8546719, Beckman Coulter) and then inserted into the coulter counter for cell counting. 500µL of the diluted cell suspension was counted, representing the number of cells per µL of the original material.

2.2.8.2.3. Seeding into tissue culture T25 and T75 vented flasks or 6 well and 96 well plates

After trypsinization and calculating the number of cells needed to be added in T25 or T75 and 6 or 96 wells, the necessary amount of volume containing cells was taken from the suspension and then inserted into the flask or plates containing a quantity of media to make the final concentration required. The total volumes of media and cells were kept at 5mL for T25, 15mL for T75, 3mL for 6 wells and 200 µL for 96 wells plates. The flasks or plates were then incubated at 37°C with 5% CO₂. When 80% confluent was reached, the cells were either treated, sub-cultured again or stored at -80 °C as pellets.

2.2.9. Freezing cells

After trypsinization, pellets of cells were re-suspended in freezing medium, and a 1mL aliquot of the suspension was transferred into labelled-cryovials. Tissue paper was wrapped around the cryovial and placed into a disposable labelled-glove and frozen at -80°C. After being left overnight or for 1-3 days, the cryovials were then transferred into liquid nitrogen (-180°C) for long-term storage.

2.2.10. In vitro cytotoxicity

It is important to note that CCK8 was used in Sichuan University whereas, in Wolverhampton University, an alternative method was used known as SRB assay.

2.2.10.1. Cell viability by cell counting kit-8 (CCK8) assay

CCK8 is a colourimetric assay that is used for the determination of cell viability in cell proliferation and cytotoxicity assays. It is a better and easier method than MTT because it uses a tetrazolium salt known as WST-8, which produces water-soluble WST-8 formazan, whereas the product MTT formazan is insoluble in water. In this case, organic solvents are required to dissolve the MTT formazan product before measuring absorbance. CCK8, therefore, requires less procedure than MTT. Moreover, MTT can present some toxicity in the cell culture media and, therefore, can result in significant well-to-well error, whereas CCK8 is the most sensitive method compared to MTT, XTT, MTS or WST-1 and because WST-8 is not cell permeable, the cells used for the assay can be reused for other experiments. Also, CCK8 involves most of the dehydrogenases in a cell, whereas MTT depends only on mitochondrial hydrogenases (Mahajan et al, 2012; Jo et al., 2015). WST-8 is reduced to a yellowish coloured formazan

product by dehydrogenases (Figure 2-5.) which is easily soluble in tissue culture medium. The amount of the formazan dye generated in cells is directly proportional to the number of living cells (Dojindo Laboratories, Kumamoto, Japan).

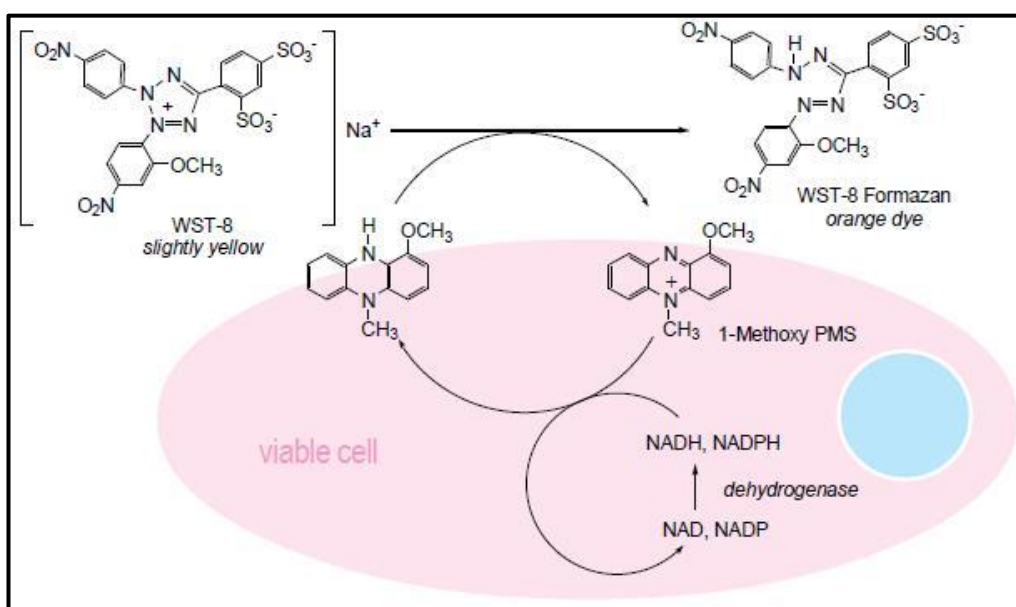


Figure 2-5. Cell viability detection mechanism with CCK-8 (Dojindo Laboratories, Kumamoto, Japan).

The cytotoxicity of the blank nanoparticles, free Dox.HCl and Dox-loaded P-PLLA and P(Lac)-PLLA nanoparticles against HepG2, and NIH3T3 cells were measured using a CCK-8 assay. Briefly, the HepG2 and NIH3T3 cells were seeded into the 96 well plates at a density of 1×10^4 per well in 100 μ L complete medium and incubated overnight. Then the cells were incubated with various concentrations of blank nanoparticles, free Dox.HCl and Dox-loaded nanoparticles for different intervals. Next, the culture medium was removed at the indicated intervals, and the cells were rinsed with PBS three times, followed by the addition of 100 μ L medium containing 10% CCK-8 into each well (light was avoided). Finally, the absorbance of the products was measured at 450nm using a microplate reader after incubating for 2hrs at 37.0 $^{\circ}$ C in the dark. The

results were expressed as the viable percentage relative to the untreated cells. The concentration that killed 50% of cells (IC50) was calculated using ORIGIN 9.0 software.

2.2.10.2. Cell viability by sulforhodamine B (SRB) assay

A cheaper alternative method to CCK8 was used for the determination of cell viability in different cell lines (Hek293, NIH3T3, HepG2 and U251). This method was developed by Skehan et al.,1990. SBR is an anionic aminoxanthene dye containing two sulfonic groups that bind to basic amino acid residues of proteins via electrostatic interaction under mild acidic conditions and then dissociate in basic conditions. The amount of bound dye is, therefore, proportional to the number of cells mass (Orellana and Kasinski, 2016). Compared to MTT and CCK8, this method does not require the measurement by metabolic activity. It is straightforward to use with only a few steps required compared to MTT. Also, it can detect densities as low as 1000-2000 cells per well. Moreover, because the SRB-stained cell monolayers are fixed by TCA and dried, they can be stored indefinitely, analysed at any time and the colour extracted by SRB is endlessly stable. For these reasons, SRB has a high level of sensitivity and can be used for large-scale screening applications (Vichai and Kirtikara, 2006).

The cytotoxicity of free Dox.HCl, free Cur, blank and loaded Dox or Cur P-PLLA, P(lac)-PLLA and PSS-PLLA nanoparticles against Hek293, NIH3T3, HepG2 and U251 cells using the SRB assay was carried out using the following method: a T-75 flask of each cell was first trypsinised, 5mL of complete media was added to the trypsinised cells, and the suspension was centrifuged in a sterile 25mL falcon tube at 1200rpm for 5 mins. Cells were counted and seeded

in 96 well plates at a density of 4×10^3 per well in 200 μ l complete media and allowed to grow for 24hrs. The media was then replaced with various concentrations of blank nanoparticles, free Dox.HCl, and Dox-loaded nanoparticles in media for different intervals. Treated cells were washed 3 times with a PBS buffer to remove any trace of drugs and then fixed with 150 μ l of 10% (wt/vol) TCA for 20-30 mins at 4 °C. It is quite convenient noting that aseptic techniques are not needed at this point. The fixed cells were washed 3 times with deionised water and left to dry. 100 μ l of 0.4% (wt/vol) SRB was then added to each well and left to stain for 20-30 mins at room temperature. Unbound dye was then removed by a 3-4-time wash with deionised water (1% acetic acid can also be used). 80-100 μ l of 10mM tris base solution was finally added to the wells and left for 10 mins to extract the protein-bound dye. The plate was then taped on the side to evenly distribute the SRB throughout the well for accuracy. The plate was then read at 510nm using a Promega Glomax plate reader and the results were expressed as the viable percentage relative to the untreated cells.

2.2.11. Flow cytometry

2.2.11.1. Cellular uptake by flow cytometry

HepG2 and U251 cells were seeded into the 6 well plates at a density of 5×10^5 per well. After incubation for 24 hrs at 37.0 °C to achieve a confluence of 70%-80%, the cells were treated with free Dox.HCl and Dox-loaded nanoparticles (Dox concentration: 5 mg/mL) for 0.5, 1 and 6 hrs. The cells were then washed with PBS and collected after trypsinisation followed by centrifugation at 1200rpm for 5 mins. Further washing two more times with cold PBS helped to remove the nanoparticles which were bound to the surface of the cells. Finally,

the cells were suspended in 30mL of PBS and the intensity of doxorubicin fluorescence in the cells was determined using FACS with a BD Accuri™ C6 flow cytometer installed with BD Accuri™ C6 software (Version 1.0.264.21).

2.2.11.2. Apoptosis

Flow cytometry was used to detect the morphologic features characterising the apoptotic programme. The membrane phospholipid phosphatidylserine (PS) is generally translocated from the inner to the outer leaflet of the plasma membrane, thereby exposing PS to the external cellular environment (Vermes et al., 1995). The apoptotic cells are stained with Annexin V which has a high affinity for PS, and necrotic cells are stained by propidium iodide (PI) due to its ability to interact with the DNA of cells under stress or when dead (Chou et al., 1987). 5×10^5 of HepG2 and U251 cells per well were seeded in a 6-well tissue culture plate and left to attend 70-80% confluency, after which they were treated with free Dox.HCl and Dox-loaded nanoparticles. After treatment, the cells were harvested by trypsinisation and washed with PBS 3 times and centrifuged at 1200rpm for 5 mins before resuspending the pellet in a binding buffer containing the dyes FITC-Annexin V and PI. After 15 mins of incubation at room temperature, each sample was analysed using the BD Accuri™ C6 flow cytometer installed with the BD Accuri™ C6 software (Version 1.0.264.21).

Q1-UL (Dead/debri) <i>[Annexin V⁻/PI⁺]</i>	Q1-UR (Late apoptotic/ Necrotic /Dead) <i>[Annexin V⁺/PI⁺]</i>
<i>[Annexin V⁻/PI⁻]</i> Q1-LL (Live)	<i>[Annexin V⁺/PI⁻]</i> Q1-LR (Early apoptotic)

Figure 2-6. Gating of cells undergoing apoptosis and necrosis using flow cytometry. The X-axis relates to the cells stained with the Annexin V FTIC, and the Y-axis relates to the cells stained by propidium iodide. The cytogram is divided into four different quadrants. Cell populations that do not take up any of the dyes are the live healthy cells and are grouped in the lower-left quadrant (Q1-LL), as shown by the BD Accuri™ C6 software. Cells that take up the Annexin V dye are those undergoing early apoptosis and are grouped in the lower-right quadrant (Q1-LR). Cell populations that take up both dyes are undergoing late apoptosis, necrosis or are considered dead and fall in the upper-right quadrant (Q1-UR). Populations that only take up the PI dye are either dead cells or debris and fall in the upper-left quadrant (Q1-UL) (Wlodkowic et al., 2011).

2.2.12. Cellular uptake by confocal studies

HepG2 and U251 cells were cultured on glass coverslips (AmScope) at a density of 1×10^5 to 70-80% confluency in 6 well tissue culture plates. Then the cells were treated with drug-loaded nanoparticles with final Dox concentration at 5mg/mL in the fresh medium. Free Dox.HCl and non-treated cells were used as a control. After incubating for either 0.5,1 or 6 hrs, the cells were washed three times with cold PBS and fixed for 10 mins with methanol on ice. The cells were rewashed with cold PBS and left to dry. The coverslips were detached from the tissue culture plate, and the side containing the fixed cells was placed onto 10µl of diluted DAPI (5:995 v/v) dropped on a microscopic slide. The edges of the

coverslips were sealed with clear nail polish. Slides were stored at 4 °C in the dark before viewing under a confocal laser scanning microscope (Zeiss LSM 880 confocal microscope, equipped with 405nm and 561nm excitation lasers using 40X/1.30 oil immersion DIC M27 objective).

2.2.13. Statistical tests

All experiments were repeated in triplicate. Data were expressed as mean values + standard deviation. The statistical differences between treatment groups were determined using two-way analysis of variance followed by Tukey's post-hoc test. All analyses were performed with SPSS 19.0 for Windows. In all tests, P values <0.05 were statistically significant.

CHAPTER 3. DESIGN AND SYNTHESIS OF ALKYNATED PEPTIDE DENDRONS

3.1. Introduction

Dendrons are hyperbranched molecules with a well-tailored architecture. They are becoming the most attractive and rapidly growing area of new chemistry as they form repetitive sequence increasing to a great extent of chemical structure (Boris and Rubinstein, 1996; Tomalia et al., 1985). Their structure is related to the one of polymers because of their repetitive structure made of monomers (Carvalho, Fernandes and Baptista, 2019) consisting of an initiator core, an interior layer (generations composed of repeating units that are attached to the initiator core) and the outer core (terminal functionality) (Tomalia et al., 1985; Nanjwade et al., 2009).

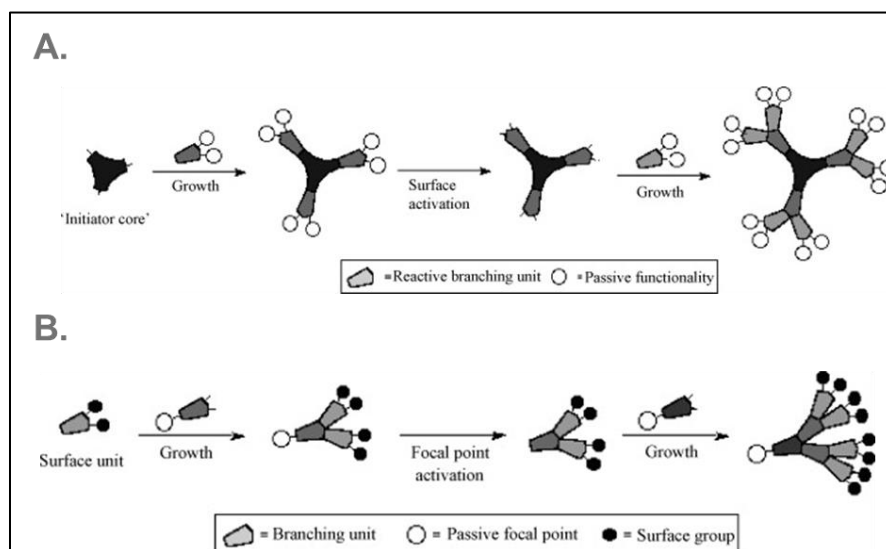


Figure 3-1. Schematic structure of the dendron synthesis method. A. Divergent method and B. Convergent method (Nanjwade et al., 2009).

Dendrons are either prepared via the divergent or convergent method. The divergent way consists of assembling monomeric modules in a radical, branch upon branch whereas the convergent method consists of reacting several

dendrons with a multifunctional core to obtain a product (Tomalia, 1996; Hawker and Frechet, 1990; Nanjwade et al., 2009). The divergent route enables dendrons of high generation to be prepared; for example, this route has been used to produce PANAM dendrimers of up to generation 10 with nearly 4096 terminal groups and molecular weight of 934720 (Noriega-Luna et al., 2014). However, purification of higher generation can be challenging, and higher generation of dendrimers increase with size (from 4 to 4096nm) resulting in more toxicity compared to smaller dendrimers of similar surface functionality (Noriega-Luna et al., 2014; Malik, 2000).

Herein, we have designed the synthesis by the divergent growth method of an alkynated peptide dendritic molecule consisting of three generation. The synthesis of alkynated peptide dendrons includes the conjugation of two or three successive additions of L-lysine into an alkyne-containing compound followed by the addition of L-arginine bearing eight hydrophobic protective groups or another L-lysine molecule. On the periphery of these molecules reside the hydrophobic 4 BOC groups and 4 PBF groups which combine alkyl, aromatic, and peptide dendritic hydrophobic segments at the same time. Compared to the structure of aromatic amino acid, PBF and BOC chemical structures show much higher hydrophobicity. PBF contains a benzene group (log P of 2.13) in which three –CH₃ are attached (CH₃ aromatic Log P 0.52), and BOC also includes three –CH₃ hydrophobic groups (CH₃- aliphatic with a log P = 0.50), determining the overall hydrophobicity of both compounds. On the other hand, the removal of protected groups would result in cationic Dendron. Both types of dendrons can then be conjugated to polymers to form non-viral systems for hydrophobic drugs or gene delivery.

3.1.1. Schematic overview of the synthesis of arginine-based dendrons

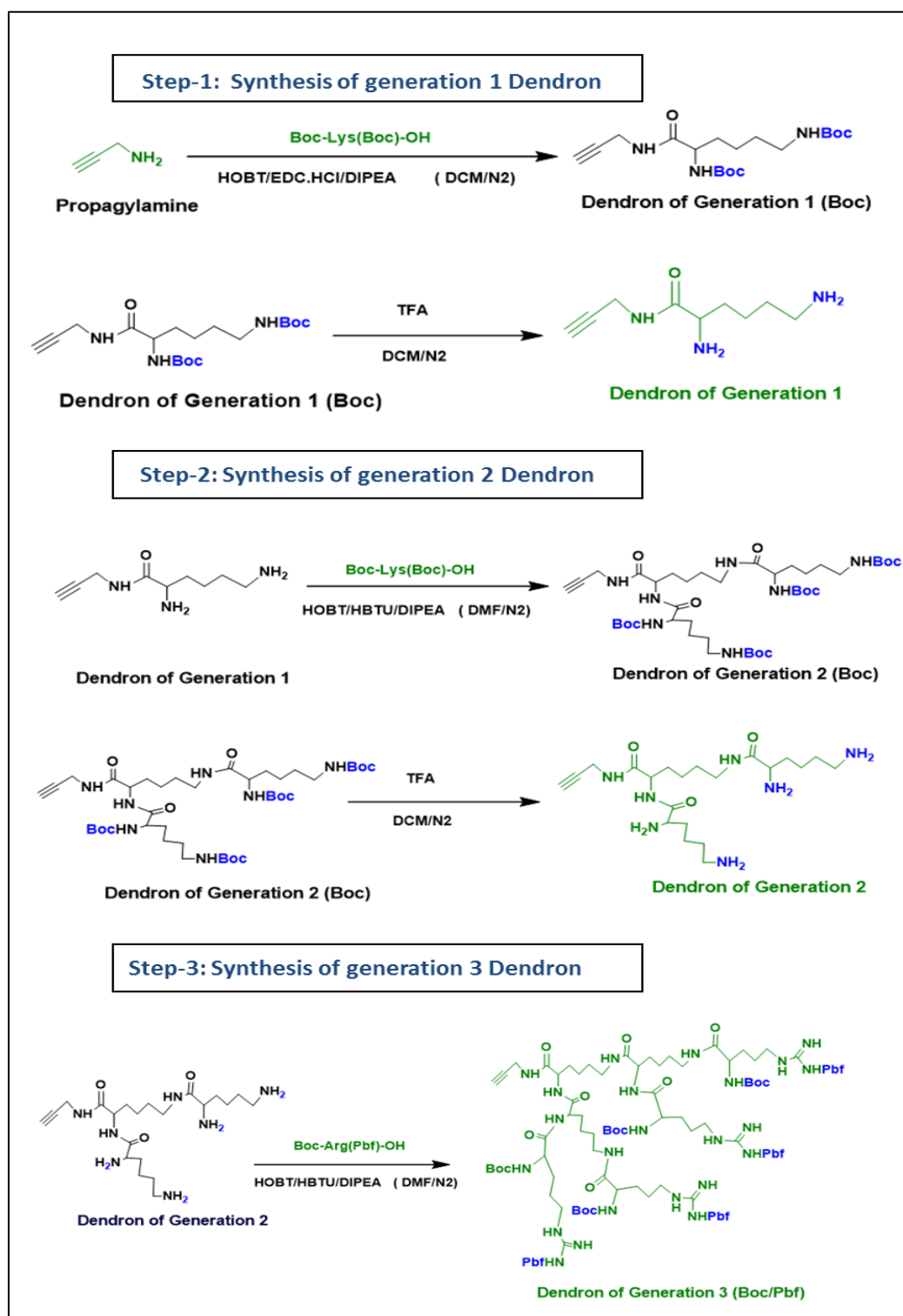


Figure 3-2. Schematic synthetic route of generation 1, 2 and 3 dendrons. Step 1: Propagylamine reaction with Boc-Lys(Boc)OH to yield Dendron of generation 1 containing terminal Boc groups, followed by the deprotection of G1 Dendron; Step 2: G1 dendron reaction with Boc-Lys(Boc)OH to yield Dendron of generation 2 containing terminal Boc groups, followed by the deprotection of G2 Dendron; Step 3: G2 dendron reaction with Boc-Arg(Pbf)OH to yield Dendron of generation 3 containing terminal BOC and PBF groups.

3.1.2. The process of dendron synthesis by peptide bond formation via the condensation of acid and amine

For each synthesis of dendrons, a peptide bond formation takes place between the amine groups of the core molecule (Propagylamine) and carboxyl groups of the molecule added (either L-Lysine or L-arginine).

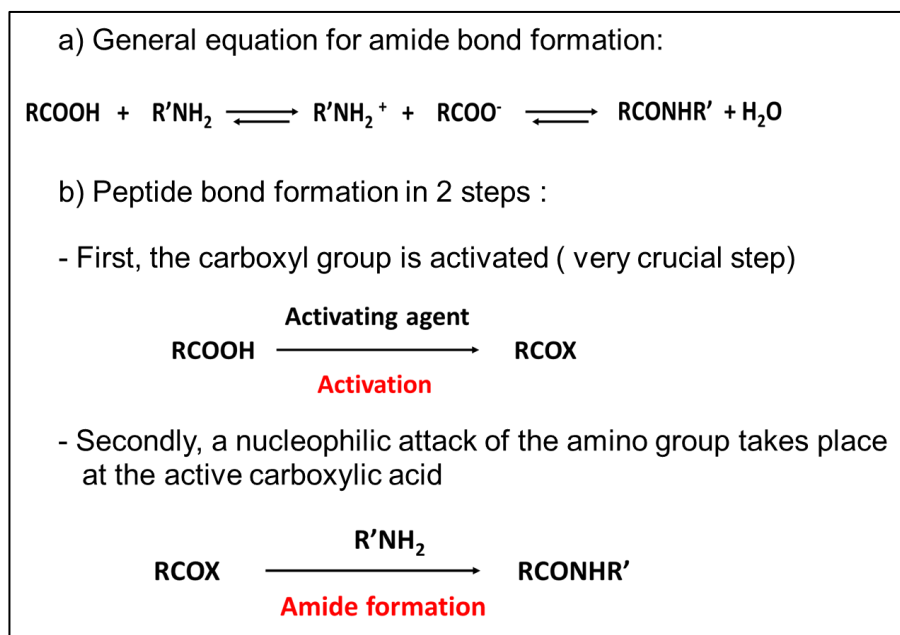


Figure 3-3. General chemical equations of peptide bond formation.

An acid-base reaction takes place at high temperature (>200 °C) in the presence of an amine and carboxylic acid to form a stable salt, but the high temperature conditions of condensation are usually incompatible. Activation of the carboxy moiety followed by the attachment of a leaving group to the acyl carbon of the acid allowing an attack by the amino group is a necessary process (Jursic and Zdravkovski, 1993; Montalbetti and Falque, 2005). Moreover, it is important that the reaction for amide formation gives a high yield of the product with ease of purification and prevented racemisation and degradation. Therefore, various coupling agents that activate the carboxy components to generate compounds such as acid chlorides, (mixed) anhydrides, carbonic anhydrides or active

esters have been developed. The first ever coupling agents to be synthesised were the carbodiimides which include dicyclohexyl-carbodiimide (DCC), diisopropyl carbodiimide (DIC), 1-ethyl-3-(3'-dimethylamino) carbodiimide HCl salt (EDC or WSC.HCl), each producing different urea product (Figure 3-4.). These react with the carboxylic acid to form the intermediate O-acylisourea mixed anhydride (figure 3-5a.) which contains a N=C group that provides powerful activation and, therefore, can directly react with the amine to yield the desired amide. However, the formation of an amide product can be accompanied with some side reactions leading to unwanted urea by-products such as dicyclohexylurea (DCU) and N-acylurea. This happens due to the nucleophilic centre on O-acylisourea, which competes with the amino component for the O-acyl residue, and this competition leads to the formation of unwanted by-product. Therefore, in addition to coupling agents, nucleophile agents (DMAP, HOBT, HOAt,..) that react faster than the competing acyl transfer are generally used in to reduce side reactions such as epimerisation and racemisation. HOBT invented in 1970 by König and Geiger, reacts with the intermediate O-acylisourea to give the OBt active ester (Figure 3-5d.) which enhances the reactivity of the activated ester by encouraging the approach of the amine via hydrogen bonding (Valeur and Bradley, 2009; Montalbetti and Falque, 2005). In contrast to activation by carbodiimides, the formation of the amide bond using these coupling agents also requires the presence of a base such as Diisopropylethylamine (DIPEA) and N-methylmorpholine (NMM) which are the most frequently used ones. This method was used for the synthesis of lysine based dendron of generation-1 because it is easily controllable, and the reaction is rapid. EDC.HCl was the carbodiimide type used because the by-product obtained is easily eliminated by washing (Figure 3-6.).

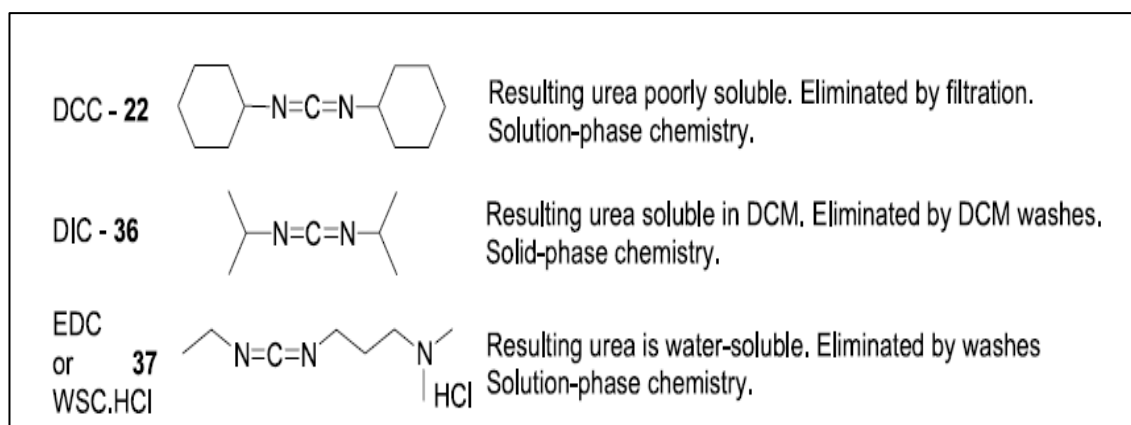


Figure 3-4. Commonly used carbodiimides and their resulting urea product obtained depending on the coupling agents used (Montalbetti and Falque, 2005).

In the case of the synthesis of the dendron of generation 2 and 3, because the number of amine groups to be conjugated increases, reactions can take longer to complete, and more undesired side reactions can occur. Therefore, higher coupling agent rates are needed to speed up the reactions and to reduce side reactions. In recent years, different types of reagents including phosphonium- and the aminium-salts (BOP, PyBOP, PyBrOP, TBTU, HBTU, HATU, COMU, and TFFH) have been developed. BOP coupling was established in 1975 by Castro et al. and was proved to be very effective compared to the carbodiimide because it is racemisation-free and exhibits superior kinetics. However, BOP is not accepted in peptide synthesis because it has some toxicity. Therefore, its analogue HBTU is more widely used as a coupling agent in combination with HOBT.

The reaction mechanism of carboxylic acid activation by EDC.HCl, HBTU or HOBT and N-acylation are summarised in the Figures 3-5 & 6.

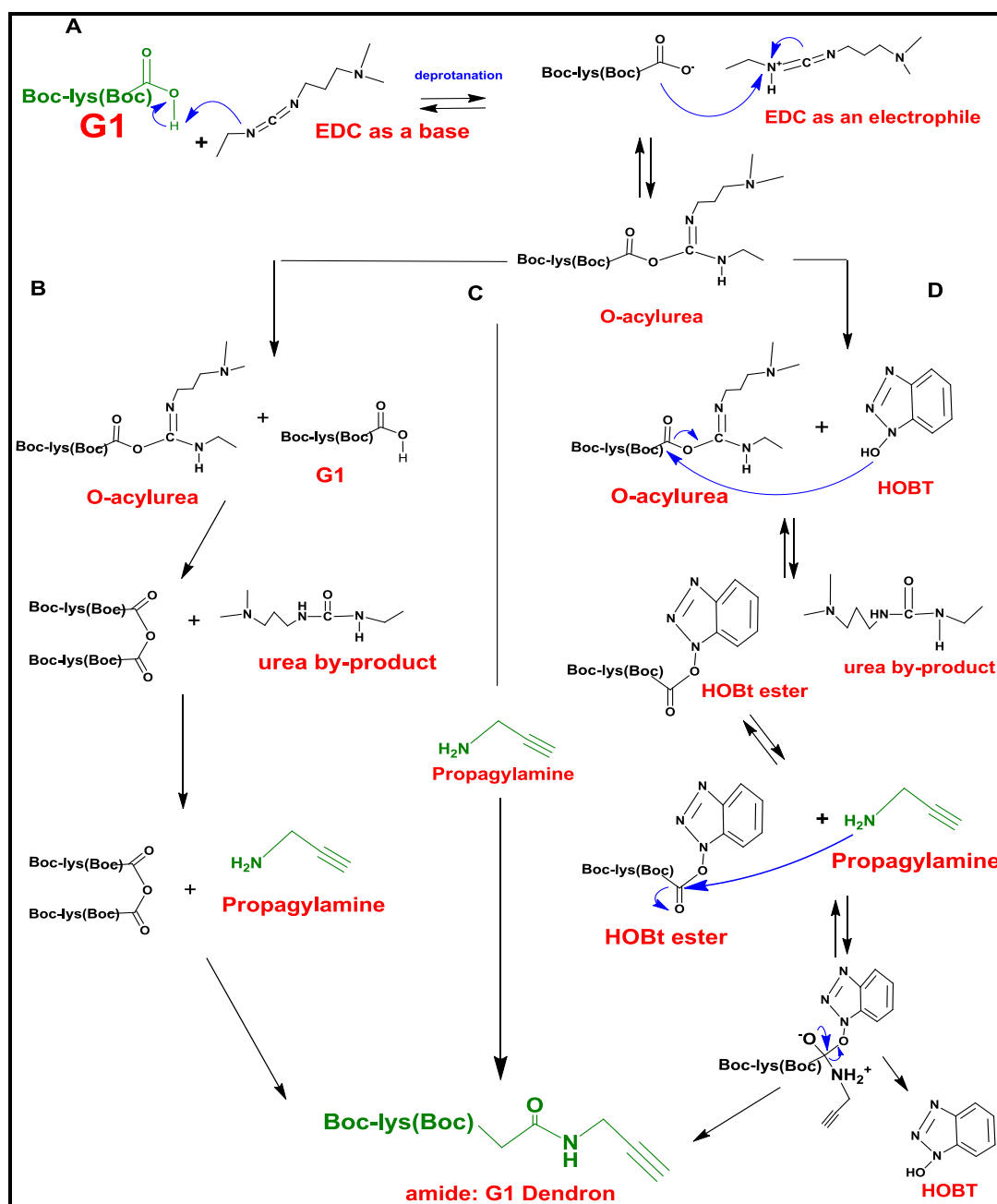


Figure 3-5. The synthesis of lysine-dendron of generation 1 by the coupling of propargylamine and Boc-Lys (BOC)-OH in the presence of EDC.HCl, HOBT and DIPEA. A. EDC.HCl and DIPEA act as the base to deprotonate the molecules. The lone pairs on the nitrogen of EDC.HCl takes the proton (H) from Boc-Lys (BOC)-OH leaving an electron behind to the oxygen. The protonated nitrogen wanting electron will withdraw some electron density away from the carbon next to it; the carbon losing some electron density will become positive and react as an electrophile whereas the oxygen of the carboxylic acid will act as the nucleophile which then attacks the electrophile to form a new bond between EDC.HCl and Boc-Lys(BOC)-OH forming the by-product O-Acylurea. The by-product can then react in 3 ways: B. React with another molecule of Boc-Lys (BOC)-OH to form an intermediate molecule Boc-Lys (BOC)-O-Boc-Lys (BOC) which then reacts with the amine group of propargylamine to give the desired amide. C. React directly with the nucleophile nitrogen of propargylamine to give the amide G1 dendron. D. React with the nucleophile HOBT to give the HOBT ester which permits the amine group of propargylamine to act as a nucleophile to form the amide bond.

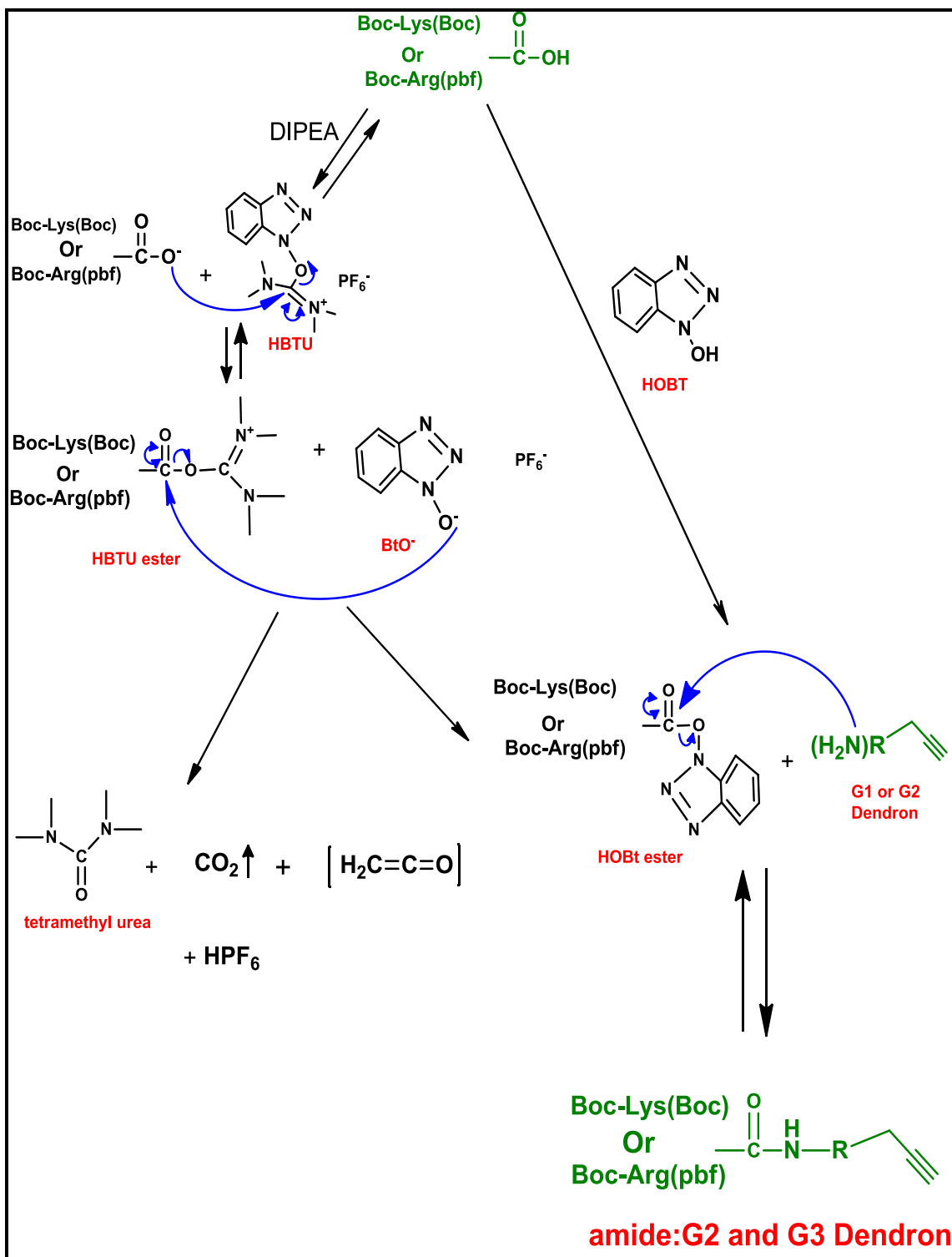


Figure 3-6. The synthesis of lysine-dendron of generation 2 and arginine-dendron of generation 3 by the coupling of the lysine-dendron of generation 1 or lysine of generation 2 and Boc-Lys (BOC)-OH or BOC(Arg)PBF in the presence of HBTU, HOBT and DIPEA. The base deprotonates the carboxylic acid to form the carboxylate anion which then attacks the electron deficient carbon atom of HBTU to form the HBTU ester and BtO⁻. The resulting HBTU ester reacts with the anion product to form the HOBT activated ester, tetramethyl urea, CO₂, ketene and PF₆. The amine reacts with the activated HOBT ester to form the amide desired product.

3.2. Aims and objective

To be able to produce a successful delivery system we aim in this chapter to confirm the successful synthesis of the hydrophobic and cationic arginine dendrons of third generation by matching the characterisation of products obtained with the predicted structures of interest, also, we aim to confirm their purity and determine if the products are fit for purpose.

3.3. Methodology

The alkynyl peptide dendrons of generation 1, 2 and 3 (G1, 2 and 3) were prepared using the previously reported methods (Li et al., 2013; Luo et al., 2012) with a few modifications.

3.3.1. Synthesis of the lysine- dendron of generation 1 (PL)

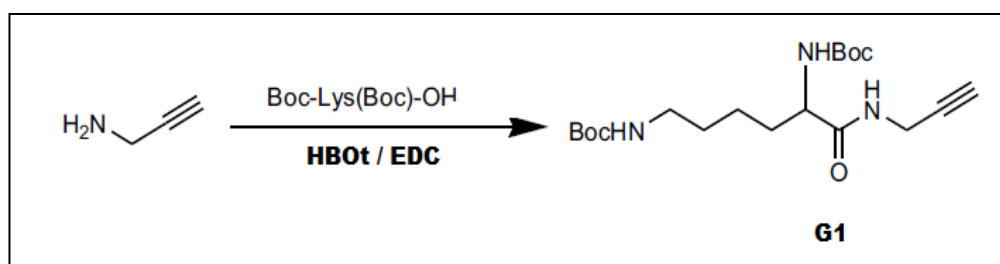


Figure 3-7. Synthesis equation of G1 dendron (PL).

First, equal molar of Boc-Lys (Boc)-OH (3.5g, 1.1mmol), HOBt (1.3g, 1.1mmol) and EDC.HCl (2.0g, 1.1mmol) were co-dissolved into 40.0mL of dried CH₂Cl₂ (DCM) under N₂ atmosphere. The flask was kept under an ice bath, and DIPEA (6.3ml, 4.0mmol) was injected into the mixture, followed by the addition of propargylamine (0.6ml, 1mmol). The mixture was first stirred at 0 °C for 30min and then brought to room temperature for 48 hrs. After the reaction, the mixture was concentrated by removing CH₂Cl₂ through rotary evaporation and then dissolved with 300mL of chloroform. The product was then washed three times

with saturated NaHCO₃, HCl (1M) and NaCl to remove Impurities. MgSO₄ was then added to the organic phase and left to stand overnight, and the organic phase was filtrated and concentrated by rotary evaporation. Further purification was carried by column chromatography using ethyl acetate/petroleum (1:1, V/V) as eluent. The final purified product obtained was dried by rotary evaporation and then by a low-pressure pump followed by vacuum drying to get a white solid.

3.3.2. Synthesis of the lysine-dendron of Generation 2 (PLL)

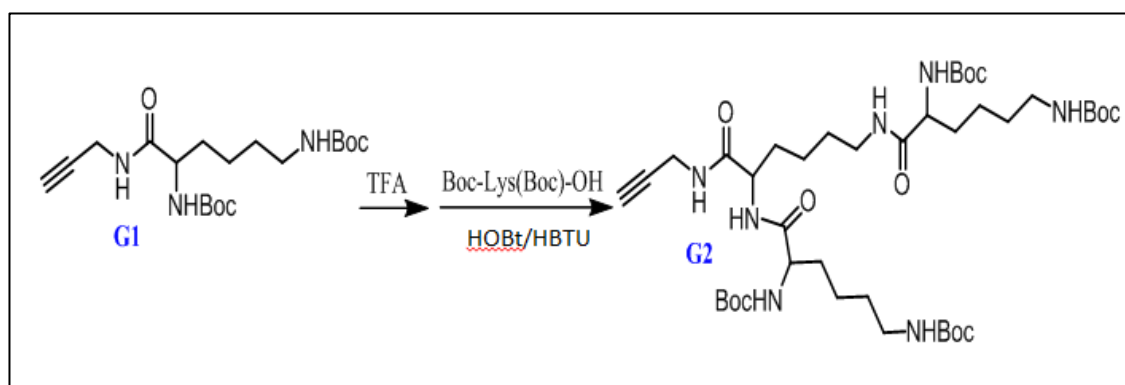


Figure-3.8. Synthesis equation of G2 dendron (PLL).

3.3.2.1. Removal of BOC from G1 dendron

For the preparation of G2 dendron, the Boc groups of G1 were first removed using TFA (20mmol). 2.60g (1mmol) of G1 was dissolved in CH₂Cl₂, followed by the addition of TFA (16ml of anhydrous TFA/CH₂Cl₂ mixture (V/V: 1.8/1) and left to stir for 5 hours at RT under N₂ atmosphere. After the solvent was removed by rotary evaporation, absolute diethyl ether was added, and precipitates appeared after stirring overnight. The precipitates were collected by centrifugation and then dried under high vacuum. TLC was used to monitor whether all the boc groups were removed.

3.3.2.2. Synthesis reaction of PLL

G2 dendron was prepared by co-dissolving equal molar of Boc-Lys (Boc)-OH (3.5g, 2.4mmol), HOBT (1.3g, 2.4mmol), HBTU (2g, 2.4mmol) and G1 (no Boc, 1mmol) into 50ml of dried DMF under N₂ atmosphere. The flask was kept under an ice bath, and DIPEA (6ml, 5mmol) was injected into the mixture. The mixture was first stirred at 0 °C for 30min and then brought to RT for 48 hrs. The pure product was obtained by the same method used to purify the G1 dendrons. The obtained crude product was purified by column chromatography (silica gel: ethyl acetate/petroleum = 4:1, V/V to remove impurities and free lysine followed by ethyl acetate/petroleum = 4:1, V/V to collect the pure product).

3.3.3. Synthesis of the dendron of generation 3 (PLLA and PLLL)

3.3.3.1. Removal of BOC from G2 Dendron

The BOC groups of G2 Dendron were removed by the same procedure as described for G1 Dendron. The obtained G2 (1mmol) was treated with 70ml of anhydrous TFA (40mmol)/CH₂Cl₂ mixture (V/V: 1.8/1) and stirred for 8 hours at RT under N₂ atmosphere. A white product (6.3g) was obtained after precipitation overnight with absolute diethyl ether. TLC was used to monitor whether all the Boc groups were removed.

3.3.3.2. Synthesis of arginine dendron of generation 3 (PLLA)

PLLA synthesis was carried out by co-dissolving equal molar of Boc-Arg (Pbf)-OH (12g, 6mmol), HOBT (3.3g, 6mmol), HBTU (8.79g, 6mmol) and deprotected G2 (1.7g, 1mmol) into 55ml of dried DMF under N₂ atmosphere. The flask was kept under an ice bath, and DIPEA (7ml, 10mmol) was injected into the mixture.

The mixture was first stirred at 0 °C for 30min and then brought to RT for 48 hrs. Purification was achieved by applying the same method used for G1 and G2 purification. The mixture was carefully washed three times with saturated NaHCO₃, HCl (1M) to avoid any emulsion. Then the organic phase was dried, concentrated and purified by column chromatography using ethyl acetate/petroleum ether (1/1 to 40/1, V/V) and then using dichloromethane/methanol (50/1 to 10/1, V/V). It is important to note that the TLC indication gave a large amount of traces that could make the separation process and the collection of the correct product more difficult.

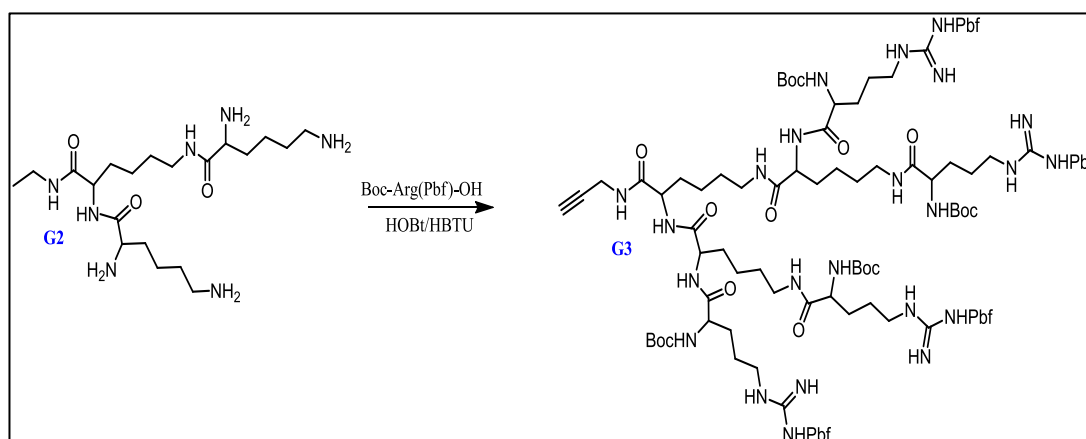


Figure 3-9. Synthesis equation of Dendron of Generation 3 (PLLA).

3.3.3.3. Synthesis of Lysine Dendron of Generation 3 (PLLL)

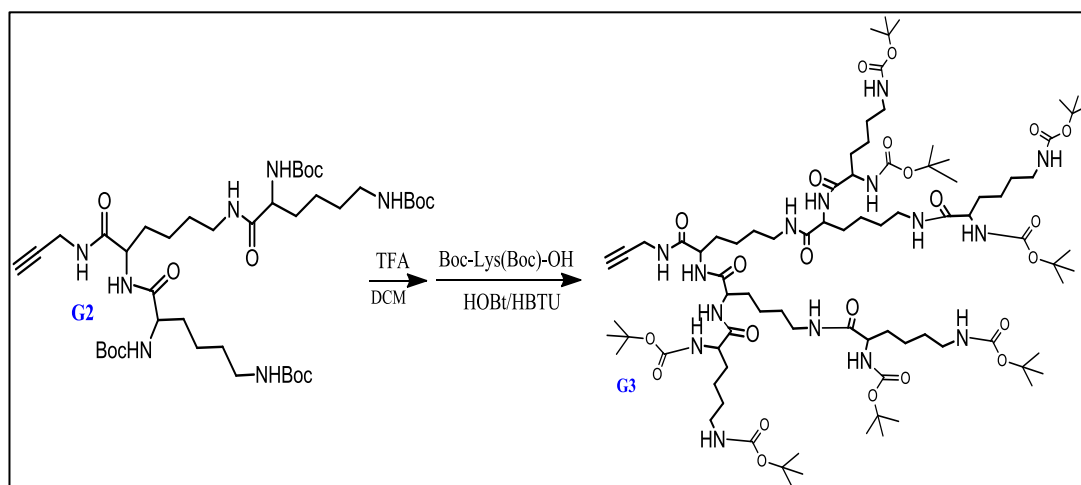


Figure 3-10. Synthesis equation of Dendron of Generation 3 (PLLL).

The removal of Boc/Pbf from PLLA to result in PLLA⁺ was not successful (see appendix section 1), for this reason, PLLL synthesis and guanidinylation of PLLL was carried out to yield into PLLA⁺. However, guanidinylation could only be carried out after conjugation of PLLL into pullulan (refer to chapter 7).

The PLLL synthesis was carried using the same method as PLLA. Equimolar equivalent of Boc-Lys (Boc)-OH (9.9g, 6mmol), HOBT (3.86g, 6mmol), HBTU (10.8g, 6mmol) and deprotected G2 (4g, 1mmol) were dissolved into 60ml of anhydrous DMF under N₂ atmosphere. The flask was kept under an ice bath, and DIPEA (8.29ml, 10mmol) was injected into the mixture. The mixture was first stirred at 0 °C for 30min and then brought to RT for 48 hrs.

The pure product was obtained by the same method used to purify the G1 and G2 dendrons by washing 3 times with saturated NaHCO₃, HCl (1M) and brine. The concentrated crude product was then purified by column chromatography using ethyl acetate/petroleum ether (1/1 to 40/1, V/V) and then followed using dichloromethane/methanol (50/1 to 10/1, V/V). Yield: 12g, 75%.

To yield PLLL⁺, the product PLLL was deprotected by removing the BOC in a similar way to G1 and G2.

3.3.4.Characterisation of Dendrons

Each generation of Dendrons synthesised was identified, and their chemical structures were confirmed by MS and H¹NMR studies. Their purity was also confirmed by TLC. Moreover, details on each characterisation method and the purification of Dendron are given in chapter 2.

3.4. Results

3.4.1. Characterisation of lysine generation 1 dendron (PL)

The reaction of the propargylamine and Lysine led to the production of the white product PL Dendron of Generation 1 with a yield of 2.60 g (74.01%). Figure 3-11. shows the mass spectra confirming the molecular weight of the PL Dendron ($C_{19}H_{33}N_3O_5$) with 2 terminal Boc groups. The most abundant peak ($m/z=406.03$) was assigned as a sodium adduct $[M+Na]^+$ and corresponded to the calculated molecular mass of dendron PL being 383.24g/mol.

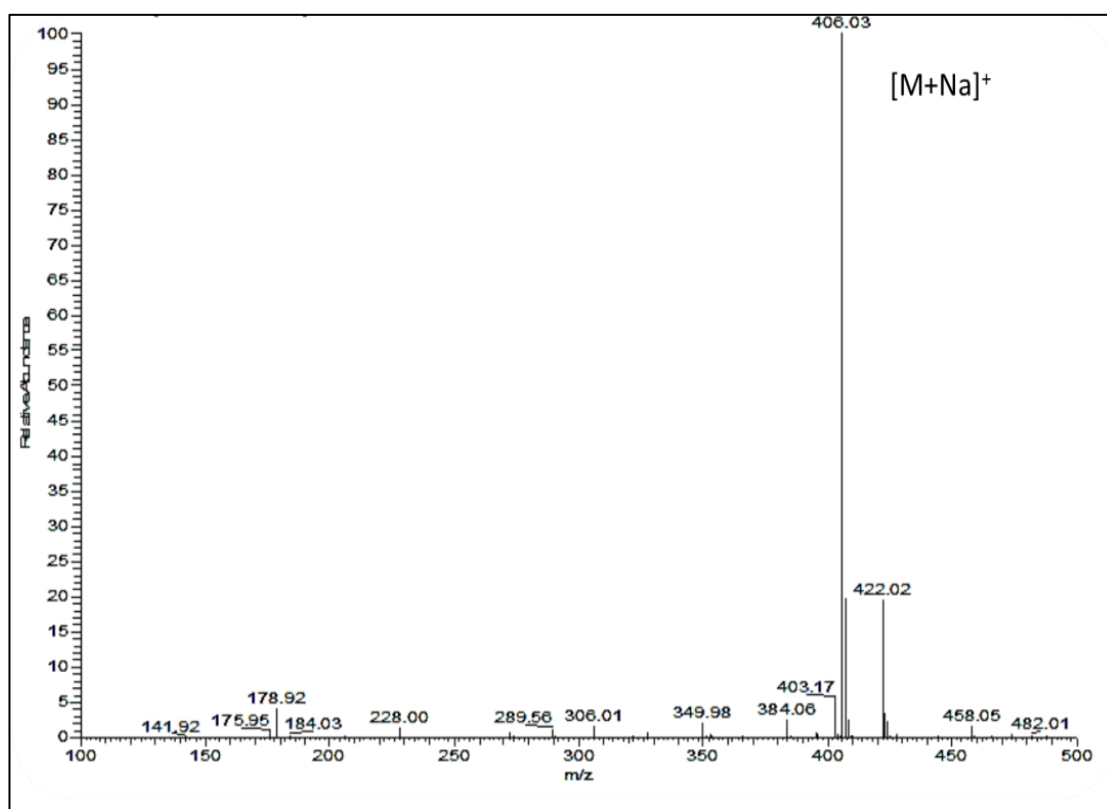


Figure 3-11. Mass spectra of the PL Dendron of generation 1. ESI-MS: $m/z=406.03$ ($M+Na^+$) (calculated 383.49 for $C_{19}H_{33}N_3O_5$).

Moreover, to further confirm the structure of the product obtained, the H^1 NMR spectrum was obtained (Figure 3.12.). The peaks in the spectrum have been labelled with numbers representing the carbon or nitrogen number in chemical

structure. The carbon or nitrogen contains 1, 2 or 3 hydrogen atoms which cause signals giving peaks in the spectrum. Therefore, the different peaks in the spectrum tell us about how many types of hydrogen bearing carbon or nitrogen there is in the chemical structure. The intensities of the signals are proportional to the number of hydrogen present.

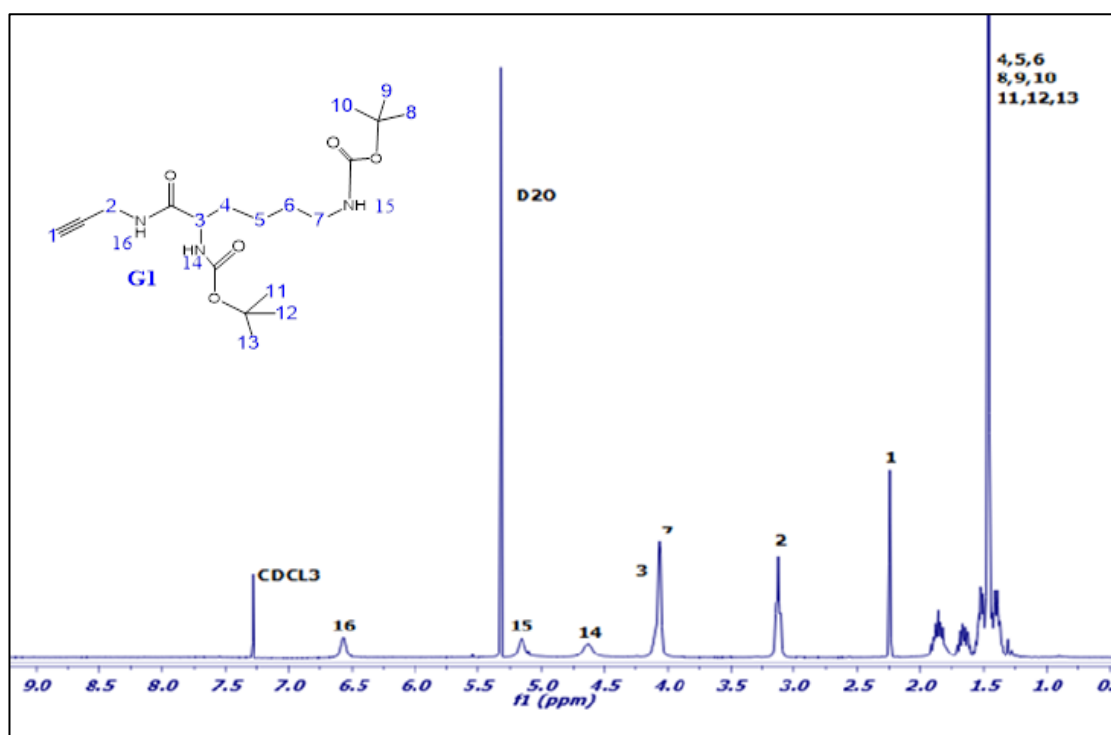


Figure 3-12. ^1H NMR spectrum of Dendron PL(400 MHz, CDCl_3): d (ppm), 1.251–1.915 (m, 24H, CH_2 Lys and CH_3 -Boc), 2.252 (s, 1H, CHCCH_2), 3.128 (m, 2H, CH_2NHCO), 4.070(s, 2H, CHCCH_2NH), 4.058 (m, 1H, COCH(R)NH), 4.664(s, 1H, CONH), 5.150 (s, 1H, CONH), 6.568(s, 1H, CONH).

The high peak seen at 1.251-1.915 ppm corresponds to the 24 hydrogens present in the lysine-BOC structure. 6 hydrogens (CH_2 -Lys) are situated in the main bone of the lysine structure at carbon number 4, 5 and 6 whereas the other 18 hydrogens are from the 2 BOC groups protecting the amine at carbon number 8, 9,10,11,12 and 13 (CH_3 -Boc). The peak at 2.252 ppm, corresponds to the hydrogen situated at carbon number 1 (CHCCH_2) of the alkyne group from propargylamine. The peak at 3.128 and 4.070 ppm have same height

peaks corresponding to the 2 hydrogens situated at carbon 2 of the propargylamine (CH_2NHCO) and carbon 7 of the lysine (CHCCH_2NH). The peak at 4.058 ppm represent the single hydrogen located in carbon number 13 (COCH(R)NH) and the hydrogen present in the 3 amine molecules (14,15 and 16) are observable by the peaks produced at 4.664 ppm (s, 1H, CONH), 5.150 ppm (s, 1H, CONH), 6.568ppm (s, 1H, CONH).

The purity of the PL product was also confirmed by TLC. After the reaction, a drop of the concentrated product was run into a TLC plate using the solvents ethyl acetate/Petroleum (1/1,V/V). Figure 3-13A. shows traces of impurities under the U-V light (Top spot of HOBT and EDC.HCl), the product (the stained middle spot) and spots of lysine (stained by ninhydrin at the bottom). The value R_f value of the product PL was determined to be 0.61. After purification by column chromatography, Figure 3-13B. shows a clear spot of the purified product PL. Separation was known to be completed when the TLC plate showed only one spot of lysine trace (Figure 3-13C.).

To create a branched structure, another lysine group was further conjugated to the terminal amine groups of G1 dendrons to lead into dendrons of generation 2 (G2). The protective Boc groups were first removed and confirmed by MS (Figure 3-14.).

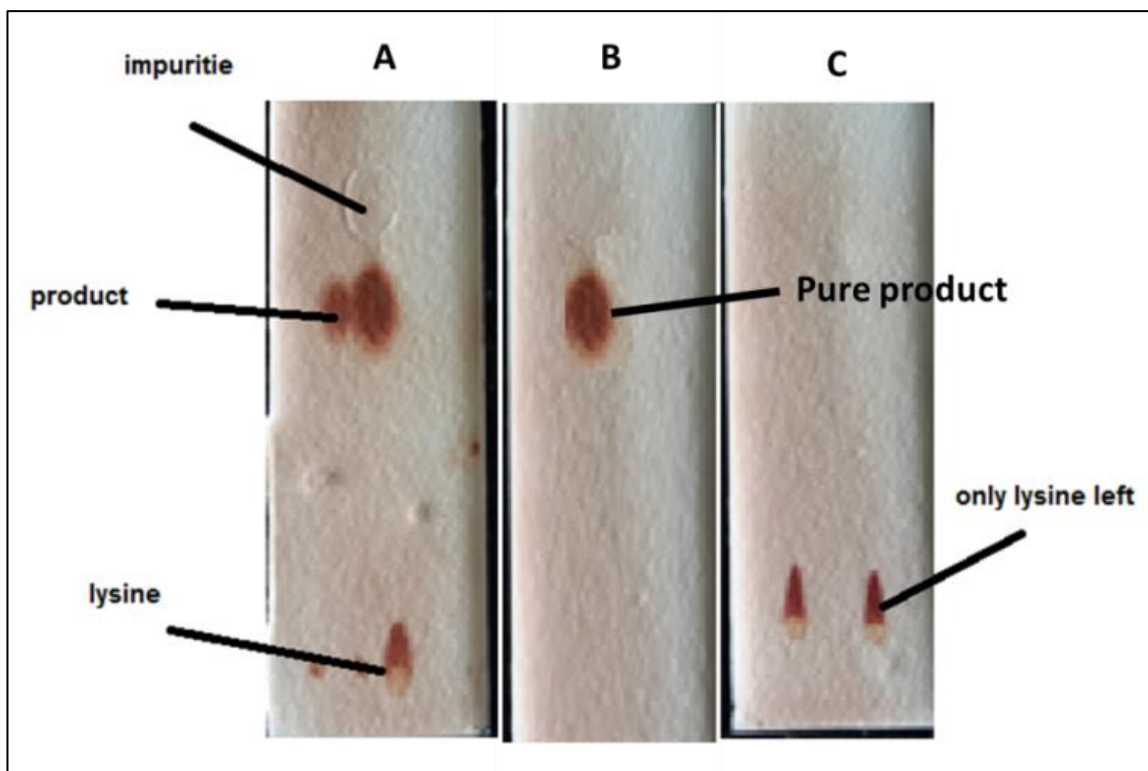


Figure 3-13. 3 TLC plates of A. product PL obtained after reaction; B. pure PL after separation and C. Lysine left after separation by column chromatography. Rf value determined to be 0.61 in the presence of PE: EA (V: V; 1:1) solvent.

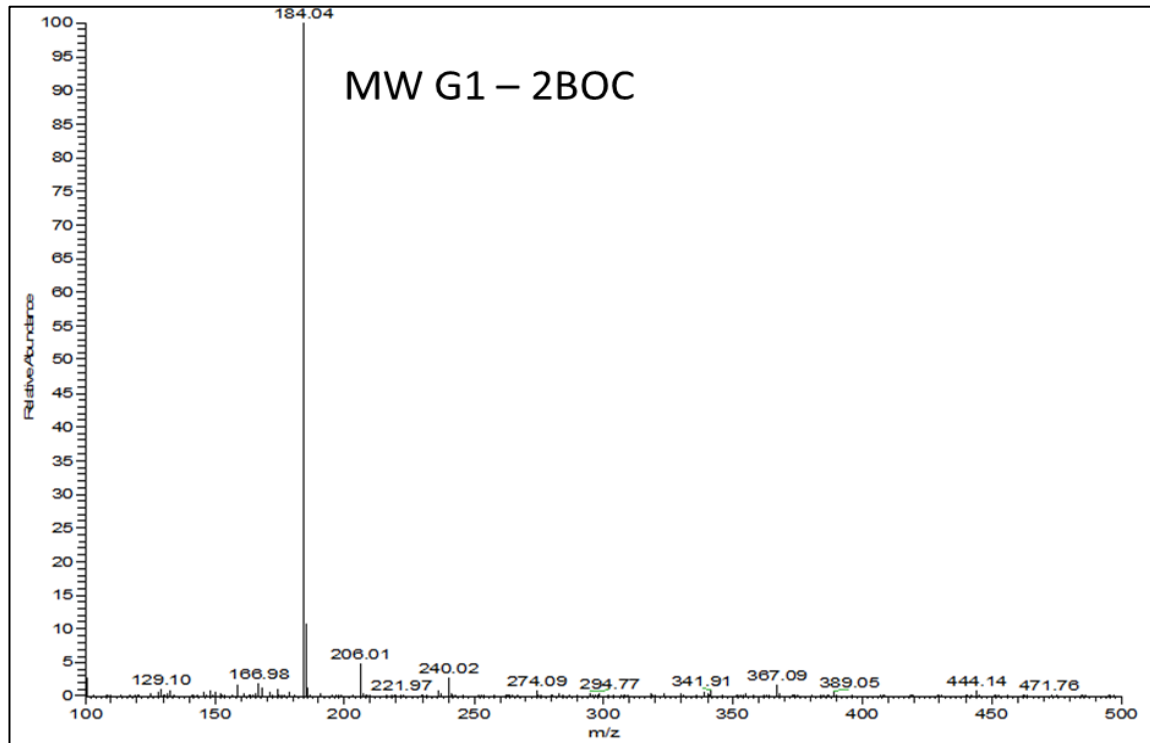


Figure 3-14. ESI-MS of the deprotected PL Generation 1 dendron (calculated 183.49).

3.4.2. Characterisation of lysine generation 2 dendron (PLL)

PLL was obtained in a yield of 12.5g (78.02%); Figure 3-15. shows the expected molecular weight of PLL being 840.23g. The higher peak shows the formation of sodium adduct $[M+Na]^+$ with a mass of 862.26g. The PLL Dendron of generation 2 contains 4 terminal amine groups which are protected with BOC groups.

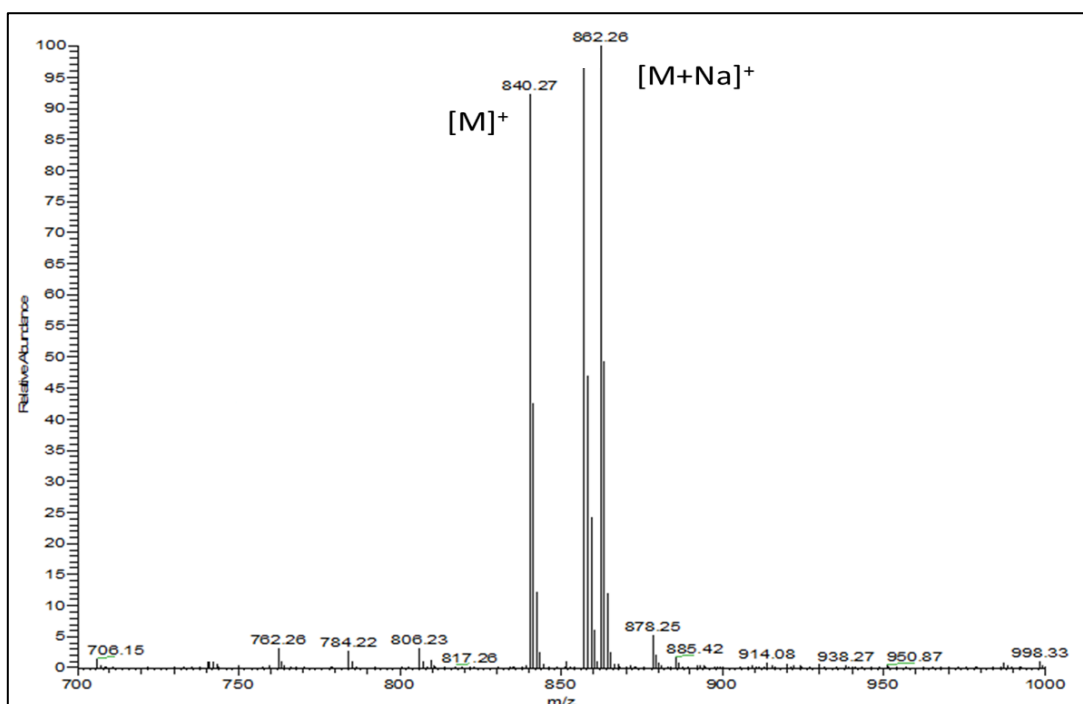


Figure 3-15. Mass spectra of the PLL Dendron of generation 1 ESI-MS: $m/z = 862.26(M + Na^+)$ (calculated 840.07 for $C_{41}H_{73}N_7O_{11}$).

The H^1 NMR spectrum in Figure 3-16. shows the ppm values for protons in a different chemical environment which confirms the chemical structure of PLL. The high peak seen at 1.207-2.180 ppm corresponds to the 54 hydrogens of the CH_2 situated on the lysine long chain and the CH_3 of the protecting BOC groups. The peak at 2.263ppm corresponds to the hydrogen present in the alkyne group of propargylamine. The peak at 3.107 corresponds to the 6 hydrogens from CH_2 groups present at the end of the long chain (CH_2NHCO).

The peak at 3.486 ppm is for the hydrogens from the CH₂ group of the propargylamine. The peak at 4.038 ppm represent the single hydrogen located in carbon 3,12, and 36 carbon from the PLL structure (COCH(R)NH) and the hydrogens of amine groups from lysine (CONH) are at 4.819, 5.543 and 5.936 ppm whereas the hydrogen of the amine of the propargylamine gave a peak at 6.942.

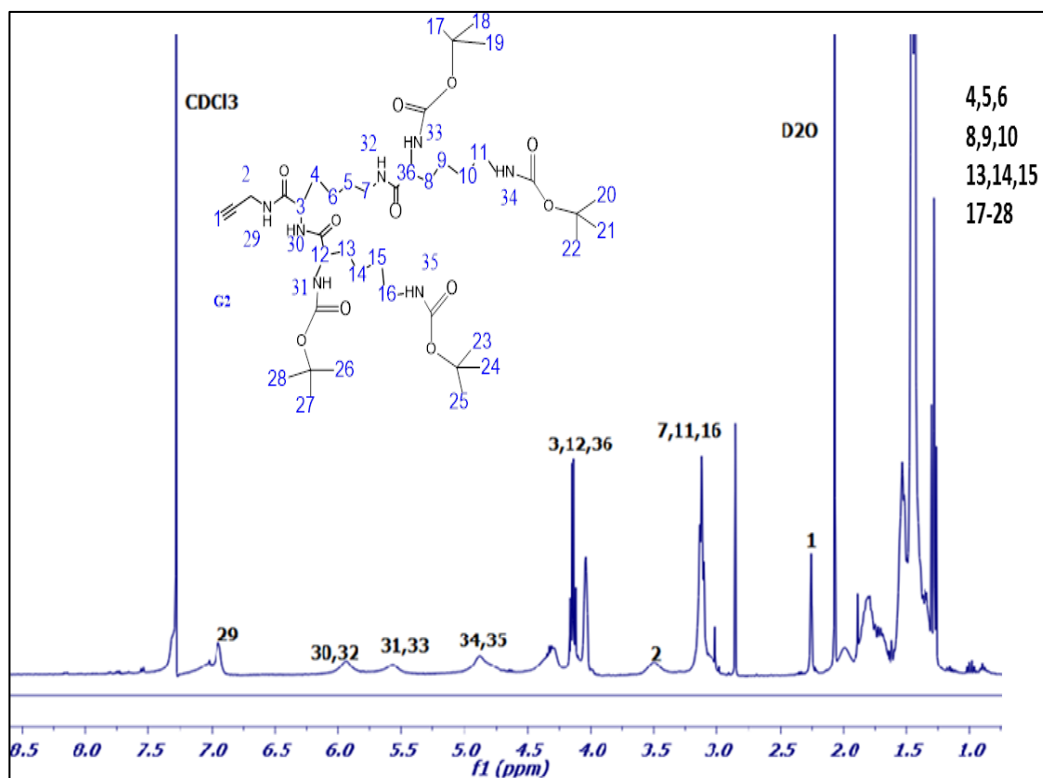


Figure 3-16. ¹H NMR spectrum of Dendron PLL (400 MHz, CDCl₃): d (ppm) , 1.207– 2.180 (m, 54H, CH₂-Lys and CH₃-Boc), 2.263 (s, 1H, CHCCH₂), 3.107(m, 6H, CH₂NHCO), 3.486(s, 2H,CHCCH₂NH), 4.038 (m, 3H, COCH(R)NH, 4.819(s, 2H, CONH), 5.543 (s, 2H, CONH), 5.936(s, 2H, CONH), 6.942(s, 1H, CONH).

TLC analysis in Figure 3-17 of the product after reaction shows some impurities visible in UV-light only, the brown stained product and traces of lysine. Impurities were first collected and discard in the presence of 1/1 volume of EA/PE and the product was obtained at 4/1 volume with a determined R_f value of 0.44, traces of lysine were easily washed off (see appendix section 9.4).

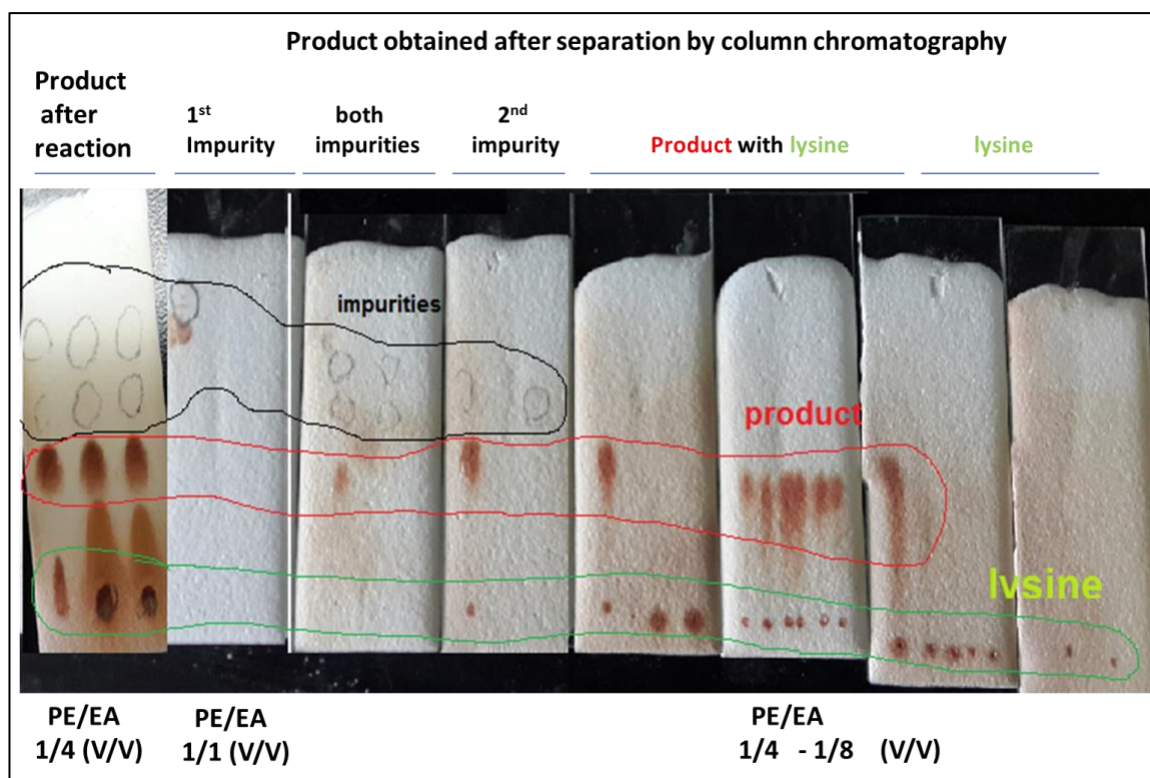


Figure 3-17. 8 TLC plates of PLL dendrons obtained at different stages of purification (PE/EA:1/1-8). The first TLC plate on the left shows different traces of impurities (top 2 clear circles), PLL dendrons (middle brown circles) and Lysine (bottom circles). The other TLC from left to right shows the products collected after separation by column chromatography over time. The impurities are first collected and discarded. Then pure product is collected separately, and the separation is stopped when traces of lysine appears on its own.

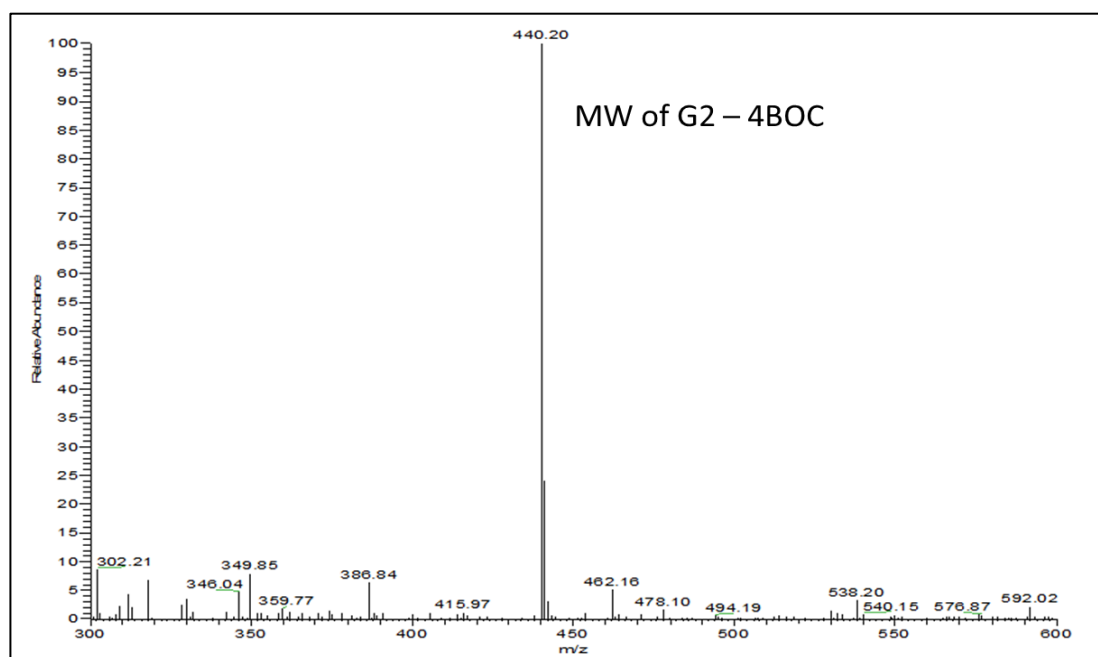


Figure 3-18. The ESI-MS of the deprotected PLL G2 dendron (calculated 440.07).

Similarly, to PL, the protective BOC groups present in PLL were also removed for further reaction, and the molecular weight 440.07 g was confirmed by Mass spectrometry (Figure 3-18.).

3.4.3.Characterisation of arginine dendron of generation 3 (PLLA (BOC/PBF))

The chemical structure and purity of PLLA (BOC/PBF) were verified by H^1 NMR (Figure 3-19.). The structure has some repeating chemical chains, therefore, the main long chain which contains all the hydrogen groups was numbered. The peak at 1.139-2.285 ppm represent the 106 hydrogens of methyl groups in lysine, BOC and PBF groups (106H, CH_2 -Lys, CH_3 -BOC and CH_3 PBF), at 2.306ppm, the peak corresponds to the single hydrogen present in the alkyne group of propargylamine. 24 hydrogens from the CH_2 protective PBF groups (position 13 and 14) are seen by the double peak at 2.410-2.806 ppm whereas the peak at 2.971 ppm represents the 8 hydrogens of the CH_2 in PBF at position 16. The peak at 3.113-3.336 corresponds to the 14 hydrogens located in position 7 and 11. The other peaks at 3.969 ppm are for the 2 hydrogens of the carbon position 2; 4.115-4.516ppm for the singlet hydrogen of the carbon at position 3 and 8 whereas the 5.792-6.212 and 6.324-6.875 are for the hydrogen available in amine groups of the lysines chains.

Purification of the product was monitored by TLC analysis. Figure 3-20 shows the TLC plate of the PLLA product before and after separation by column chromatography in different solvents mixture ratio (1/1, 1/40 (PE/EA) and 1/10 and 1/50 (DCM/MeOH)). In the presence of PE and EA, the product does not move from the mobile phase whereas the R_f value is determined to be 0.59 with ratio 1/50 (DCM / MeOH) and 0.50 for 1/10 ratio.

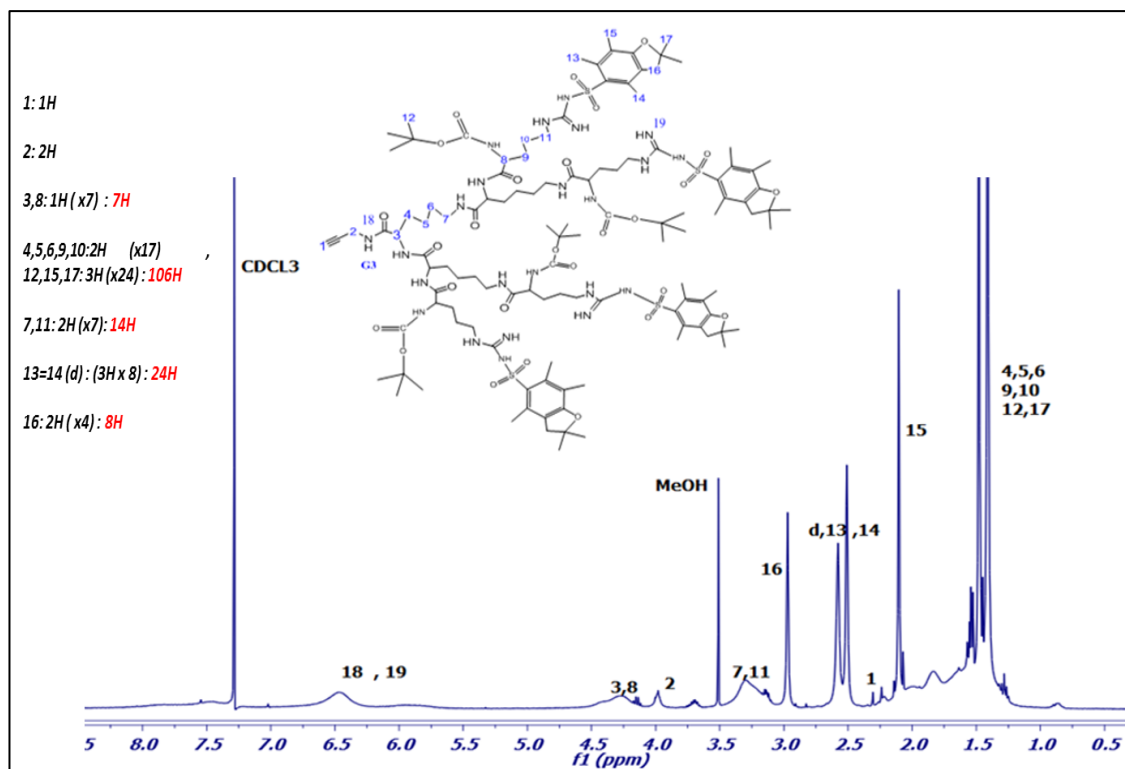


Figure 3-19. ^1H NMR spectrum of dendron PLLA (CDCl_3), d (ppm), 1.139-2.285 (106H, $\text{CH}_2\text{-Lys}$, $\text{CH}_3\text{-Boc}$ and CH_3 PBF), 2.306 (1H, s, CHCCH_2), 2.410- 2.806 (24 H, d, CH_2 PBF), 2.971 (8H, CH_2 PBF) , 3.113-3.336 (14 H, m, CH_2NHCO), 3.969 (2H, $\text{CH}^{\wedge}\text{CCH}_2\text{NH}$), 4.115-4.516 (7H, m, COCH(R)NH), 5.792-6.212(8 H, s, NHCO), 6.324-6.875(12 H, s, NHCO).

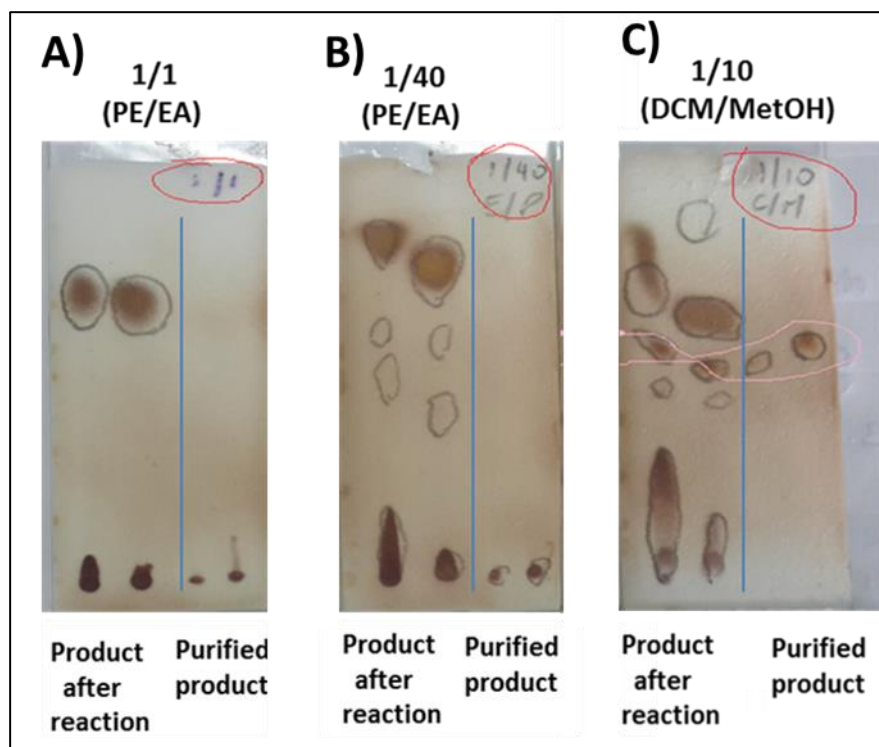


Figure 3-20. 3 TLC plates of PLLA dendrons before and after purification under the presence of: A. 1/1 (V/V) PE/EA solvent; B. 1/40 (V/V) PE/EA solvent and C. 1/10 (V/V) DCM/MetOH solvent. The Brown dots on top shows the traces of the product whereas the ones at the bottoms are traces of impurities.

PLLA dendron were also confirmed by MS (Figure 3-21). The mass is shown as half the mass (2472.41g) with a sodium adduct. The yield of the product PLLA dendron was 7g (73.20%).

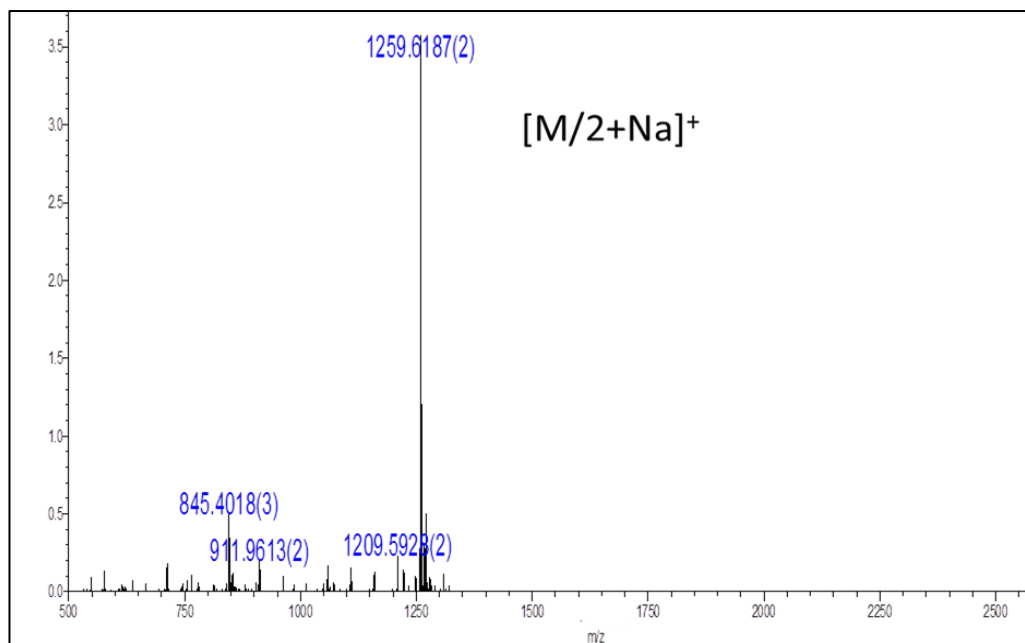


Figure 3-21. ESI-MS of PLLA dendron, $m/z = 1259.6187(M/2+Na)^+$ (calculated 2472.41 for $C_{121}H_{201}N_{23}O_{23}S_4$).

3.4.4. Characterisation of the lysine generation 3 dendron (PLLL⁺)

Figure 3-22 shows the successful synthesis of PLLL containing 8 protective BOC groups (MW=1752.13) due to the highest peak corresponding to half of the mass of PLLL with 2 sodium adducts ($[M+2Na]$ at $m/z = 899.5543$). Similarly, to PLLA, the PLLL structure was confirmed by H^1NMR (Figure 3-23). To produce positive bearing amine based Dendron, the protective 8 BOC were removed and the mass spectrum of $[M + 3H]^{+++}$ at $m/z = 318.24$ (Figure 3-24) was corresponding to the signal of PLLL⁺ dendron, indicating the lysine dendron of generation 3 bearing eight free primary amines had been successfully synthesised.

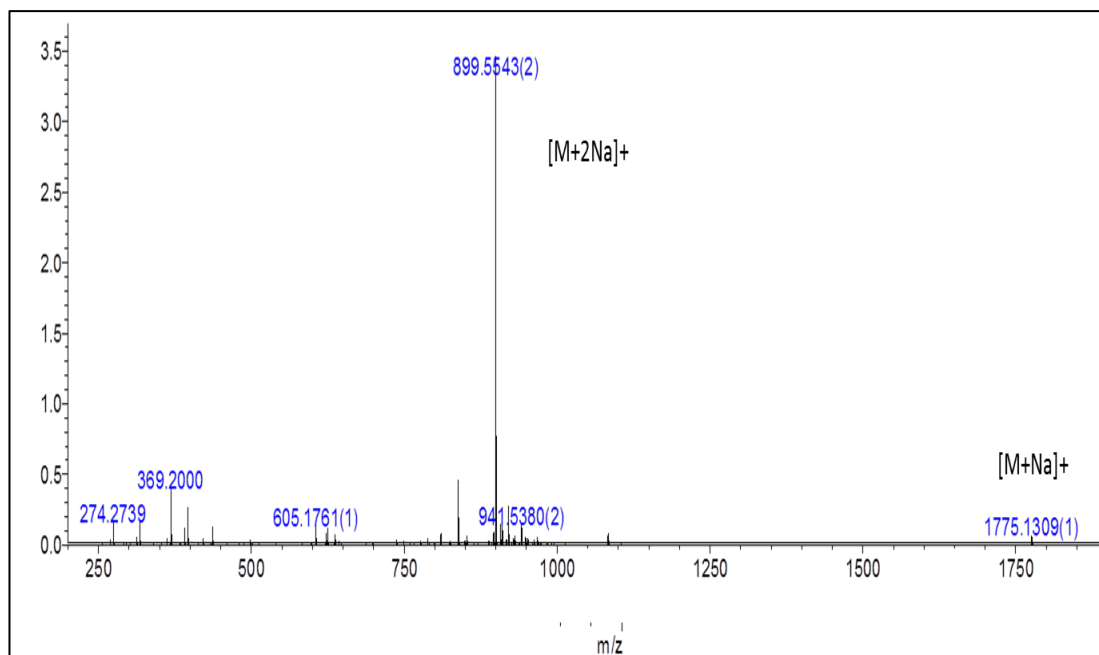


Figure 3-22. ESI-MS of PLL dendron, $m/z = 899.5543 [M+2Na]^+$ (calculated 1752.13 for $C_{121}H_{201}N_{23}O_{23}S_4$).

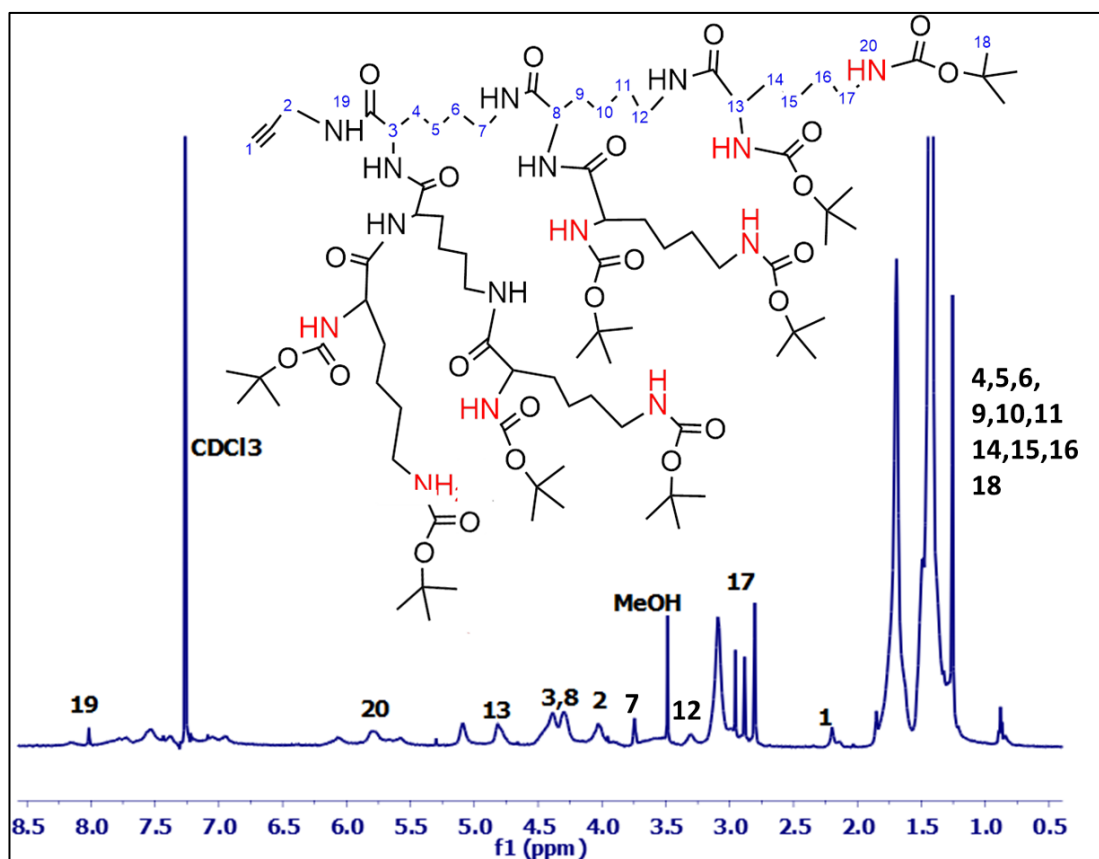


Figure 3-23. 1H NMR spectrum of dendron PLL ($CDCl_3$), δ (ppm), 1.182-1.888 (114H, CH_2 -Lys, CH_3 -Boc), 2.201 (1H, s, $CHCCH_2$), 3.250- 2.755 (8H, q, CH_2NHCO), 3.371 (2H, CH_2NHCO), 3.751 (4H, m, CH_2NHCO), 4.023 (2H, CH^CCH_2NH), 4.598-4.199 (7H, d, $COCH(R)NH$), 4.818 (4 H, s, $COCH(R)NH$), 5.803 (8 H, s, $NHCO$), 8.017 (7H, s, $NHCOCH$).

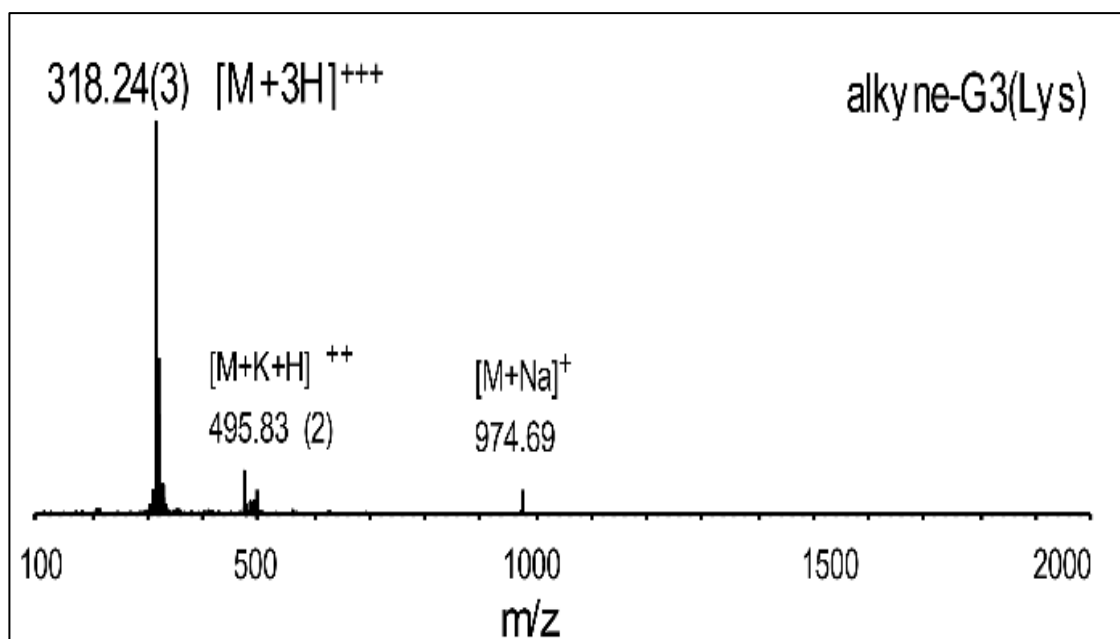


Figure 3-24. The ESI-MS of the deprotected PLL G3 dendron (calculated 952.13).

3.5. Discussion

Dendrimers show several advantages over linear polymers; they have been found to be easily modified, providing an ability to interact with several drugs and genes. In this chapter, we have been concentrating on the synthesis of 2 different peptide-based dendrons. Both dendrons are of the third generation and consist of the same initiator core and interior layer but differ with their periphery. The initiator core consists of an alkyne group that can undergo click reactions with azidated polymers (see chapter 4, 5, 6 and 7). The interior layer is connected with the initiator core and is made up of a repetitive generation of lysine units and arginine. One dendron is characterised by 8 hydrophobic terminal groups (BOC/PBF) whereas the other consists of 8 terminals positively charged amine groups. Results show the successful synthesis of dendrons by the repetitive synthesis process to increase the generation. For each dendron generation, the yield of more than 70% was obtained (74.01% for G1, 78.02% for G2 and 73.20% for G3). This high yield could be due to the use of HOBt as it has been shown that the use of this additive yields to higher product and lower

epimerization (Valeur and Bradley, 2009). Moreover, the method used here seems to be very efficient yielding dendrons in high quantities and in gram scale which is advantageous for extensive biological testing compared to the solid phase method which produces lower generations dendrons in milligram scale (Janiszewska et al., 2016). During activation of carboxyl groups, it is known that the main side reaction known as racemisation can occur however the use of protected BOC amino acids helped to retain the optical purity upon activation of the lysine and arginine at each generation reaction (documents.bachem.com). Moreover, the use of peptides such as lysine and arginine easily helped to detect the violet colour products in TLC plates because of the presence of ninhydrin which interacted with the amino acids to form a Ruhemann'purple complex. The hydrogen bonding interactions in a chloroform solution of each Dendron products were investigated by ¹HNMR which confirmed their structure, and their molecular weight was confirmed by mass spectrometry. As the generation increases from G1 to G3, the molecular weight was also observed to increase, which also suggest an increase in size. The process to obtain the dendrons via divergent synthesis required excess time due to all the process involved such as a reaction and long chromatographic separations, particularly with dendron of generation 3 (Svenson and Tomalia, 2012). However, the process was easily repeated, and higher yield was obtained. We also aimed to obtain the amine terminal bearing generation 3 Dendron by the removal of BOC and PBF from the surface. However, treatment by TFA did not allow the full deprotonation of the dendron. Instead, unexpected mass results were opened (appendix section 9.1&2). The mass of arginine Dendron of the third generation bearing eight amine group at the periphery was expected to be 1063.73. However, products obtained after deprotonation did not match to the mass

expected. Also, the poor solubility in water of the deprotected products confirmed the unsuccessful deprotonations. There is a possibility that the dendrons did undergo racemisation during deprotection reaction, therefore, resulting in different products. For this reason, a new way was designed, lysine dendron of third generation bearing 8 BOC groups was synthesised following the method of Ma et al., 2013 and Li et al., 2013. To then obtain a terminal arginine structure we proposed to conjugate the terminal amine groups of lysine from PLLL⁺ with guanidine groups (see chapter 7). The fact that Dendrons can be modified at any point to obtain desired terminal functional groups makes them very special and the ideal molecules for drug and gene delivery. The successfully synthesised dendrons PLLA and PLLL can be conjugated into polymers to form nanocarriers for drug and gene delivery. PLLA can be used to carry hydrophobic drugs and improve their solubility, whereas, PLLL bearing positively charged amine can easily interact with negatively charged DNA for gene delivery.

In Conclusion, this chapter presents a deep understanding of the production of dendrons and various alternations choices to produce Dendron with different terminal groups.

CHAPTER 4. MICELLAR DENDRONS FOR THE DELIVERY OF DOXORUBICIN IN VITRO CELL MODELS

4.1. Introduction

Chemotherapy is one of the most effective therapies against many types of cancer. However, chemotherapeutic agents that are toxic to tumour cells are usually also toxic to healthy cells (Ahles and Saykin, 2007; Cheek, 2012; Huang et al., 2017), suffer from resistance or present low bioavailability due to their poor solubility in water (Kalepu and Nekkanti, 2015), therefore results in severe side effect or in reduced therapeutic efficiency. For this reason, many new carrier systems have been developed for targeted drug delivery to achieve desirable efficiency and to minimise side effects. It is, however, important to note that any carrier systemically administered will also have to overcome many obstacles within the body. To reach the targeting site, it is essential that the carrier resists from plasma proteins, opsonisation (or evade uptake by macrophages), clearance by renal filtration and degradation by endogenous nucleases (Alexis et al., 2008).

Moreover targeting tumours in large organs of the body is very challenging due to their very complex anatomical organisation characterised by various barriers that stop foreign materials. Examples include the Blood-brain barrier (BBB) in the brain and barriers preventing access of parenchymal cells by Sinusoidal endothelial cells and Kupffer cells clearance in the liver.

The brain survives from a system consisting of neural cells (brain parenchyma, 70-80%), the vascular system (3-5%) and the brain interstitial system (ISS, 15-20%). The two main functional neural cell types are neurons and glial cells

(astrocytes, oligodendrocytes and microglia) (Lyon et al., 2017; Lei et al., 2017; Fumagalli, Ortolano and De Simoni, 2014). The capillaries in brain tissues contain some barriers that separate the circulating blood from the brain parenchyma, including the most selective barrier blood-brain barrier (BBB) (Abbott, 2005; Kipnis, 2016). In the case of a Brain tumour, the BBB is breached therefore can allow the passage of immune cells into brain parenchyma. It has been reported that higher grade brain tumours can lead to exacerbated irregular vascularisation, tumour necrosis, BBB disruption, antigen expulsion and elevated interstitial pressure of the fluid that can influence therapeutic infiltration (Charles et al., 2011; Dubois et al., 2014; Goel et al., 2011). Although the BBB is known to be leaky in a brain tumour, there is still presence of intact BBB in some region that present barriers for drug delivery and immunotherapy (Van Tellingen et al., 2015), the BBB can prevent the passage of 98% of small molecular drugs and 100% of large molecular drugs within the bloodstream (Zhou et al., 2013).

On the other hand, the liver is composed of 80% of parenchymal cells (hepatocytes cells) and 20% of non-parenchymal cells (sinusoidal cells). The sinusoidal cells comprise 70% of sinusoidal endothelial cells (SECs), 20% of Kupffer cells (KCs, the liver macrophages), 10% of hepatic stellate cells (HSCs, the fat-storing cells or Ito cells) and less than 1 % of pit cells (natural killer cells) (Do et al., 1999; Sasse, Spornitz and Piotr Maly, 1992; Blouin, 1977; Knook and Sleyster, 1980 ; Jacobs et al., 2012 ; Mohar et al., 2015). Moreover, like all the other endothelial cells within the body, the sinusoidal endothelial cells form highly specialised capillaries with endothelial lining that contains fenestrae which then provides an open pathway between the sinusoidal lumen and the

space of Disse in which numerous microvilli from parenchymal liver cells protrude (Braet et al., 2009; Jacobs et al., 2012). Although these fenestrations can provide direct access for delivery systems to hepatocytes cells, they can also restrict the entrance of large particle sizes since the fenestrae measure 100 to 200 nm. Also, the efficiency of delivery systems can be limited by the uptake of sinusoidal endothelial cells and Kupffer cells before reaching to hepatocytes cells. The sinusoidal endothelial cells have been reported to be scavengers cells that can internalise particles of sizes up to 230nm whereas Kupffer cells present in sinusoid capillaries account for 80-90% of resident macrophage in the entire body, therefore, forming the major part of the RES system (Mishra et al., 2013; Shiratori et al., 1993; Xu et al., 2008; Jacobs et al., 2012).

As we have described before in chapter 1, particle size, surface properties such as charge, solubility and targeting ligands to cells of interest are the key importance to overcome these challenges.

4.2. Aims and objective

The specific above obstacles faced by delivery systems in large organs have led us to develop a new delivery system that can deliver hydrophobic therapeutic agents successfully to their target. Nanoparticles systems can be the primary way of reducing drug elimination and also can be a way to overcome the BBB challenge (Von Maltzahn et al., 2011).

Since we have already successfully synthesised hydrophobic arginine dendron bearing terminal PBF and BOC groups (PLLA-PBF/BOC) that can form a cavity for drugs. We propose the synthesis of a polymeric micellar dendrons based

system capable of delivering the drug Dox into liver or brain tumour cells. To form targeting micelles, the hydrophilic polysaccharide pullulan is chosen because of its recognition of Asialoglycoprotein receptor (ASGPR) expressed uniquely and in large numbers on hepatocytes (Li et al., 2016). We, therefore, hypothesise that the amphiphilic system consisting of pullulan conjugated hydrophobic arginine dendron (P-PLLA) can self-assemble into nanocarriers in aqueous solution and therefore encapsulate hydrophobic drugs such as Dox for the treatment of hepatic cancer and brain tumours. Our primary objective is to form nanocarriers of small sizes so that the pullulan bearing conjugate could gain access to hepatocytes or glioblastoma cell by passing through the fenestrated endothelium of the sinusoid or efficiently bypass the BBB barriers. Once inside the cells of interest, the drug can be released at lower pH inside cancerous cells and reach their site of action to stop or reduce cell proliferation. Specifically, we aimed to develop and characterise the nanocarrier system P-PLLA and investigate:

- 1) the loading and encapsulation efficiency of doxorubicin;
- 2) the stability of the blank and loaded nanoparticles;
- 3) the drug release studies;
- 4) the toxicity against an experimental brain and liver cancer cell line in vitro and;
- 5) the ability to uptake the doxorubicin-loaded nanoparticles into brain and liver cancer cells.

4.3. Methodology

4.3.1. Synthesis of the arginine dendron of generation 3 (PLLA)

Refer to chapter 3

4.3.2. Pullulan azidation (PN3)

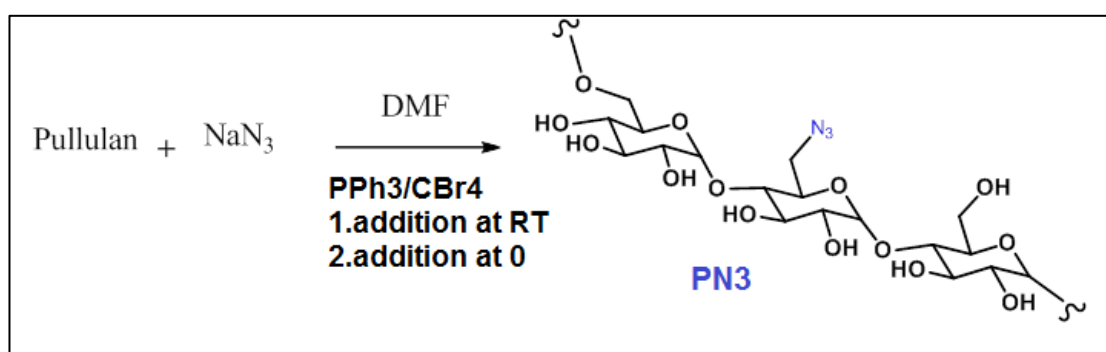


Figure 4-1. Synthesis equation of the azidated pullulan PN3.

Two reactions were carried out at the same time. First, 0.98g (1mmol, the equivalent of anhydrous glucoside units) of Pullulan and 3.15g (8mmol) NaN_3 were dissolved in 30mL of anhydrous DMF at 80°C for 2 hours under N₂ atmosphere. After cooling to RT, an ice bath was added in one flask, and the other flask was left at RT. A freshly prepared solution of PH₃P (2g in 5ml DMF, 1.6mmol) was then added in each flask followed by the addition of a CBr₄ solution (3g in 5ml DMF, 1.6mmol). The ice bath was removed after 30min of stirring, and both reactions were allowed to stir for 20hrs at RT. The solution was then exposed to air and methanol (5ml) was added and left to stir for 5 min to quench the reaction. Finally, the azidated pullulan was precipitated into 300ml of ethanol. The precipitate was recovered by centrifugation and then washed with 100mL of a 7:3 ethanol/water solution followed by 100mL ethanol. The solid obtained was then allowed to dry at 60°C overnight in a vacuum.

4.3.3. Click reaction between azidated pullulan and PLLA dendron

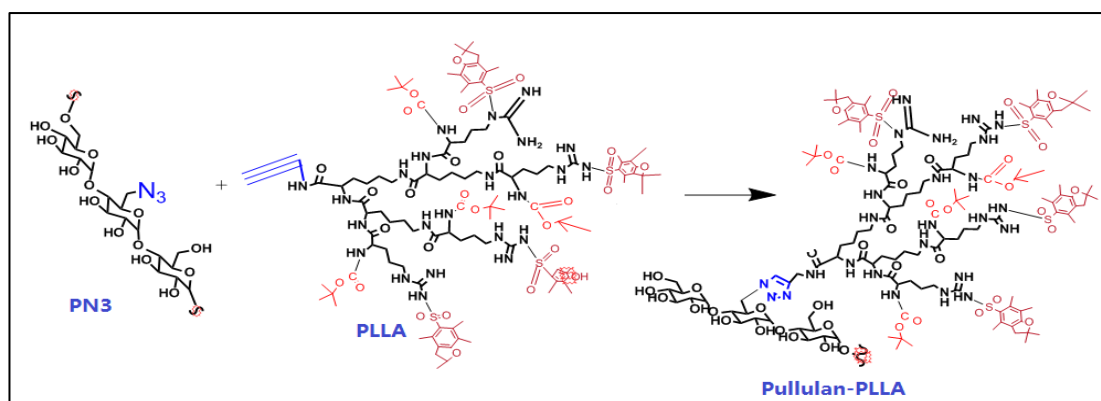


Figure 4-2. Synthesis equation of Pullulan clicked PLLA (PG3or P-PLLA).

PLLA (2.35g, 2 mmol) and PN3 (0.1g, 1mmol) were added successively in 30 ml of DMSO and stirred to dissolve under an N₂ atmosphere at 50 °C for 1hr. The mixture was then brought to RT and passed into argon under stirring. Then 5ml of a deoxygenised aqueous solution of sodium L-ascorbate (0.075g, 0.4mmol) and 5ml of deoxygenised blue aqueous solution of copper (II) sulphate pentahydrate (0.048g, 0.2mmol) was injected successively into the reaction. The yellowish resultant reaction mixture was stirred under argon for 55 hrs at 40 °C. After the reaction, the flask was left to stir in the presence of oxygen to allow de-activation of the agents. A small amount of EDTA was added and left to stir for 2-3 hrs until the solution turned blue. The resulting solution was dialysed against distilled water containing a lower amount of EDTA for 1 day and against distilled water for 2 days (MWCO=3500). The final yellowish solution was then lyophilised to yield the product PG3.

4.3.4.Characterisation

The characterisation was carried by FTIR, NMR and EA, the details of each method are given in chapter 2. In addition, Chapter 2 contain the method details

of micelle formation of P-PLLA, Dox loading and drug release, characterisation details by SEM, TEM and DLS, stability studies (CAC studies), cell culture, in vitro cytotoxicity in 3T3, Hek293, U251 and HepG2 cells, flow cytometry, FACS studies and apoptosis.

4.4. Results

4.4.1. Characterisation of the azidated pullulan

Different conditions of azidation reactions were carried out to investigate the best parameter for giving more azidation. Table 4-1 lists the conditions employed as well as elemental analysis with the calculated DS (defined here as the degree of substitution per anhydroglucose unit). As seen, ten equivalent molar of sodium azide gave a higher conversion (232.16%) in a condition where equimolar quantities of $\text{Ph}_3\text{P}/\text{CBr}_4$ were added in the presence of ice bath compared to a lower conversion (155.04%) when added at room temperature.

Table 4-1. Determination of the substitution degree of azidated pullulan by elemental analysis.

Pullulan derivative/% element	Pullulan: NaN_3 (temperature)	C (%)	H (%)	N (%)	DS (% per unit)
Pullulan	–	40.33	6.66	–	–
PN₃(1)	1: 10 (RT)	39.34	5.68	11.86	155.04%
PN₃(2)	1:10 (0°C)	32.94	5.62	14.87	232.16%
PN₃(3)	1:9 (0°C)	39.51	6.67	5.93	77.19%
PN₃(4)	1:8 (0°C)	39.24	6.56	3.74	49.02%

In addition to the Elemental analysis, the FTIR analysis also confirms the successful azidation to pullulan. Figure 4-3 shows the FTIR spectra for pullulan

and PN_3 . On both Spectra, broadband appeared at 3401 cm^{-1} due to $-\text{OH}$ stretching and a sharp band at 2918 cm^{-1} was characteristic of C-H stretching.

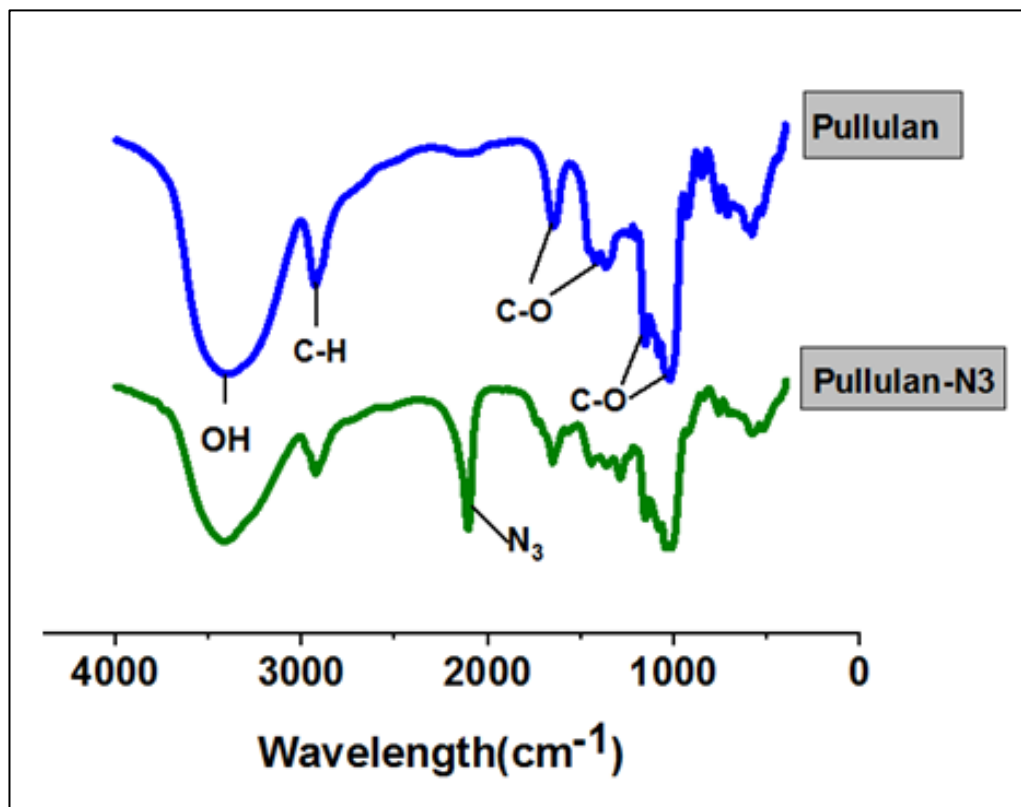


Figure 4-3. IR spectrum of Pullulan and Azido-Pullulan (4) PN_3 containing a strong C-N_3 stretching vibration at 2107 cm^{-1} which matches that of published data.

The peaks at 1413 , 1156 , 1014 and 590 cm^{-1} were due to C-O-H bending, C-O-C stretching, C-O stretching and alpha configuration, respectively. The band at 1646 cm^{-1} corresponds to the vibrations of the C-O-C bond and glycosidic linkage (Sugumaran et al., 2013; Saber-Samandari et al., 2014). The FTIR spectra of the PN_3 show an extra strong C-N_3 stretching vibration at 2107 cm^{-1} which confirm the successful azidation.

4.4.2. Characterisation of clicked $\text{PG}_3(\text{BOC}/\text{PBF})$ product

A classic copper-catalysed reaction was used to synthesise the pullulan conjugate $\text{PG}_3(\text{BOC}/\text{PBF})$ by reacting the alkyne-functionalized PLLA dendron

with the azidated pullulan containing 77.19% of azide groups. In Figure 4-6, three spectra are given for comparison of peaks produced by azidated pullulan, dendron of generation 3 PLLA and their clicked product.

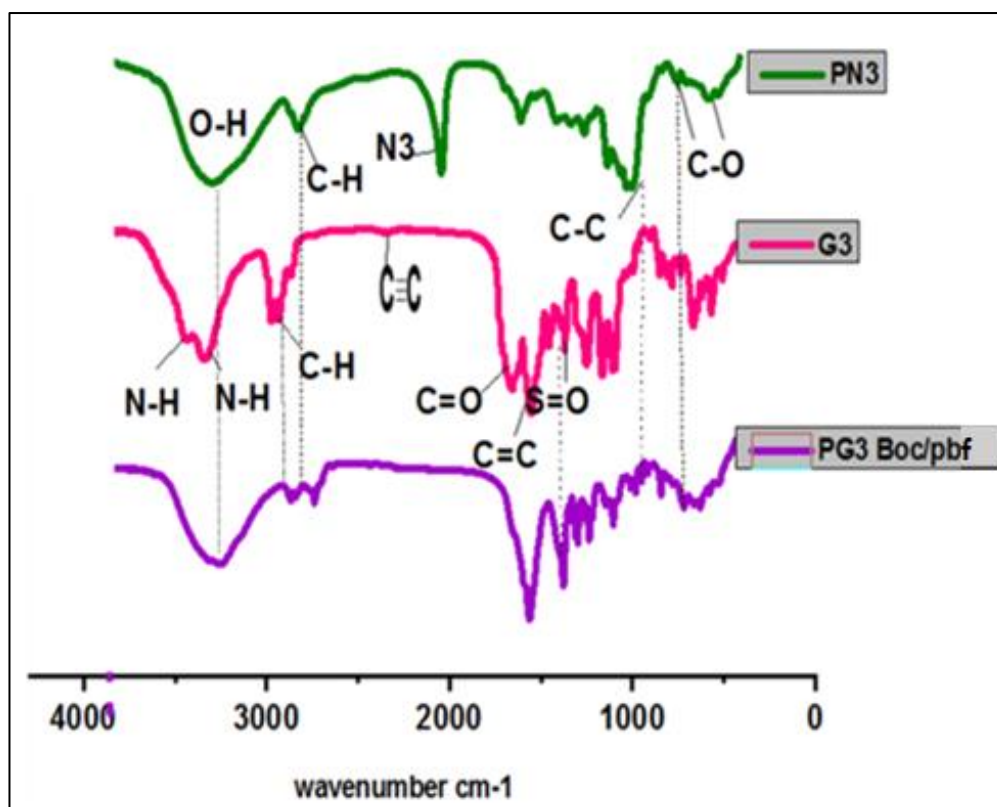


Figure 4-4. FTIR spectrum of the azidated Pullulan, dendron of generation 3 PLLA and clicked product PG3 BOC/PBF.

All peaks present from PN3 and PLLA are also observable in the product PG3(BOC/PBF) spectrum suggesting the strong click reaction. The presence of pullulan is confirmed by the adsorption peak at 3000-3500 cm⁻¹ due to O-H stretch and 2932 cm⁻¹ due to C-H stretch. The N-H stretch at 3348 cm⁻¹ of G3 is overlapped with the O-H stretch of pullulan whereas the absorption peak at 1532 cm⁻¹ due to C=C and 1375 cm⁻¹ due to S=O present in the PBF groups of G3 are also present in the clicked product. Furthermore, the disappearance of the azido group peak at 2107cm⁻¹ in PN3 and the alkyne peak at 2347 cm⁻¹

assigned to the dendrons G3 suggest the full clicked conjugation of G3 into pullulan.

Moreover, the ^1H NMR spectra of the clicked product PG3(BOC/PBF) showed a signal at 7.90 ppm (He) indicating the triazole proton present in the 5-membered heteroatom ring formed from the click chemistry.

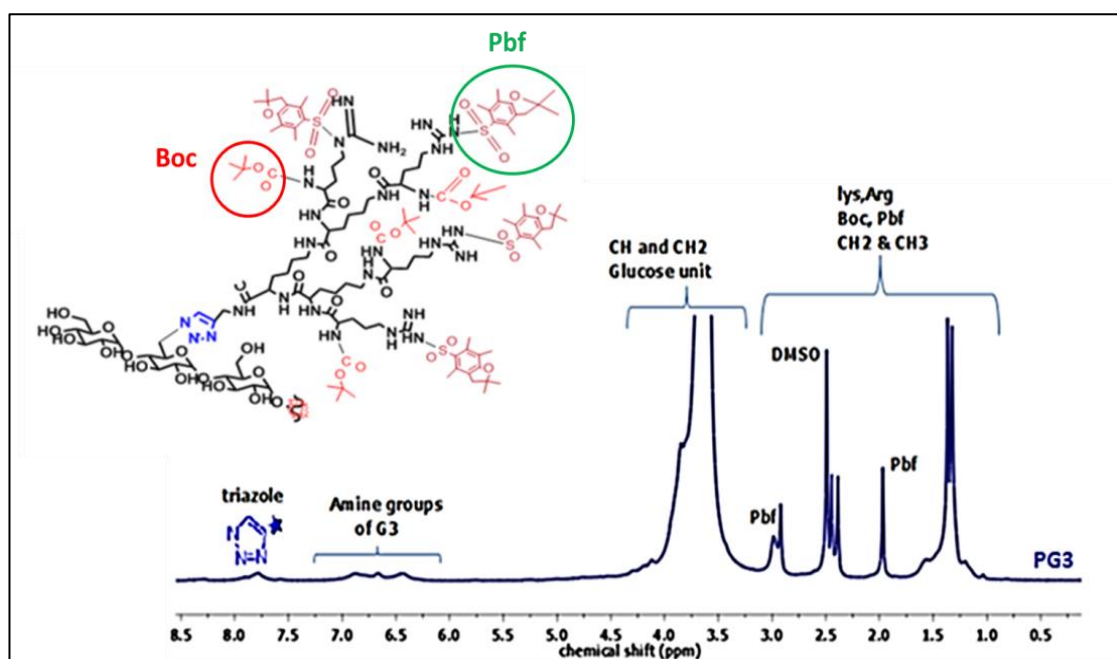


Figure 4-5. ^1H NMR (400 MHz, DMSO- d_6) of clicked PG3.

The characteristic peaks in ^1H NMR corresponds to particular hydrogens in the structure: 0.734-1.154 (d, 12H, CH₃-PBF, G3); 1.546 (s, 24H, CH₃-BOC-PBF, G3); 1.964-2.103 (s, 12H, CH₃-PBF, G3); 2.410- 2.806 (d, 24 H, CH₃-PBF, G3); 4.8 (d, 66H per 100 glucose units, pullulan C1 H (1-4)); 5.0 (s, 33H per 100 glucose units, pullulan C1 H (1-6)); 7.90 (s, 1H, NCHCH, triazole ring). Also, the graft level of G3 dendrons onto the azidated pullulan was 20.32%, according to the integral intensities of Hh in G3 and Ha in pullulan.

4.4.3. The self-assembly of P-PLLA(BOC/PBF) or PG3

PG3(BOC/PBF) form an amphiphilic system that could self-assemble to form micelles in aqueous media due to the enhancement of the hydrophobic effect. The size distribution of PG3 based nanoparticles (1mg/ml) in distilled water was measured by dynamic light scattering (DLS); TEM; and SEM (Figure 4-6). PG3 showed an average size of 87.07nm with a PDI of 0.241. Moreover, TEM and SEM images showed monodispersed spherical nanoparticles with an average size similar to the one obtained with DLS analysis.

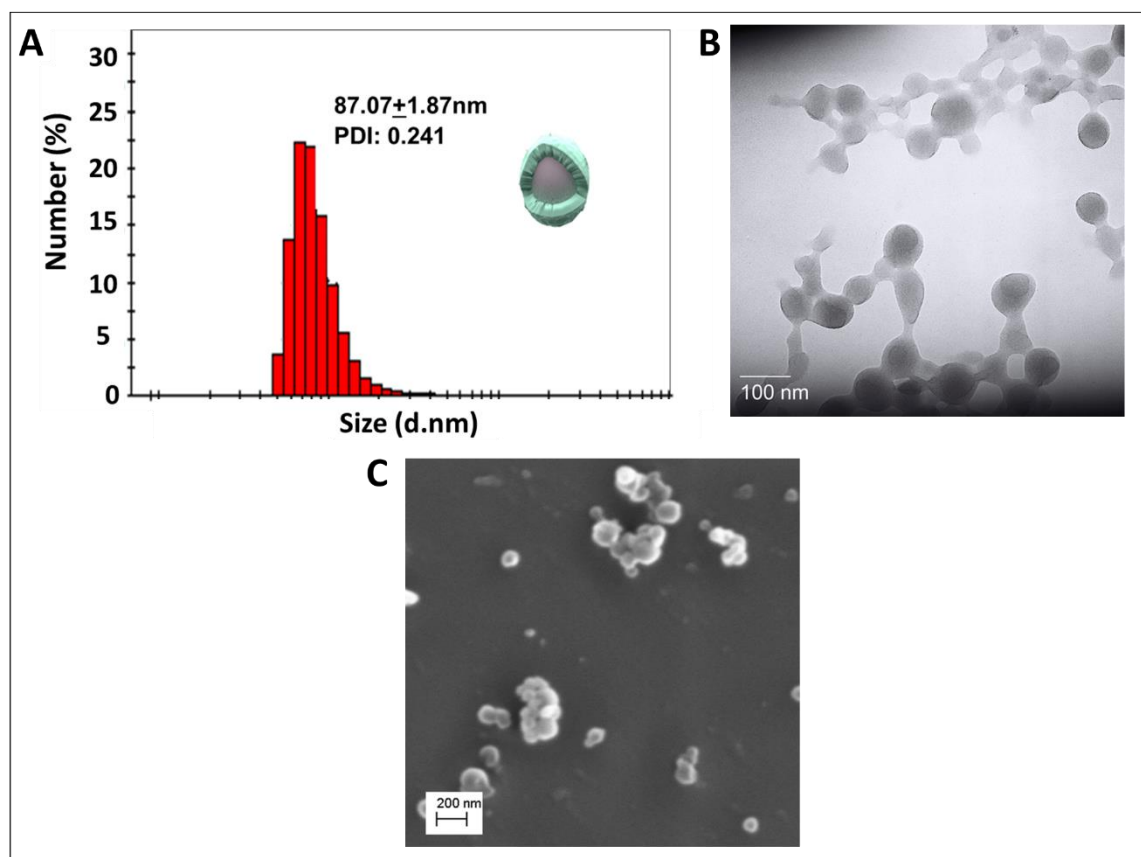


Figure 4-6. Size distribution and morphology studies of blank of PG3 by A. DLS, B. TEM and C. SEM.

4.4.4. CAC and Stability studies of PG3(BOC/PBF) micelles

The CAC of the PG3 was determined by fluorescence technique, using pyrene as a hydrophobic probe. Figure 4-7 shows the plots of the fluorescence intensity

ratio I337 / I334 against the logarithm of the PG3 micelles concentration. For PG3, a value of 10.47ug/ml was obtained, which indicates high stability of mixed micelles and excellent stability upon dilution in body fluid.

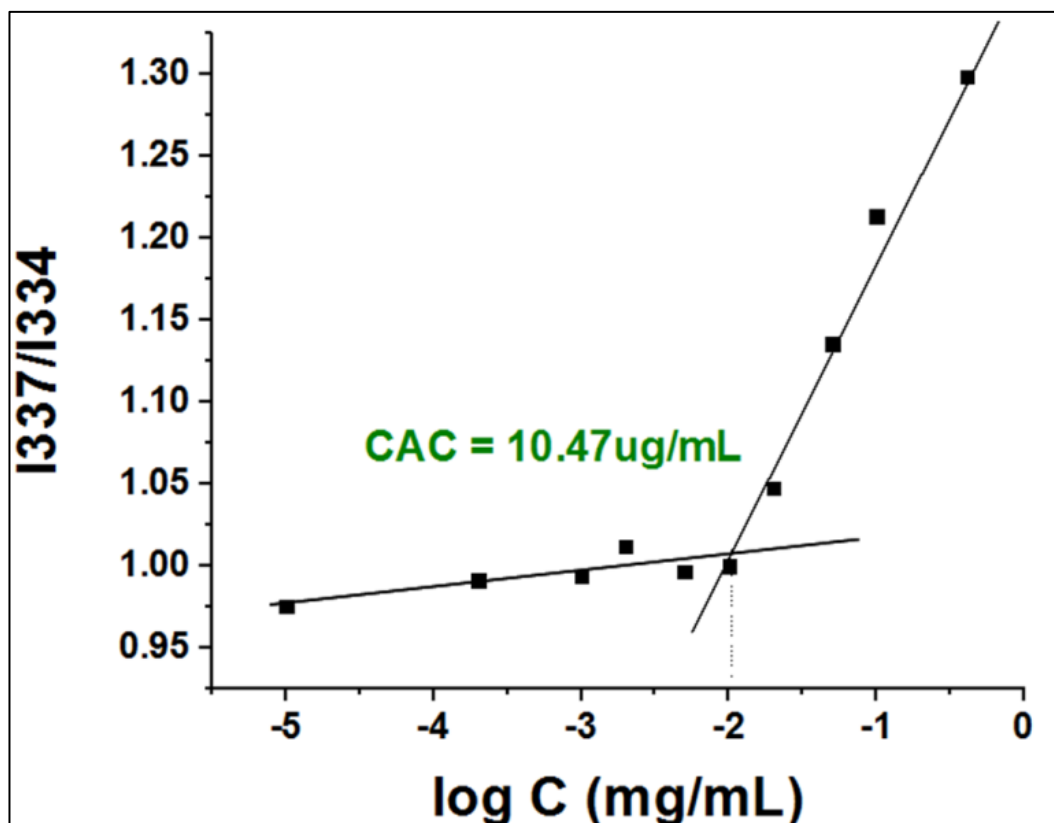


Figure 4-7. Critical association concentration of PG3 measured using the fluorescent dye pyrene.

4.4.5. Drug loading into P-PLLA (P-PLLA-Dox)

The drug doxorubicin was physically entrapped and stabilised in the hydrophobic dendron core of the micelles PG3 via hydrophobic-hydrophobic interaction.

The loading and encapsulation efficiency were determined using the line of equation of the standard curve of doxorubicin being $y=5.0939x-0.5728$ (Figure 4-8)

Drug loading was carried out with a different weight ratio between the carrier and the drug Dox. As seen in table 4-2, the loading content of P-PLLA-Dox at

ratio 5:1, 2:1 and 1:1 micelle was 19.17%, 22.77% and 27.14%, respectively whereas the encapsulation efficiency was 64.15%, 53.20% and 40.64%, respectively.

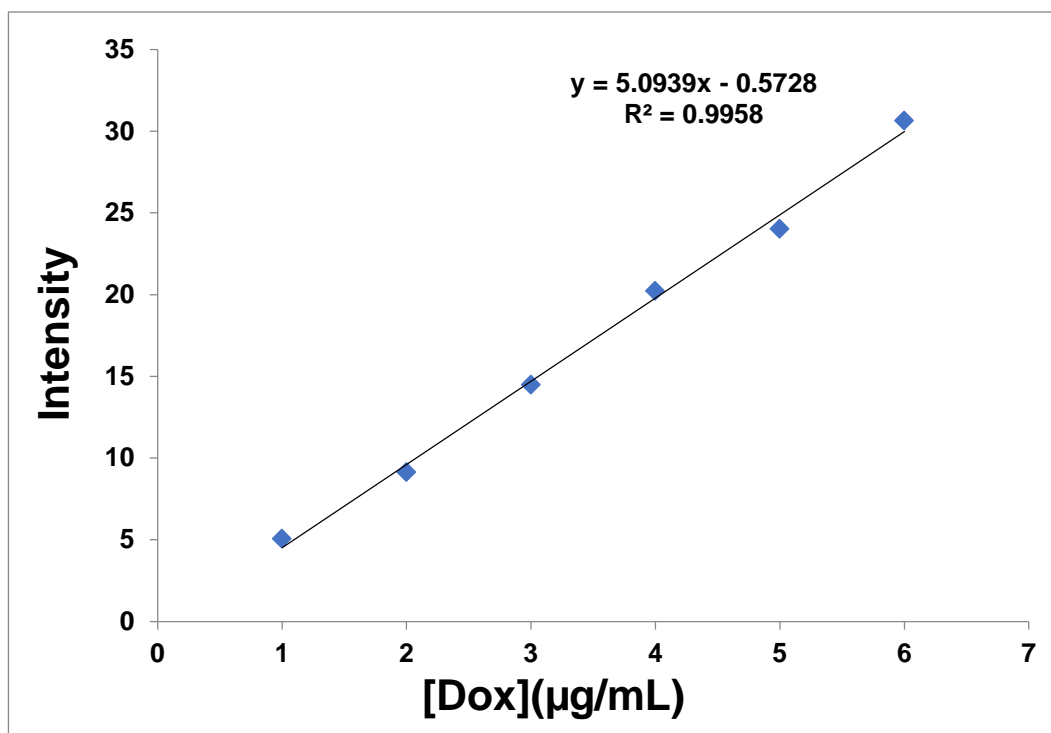


Figure 4-8. A standard curve of Doxorubicin determined at 480nm.

PG3 loaded with Dox at ratio 5:1 showed the highest encapsulation efficiency with excellent distribution of PG3-Dox in aqueous media and was therefore used for further studies.

Table 4-2. Drug loading content (LC) and encapsulation efficiency (EE) of P-PLLA

PG3:DOX (ratio)	PG3(BOC/PBF)	
	LC%± Std.dev	EE% ±Std.dev
5:1 (20%)	19.17±1.50	64.15±6.25
2:1 (50%)	22.77±2.92	53.20±5.35
1:1 (100%)	27.14±1.75	40.64±4.66

DLS, TEM and SEM measurements showed an increase of the average size of the Dox-loaded P-PLLA nanoparticles with a mean of 138nm compared to blank

P-PLLA micelles (Figure 4-9). The successful loading of the drug is therefore evidenced by the increase in size because the Dox molecules loaded into the micelles increased the inner space of the micelles (Zhou et al., 2016; Fan et al., 2018).

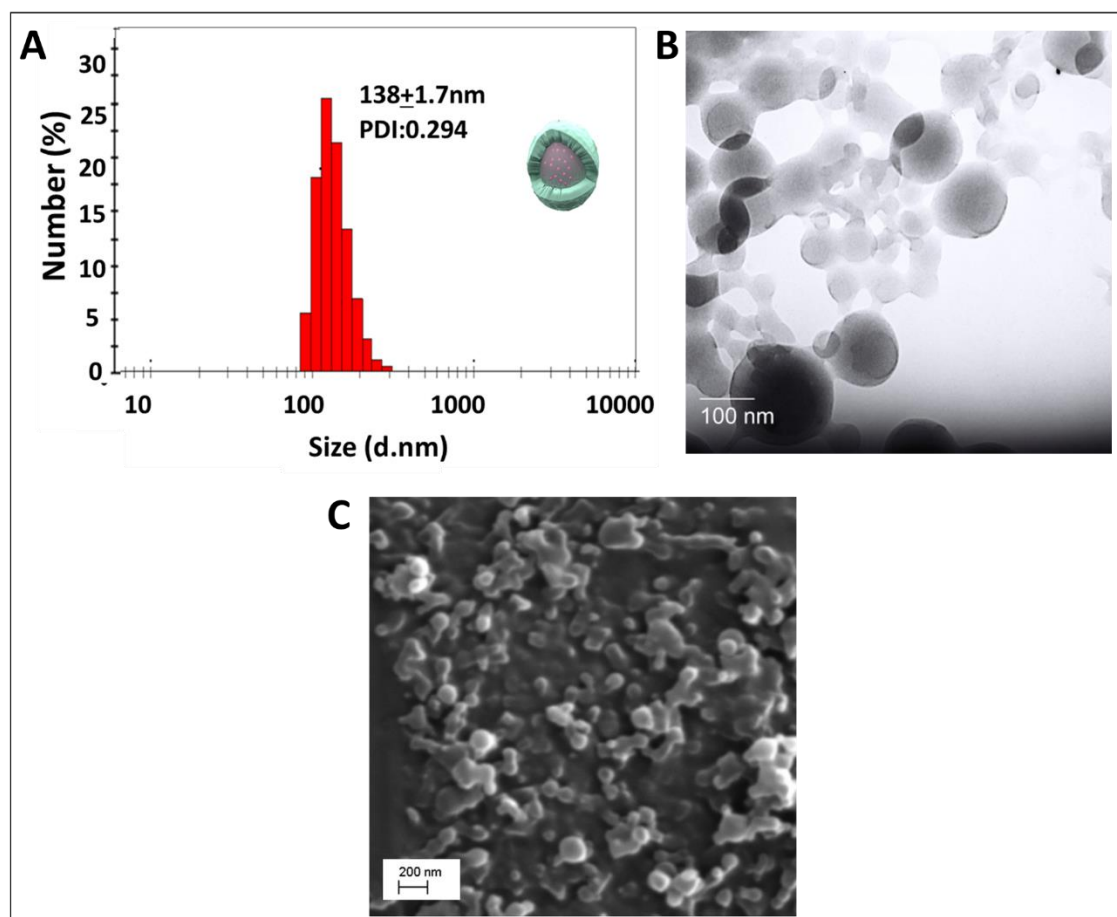


Figure 4-9. Size distribution of DOX-loaded PG3 micelles in water determined by A. dynamic light scattering and B. TEM and C.SEM.

4.4.6. In vitro drug Release studies of P-PLLA-Dox NPs

Since the pH change occurs at many specific or physiological sites in the body, the release of Dox from PG3 was investigated at different pH (5.0, 6.8 and 7.4).

Throughout 60hours, the higher sustained release rate of up to 53% of the drug load was observed under pH 5 condition (intracellular environment pH) whereas only 23 % was released at pH 6.8 and 16% at pH 7.4 (blood pH). This phenomenon can be due to the protonation of the amine group in Dox (NH_3^+)

with hydrophilicity enhancement at lower pH values (Quader et al., 2014 and Ma et al., 2015).

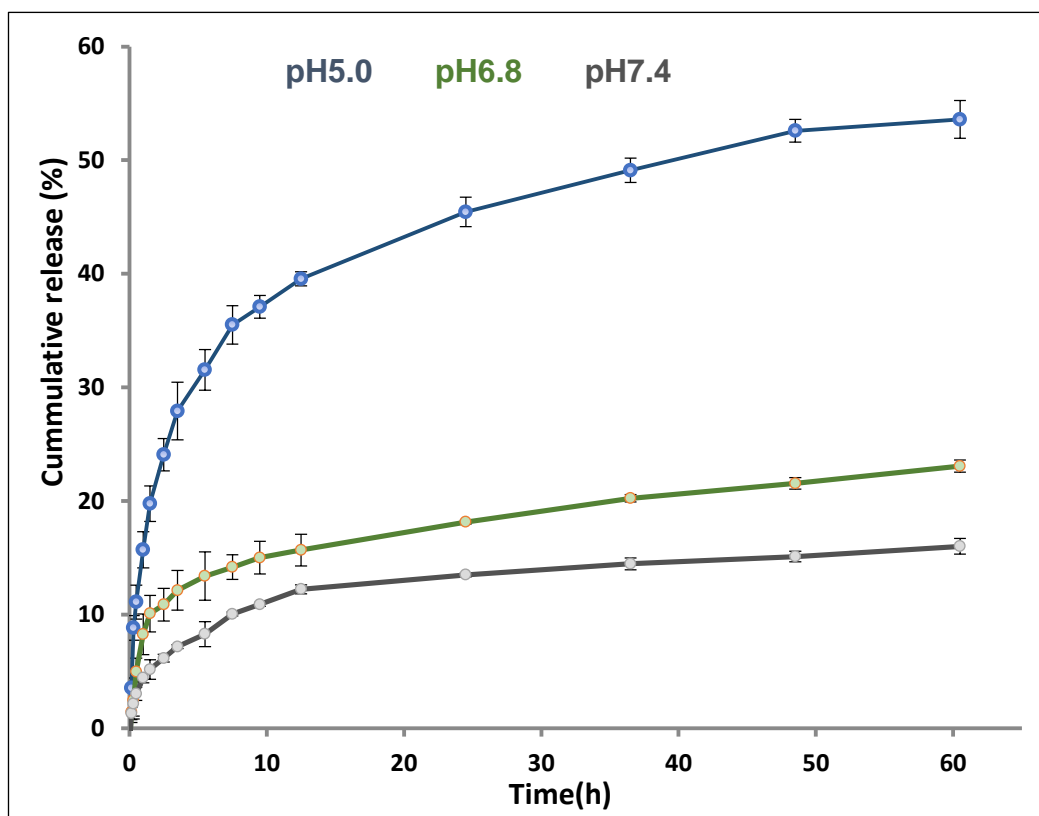


Figure 4-10. pH sensitive release of Dox from PG3 (BOC/PBF) micelles.

4.4.7. Stability of blank and Dox-loaded PG3 micelles

The micelles formulations were stored as a freeze-dried powder (Figure 4-11A) at -20°C , whereas blank and Dox-loaded micelle suspension in DI water (Figure 4-11B&C) was stored at 4°C for 3 months.

From the stored sample, no sedimentation, no precipitation, no aggregations or phase separation were observed in 3 months stability test showing that the micelles were stable, and that no chemical degradation took place.

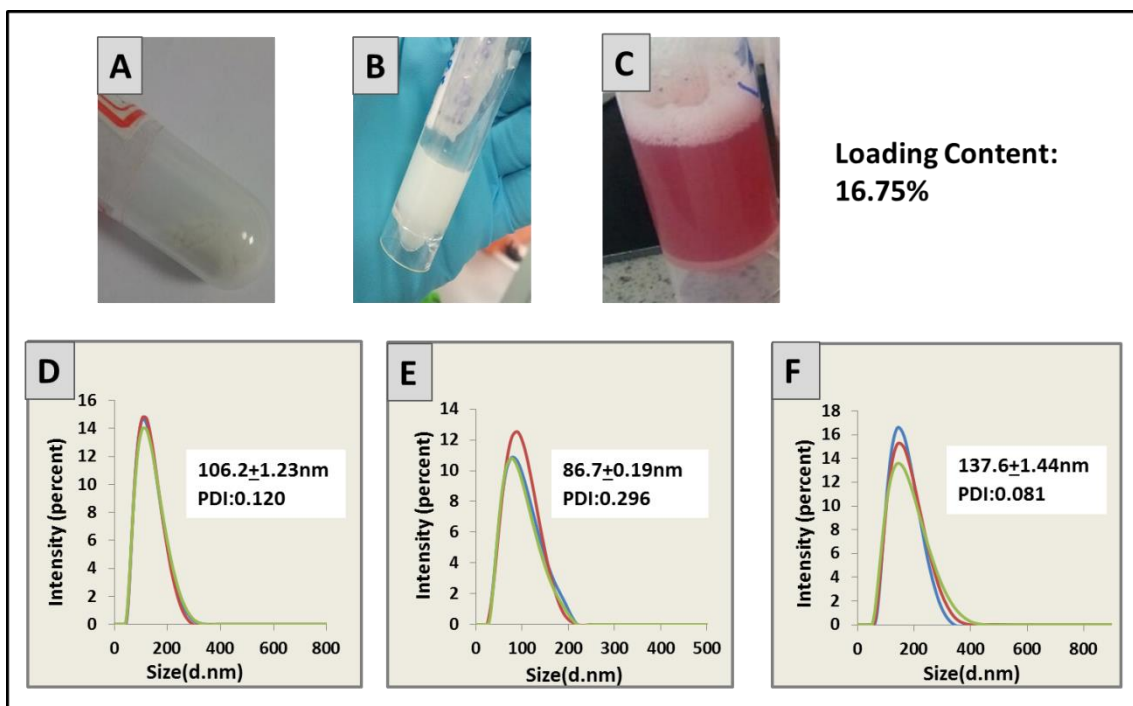


Figure 4-11. Images and size distribution of blank PG3 and loaded Dox-PG3 micelles stored for 3 months: A. lyophilised PG3 micelles in powder form; B. Blank PG3 micelle suspension in DI water; C. Dox-loaded PG3 micelle suspension in DI water; D. Size distribution of blank freeze dried PG3 powder by dynamic light scattering; E. Size distribution of blank PG3 suspension in DI by dynamic light scattering; F. Size distribution of Dox-Loaded PG3 suspension in DI by dynamic light scatter. Note: Size distribution of the samples were determined in triplicate (peak colours blue, red and green in D, E and F).

Furthermore, changes in size were also monitored; there were no significant changes in sizes for the micelles in suspensions showing the high storage stability. Although micelles in dried form showed a higher particle size of 106nm, they showed good stability profile. Also, in 3 months, there was a slight decrease in the drug content from 19.17% to 16.75% this is maybe due to the slow release of Doxorubicin from micelles.

4.4.8. Cytotoxicity of Dox.HCl, blank and loaded Dox-P-PLLA

The in vitro cytotoxicity study of the blank P-PLLA micelles was carried out against normal cell lines (Hek293 and NIH3T3) and cancerous cell lines (HepG2 and U251) for 72hours. Figure 4-12 shows that all cell types exposed to the blank PG3 micelles stayed more than 80% confluence in the period of

72hours. The blank micelles, therefore, had no cytotoxicity in the concentration of 0-100 μ g/mL. In comparison between cell lines, normal cells Hek293 and NIH3T3 were almost 95% confluent, which indicates the safe use of blank micelles PG3 as a nanocarrier for cancer therapy. The cytotoxicity of Dox loaded P-PLLA and their in vitro antitumour effect was also investigated against HepG2, U251, Hek293 and NIH3T3 cells. As seen in Figure 4-13, the toxicity of P-PLLA-Dox exhibited concentration and time dependence against each cell lines. As the concentration of Dox.HCl and P-PLLA-Dox concentration increased from 0 to 200 μ g/mL, cytotoxicity to cells also increased.

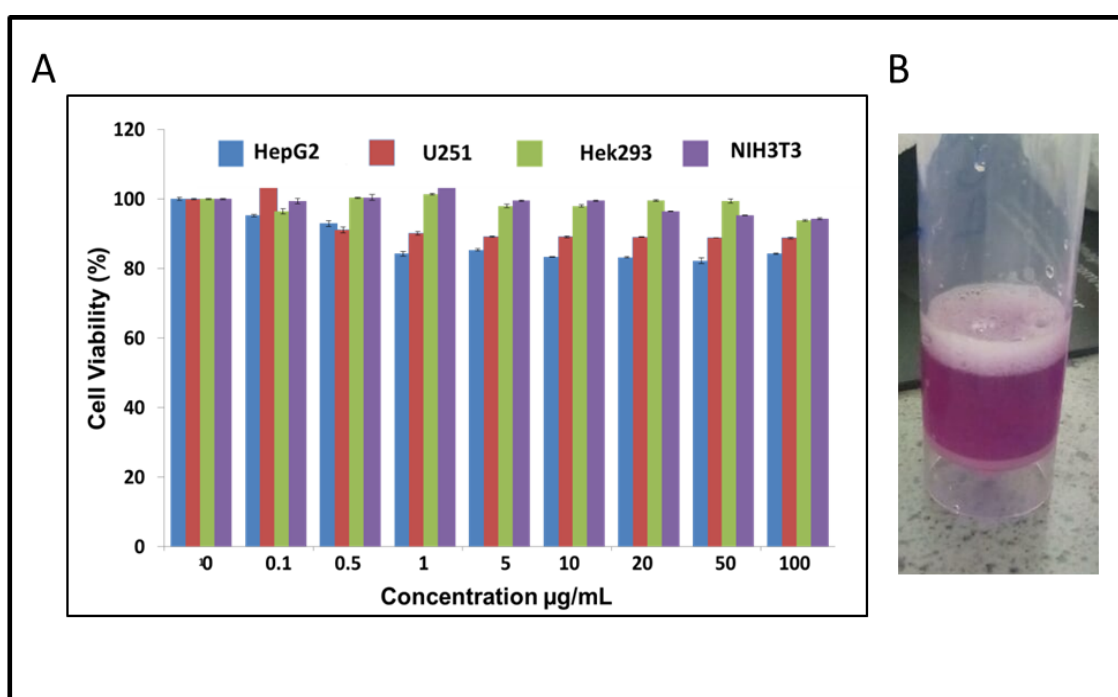


Figure 4-12. A. Biocompatibility assay of HepG2, U251, Hek293 and NIH3T3 cells against blank PG3 nanoparticles for 72h B. Image of the PG3 micelles suspension in DMEM containing 10% (V/V) FBS.

Table 4-3 shows the calculated IC₅₀ values of free Dox.HCl and PG3-Dox in each cell lines at a varying time. As seen the IC₅₀ of loaded Dox in PG3 was always higher than that of free Dox.HCl in each cell and at all-time intervals. These observations might be because of hydrophilic Dox.HCl could be easily

transported into the cells and accumulated rapidly in nuclei, whereas hydrophobic Dox-loaded P-PLLA NPs may be internalised by endocytosis followed by the disassembly of the nanoparticles, releasing Dox from cytosolic compartments in a sustained manner and continuously producing a toxic effect after incubation (Eliaz et al., 2004).

Table 4-3. Calculated IC50 values of free Dox.HCl and PG3-Dox in HepG2, U251, Hek293 and NIH3T3 cell lines at a varying time

Cells lines/time of incubation		IC50 ($\mu\text{g}/\text{mL}$)			
		HepG2	U251	Hek293	NIH3T3
24h	Dox.Hcl	0.084	0.256	6.876	5.876
	PG3-Dox	1.765	3.876	10.874	9.876
48h	Dox.Hcl	0.058	0.154	3.857	3.758
	PG3-Dox	1.246	2.765	8.975	8.158
72h	Dox.Hcl	0.049	0.096	2.276	1.745
	PG3-Dox	0.276	1.176	7.847	5.654
96h	Dox.Hcl	0.041	0.056	0.876	0.654
	PG3-Dox	0.174	0.976	5.875	4.643



Figure 4-13. Image of the PG3-Dox micelles suspension In DMEM containing 10% (V/V) FBS

It is also observable that the toxicity of P-PLLA-Dox in cancerous cells HepG2 and U251 is higher compared to normal cells Hek293 and NIH3T3 and that the cell viability of HepG2 decreased the most. These results suggest that P-PLLA-Dox had a higher affinity toward the HepG2 cells and could kill both tumour cells but were less toxic to normal cells.

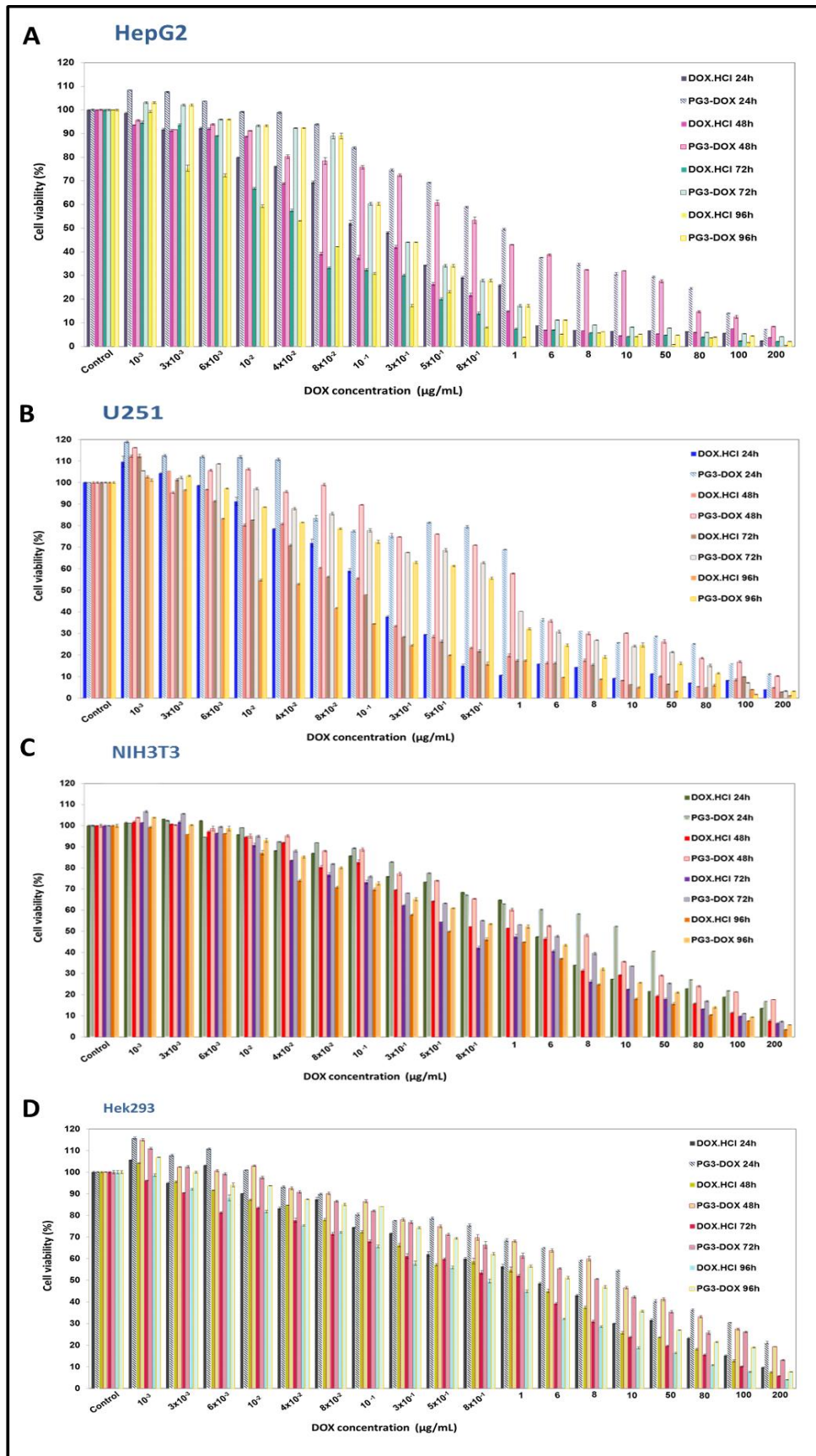


Figure 4-14. The in vitro cytotoxicity of Dox.HCl and PG3-Dox after 24, 48, 72 and 96 hours of incubation against A. HepG2 cells, B. U251 cells, C. NIH3T3 cells and D. Hek293.

4.4.9. Cellular internalisation by Flow cytometry and confocal studies

Doxorubicin is fluorescent with a maximum excitation and emission wavelength of 470 and 560 nm, respectively (Kauffman et al., 2016). Laser flow cytometry has been widely used for monitoring the accumulation in cells of fluorescent anticancer drugs (e.g. Doxorubicin), other fluorochromes and antibodies (Krishan and Hamelik, 2005). Therefore, flow cytometry has been used here for the quantitative determination of Dox uptake in HepG2 and U251 cells.

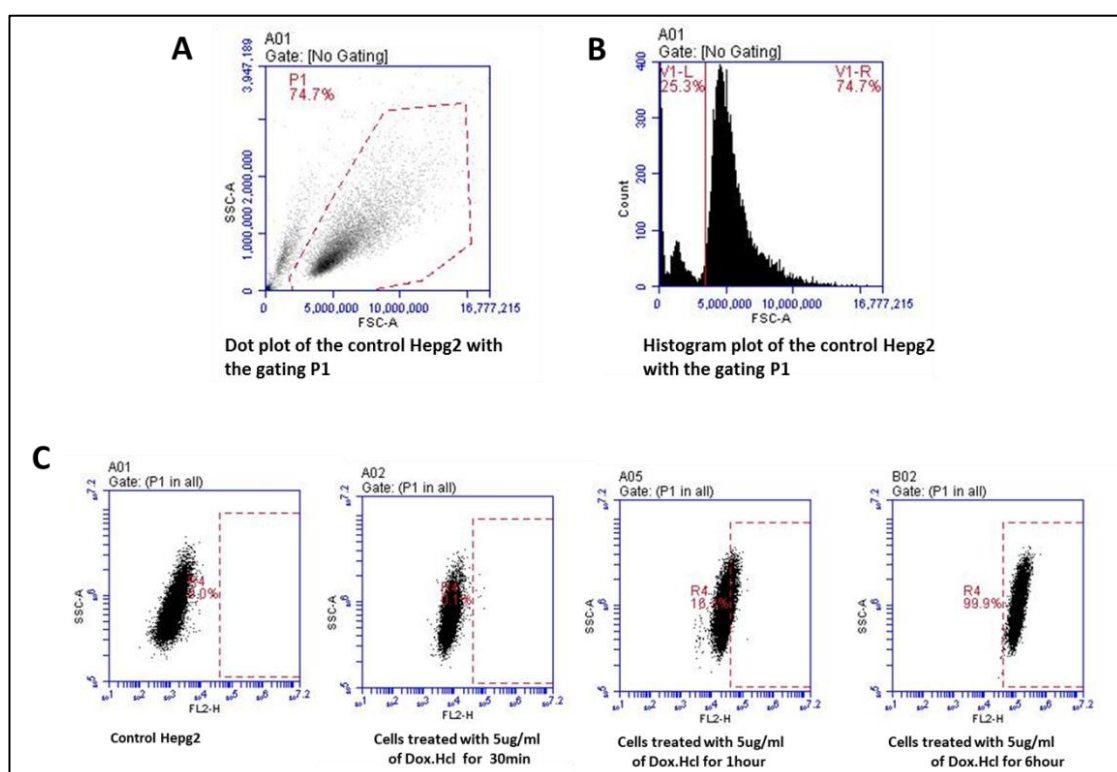


Figure 4-15. Flow cytometry plots. A. Dot plot of HepG2 control gated as P1, B. histogram plot of the control HepG2 cells and C. Dot plot showing the Dox fluorescence intensity of hepG2 cells treated with 5µg/mL of Dox.HCl at various time.

Cells without any Dox treatment were used as a negative control. The internalisation of Dox.HCl was investigated for the duration of 0.5, 1 and 6 hours incubation. Figure 4-15 shows a shift of fluorescence intensity to the right as the

time increases, which is directly proportional to the amount of Dox internalised in cells.

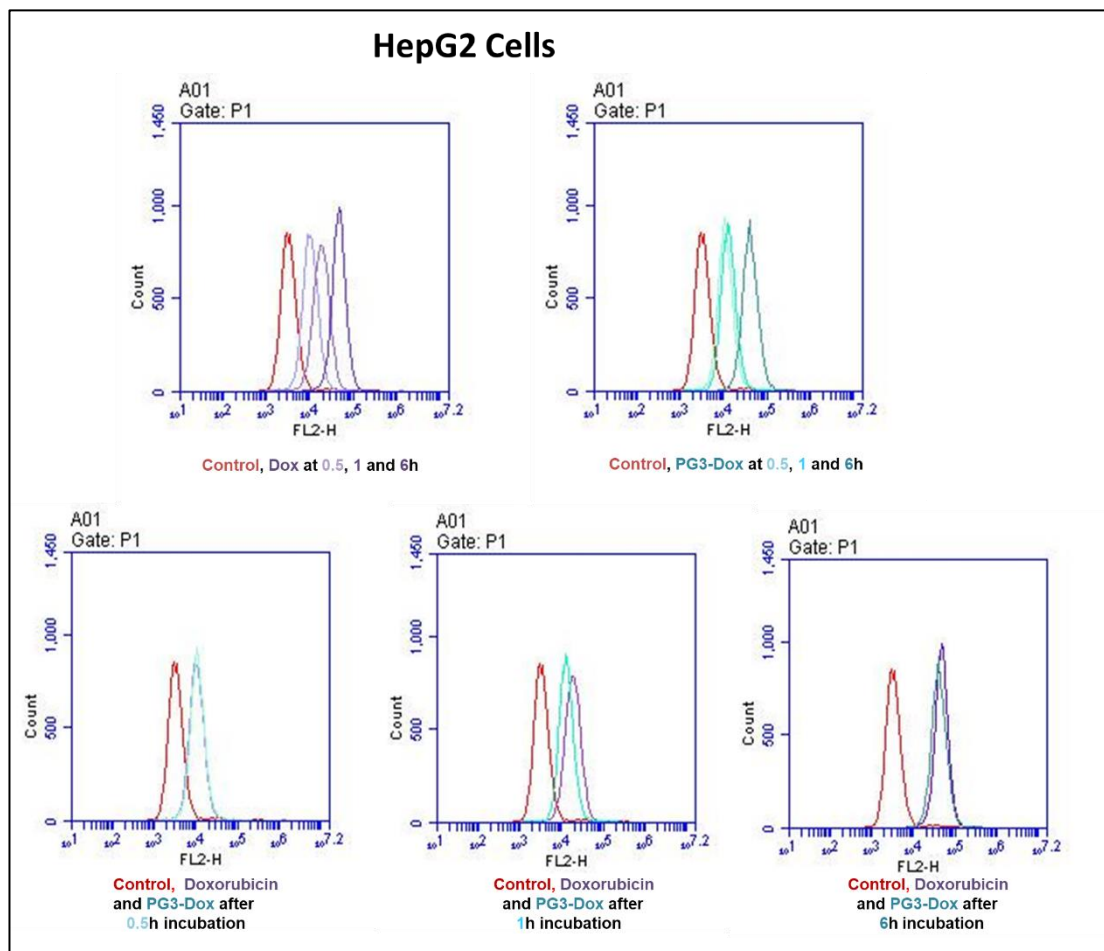


Figure 4-16. The cellular uptake by Flow Cytometry of Dox.HCl and PG3-Dox nanoparticles at 0.5, 1 and 6 hours in HepG2 cells. The flow cytometry histograms are represented in 2 ways: first top 2 histogram plots represent separate plots of the changes in fluorescence intensity of Dox.HCl treated HepG2 cells (peaks in purple), and PG3-Dox-treated HepG2 (peaks in Blue) over time whereas the three bottom plots compare the fluorescence intensity of Dox.HCl and PG3-Dox-treated HepG2 cells at each time intervals. Untreated HepG2 cells were also used as control (peaks in Red).

Treatment to both tumour cells showed that the internalisation of Dox-PG3 was also time dependent and lower fluorescence intensity compared to Dox.HCl treated cells at 0.5 and 1hour incubation was observed indicating the slower uptake of PG3-Dox compared to Dox.HCl (Figure 4-16 and 4-17). In addition to flow cytometry plots, confocal studies (Figure 4-18 and Figure 4-19) also showed the increase with time of strong red signals inside cells, which indicates the successful uptake of Dox.HCl and PG3-Dox inside cells.

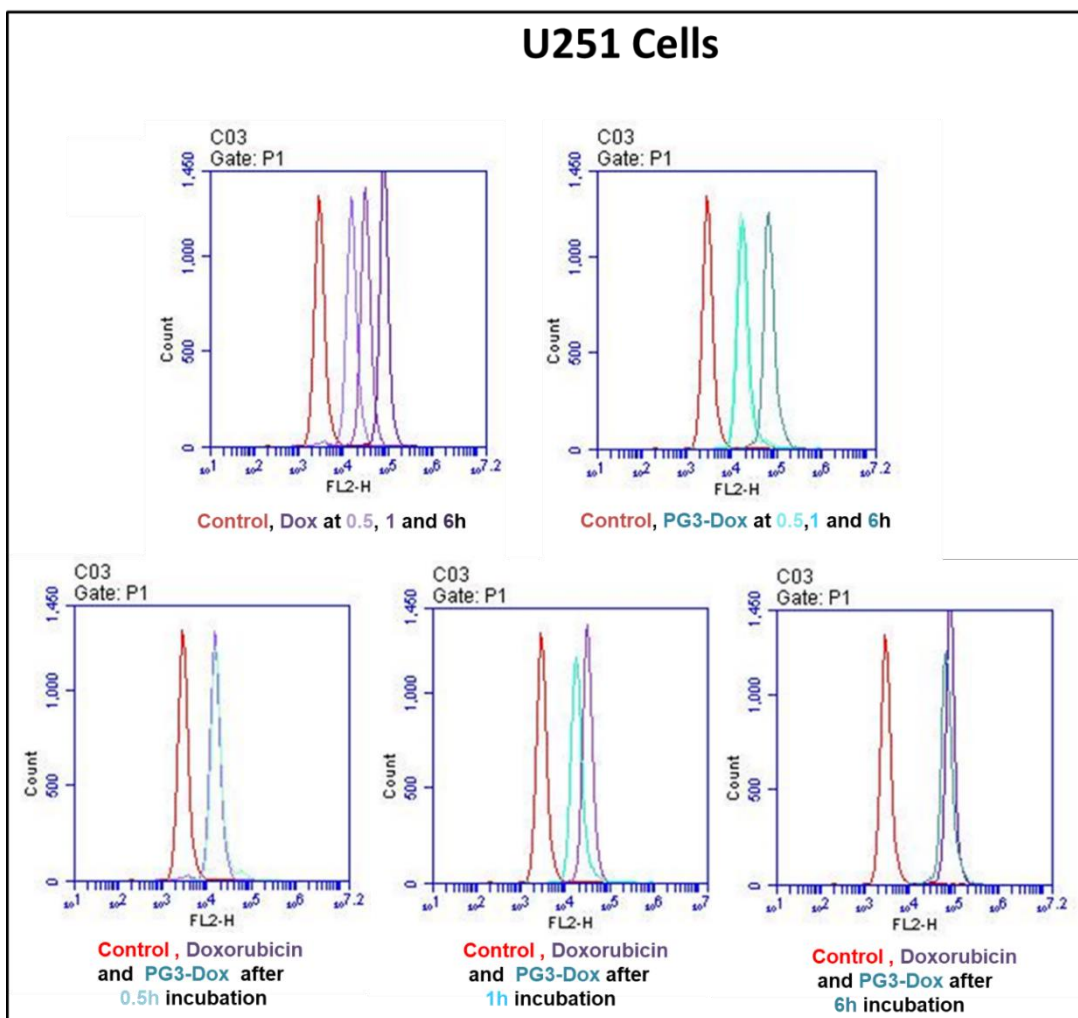


Figure 4-17. The cellular uptake by Flow Cytometry of Dox.HCl and PG3-Dox nanoparticles at 0.5, 1 and 6 hours in U251 cells. The flow cytometry histogram represented in 2 ways: first top 2 histogram plots represent separate plots of the changes in fluorescence intensity of Dox.HCl treated U251 cells (peaks in purple), and PG3-Dox-treated U251 cells (peaks in Blue) over time whereas the three bottom plots compare the fluorescence intensity of Dox.HCl and PG3-Dox-treated U251 cells at each time intervals. Untreated U251 cells were also used as control (peaks in Red).

For both cells, the pathway of internalisation of Dox.HCl and the PG3-Dox nanoparticles were different because the distribution of the red signals representing Dox in cells treated with Dox.HCl was different from that of cells treated with PG3-Dox nanoparticles. In Figure 4-18 and 4-19, at 0.5h, HepG2 and U251 treated cells with Dox.HCl showed strong red fluorescence in the cytoplasm and weak fluorescence in cell nuclei.

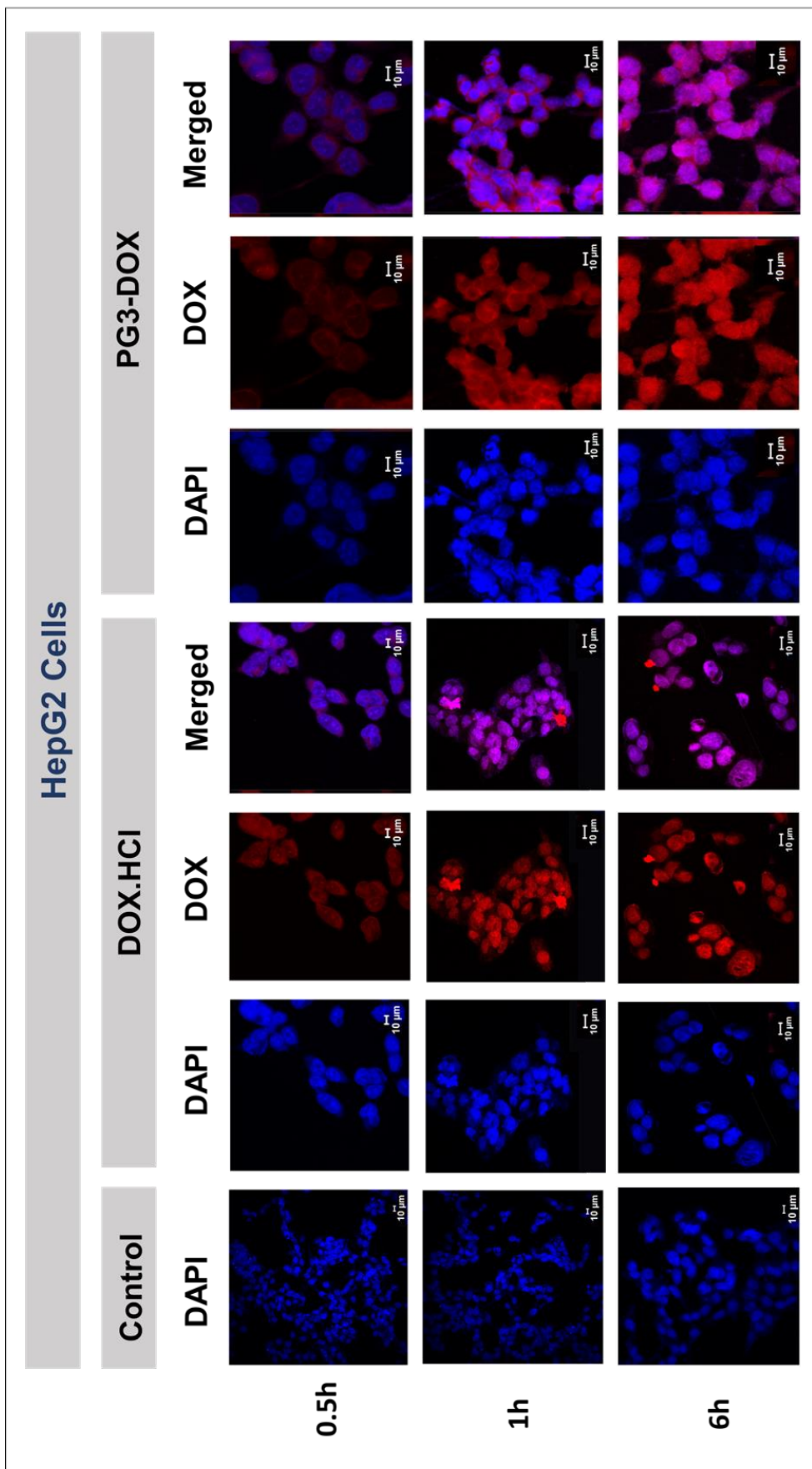


Figure 4-18. The cellular uptake results by confocal laser scanning microscopy against HepG2 cells treated with DOX.HCl and PG3-DOX nanoparticles for 0.5, 1 and 6 hours. For each panel, the images from top to bottom indicate cells treated after 0.5, 1 and 6 hours. The first column indicates the untreated cells with their nucleus stained with DAPI (Blue) which is used here as a control. The next 3 column represents cells treated with DOX.HCl shown here with DAPI stain only (blue), with DOX stain only (red) and overlays of the two channels (Purple). Similarly, the last three columns represent cells treated with PG3-DOX.

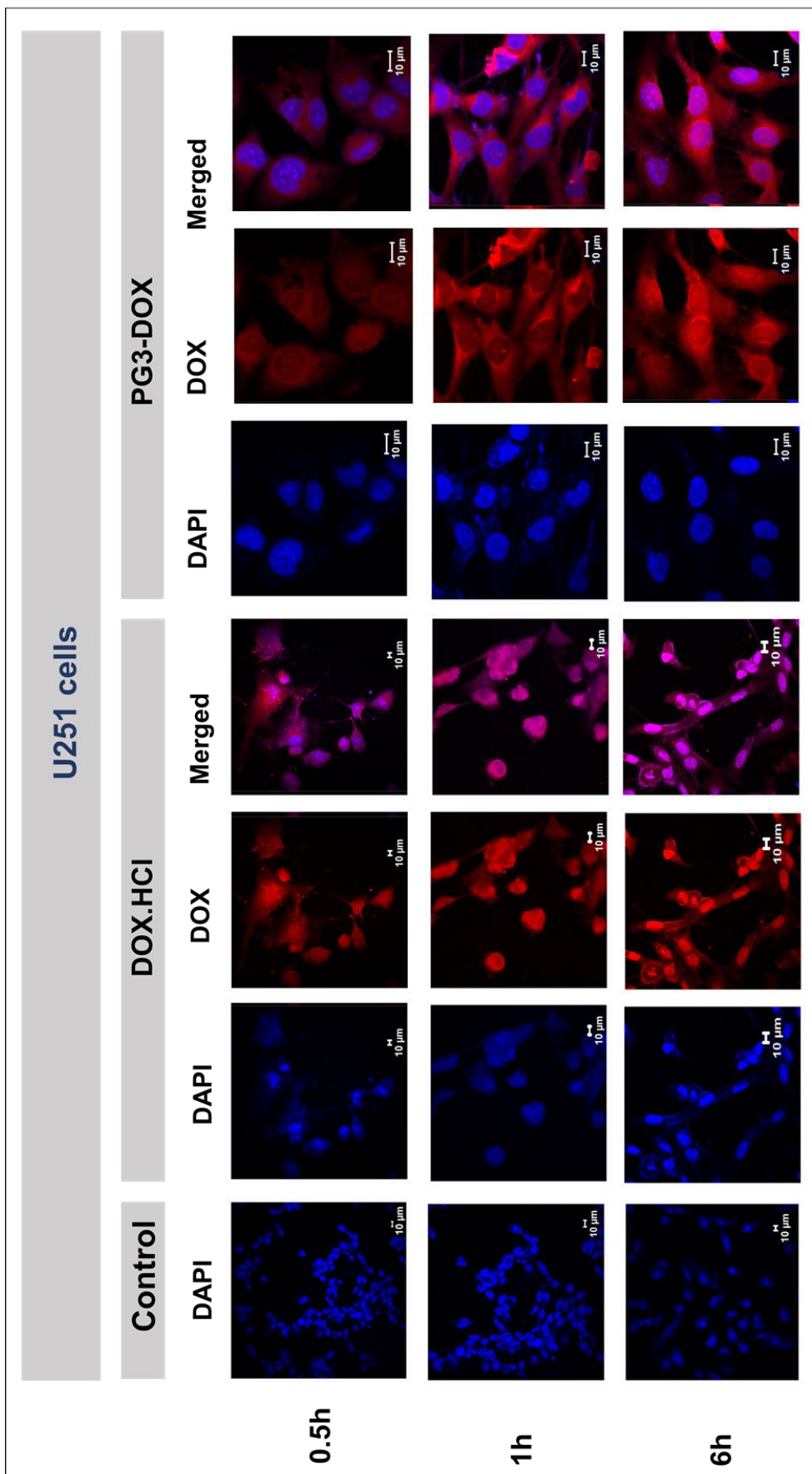


Figure 4-19. The cellular uptake results by confocal laser scanning microscopy against U251 cells treated with DOX.HCl and PG3-DOX nanoparticles for 0.5, 1 and 6 hours. For each panel, the images from top to bottom indicate cells treated after 0.5, 1 and 6 hours. The first column indicates the untreated cells with their nucleus stained with DAPI (Blue) which is used here as a control. The next 3 column represents cells treated with DOX.HCl shown here with DAPI stain only (blue), with DOX stain only (red) and overlays of the two channels (Purple). Similarly, the last three columns represent cells treated with PG3-DOX.

As the hours of incubation increased to 1 and 6h, stronger red fluorescence was observed in both cells nuclei in addition to a very weak fluorescence in the cytoplasm. This observation indicates the rapid intercalation of intracellular Dox.HCl by passive diffusion into the HepG2 and U251 cells. On the other hand, throughout all 6hrs of incubation, HepG2 and U251 cells treated with PG3-Dox showed strong red fluorescence throughout the cytoplasm, revealing that PG3-Dox Nps were initially trapped within endosomal compartments after cellular uptake. At 6hours, both HepG2 and U251 treated cells with PG3-Dox showed some red fluorescence in the nuclei as well, indicating that Dox was successfully released from the PG3 carriers and successfully delivered to the nuclei where its mechanism of action takes place.

4.4.10. Apoptosis studies

Flow cytometry was also used to quantitatively investigate the apoptosis of HepG2 and U251 cells after 12h treatment with Dox.HCl and PG3-Dox. The cells were stained with FITC-labeled Annexin V and propidium iodide (PI) and then analysed with triplicate determinations.

From the Figure 4-20, after the incubation for 12h, the control sample containing non-treated HepG2 cells showed an apoptotic rate of 4.0% including the early and late apoptosis rate of 0.9% and 3.1%, respectively. The early and late apoptosis rate of the Dox.HCl treated HepG2 cells were 21.2 % and 4.2%, respectively, whereas those treated with PG3-Dox were 20.3% and 3.4%, respectively. This indicates that the apoptosis rate induced by PG3-Dox was not much different from that of Dox. Similar results were obtained with treated U251 cells, the early and late apoptosis rate of the Dox.HCl treated U251cells were

9.1 % and 0.9%, respectively, whereas those treated with PG3-Dox were 7.6% and 1.2%, respectively.

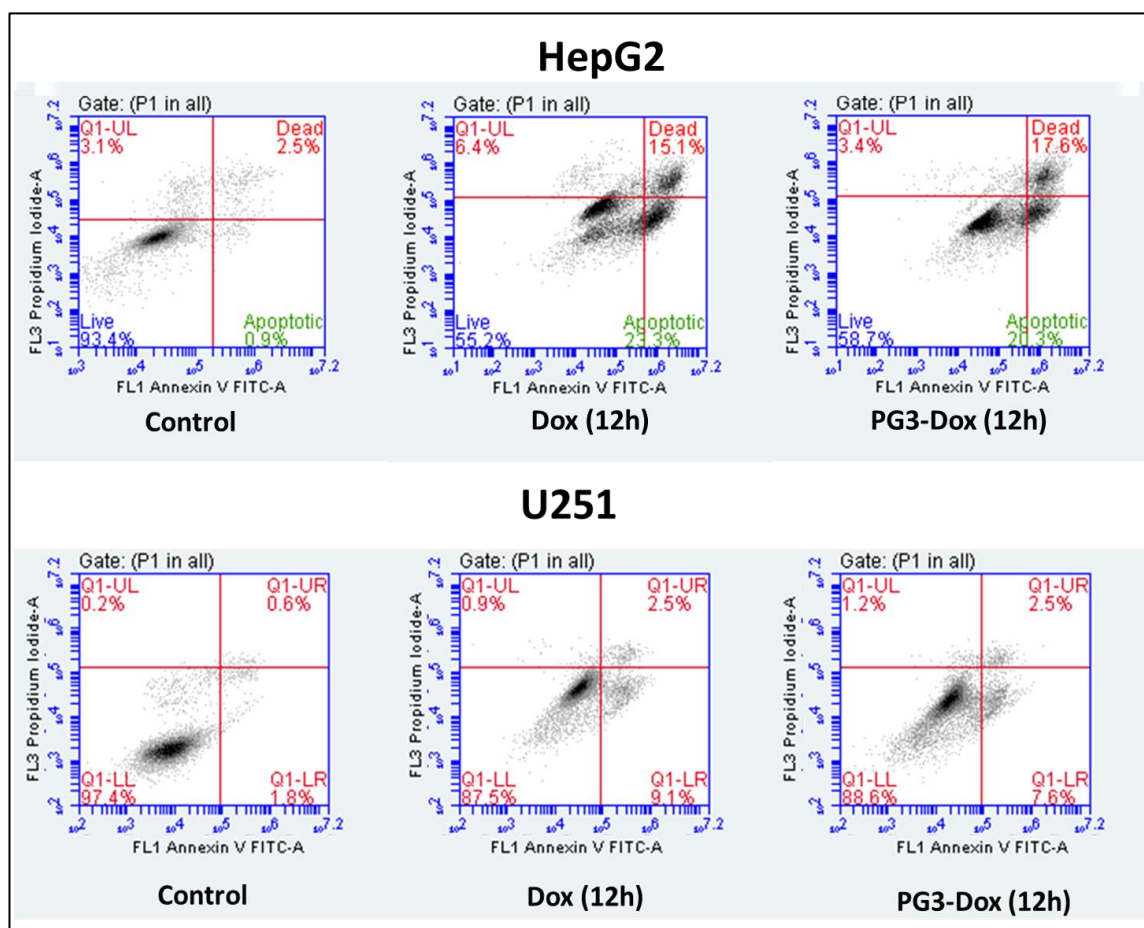


Figure 4-20. The effect of free Dox.HCl and Dox-loaded PG3 on the induction of apoptosis in HepG2 and U251 cells. Tumour cells were quantified by flow cytometric analysis of Annexin V FITC staining in tumour cells following 12h treatment with 5µg/mL equivalent Dox concentration. The lower left (LL) quadrant represents live/healthy cells, the lower right (LR) quadrant represents early apoptosis, and the upper right (UL) represents cells in late apoptosis, while the top left (UR) represents the percentage of Dox uptake/dead cells. The percentage of cells undergoing early or, late apoptosis is indicated in the respective quadrants.

4.5. Discussion

Amphiphilic Dendronised Polymer-based NPs that self-assemble to form micellar structure are the new systems extensively been studied for the solubilisation and the safe delivery of hydrophobic drugs in cancer therapy. One of the most common hydrophobic drugs used to test such a carrier system is

the anthracycline antibiotic doxorubicin (Dox) which is presently used in the treatment of a wide variety of cancers. We have developed an amphiphilic dendronised polymer based nanocarrier for the delivery of the hydrophobic drug Dox in liver and Brain cancer cells. Polysaccharides including Hyaluronic acid, Dextran, Chitosan, Heparin, cyclodextran, pullulan,... have shown to be the most important group of polymers used in delivery systems (Goodarzi et al., 2013). Pullulan was chosen here as the ideal backbone of the nanocarrier since its neutral, non-toxic, non-immunogenic, noncarcinogenic and non-mutagenic, can target liver cells and most important can readily undergo chemical modification (Kumar et al., 2012). Here, we have successfully conjugated the hydrophobic arginine dendron of the third generation into pullulan through an approach known as Huisgen azide-alkyne 1, 3-dipolar cycloaddition or “click” reaction. Pullulan consists of maltotriose units connected by α (1 \rightarrow 4) glycosidic bond, whereas consecutive maltotriose units are connected by α (1 \rightarrow 6) glycosidic bond. There are nine OH groups per repeating unit available for substitution in the pullulan structure. Azidation of various polysaccharide such dextran (Mai et al., 2015), starch (Shey et al., 2006) and amylose (Cimecioglu et al., 1997; Pang et al., 2015) have been achieved before. Since the click chemistry consists of the cycloaddition of azides and terminal alkynes to form 1,2,3-triazoles, we have successfully converted up to 232.16% of OH into azides groups per unit of pullulan in a condition where equimolar quantities of $\text{Ph}_3\text{P/CBr}_4$ were added in the presence of an ice bath with a ratio of pullulan: NaN_3 being 1:10. The characteristic strong absorption peak at 2107 cm^{-1} was observed in the FTIR of PN3, which matches that of published data and confirmed the vibration of azido groups present in pullulan. Compared to the azidation of starch by cimeciogluin 1997 and Pang in 2015, which was carried in

the same conditions as our experiment, only 40-75% of conversion was achieved. The authors reported that the conversion could easily be affected by moisture content; therefore, during the azidation of pullulan, any source of moisture was avoided. Moreover, the experimental conditions we used for pullulan azidation was much more straightforward, efficient and quicker compared to the method used by Mai et al., in 2015 who first carried the oxidation of dextran to then achieve the azidation of dextran.

The successful azidated pullulan was then clicked with alkyne containing dendron PLLA G3 (BOC/PBF) which was confirmed by FTIR and H^1NMR . The click reaction was very reliable and easy to perform, not very elevated temperature was needed, and the reaction was taken place in deoxygenated water. High yield was also obtained, and purification of the product was simple. These convenient factors have been reported previously by Hein, Liu and Wang in 2008 who describes the wide application of click chemistry in biomedical and especially in pharmaceutical sciences and its emerging applications in drug delivery and nanomedicine. The authors also report that click chemistry is a powerful linking reaction catalysed by Cu^I , which makes the reaction 107 times faster than the uncatalyzed version.

The final clicked product PG3 (PLLA) was therefore composed of a hydrophilic backbone in which 20.32% of hydrophobic dendron was introduced. The amphiphilic structure was also confirmed by the fact that PG3 was able to self-assemble in aqueous solution to form spherical nanomicelles of 87.07nm with a PDI of 1.87. The particle size distribution and polydispersity index (PDI) of nanocarriers are highly critical physical characteristics to be considered. The size of particles gives us an overview of how efficiently the carriers can reach

their target without being eliminated in the bloodstream, whereas the PDI represents the distribution of the size population within the sample. A PDI value lower than 0.05 is mainly seen with highly monodisperse standards whereas a PDI value bigger than 0.7 indicates that the sample has an extensive particle size distribution and is probably not suitable to be analysed by the dynamic light scattering (DLS) technique (Danaei et al., 2018).

For this reason, PG3 has shown excellent physical characteristics in term of size and PDI as their sizes are within 30-200nm with a PDI lower than 0.7.

Moreover, stability studies showed that PG3 stayed stable even after 3 months with no change in size. However, following intravenous administration, the polymer concentration may fall below the critical association (CAC), in this case, PG3 also showed a low value of CAC 10.47 μ g/mL which shows high assembly stability in aqueous solution (Allen, Maysinger and Eisenberg, 1999).

In addition to enormous size and stability properties, PG3 nanocarriers showed to be a safe carrier as no toxicity of the carrier was observed in Hek293, NIH3T3, U251 and HepG2 cells. These results suggest that the neutral amphiphilic PG3 nanocarrier would be an ideal carrier to improve the solubility of hydrophobic drugs and deliver hydrophobic drugs safely into cancerous cells since their sizes would permit their escape from RES clearance and bypass barriers in the liver and brain.

To investigate the ability of PG3 to deliver hydrophobic drugs into liver and brain cancer cells, the hydrophobic drug Dox was incorporated inside PG3 via physical entrapment. 19.17% of drug Dox was successfully loaded into PG3, and the loaded carrier size was increased to 138nm which is still convenient as

a carrier size for the delivery of doxorubicin in liver and brain cancer cells. As expected, the rate of drug release was affected by pH of the environment, where acidic pH resulted in Dox release into the surrounding media while the conjugate retained its stability at neutral pH and even when stored for 3 months. PG3 also displayed effective cellular toxicity towards all cell lines. However, higher toxicity was observed in cancer HepG2 and U251 cells compared to normal Hek293 and NIH3T3 cells lines, which suggested that PG3 enhanced the delivery of doxorubicin into cancerous cell lines. Moreover, in vitro cellular uptake of the drug-loaded PG3 was also confirmed by flow cytometry, confocal studies and even apoptosis assays. It was noted that by the time of 6 hours, a similar amount to free Dox could be taken inside both U251 and HepG2 cells by PG3 however free Dox would almost be internalised inside the nucleus whereas most of Dox-loaded PG3 was still localised in cells cytoplasm. In addition, in 12hours incubation, PG3-Dox-induced the apoptosis of 23.7% of HepG2 cells, whereas only 8.8% of U251 cells did undergo apoptosis. These results could confirm that pullulan was able to target HepG2 cells and influence the uptake of the carrier which also affected the higher toxicity of HepG2 cells more than U251 cells since the determined IC50 in HepG2 treated with PG3Dox at different interval of time was much lower than those in U251 cells.

4.6. Conclusions

In this study, we have described the feasibility of using the amphiphilic pullulan grafted Dendron bearing hydrophobic PBF and BOC groups as a carrier for the delivery of anticancer hydrophobic drugs such as Doxorubicin. The loaded PG3-Dox micelles presented well enough physical characteristic to be able to deliver Dox in liver or Brain tumours. The carrier system could rapidly organise into

remarkably stable, nanosized micelles that possess some unique physical properties, including extremely low CMC and cytotoxicity, excellent pH-responsive behaviour and micellar stability. Moreover, CLSM and flow cytometric analyses further confirmed the efficient uptake via endocytosis of the loaded PPLLA-Dox in HepG2 and U251 cells. These results strongly suggest that PG3 could be employed to dramatically improve the effectiveness of chemotherapy in the low pH tumour microenvironment, while its sustained drug release profile would reduce the toxicity effects in healthy cells under normal physiological conditions.

CHAPTER 5. MODIFIED MICELLAR DENDRON FOR TARGETED DOX DELIVERY IN VITRO

5.1. Introduction

Until today, Hepatocellular carcinoma (HCC) remains the leading cause of death among cirrhotic patients, with 782,451 cases diagnosed and 745,533 deaths in 2012, it is the third cause of cancer-related mortality worldwide (El-Serag, 2004, Parkin et al., 2005, Gorad, Mandlik and Gujar, 2013, Wong et al., 2017). Nanoparticle-based drug delivery systems have been developed to treat and improve the existing therapies for HCC. Previously in chapter 4, we have described the physiological barriers that nanocarriers may face during delivery of therapeutic agent into liver tumour cells. Fortunately, there are ways to improve nanocarriers safety and to overcome these challenges through the passive accumulation of nanocarrier therapeutics and active targeting by surface modifications of nanoparticles with specific ligands such as carbohydrates, peptides, proteins and antibodies. Nanocarriers can easily reach the liver, but it is essential that they target the cell of interest at the same time. Thus, the challenge is to obtain a selective accumulation of drugs in one specific cell type and to sustain intracellular levels for a more extended period (Mishra et al., 2013). Since, hepatocytes consist of 80% of the cells in the liver and are the primary cells that play the major functions in term of metabolic and secretory activities of the liver, any mutation or malfunction related with these cells can result to severe damage of the liver and other diseases (including hepatocellular carcinoma). Targeting the hepatocytes cells in the liver would, therefore, be an essential strategy for liver cancer therapy and other conditions

related to hepatocytes malfunction. It has been reported that improved delivery (enhanced localisation) to the parenchyma is achieved with small size delivery system that is ≤ 50 nm which can also diffuse deeper in the space of Disse. Moreover, the delivery system of sizes 150nm can avoid Kupffer cells and diffuse the sinusoids through the fenestrations and reach hepatocytes plates (Ogawara et al., 1999; Allen et al., 1991; Mishra et al., 2013). The size of the delivery system therefore always comes into consideration. Furthermore, specifically targeting the hepatocytes can be achieved by grafting targeting moieties into the delivery systems that can target receptors overexpressed in hepatocytes. Receptors that can be targeted in hepatocytes for treatment and that constitute a possible pathway of entry mechanisms in these cells are asialoglycoprotein receptor (ASGP-R), HDL-R, LDL-R, IgA-R, scavenger R (Class BI), transferrin R and insulin R (Harashima, 1994; Mishra et al., 2013).

The asialoglycoprotein receptors also known as hepatic lectin are the most commonly exploited target expressed on the sinusoidal surface of the hepatocytes cells and recognises carbohydrates (mainly galactose and N-acetylgalactosamine) in high affinity. Once the carbohydrate residues bind to the carbohydrate recognition domain in the extracellular space of hepatocytes, the cells then take up the carbohydrate residues containing molecules via receptor-mediated endocytosis and the ligands are then released into endosomes-lysosomes by their segregation from the receptor due to the low pH in endosomes-lysosomes (Wragg and Drickamer, 1999; Wu, 2002; Mishra et al., 2013). Various ligands have been used to target ASGP-receptors including galactose moieties (Yan et al., 2017), lactose moieties (Thao et al., 2017), Asialofetuin (Detampel et al., 2013), Lactoferrin (Xu et al., 2015), soybean-

derived sterylglucoside (SG) and polymers such as poly-(N- ρ -vinylbenzyl-O-b-D-galactopyranosyl-[1-4]-D-gluconamide(PVLA)) (Watanabe et al., 2000) and pullulan (Li et al., 2016).

5.2. Aim and objective

In chapter-4, we demonstrated that the targeting pullulan-based arginine dendron nanocarrier could successfully load the hydrophobic DOX and efficiently be internalised into liver cancer cells. However, we could not confirm that the carrier was internalised via receptor-mediated endocytosis by the targeting of pullulan into ASGP-receptor. Similarly, the work of Guhagarkar et al. in 2011 evaluating the in vitro ASGPR-mediated uptake of pullulan-functionalized Dox nanoparticles in HepG2 cell lines showed that in vitro studies does not assess thoroughly the ASGPR-mediated uptake of polysaccharide-based ligands. For this reason, since no one has done this type of work, we proposed to modify our PG3 system by adding the ligand lactose to enhance the targeting of pullulan for ASGP receptors and therefore increase the overall efficiency of the carrier in HepG2 cells by increasing high cellular uptake. Lactose is not only used here to improve the targeting of pullulan but also is used as the addition of polar groups to yield a higher solubilisation of the modified pullulan and therefore increase the micellation process of the amphiphile structure. Pullulan is still used here because of its reported tropism in liver (Farris, 2014; Yamaoka, Tabata, and Ikada, 1993; Kaneo, 2001), its excellent biological and physiochemical features (Ambattu and Rekha, 2015; Belbekhouche, 2011). We, therefore, aim in this work:

- To successfully conjugate lactose into PG3

- Improve the active targeting of ASGP receptors in HepG2 cells by the lactosilated carrier
- Improve the passive targeting by reducing the size of the nanocarrier
- increase the micellation process of the amphiphile structure

5.3. Methodology

5.3.1. Dendron synthesis and pullulan azidation

G3 Dendrons PLLA (BOC/PBF) synthesised and Pullulan azidated containing 49.02% azide groups were used. Their synthesis details are described in details in chapter 3 and 4.

5.3.2. Conjugation of lactose to azidated Pullulan (P(lactose)N3)

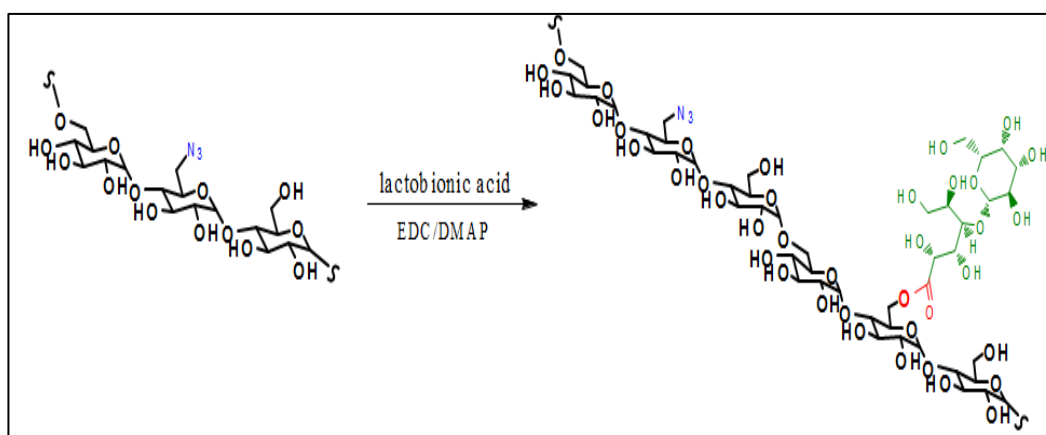


Figure 5-1. The synthesis equation of the azidated pullulan modified lactose.

Firstly, Pullulan bearing the azide groups (0.77g, 1mmol equivalent of anhydrous glucoside units) was completely dissolved for 2-3h in 20 mL of anhydrous DMSO at 60°C. Lactobionic acid (10.5g, 8mmol), EDC.HCl (3.8g, 5.4mmol) and DMAP (2.24g, 5mmol) was dissolved in 40mL of anhydrous DMSO and stirred at 50–60°C for 30min under N₂ atmosphere to activate the

carboxyl group. To this solution, the PN3 solution was then added dropwise, and the dark brown mixture was left to stir for 48hrs at 60°C. Purification of the product was achieved by dropping the mixture into 90% of ethanol (300.00 mL) under vigorously stirring and then the precipitated product was dialysed against DI water (MWCO 3500 Da) for one day. The brown solids appeared in the dialysis bag were then collected by lyophilisation.

5.3.3. Click reaction between pullulan bearing lactose and PLLA

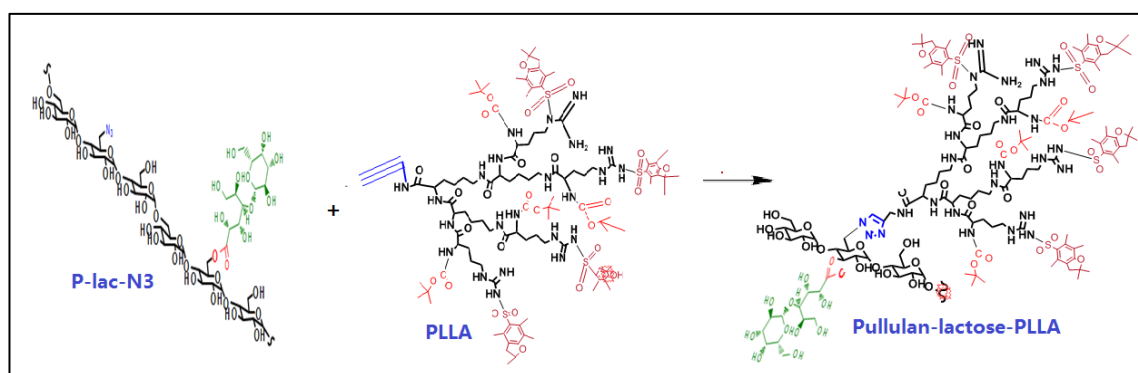


Figure 5-2. The synthesis equation of pullulan bearing G3 clicked PLLA (P(Lac)G3).

The click reaction was carried out with the same method used in chapter 4. Briefly, PLLA Dendron G3(2.35 g, 2 mmol) and P(Lac)N₃ (0.10 g, 1 mmol) were dissolved in 30 mL DMSO under N₂ atmosphere at 50 °C for 1 h. The mixture was then brought at RT and passed into argon, then 5. mL of a deoxygenated aqueous solution of sodium L-ascorbate (0.08 g, 0.40 mmol) and 5.00 mL of copper (II) sulfate pentahydrate (0.05 g, 0.20 mmol) were added successively into the reaction. The resultant yellowish mixture was stirred for 55h. After the reaction, a little amount of EDTA₂Na was added and left to stir for 2-3h. The resulting solution was finally dialysed against DI water for 2 days (MWCO 3500 Da) and then lyophilised to yield the product Pullulan (Lac) PLLA.

5.3.4. Characterisation

The characterisation was carried by FTIR and NMR, the details of each method are given in chapter 2, and the other experiments were similarly carried as in chapter 4.

5.4. Results

5.4.1. Characterisation of the lactose conjugated pullulan (P(LAC)N₃)

To achieve a liver-targeted system, pullulan modification was further conducted by directly conjugating lactobionic acid onto the surface of PN₃ via EDC chemistry to gain azido-lactosylated pullulan (P(Lac)N₃) which was confirmed by FTIR and ¹HNMR analysis.

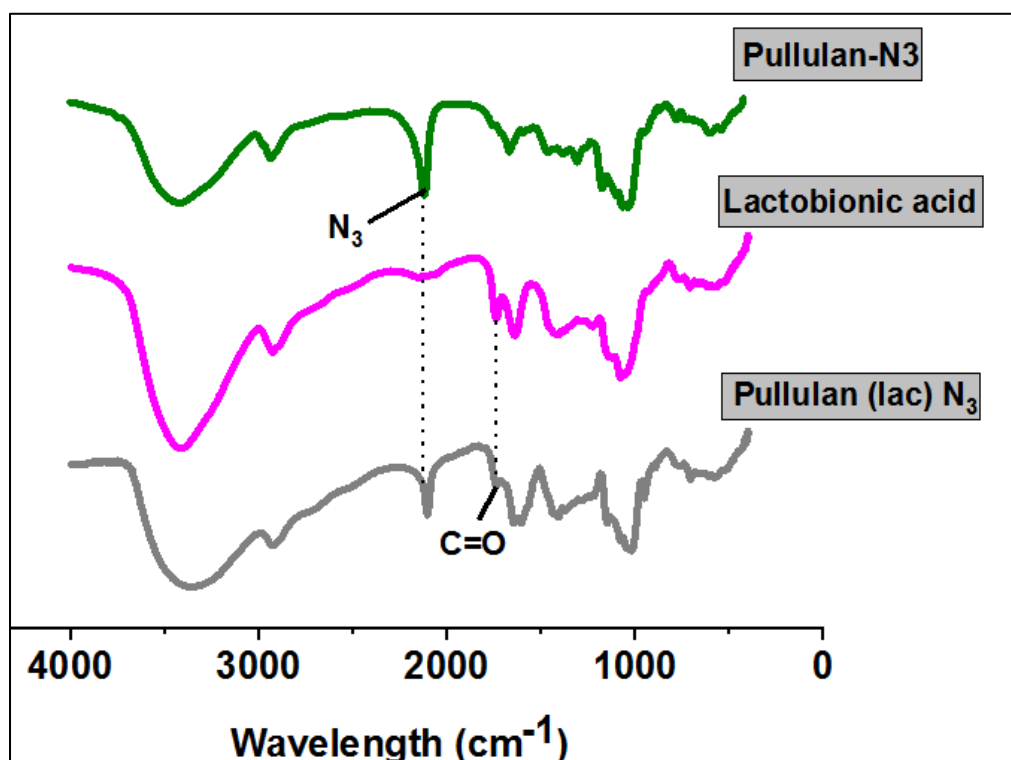


Figure 5-3. IR spectrum of Pullulan, lactobionic acid and lactose conjugated azidated pullulan (P(Lac)N₃) showing the ester peak at 1746cm⁻¹.

Figure 5-3 shows 3 spectra of FTIR showing the azidated Pullulan (2), pure lactobionic acid and conjugated lactobionic acid into pullulan. The appearance

of a sharper peak at 1746 cm^{-1} in the spectra of the $\text{P}(\text{lac})\text{N}_3$ FTIR was the stretching vibration absorbance of $\text{C}=\text{O}$ in ester bonds which confirmed the conjugation between carbonyl groups of the lactobionic acid and hydroxyl groups of the pullulan.

Moreover, the ^1H NMR spectrum (Figure 5-4) show the peaks at 4.2 and 4.6 ppm in $\text{P}(\text{Lac})\text{N}_3$ related to the H_a and H_b signals of lactobionic acid moiety, respectively. The peaks at 4.8 and 5.0 ppm correspond to the 33 H per 100 glucose units of pullulan C1 H (1-6) and 66H per glucose units of pullulan C1 H (1-4) (Sasaki et al., 2011).

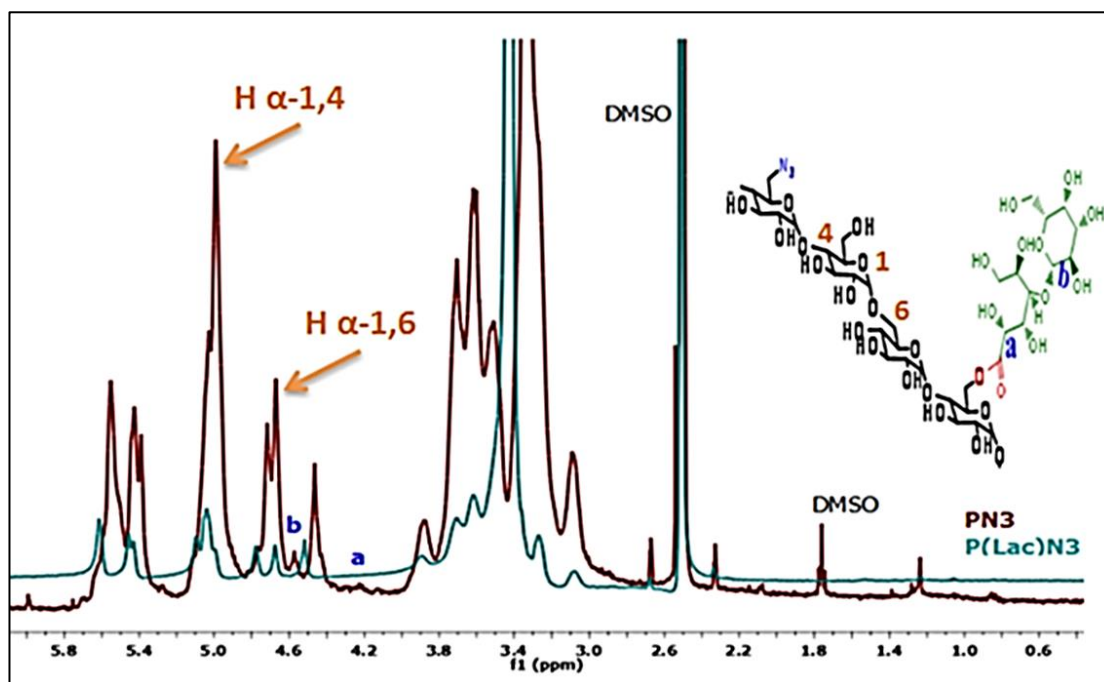


Figure 5-4. ^1H -NMR (DMSO), d (ppm) of pullulan and $\text{P}(\text{lac})\text{N}_3$.

The chemical composition of lactobionic acid in PN_3 at C-6 per anhydroglucose unit was determined to be 34.45% by assigning the protons of H_d in pullulan and the proton of H_b in lactobionic acid. It should be noted that the PN_3 used at this step contained 49.02% azide groups to allow more chances of lactobionic acid to be conjugated.

5.4.2. Characterisation of the clicked product P(Lac)G3

The chemical structures of graft copolymers were verified by FTIR (Figure 5-5). The click conjugation was confirmed by the disappearance of the azido group peak at 2108 cm^{-1} in P(Lac)N3 and all the characteristic peaks of pullulan conjugated lactose and of dendron G3 are present in the FTIR of P(Lac)G3.

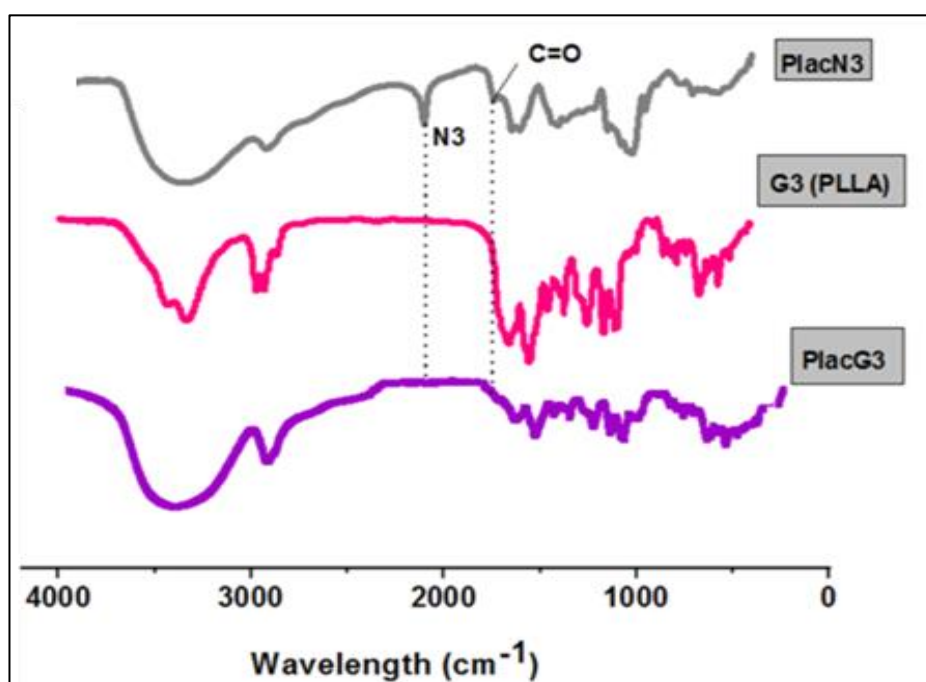


Figure 5-5. FTIR spectrum of azidated lactose bearing pullulan, Dendron of generation 3 PLLA and clicked product P(Lac)G3.

Moreover, the ¹HNMR spectra of P(Lac)G3 in Figure 5-6 showed a signal at 7.90 ppm (He) indicating the triazole proton present in the 5-membered heteroatom ring formed from the click chemistry. The peaks details are as follow: ¹HNMR (400 MHz, DMSO-d₆):d(ppm), 0.734-1.154 (d, 12H, CH₃-PBF, G3); 1.546 (s, 24Hh, CH₃-BOC-PBF, G3); 1.964-2.103 (s, 12Hg, CH₃-PBF, G3); 2.410- 2.806 (d, 24 Hf, CH₃-PBF, G3); 4.2 (s, 1Hc, OHCHCO, lactobionic acid); 4.6 (s, 1Hd, CHCHCO, lactobionic acid); 4.8 (d, 66Hb per 100 glucose units, pullulan C1 Hb (1-4); 5.0 (s, 33Ha per 100 glucose units, pullulan C1 Ha

(1-6)); 7.90 (s, 1H, NCHCH, triazole ring). Also, the graft level of G3 dendrons onto the lactosylated pullulan was 18.51%, according to the integral intensities of Hh in G3 dendron and Ha in pullulan.

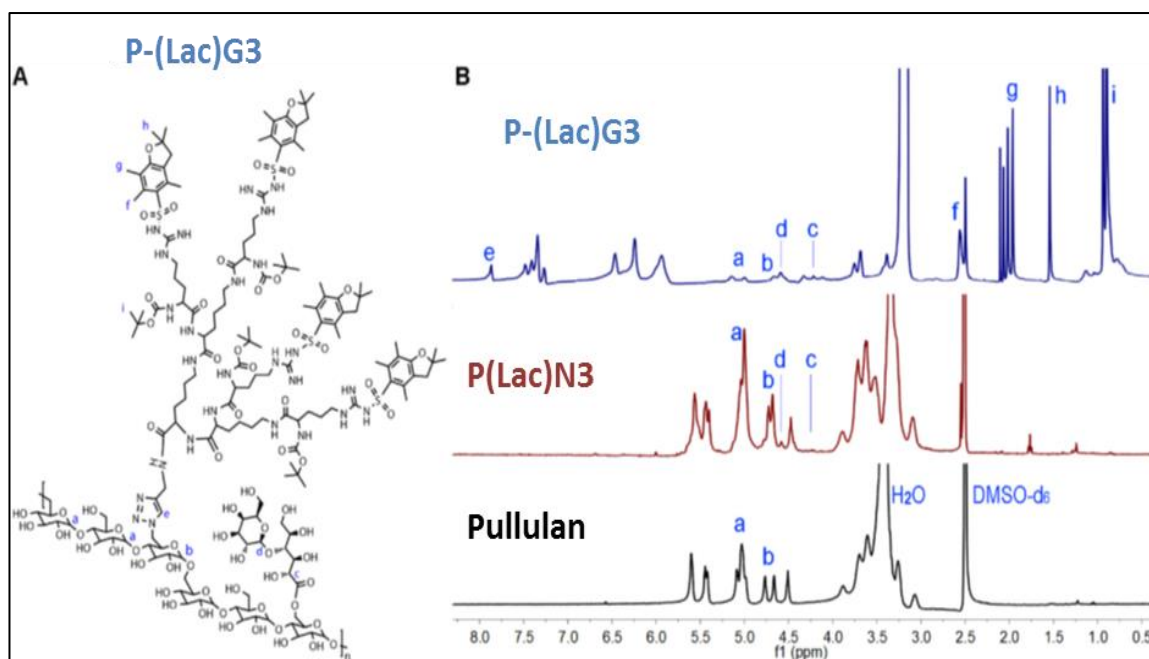


Figure 5-6. (A) Chemical structure of P(Lac)G3, and (B) ¹H NMR (400 MHz, DMSO-d₆) of pullulan, P(Lac)N3 and P(Lac)G3.

5.4.3. The self-assembly of P(Lac)G3

Similarly to PG3 in chapter-4, bearing the same chemical components like PG3, the clicked P(Lac)G3 also consist of an amphiphilic structure that could self-assemble to form micelles structure in aqueous solution. The size and size distribution of P(lac)G3 nanoparticles in DI water presented a lower average size (54 ± 8 nm with PDI 0.131) (Figure 5-7). Moreover, the morphology of the micelles was determined by TEM and SEM images which shows spherical shaped nanoparticles of sizes around 50nm.

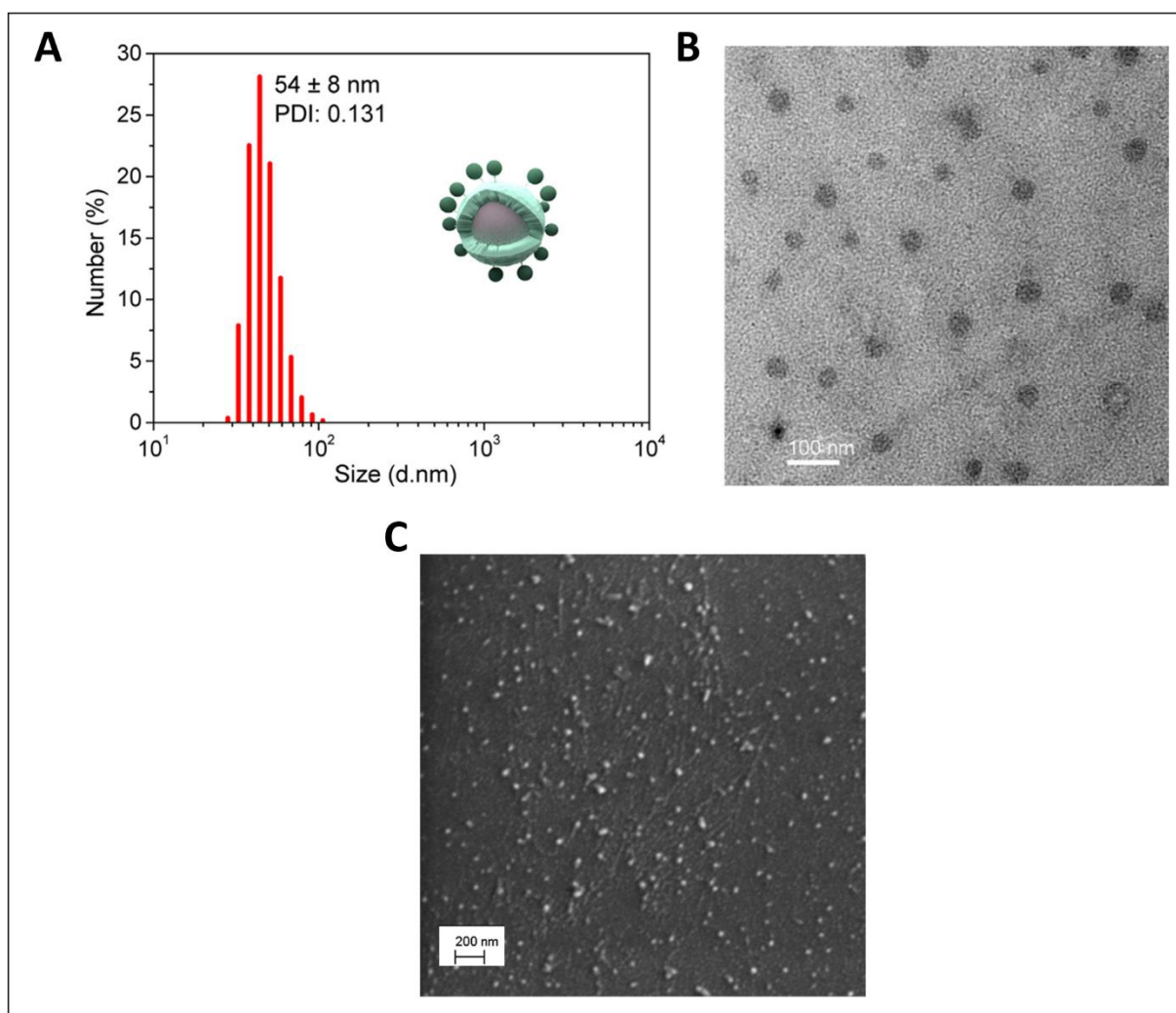


Figure 5-7. Size distribution and morphology studies of blank of P(Lac)G3 by A. DLS, B. TEM and C. SEM.

5.4.4. CAC and Stability studies of P(Lac)G3 micelles

The micellisation behaviour was investigated in aqueous media by fluorescence spectroscopy in the presence of pyrene. Figure 5-8 shows an increase in the value I_{337}/I_{334} ratio with the increase of the log concentration of micelles and the determined CAC value being $8.87 \mu\text{g/mL}$.

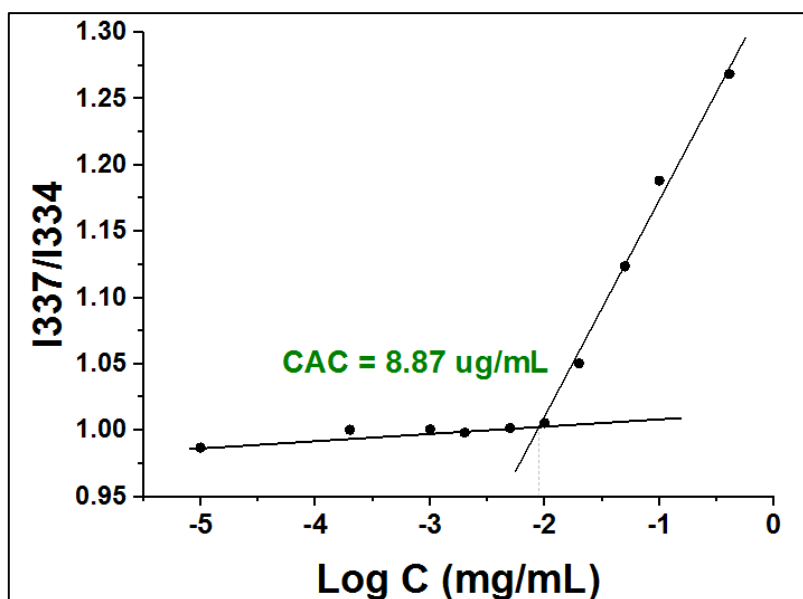


Figure 5-8. Critical association concentration of P(Lac)G3 measured using the fluorescent dye pyrene.

5.4.5. Drug loading in P(Lac)G3

P(lac)G3 could be used as a novel nanocarriers for the application in anticancer therapy. These nanocarriers were used as drug delivery systems for the anticancer drug doxorubicin to try and minimise the drug harmful side effects and increase its therapeutic efficacy in liver cancer cells. Dox was successively entrapped physically into the hydrophobic core of P(lac)G3 and the amount of entrapped doxorubicin and encapsulation efficiency at ratio 5:1, 2:1 and 1:1 was calculated using the standard curve of Doxorubicin presented in chapter-4.

Table 5-1. Drug loading content (LC) and encapsulation efficiency (EE) of P(Lac)G3

	P(LAC)G3	
P:DOX (ratio)	LC%± Std.dev	EE%± Std.dev
5:1(20%)	16.89±2.41	56.34±4.66
2:1(50%)	18.99±3.53	46.13±8.70
1:1(100%)	23.07±1.26	33.04±7.44

The loading content was 16.89%, 18.99% and 23.07% whereas the encapsulation efficiency was 56.34%, 46.13% and 33.04%, respectively.

Furthermore, DLS, TEM measurements (Figure 5-9) showed the excellent distribution of drug loaded Dox-P(Lac)G3 nanoparticles in aqueous media. An increase of the average size of the Dox-loaded P(Lac)G3 nanoparticles was observed with a mean of 68 ± 9 nm. TEM images showed spherical shaped Dox-P(Lac)G3 micelles, and self-aggregated micelles observable by SEM were also roughly spherical.

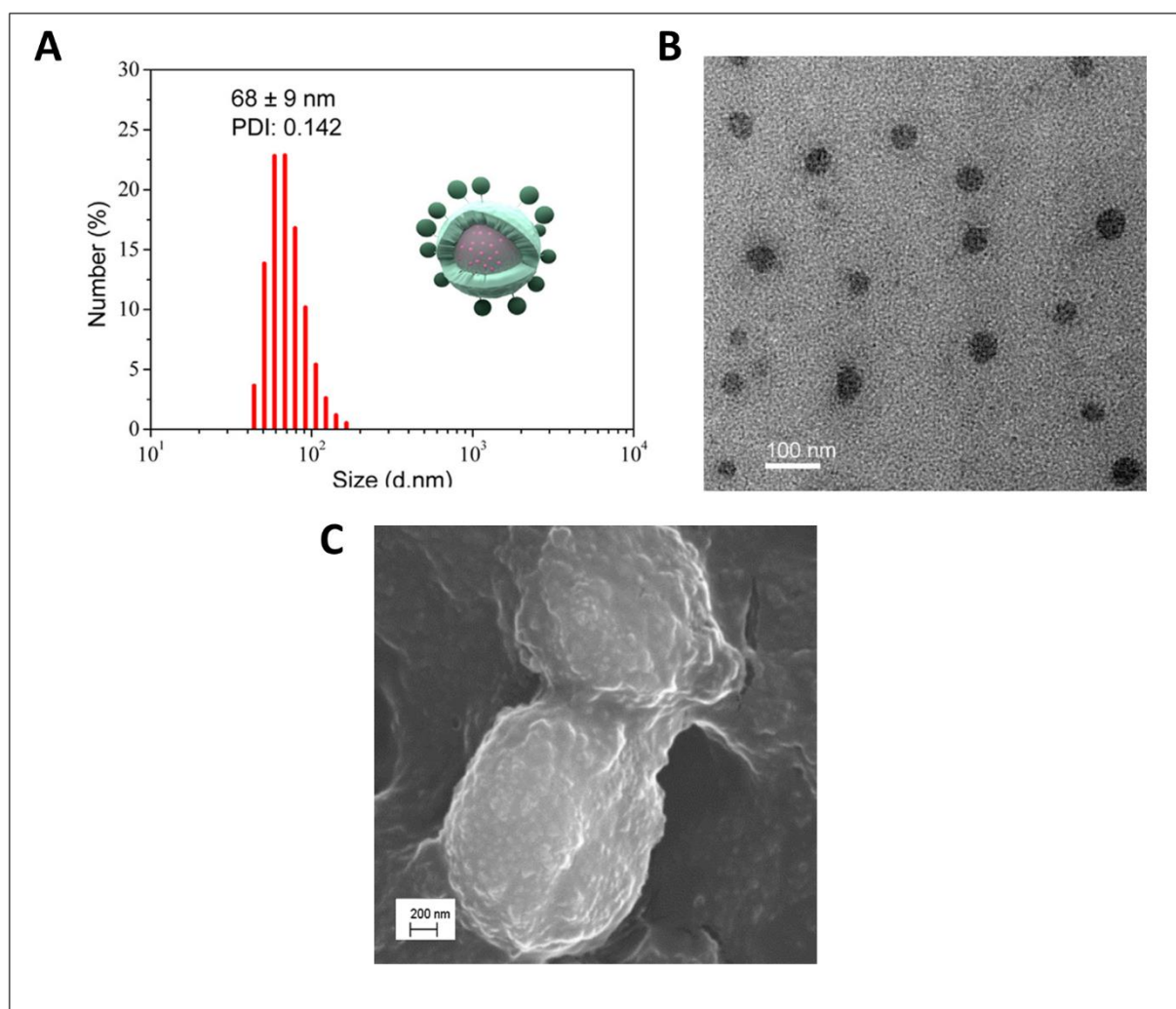


Figure 5-9. Size distribution of Dox-loaded P(Lac)G3 micelles in water determined by A. dynamic light scattering; B. TEM and C.SEM.

5.4.6. In vitro drug release studies of Dox-P(lac)G3 nanoparticles

In vitro drug release of Dox from Dox-P(Lac)G3 nanoparticle was investigated at different pH (5.0, 6.8 and 7.4) conditions. As illustrated in Figure 5-10, the Dox-P(Lac)G3 nanoparticles had brought about approximately 6 wt% of Dox released at pH 7.4 after 62 h.

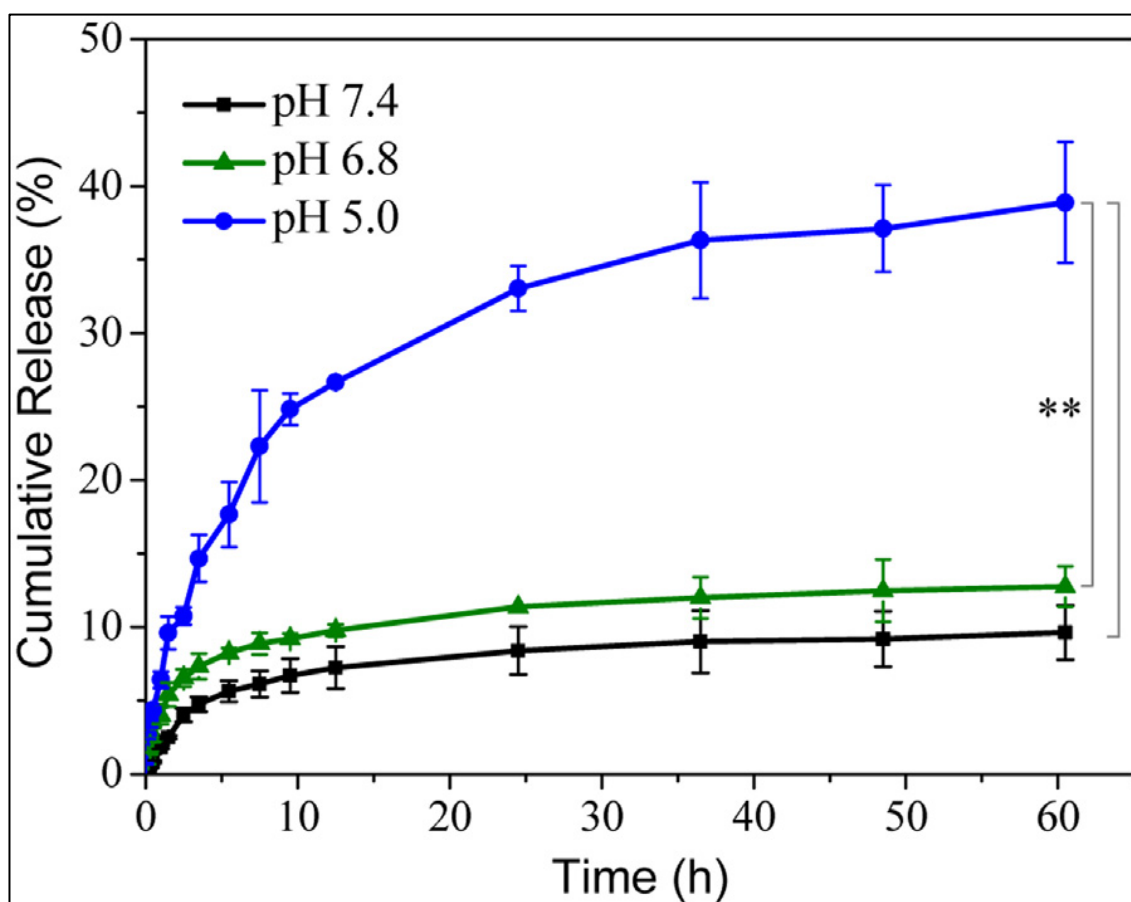


Figure 5-10. The pH-sensitive release of Dox from P(Lac)G3 micelles.

The Dox release rate was increased along with the decrease of pH value. The cumulative release of Dox showed only a slight increase and reached 10 wt% at pH 6.8 at the same timescale. In an acidic pH condition (pH 5.0, mimicking endo/lysosomal state), the Dox drug release was much faster than in a physiological pH as it showed a quicker release to reach over 25 wt% within 10 h, continued a sustained release to reach almost 40 wt% after 62 h.

5.4.7. Stability of blank and Dox-loaded P(Lac)G3 micelles

To explore the long-term stability of the Dox-P(Lac)G3, the NPs were suspended in DI water, 10% (V/V) FBS diluted with DI water, and DMEM containing 10% (V/V) FBS up to 120 h.

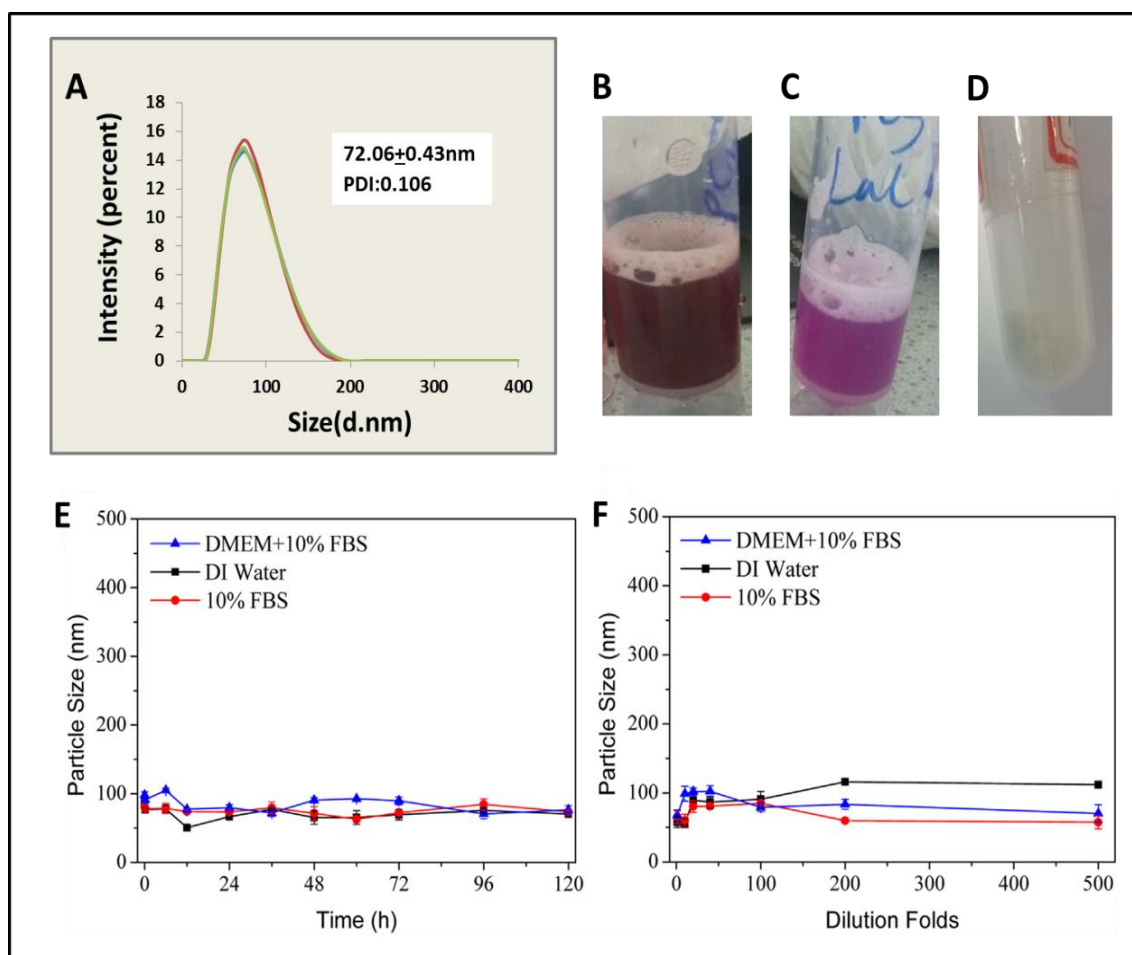


Figure 5-11. (A) DLS results of Dox-P(Lac)G3 nanoparticles after 3 months storage in DI water, (B) Image of Dox-P(Lac)G3 nanoparticles in DMEM containing 10% (V/V) FBS, (C) Image of Dox-P(Lac)G3 nanoparticles in DMEM containing 10% (V/V) FBS, (D) image of lyophilised P(Lac)G3 micelles in powder form, (E) DLS results of Dox-P(Lac)G3 nanoparticles after long time incubation in DI water, 10% (V/V) FBS and DMEM containing 10% (V/V) FBS, respectively. (F) Particle size changes of Dox/LP-g-G3P nanoparticles after dilution of different times with DI water, 10% (V/V) FBS and DMEM containing 10% (V/V) FBS, respectively.

DLS measurement showed there were few size distribution changes in three different media as the time increased even to 120 h (Figure 5-11E), which

signified that these three different media did not affect the size distribution and PDI of the Dox-P(Lac)G3 nanoparticles. The stability of Dox-P(Lac)G3 throughout 3 months was also investigated. Images in Figure 5-11B, C and D are images of the micelles suspension of Dox-P(Lac)G3, P(Lac)G3 in DMEM containing 10% (V/V) FBS and lyophilised micelles which were stored at 4°C for 3 months. The samples showed well-dispersed micelles with no precipitation and the size of Dox-P(Lac)G3 was slightly increased to 72.06nm from 68nm (Figure 5-11A).

5.4.8. Cytotoxicity of Dox.HCl, blank and loaded Dox-P(Lac)G3

Toxicity of the Blank P(Lac)G3 NPs were investigated in both HepG2, and NIH3T3 cell by CCK8 assay (Figure 5-12B) whereas measurement by SRB assay was done for HepG2, Hek293 and NIH3T3 cell lines (Figure 5-12A).

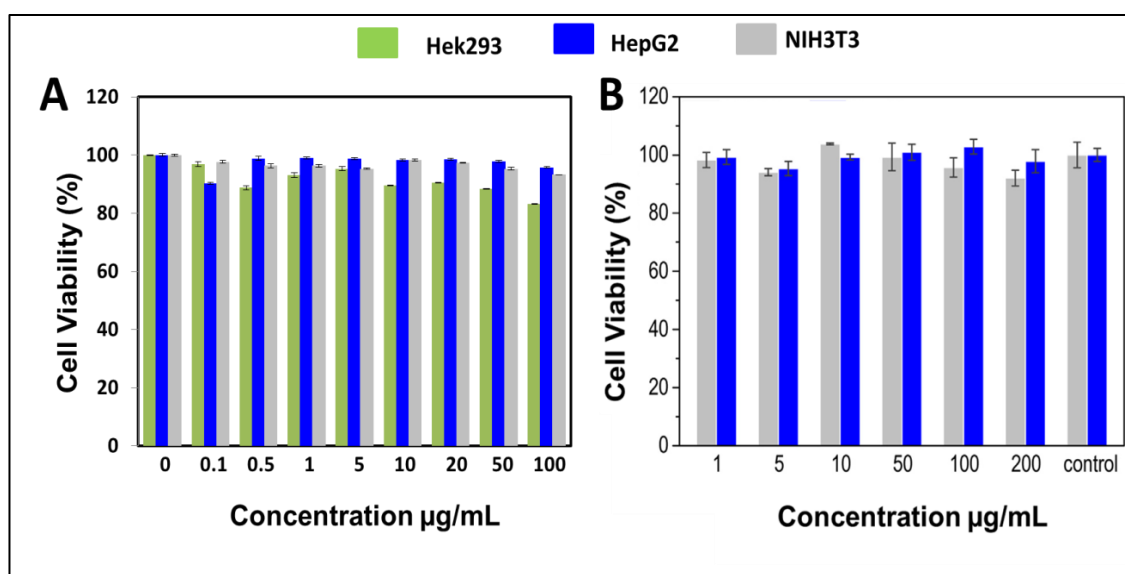


Figure 5-12. Biocompatibility assay of (A) HepG2, Hek293 and NIH3T3 cells against blank P(Lac)G3 nanoparticles for 24h by the SRB assay and (B) HepG2 and NIH3T3 cells against blank P(Lac)G3 nanoparticles for 24h by the CCK8 assay.

Results show that both assays produce similar cell viability percentage values which demonstrate that SRB assay can be used as an alternative to CCK8 assay. Also, both assays showed no significant cytotoxicity (viabilities remained above 80%) of blank P(Lac)G3 observed in HepG2, Hek293 and NIH3T3 cell lines even at a higher concentration up to 100-200 $\mu\text{g/mL}$.

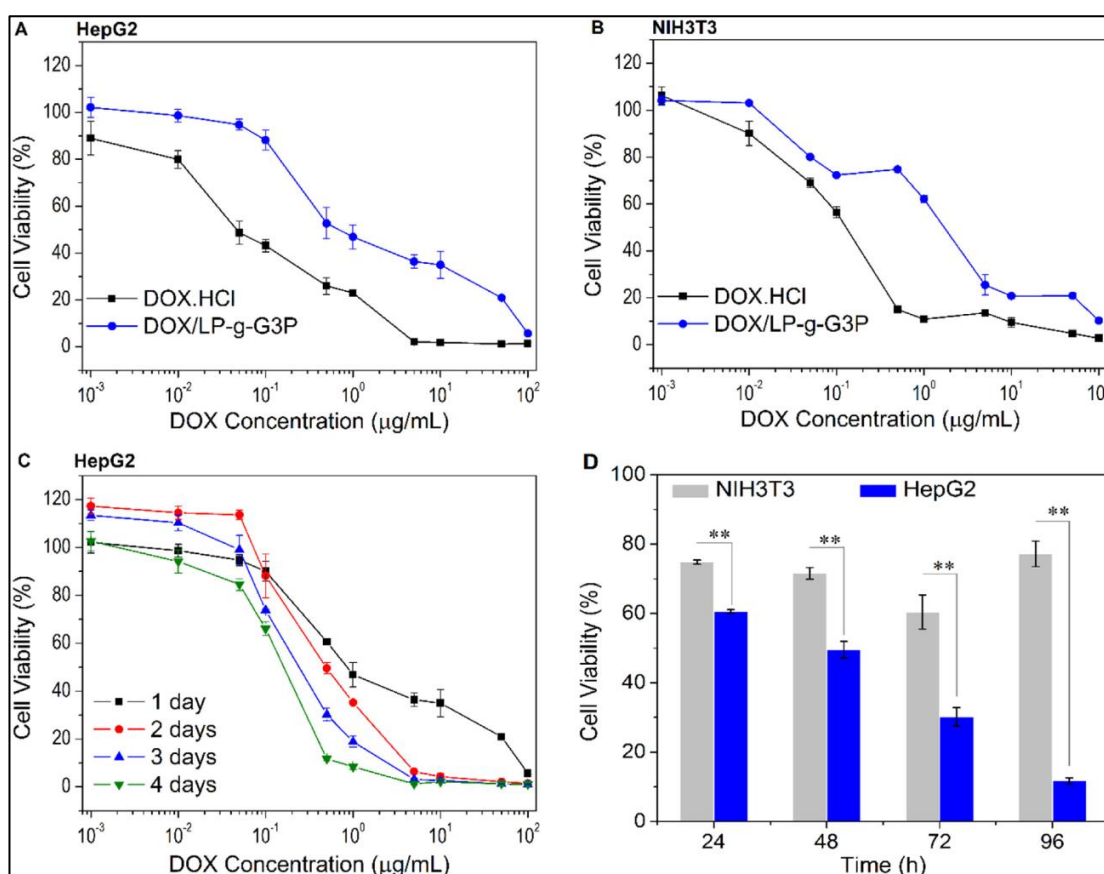


Figure 5-13. Dose-dependent cytotoxicity of (A) HepG2 and (B) NIH3T3 cells against Dox-P(Lac)G3 nanoparticles and free Dox.HCl solutions for 24 h. (C) Enhanced cytotoxicity of the Dox-P(Lac)G3 nanoparticles in HepG2 cells for varying time periods. (D) Cell viability against HepG2 and NIH3T3 cells incubated with the Dox-P(Lac)G3 nanoparticles at the Dox equivalent 0.5 $\mu\text{g/mL}$ for different time intervals (n = 6, **p < 0.05 by two-way ANOVA, followed by Tukey's post-hoc test).

Moreover, Viability of cells treated with Dox.HCl was also investigated using CCK8 and SRB assay for 24hours. HepG2 and NIH3T3 cells were ASGPRs and RCA120 positive and negative cells, respectively.

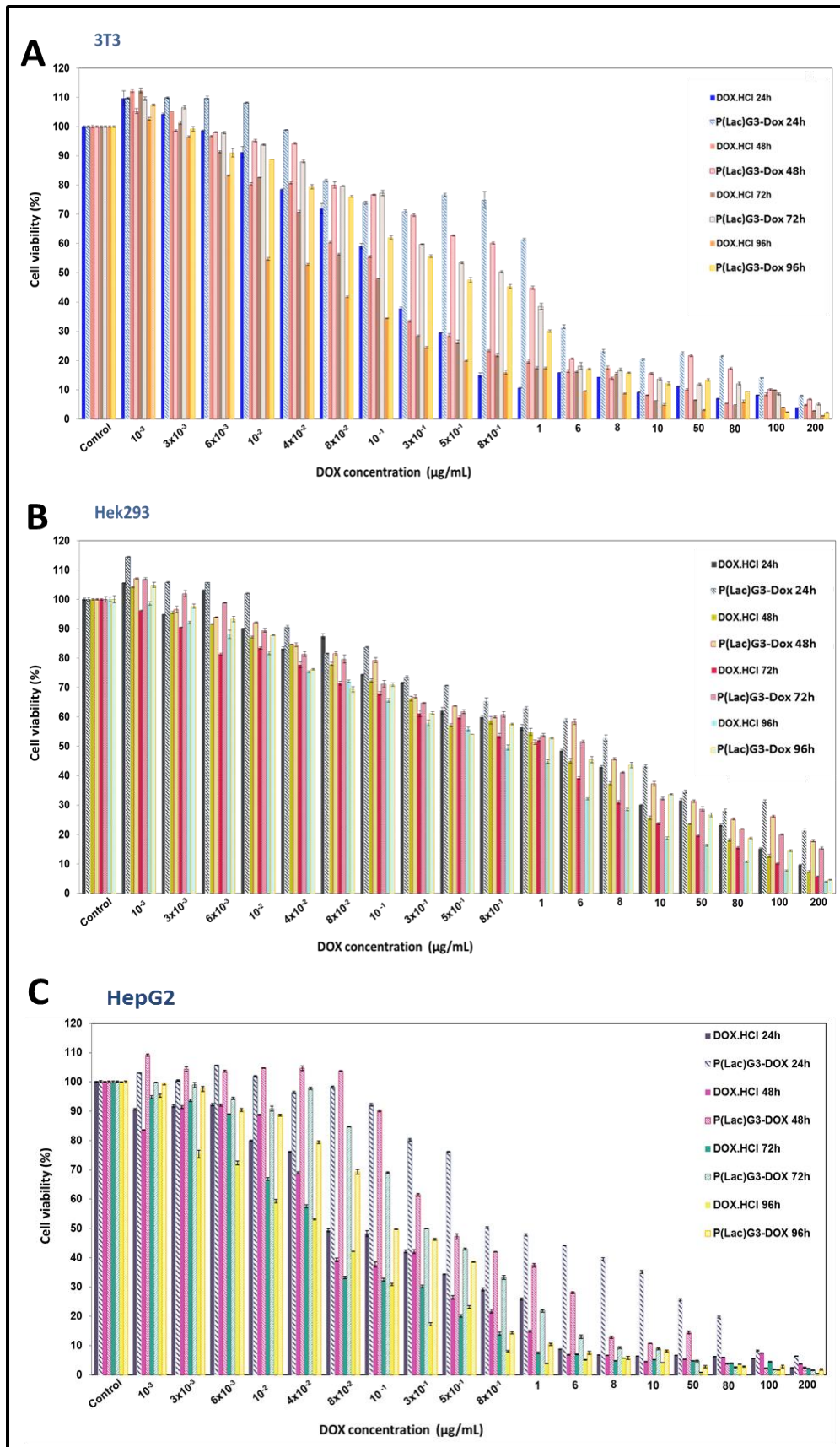


Figure 5-14. The in vitro cytotoxicity by SRB assay of Dox.HCl and Dox-P(Lac)G3 after 24, 48, 72 and 96 hours of incubation against A. NIH3T3 cells; B. Hek293 cells and C. HepG2 cells.

In both assays (Figure 5-13A&B and Figure 5-14A&C), cytotoxicity was concentration dependent and increased with increasing Dox concentration for both free Dox.HCl solution and Dox-P(Lac)G3 nanoparticles treated HepG2 and NIH3T3 cells.

Table 5-2. Calculated IC₅₀ values of free Dox.HCl and Dox-P(Lac)G3 in HepG2, Hek293 and NIH3T3 cell lines at a varying time by CCK8 and SRB assays

Cell lines(CCK8/SRB) /Time of incubation		IC ₅₀ (µg/mL)				
		HepG2		NIH3T3		Hek293
		CCK8	SRB	CCK8	SRB	SRB
24h	Dox.HCl	0.046	0.084	0.129	0.258	5.754
	Dox-P(Lac)G3	0.675	0.847	1.701	2.153	9.763
48h	DOX.HCl	-	0.058	-	0.234	4.267
	Dox - P(Lac)G3	0.507	0.475	-	0.976	7.489
72h	Dox.HCl	-	0.049	-	0.165	3.588
	Dox - P(Lac)G3	0.242	0.317	-	0.856	6.358
96h	Dox.HCl	-	0.041	-	0.069	0.943
	Dox - P(Lac)G3	0.162	0.195	-	0.469	5.699

***Important note: The CCK8 assay was only carried out in HepG2 and NIH3T3 cell lines and at an only particular time for publication purpose.**

Similarly, the IC₅₀ (the concentration that caused 50% cell death) value was also obtained with Dox concentration varied from 0.001 to 200 µg/mL. The IC₅₀ of the free Dox.HCl solution and Dox-P(Lac)G3 nanoparticles determined by CCK8 were calculated to be 0.046 µg/mL and 0.675 µg/mL, respectively in HepG2 cells, while 0.129 µg/mL and 1.701 µg/mL, respectively, were calculated for NIH3T3 cells. In comparison, the IC₅₀ determined by SRB were calculated to be 0.084 µg/mL and 0.847 µg/mL, respectively, in HepG2 cells whereas

0.258 µg/mL and 2.153 µg/mL, respectively, were obtained in NIH3T3 cells (table 5-2). Cell viability analysis by both SRB and CCK8 showed that the cytotoxicity of the Dox-P(Lac)G3 nanoparticles in HepG2 cells was time-dependent as well. The IC₅₀ values by CCK8 (SRB) assays after 1, 2, 3 and 4 days were 0.675 (0.847), 0.507(0.475), 0.242 (0.337) and 0.160(0.307) µg/mL, respectively. Meanwhile, cytotoxicity of Dox.HCl and Dox-P(Lac)G3 by SRB assay were determined in Hek293 and NIH3T3 cells lines after 1,2,3 and 4 days (Figure 5-14A&B). The IC₅₀ values given in table 5-2 were very high for Hek293 cells and NIH3T3 cells compared to HepG2 cells which implied that the Dox-P(Lac)G3 nanoparticles had a better affinity toward the HepG2 cells and could kill the tumour cells.

5.4.9. Cellular internalisation by Flow cytometry and confocal studies

It is likely that lactosylated pullulan serving as the hydrophilic shell of P(Lac)G3 nanoparticles could facilitate liver-targeted delivery. To preliminarily investigate the cellular internalisation efficiency of the Dox-P(Lac)G3 nanoparticles, confocal laser scanning microscopy and flow cytometry were performed. Free hydrophilic Dox.HCl solution and Dox-P(Lac)G3 nanoparticles with an equivalent amount of Dox (5 mg/mL) were added to exponentially growing cells for 0.5, 1 or 6 h. As presented in Figure 5-15, after 0.5h, both Dox. HCl and Dox-P(Lac)G3 treated cells exhibited some weak red signals in the cytoplasm, whereas for the time increased to 1 and 6h, the cells treated by Dox.HCl already presented very strong signals inside the nucleus in addition to a very weak fluorescence in the cytoplasm. The Dox-P(Lac)G3 treated cells instead

showed speckled red dots throughout the cytoplasm for all 6 hours incubation revealing the efficiently transport of Dox inside HepG2 cells via endocytosis.

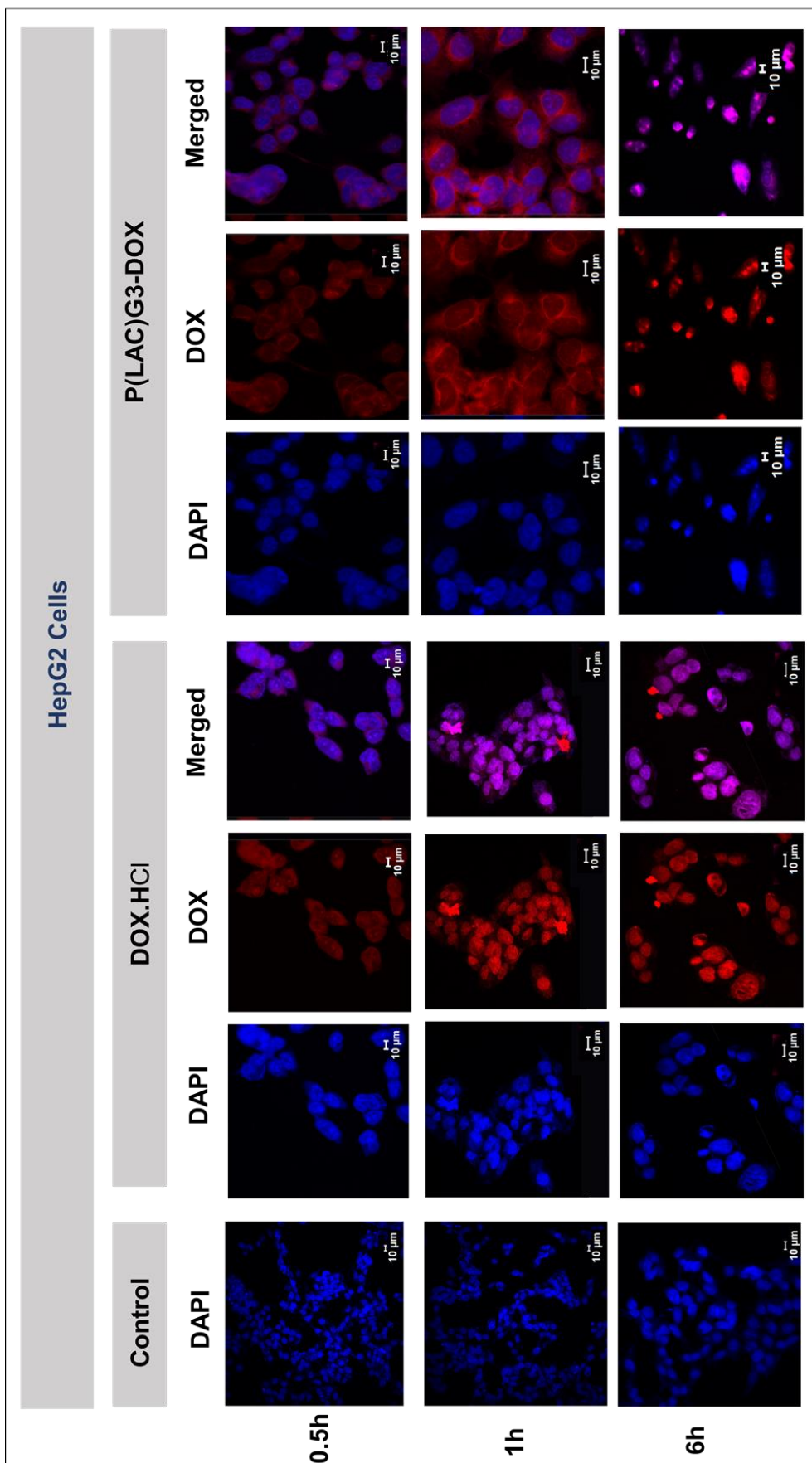


Figure 5-15. The cellular uptake results against HepG2 cells treated with Dox.HCl and Dox-P(Lac)G3 nanoparticles for 0.5, 1 and 6 hours by Confocal laser scanning microscopy. For each panel, the images from top to bottom indicate cells treated after 0.5, 1 and 6 hours. The first column indicates the untreated cells with their nucleus stained with DAPI which is used here as a control. The next 3 columns represent cells treated with Dox.HCl shown here with DAPI stain only, with Dox stain only and overlays of the two channels. Similarly the last 3 columns represent cells treated with Dox-P(Lac)G3.

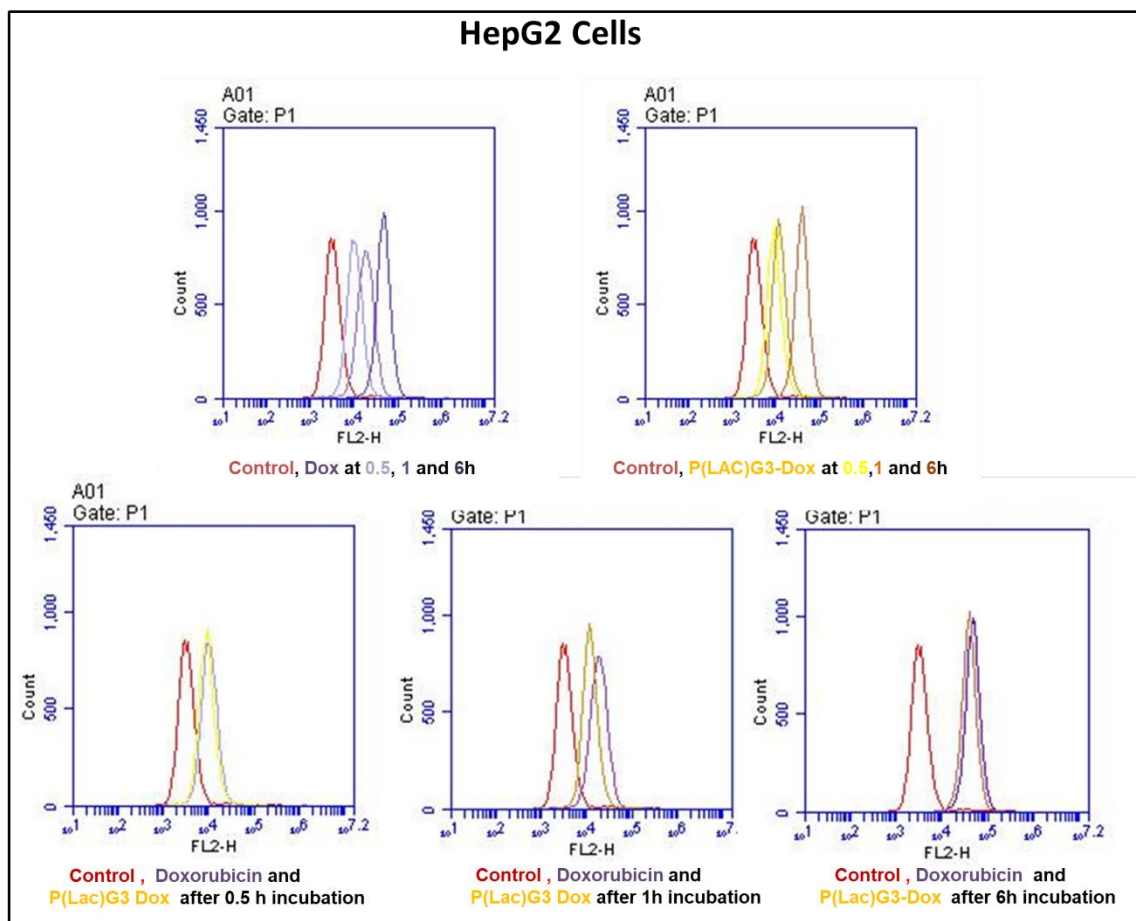


Figure 5-16. The cellular uptake by Flow Cytometry of Dox.HCl and PG3(lac)-Dox nanoparticles at 0.5, 1 and 6 hours in HepG2 cells. The Flow cytometry histograms are represented in 2 ways: first top 2 histogram plots represent separate plots of the changes in fluorescence intensity of Dox.HCl treated HepG2 cells (peaks in purple) and Dox-P(Lac)G3 treated HepG2 (peaks in yellow) over time whereas the 3 bottom plots compare the fluorescence intensity of Dox.HCl and Dox-P(Lac)G3 treated HepG2 cells at each time intervals. Untreated HepG2 cells were also used as control (peaks in red).

The flow cytometry (Figure 5-16) also indicated that the hydrophobic Dox was successfully transported into cells by being loaded in Dox-P(Lac)G3 nanoparticles as the fluorescence intensity was increased with time.

5.4.10. Apoptosis studies

To further demonstrate that Dox was effectively released from P(Lac)G3 nanocarriers, the carriers containing Dox were treated with HepG2 cells to investigate if they could induce apoptosis.

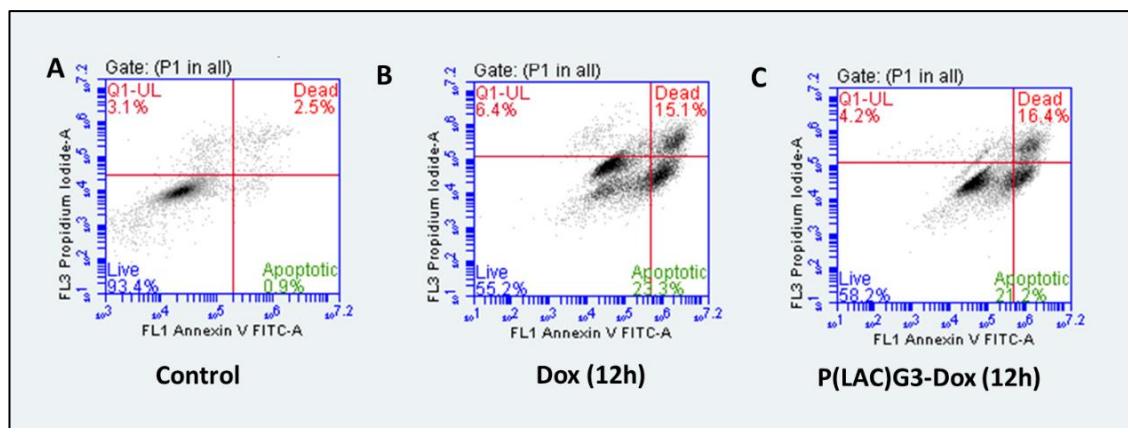


Figure 5-17. The effect of free Dox.HCl and Dox-P(Lac)G3 on the induction of apoptosis in HepG2 cells. Tumour cells were quantified by flow cytometric analysis of Annexin V FITC staining in tumour cells following 12h treatment with 5 μ g/mL equivalent Dox concentration. The lower left (LL) quadrant represents live/healthy cells, the lower right (LR) quadrant represents early apoptosis, and the upper right (UL) represents cells in late apoptosis, while the upper left (UR) represents the percentage of Dox uptake/dead cells. The percentage of cells undergoing early or, late apoptosis is indicated in the respective quadrants.

The total apoptotic ratio of Dox.HCl was 29.7% obtained by summation of the early apoptotic ratio of 23.3% and the late apoptotic ratio of 6.4%, which was higher than that obtained with Dox-P(Lac)G3 being 23.7%.

5.5. Discussion

Herein, we have successfully synthesised the amphiphilic lactobionic acid modified pullulan bearing hydrophobic arginine dendrons P(Lac)G3 which was prepared similarly to PG3 (chapter-4) using azide-alkyne click chemistry between hydrophilic lactosylated pullulan and PLLA. The azidated pullulan containing 49.02% of N₃ per unit was first modified by the addition of lactobionic acid through an esterification reaction between the non-azidated OH group of pullulan and carboxyl COOH group of lactobionic acid to form the ester P(Lac)N₃. Esterification of pullulan has previously been achieved by few methods available in literature using acetyl chloride with pyridine, acetic anhydride, pyridine and 4-dimethylaminopyridine, carboxylic acids in situ

activated with tosyl chloride, N, N-Dicyclohexylcarbodiimide and 4-dimethylaminopyridine, iminium chloride and 1,1-carbonyldiimidazole and acetic anhydride activated with strong acids or metallic catalysts (Teramoto and Shibata, 2006, Kumareswaran, Gupta and Vankar, 1997, Hussain et al., 2010, Zhang et al., 2009). We have demonstrated the simple esterification process of lactobionic acid into pullulan using EDC.HCl and DMAP which resulted in high yield and conjugation of 34.45% per unit. 18.51%/unit of arginine dendrons were then successfully clicked to the azidated lactose bearing to form an amphiphilic nanocarrier. The amphiphilic system could self-assemble to form well polydisperse micelles with great stability profile (54nm in size and CAC value of 8. 87 μ g/mL). Compared to PG3, P(LAC)G3 was made of 1.81% less hydrophobic moieties and higher hydrophilic backbone (due to the lactosylated pullulan) resulting in much lower particle size (PG3 of 87.07nm whereas P(Lac)G3 is of 54nm). The self-assembly of these amphiphilic systems is driven by the weak non-covalent intermolecular forces including the hydrophobic interactions (within BOC/PBF groups) and π - π interaction (within phenyl groups) which attract each dendron molecules to aggregate together minimising their contact to water molecules while optimizing the repulsion between the hydrophilic pullulan or lactosylated pullulan. The repulsive interaction is due to electrostatic or steric repulsion between the hydrophilic molecule which stays in contact with water. Unexpectedly, the extreme lower particle size reduction of P(Lac)G3 compared to PG3 could possibly due because of a higher hydrophilic periphery of the micelle enhancing a tighter hydrophobic core since it is known that the self-assembly of amphiphilic structures can be varied by controlling the ratio of hydrophilic and hydrophobic segments (Xia et al., 2017). Moreover, Ree et al. in 2017 also report the stabilisation of micelles by altering the ratio of

hydrophilic and hydrophobic blocks; the authors report that in contrast to a simple hydrophilic linear polymer backbone, hydrophilic bristles possess the ability to stabilise the micelle corona structurally. Therefore, we deduce that the addition of lactobionic acid into pullulan has extensively increased its overall hydrophilicity. It has also been reported that an increase in the length of the hydrophilic block is associated with an increase in the CMC (Rosen et al., 1982, Kulthe et al., 2012). However, P(Lac)G3 had a CAC value of 8.87 μ g/mL which was lower than that of PG3, this shows that the increased hydrophilicity did not affect the stability of micelles maybe because the targeting moieties are added on the surface of few units of the polymer and is not related with the polymer lengthening. To investigate if P(Lac)G3 could improve the targeting of HepG2 cells, the hydrophobic drug Dox was incorporated into P(Lac)G3. PG3 contain a larger number of Hydrophobic segments, therefore, has a larger core size resulting in a greater ability to entrap hydrophobic drugs (Kulthe et al., 2012). The size of loaded P(Lac)G3 is only 68nm which shows that these nanocarriers have the most desirable size to deliver therapeutic agents into cancerous liver cells. It is known that in general, micelles with sizes between 20 and 50 nm can efficiently enter cancerous tissues through the openings of loosely packed cancer cells via the EPR effect (Danhier, Feron and Pr at, 2010, Ree et al., 2017). Therefore, P(Lac)G3-Dox of sizes 68nm would not only reach a tumour passively but would easily avoid Kupffer cells uptake, diffuse deeper in the space of Disse and diffuse the sinusoids through the fenestrations and reach hepatocytes plates to target them actively. In vitro release studies of Dox from Dox-P(Lac)G3 nanoparticles also showed a sustained release behaviour which could be the advantageous feature in therapy: the primary high drug release (25 wt% within 10h) provides an initial dose, followed by a sustained release.

Furthermore, owing to the dilution that can be caused by the bloodstream when the Dox-P(Lac)G3 nanoparticles are injected into the body, the nanoparticles would suffer from the dissociation of self-assemblies leading to the premature release of the loaded drug. Therefore, we explored the stability of the Dox-P(Lac)G3 nanoparticles against dilution with three different media. As shown in Figure 5-11F, there were no obvious changes in three media even after 500-fold dilution, which implied the Dox-P(Lac)G3 nanoparticles had good stability against dilution. To preliminarily investigate the tumour cellular effect of the Dox-P(Lac)G3 nanoparticles, cell viability by CCK8 and SRB assays, confocal laser scanning microscopy, flow cytometry and apoptosis assays were performed. The toxicity of Dox-P(Lac)G3 in HepG2 cells carried by SRB assay was much higher than that of PG3-Dox at 24h and 48h (IC₅₀ for Dox-PG3 and Dox-P(Lac)G3 was 1.765 and 0.847 µg/mL, respectively at 24h and 1.246 and 0.475 µg/mL, respectively at 48h). Whereas at 72 and 96h, the IC₅₀ were nearly identical (0.276 and 0.317 µg/mL, respectively at 72h and 0.174 and 0.195 µg/mL, respectively at 96h). Since the high rate of release of Dox from the carriers more likely takes place inside the endosome-lysosome (low pH environment) compartment after internalisation of the loaded carriers, the toxicity results indicate that the HepG2 cells internalise quicker the Dox-P(Lac)G3 nanoparticles which then have a quicker toxic effect compared to Dox-PG3 nanoparticles. Ghagada et al. in 2005 carried out a study where the factors influencing the uptake of folate-based liposomal in FR-expressing cells was observed. These factors were reported to be the ligand number, exposure time and carrier concentration. Increasing the incubation time increased the uptake for liposomes containing a low number of ligands whereas liposomes with a high number of ligands reached saturation rapidly decreasing the uptake

rate. The authors further reported that the internalisation process in cells is slower than the binding process of liposomes to the cell surfaces. However, in our study, we observed that the increase of ligands by the addition of lactobionic acid in pullulan increased the toxicity in HepG2 cells which may be related to increased uptake rate of P(Lac)Dox, therefore, resulting in higher toxicity. But the analysis of internalisation by confocal and flow cytometry does not correspond to these observations since the distribution of Dox after 0.5, 1 and 6h in treated Dox-PG3 and Dox-P(Lac)G3 HepG2 cells does not differ and treated cells by both loaded systems exhibited same amount of fluorescence intensity after incubation at 0.5, 1 and 6h (refer to chapter 8).

5.6. Conclusion

In summary, we have successfully developed an original amphiphilic glycopolyptide analogue, lactosylated pullulan-graft-arginine dendrons (P(Lac)G3) that could form core-shell nanoassemblies with an average diameter of about 54 nm by the fine-tuning of intra- and intermolecular interactions which could also provide a safe and spacious harbour for the hydrophobic drugs. Blank P(Lac)G3 nanoparticles exhibited excellent biocompatibility both in the normal and tumour cells, whereas Dox-loaded P(Lac)G3 NPs could be effectively internalised into the hepatoma carcinoma cells and dramatically inhibited cell proliferation. Thus, this study produced a liver targeting nanocarrier of excellent size distribution with higher toxicity effect to HepG2 cells in comparison to PG3 loaded Dox nanocarriers. Also, we demonstrated that varying the ratio between hydrophilic segment to hydrophobic segments within micelles could improve their size which is the

primary physical characteristic of a nanocarrier system for the delivery of hydrophobic drugs in liver cancer therapy.

CHAPTER 6. CO-DELIVERY OF DOXORUBICIN AND CURCUMIN USING REDOX-BASED MICELLAR DENDRONS

6.1. Introduction

Within the last decade, persistent efforts have been made in the development of stimuli-responsive drug delivery systems that can, when exposed to intracellular stimuli, produce physicochemical changes that favour drug release at the target site. We have introduced in chapter 1 the different types of biological stimuli that have been exploited for triggered drug release including temperature (Zhan et al., 2015), pH (Ma et al., 2015), magnetic field (Qin et al., 2009), redox potential (Li et al., 2009), enzymes (Li et al., 2014) or two parameters at the same time (Chen et al., 2013). Among these, redox stimuli-responsive nanocarriers characterised by disulphide bonds in the main chain, at the side chain or in the crosslinker for enhanced intracellular drug release has attracted more and more attention (Wang et al., 2014). This attention is driven by the great difference in the redox potential between the mildly oxidising extracellular milieu and the intracellular reducing milieu which are even higher in cancerous cells (Jhaveri, Deshpande and Torchilin, 2014, Wang et al., 2014). The reducing environment in the intracellular compartment is due to the presence of higher levels of the glutathione tripeptide (γ -glutamyl-cysteinyl-glycine) (GSH) in the cytosol and subcellular compartments (approximately 2–10 mM), which are about 100–1000 times higher than in the extracellular compartment (approximately 2–20 μ M) (Schafer and Buettner, 2001, Li et al., 2012, Jhaveri, Deshpande and Torchilin, 2014). GSH can reduce disulphide bonds and is reported to be at several times higher concentrations in tumour tissues compared with normal

tissues (Wang et al., 2014, Li et al., 2012). Moreover, there are other types of source of redox reduction besides GSH in the intracellular compartments. These include thioredoxin reductase and cysteines present in lysosomes. The cysteines keeps low mass iron in the reduced state (Fe^{2+}) in the acidic compartment and therefore increases the lysosomal redox potential, also, cysteines assist the disulfide cleavage in endosomes (Söderberg, Sahaf and Rosén, 2000; Kurz, Eaton and Brunk, 2010; Cheng et al., 2011; Li et al., 2012; Jhaveri, Deshpande and Torchilin, 2014). Many carriers have been developed using redox-responsive materials for the delivery of chemotherapeutic agents and have also been used in combination therapy as well, more specifically for the co-delivery of therapeutic agents (Jhaveri, Deshpande and Torchilin, 2014). Co-delivery systems are new methods developed that are capable of simultaneously transporting and releasing multiple therapeutics at a disease site. When a single therapeutic fail, treatment with 2 or more therapeutics at the same time can succeed. A main example of co-delivery involves targeting multi-drug resistance (MDR) pathways (details in chapter 1) either through transporter inhibitors or targeting of MDR genes, while also delivering a chemotherapeutic. Many researchers have focused on the enhancement of Doxorubicin delivery by the co-delivery of Dox with Combrestatin, verapamil, cyclophosphamide, paclitaxel, P-gp siRNA, survivin mutant gene and p53 antitumor gene to overcome drug resistance, increase its accumulation in tumour cells and the permeability in tumour microvessels (Dai et al., 2012; Wu et al., 2007; Ishida, Shiraga, and Kiwada, 2009; Wang et al., 2011; Meng et al., 2010; Xiao et al., 2010; Zhao et al., 2012; Godsey, Suryaprakash, and Leong, 2013). Furthermore, inhibition of p-gp-dependent drug efflux activity has shown to be achievable using the natural compound curcumin (CHANG et al., 2013;

Bar-Zeev, Livney and Assaraf, 2017). Curcumin, isolated from turmeric is a poor water-soluble compound that possesses anticancer and anti-inflammatory activity which are both critical for the suppression, formation and progression of cancer (Bar-Zeev, Livney and Assaraf, 2017; Basniwal, Khosla and Jain, 2014). Rivera-Espinoza and Muriel in 2009 have reported the possible ability of curcumin to cure and ameliorate hepatic disorders since curcumin has the ability to inhibit factors such as nuclear factor-kB, has anti-oxidant properties, can attenuate liver injury induced by ethanol, thioacetamide, iron overdose, cholestasis and acute, subchronic and chronic carbon tetrachloride (CCl₄) intoxication; moreover, it reverses CCl₄ cirrhosis to some extent.

Structural Characteristics of Curcumin

Curcumin also known as diferuloylmethane ((1E,6E)-1,7-bis(4-hydroxy-3-methoxyphenyl)-1,6-heptadiene-3,5-dione) has a chemical formula of C₂₁H₂₀O₆, and molecular weight of 368.38.

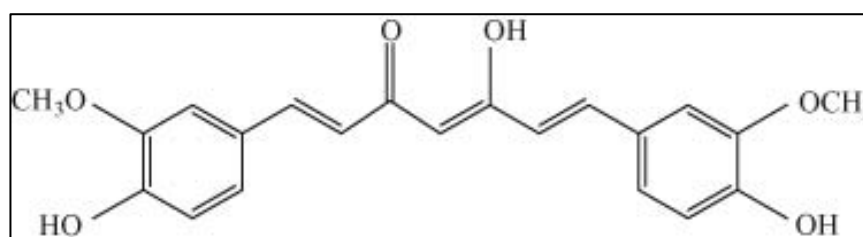


Figure 6-1. Chemical structure of curcumin (Priyadarsini, 2014).

The structure of curcumin consists of two aromatic ring systems containing o-methoxy phenolic groups, connected by a seven carbon linker consisting of an α,β -unsaturated β -diketone moiety. Curcumin can be in different isoforms depending on the environment. Mostly it is in crystal form either as cis-enol and keto form. It is a hydrophobic molecule with a log P value of ~ 3.0 which is

soluble in DMSO, methanol, ethanol, acetonitrile, chloroform, ethyl acetate, etc., and therefore curcumin has shown to have a low bioavailability when administrated orally or intravenously (Priyadarsini, 2014; Yallapu, Jaggi and Chauhan, 2012). For this reason, researchers have been working on solving the limiting factors of curcumin by improving its bioavailability, protecting its degradation and metabolism and by increasing its targeting capacity into tumour cells via its incorporation into a different type of nanoparticles (Yallapu, Jaggi and Chauhan, 2012).

6.2. Aims and objective

In this work, we aim to improve the release rate of pullulan modified arginine dendron PLLA by adding a reductive disulphide linkage between pullulan and the hydrophobic dendron to form PSSG3. As we previously could not identify any difference between the internalisation of PG3 and P(Lac)G3 into HepG2 cells. We choose here to keep it simple and produce pullulan modified G3 nanocarriers via a disulphide linkage which can stay stable at oxidising extracellular conditions but undergoes rapid breakdown or thiol-disulfide exchange in the presence of reducing agents like GSH in the intracellular compartment of liver cancer cells. Moreover, previous studies have shown that hepatocellular carcinoma cells exhibit increased resistance against re-treatment of Doxorubicin (Buschauer et al., 2018), therefore to improve the anti-cancer toxicity effect of loaded Dox nanocarriers compared to free Dox.HCl, the two hydrophobic drugs curcumin and Doxorubicin were chosen here to be loaded at the same time into PSSG3 to form overall a co-delivery system. Curcumin not only is a cheap natural anticancer drug but also could enhance the antitumor efficiency of Doxorubicin in HepG2 cells. We, therefore, aim in this study to:

- successfully synthesise and characterise the pullulan modified G3 bearing a disulphide linkage (PSSG3),
- investigate the self-assembly, morphology and stability of PSSG3,
- investigate the loading and encapsulation efficiency of doxorubicin (PSSG3-Dox), curcumin (PSSG3-cur) and both doxorubicin and curcumin in PSSG3 (PSSG3-Dox/Cur),
- investigate the in vitro toxicity of PSSG3, PSSG3-Dox, PSSG3-cur and PSSG3-Dox/Cur against HepG2, NIH3T3 and Hek293 cells,
- Investigate the ability to uptake the doxorubicin and curcumin loaded nanoparticles into HepG2 cancer cells.

6.3. Methodology

6.3.1. Dendron synthesis

Hydrophobic G3 Dendrons PLLA (PBF/BOC) synthesised was used in this study. Their synthesis details are described in chapter 3.

6.3.2. Addition of disulphide bond to Pullulan (P-SS-COOH)

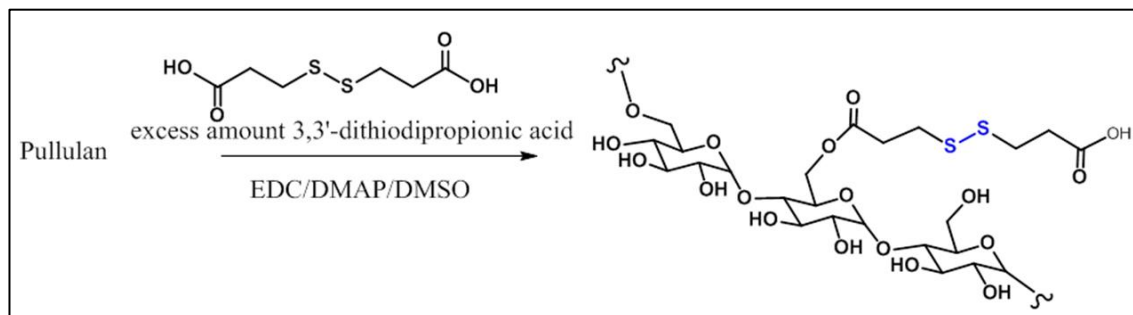


Figure 6-2. Synthesis equation of disulfide-linked pullulan PSS-COOH.

Briefly, pullulan (1mmol) dissolved in 25ml of DMSO was added to a 50mL solution of a mixture of DTDPA (8mmol), EDC.HCl (5.4mmol) and DMAP

(5mmol) in DMSO. The reaction was left to stir for 2 days at 50-60 °C under N₂ atmosphere. The solution turned to dark brown within a day.

The solution was then dropped (dropwise) into 90% of ethanol (300ml) under vigorous stirring, and the precipitated product was dialysed against distilled water (MWCO 35000) for a day. The brown solids appearing in the dialysis bag were then collected by lyophilisation.

6.3.3. Azidation of disulphide modified pullulan (PSS-N₃)

To yield PSS-N₃, the carboxyl groups of the product PSS-COOH were reacted with the amine group of 3-azido propargylamine by a condensation reaction.

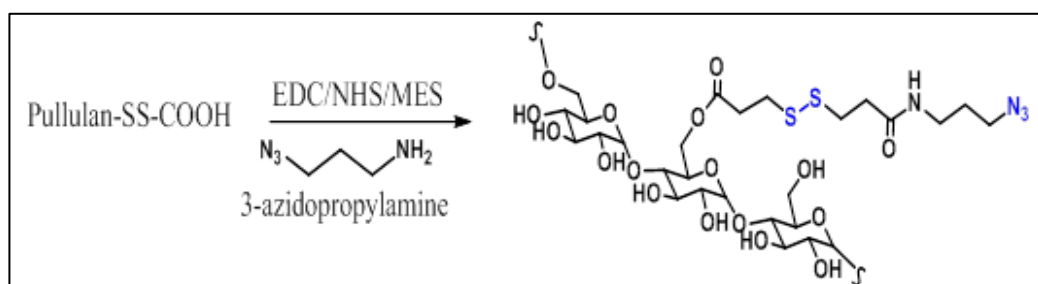


Figure 6-3. Synthesis equation of azidated disulfide linked Pullulan (PSSN₃).

First, P-SS-COOH (0.35g, 1mmol) was first dissolved in 50ml MES buffer and 25ml of DMSO (0.1M, PH6). Then EDC (0.13g, 0.668mmol) and NHS (0.08g, 0.668mmol) were added, and the mixture was left to stir at 4°C for 4hrs in the absence of O₂ to activate the carboxyl groups. 3-azidopropylamine (0.1g, 1mmol) was lastly added, and the reaction mixture was left to stir for 36h at RT.

The resulting yellowish solution was dialysed against water to remove unreacted agents (MWCO 3500) for 2 days. Finally, the PSSN₃ solution was lyophilised and stored at 4 °C until further use.

6.3.4. Click reaction between PSSN₃ and PLLAG₃ dendron

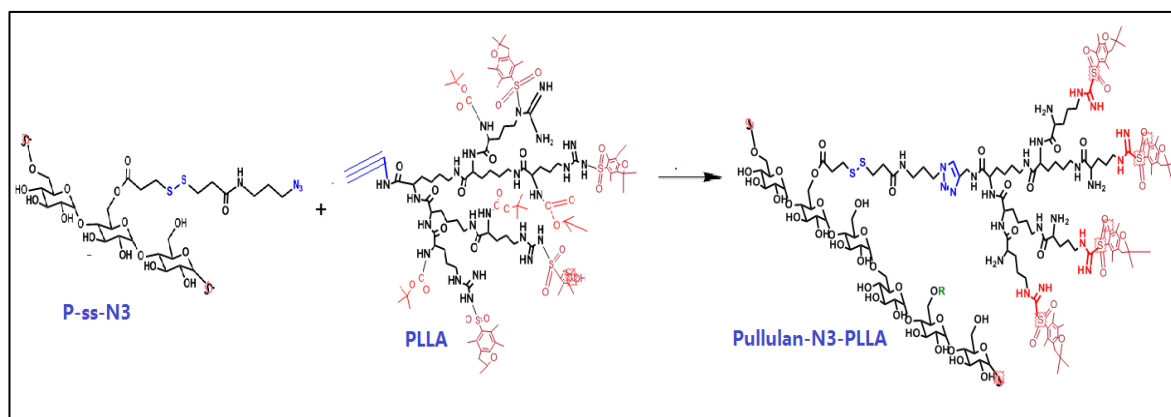


Figure 6-4. Synthesis equation of disulphide pullulan modified G3 bearing a disulphide leakage (PSSG3).

The PSSG3 was obtained by click reaction in a similar way as PG3 and P(Lac)G3 formation (details in chapter 4 and 5).

6.3.5. Characterisation

The characterisation was carried by FTIR and NMR, details of each method is given in chapter 2 and the other experiments were similarly carried as in chapter 4 and 5.

6.4. Results

6.4.1. Characterisation of the PSS-COOH and P-SS-N3 conjugates

Addition of the disulphide bond into Pullulan was synthesised by condensing the carboxyl acid group of 3, 3'-dithiodipropionic acid and the hydroxyl group of Pullulan. After the addition of DTDPA into pullulan, the terminal COOH group from DTDPA were then reacted with the amine group of 3-azidopropylamine to form an amide bond-containing product with a terminal azide group. Figure 6-5 shows the FTIR spectrum of the successful conjugation of DTDPA which is

confirmed by the characteristic absorption band at 1732 cm^{-1} indicating the carbonyl group (C=O) stretching vibration of the ester group (Li et al., 2014). Moreover, the azido group added to the disulphide linkage was also confirmed by the appearance of the strong absorption peak at 2111 cm^{-1} which corresponds at the N_3 group of the 3-azidopropylamine.

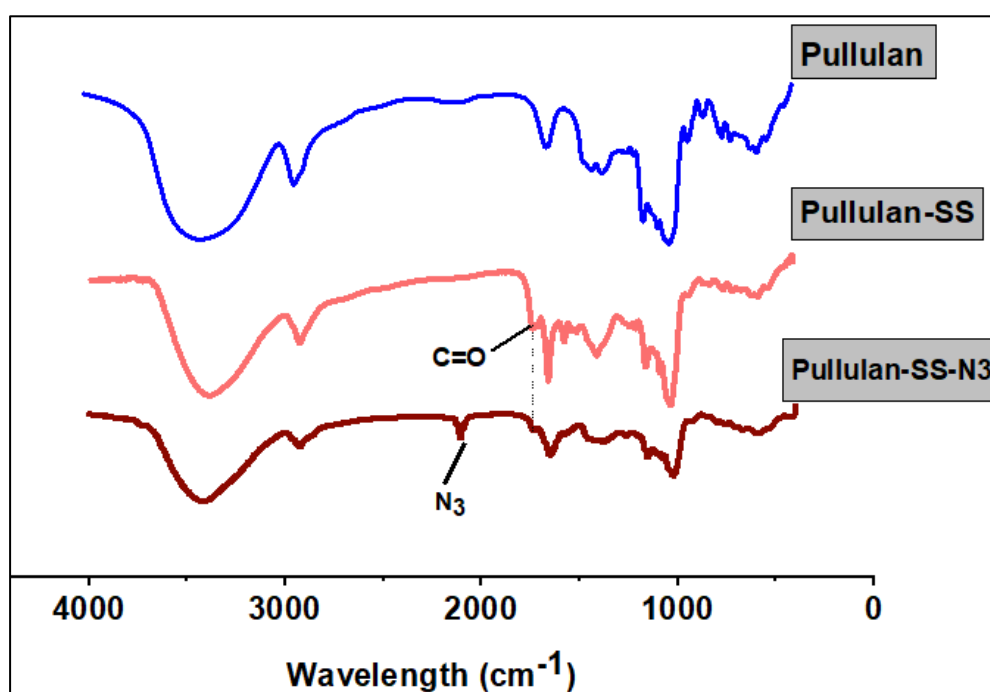


Figure 6-5. FTIR spectrum of pure pullulan, pullulan-SS-COOH and Pullulan-SS-N3 conjugates.

The successful conjugation of DTTPA in pullulan was also confirmed by $^1\text{H-NMR}$. Figure 6-6. shows the $^1\text{H-NMR}$ spectrum in which the characteristic peak of pullulan and DTPA are identified and matches with that of published data (Akiyoshi et al., 1993; Yang et al., 2014; Sivakumar and Panduranga Rao, 2003). The proton identified are 2.66 ppm (4H, m, a-H₂,DTPA), 2.71 (4H, m, b-H₂,DTPA), 2.99-3.94 ppm (4H, glucose C2, C3, C4, and C5,Pullulan), 4.42-5.75ppm (glucose,-OH, Pullulan), 4.66 ppm (1H, s, 1-glucose α -1,6, Pullulan), 5.00 ppm (1H, s, 2-glucose α -1,4, Pullulan). The degree of substitution of DTTPA in pullulan (DS; number of DTPA residues per 100 glucose units in

pullulan) was determined to be 16% by calculating the ratio of methylene group protons of DTDPA (2.66 ppm) to sugar protons of pullulan (C1 position of α -1,6 and α -1,4 glycosidic bonds, 4.66 and 5.00 ppm).

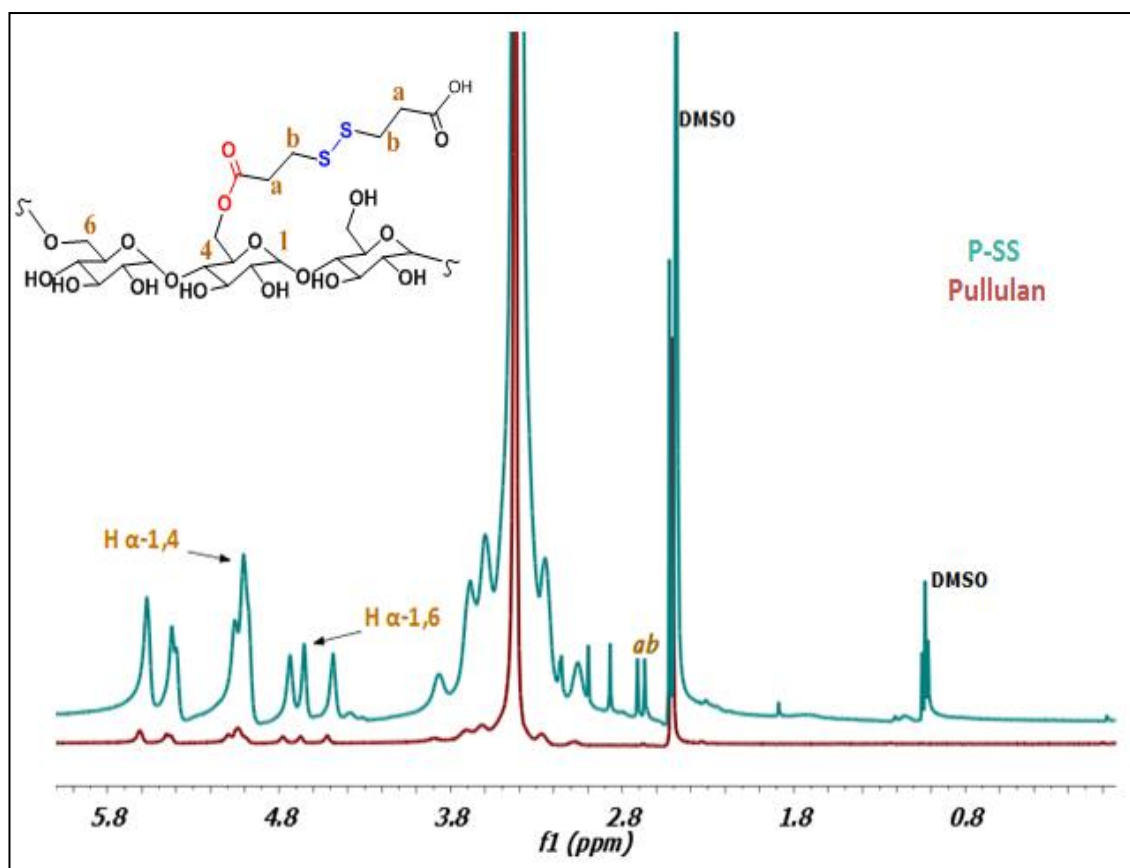


Figure 6-6. $^1\text{H-NMR}$ spectrum of pullulan and Pullulan-SS-COOH conjugate.

6.4.2. The self-assembly of PSSG3 and their stability studies

The successful conjugation of dendrons G3 (PBF/BOC) linked via disulphide bond in pullulan (PSSG3) was confirmed by the fact that PSSG3 could self-assemble into spheroidal nanoparticles of size 68.1nm as figure 6-7A&B shows. Moreover, the PSSG3 exhibited great stability throughout 3-month storage. In 3 months, no significant change in size was observed showing that the NPs retained their micellar structure. Moreover, in the presence of 10mM DTT, the nanoparticles exposed in DTT for 24hours showed that the disulphide linkage breaks resulting in various increased size distribution with a mean of 615nm.

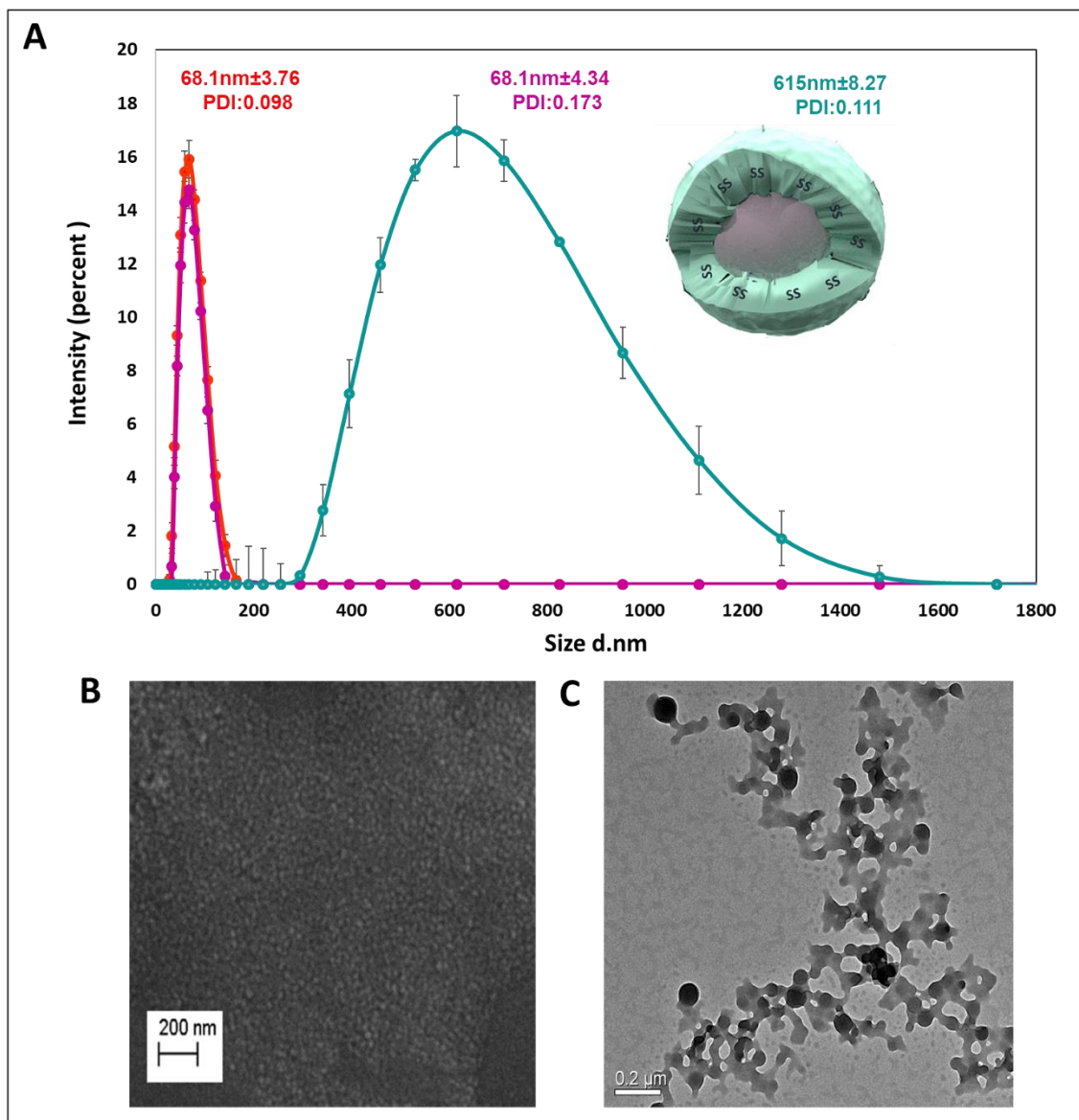


Figure 6-7. Size distribution and morphology studies of the blank PSSG3. DLS images at 0h (in red), after 3 months storage (in purple) and in the presence of 10mM DTT for 24hrs (in Blue) (A), SEM images at 0h (B) and TEM images at 0h (C).

High stability of the micelles PSSG3 was further confirmed by their low critical aggregation concentration value being 9.93μg/mL.

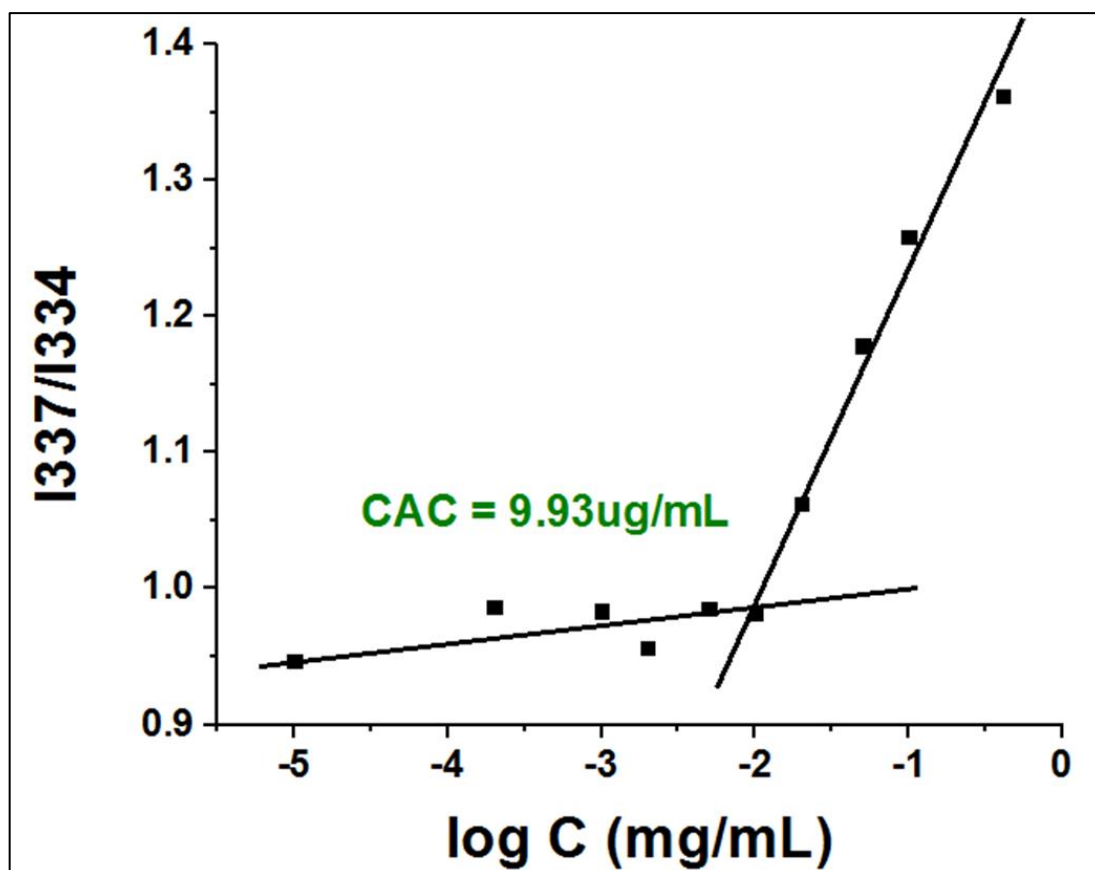


Figure 6-8. Critical association concentration of PG3 measured using the fluorescent dye pyrene.

6.4.3. Drug loading into PSSG3 nanocarriers

Since PSSG3 showed good stability profile, the carrier capability of loading hydrophobic drugs was investigated. Doxorubicin and Curcumin were loaded individually and in combination into the PSSG3 carrier. The loading and encapsulation efficiency were determined using the line of equation of the standard curve of doxorubicin being $y=5.0939x-0.5728$ (chapter 4) and the line of equation of the standard curve of doxorubicin being $y=0.1252x-0.0541$.

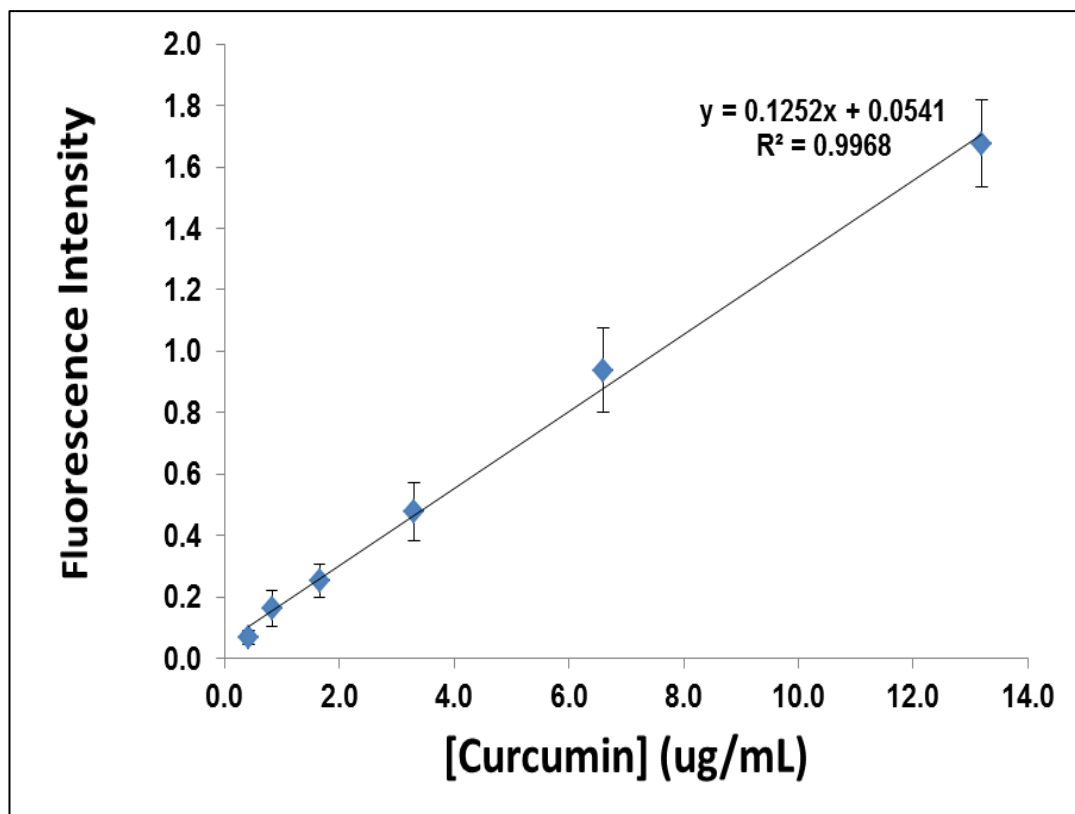


Figure 6-9. A standard curve of curcumin determined at 425nm.

Drug loading was carried out at a ratio of 5:1 (PSSG3: Dox or Cur or Dox/Cur). Table 6-1 shows that the drug loading and encapsulation efficiency of Dox into PSSG3-Dox is 18.14% and 59.74 %, respectively which is higher than that from PSSG3-Dox /cur being 15.59% and 57.80%, respectively. Similarly, the drug loading and encapsulation of curcumin from PSSG3-Cur is 19.21% and 91.44%, respectively, which was also higher than that from PSSG3-Dox/cur being 17.01% and 88.72%, respectively.

Table 6-1. Drug loading content (LC) and encapsulation efficiency (EE) of Dox and Cur in PSSG3 nanocarriers

P:Dox:Cur Ratio	Doxorubicin		Curcumin	
	LC%±std dev	EE%±std dev	LC%±std dev	EE%±std dev
5:1:1 (20%)				
PSSG3-Dox	18.14±3.50	59.74±7.44	N/A	
PSSG3-cur	N/A		19.21±3.01	91.44±1.11
PSSG3-Dox/cur	15.59±5.30	57.80±4.73	17.01±2.13	88.72±2.00

The size and morphology of the various drug-carrier conjugates were also investigated. The sizes of PSSG3-Dox was 91.28nm with similar size seen by SEM images (Figure 6-10B), and red spherical small particles are visible in fluorescence microscopy. However, a slightly increased to 118.46nm in size was observed after 3 months, which is maybe due to the slow release of the drug in normal PBS conditions. In the presence of 10mM DTT, broad size distribution is observed indicating the distribution of the free drug and disassembled carrier sizes.

The morphology and size distribution of the loaded curcumin into PSSG3 (Figure 6-11) are similar to that of PSSG3-Dox. The mean size is 78.82nm at 0h, which increases to 164.18nm after 3 months, and in the presence of DTT, the size distributions increase from 274.92nm to over 955.64nm. The greenish fluorescence inside the nanocarrier is also visible under fluorescence microscope showing the spherical morphology of the loaded PDDG3-Cur.

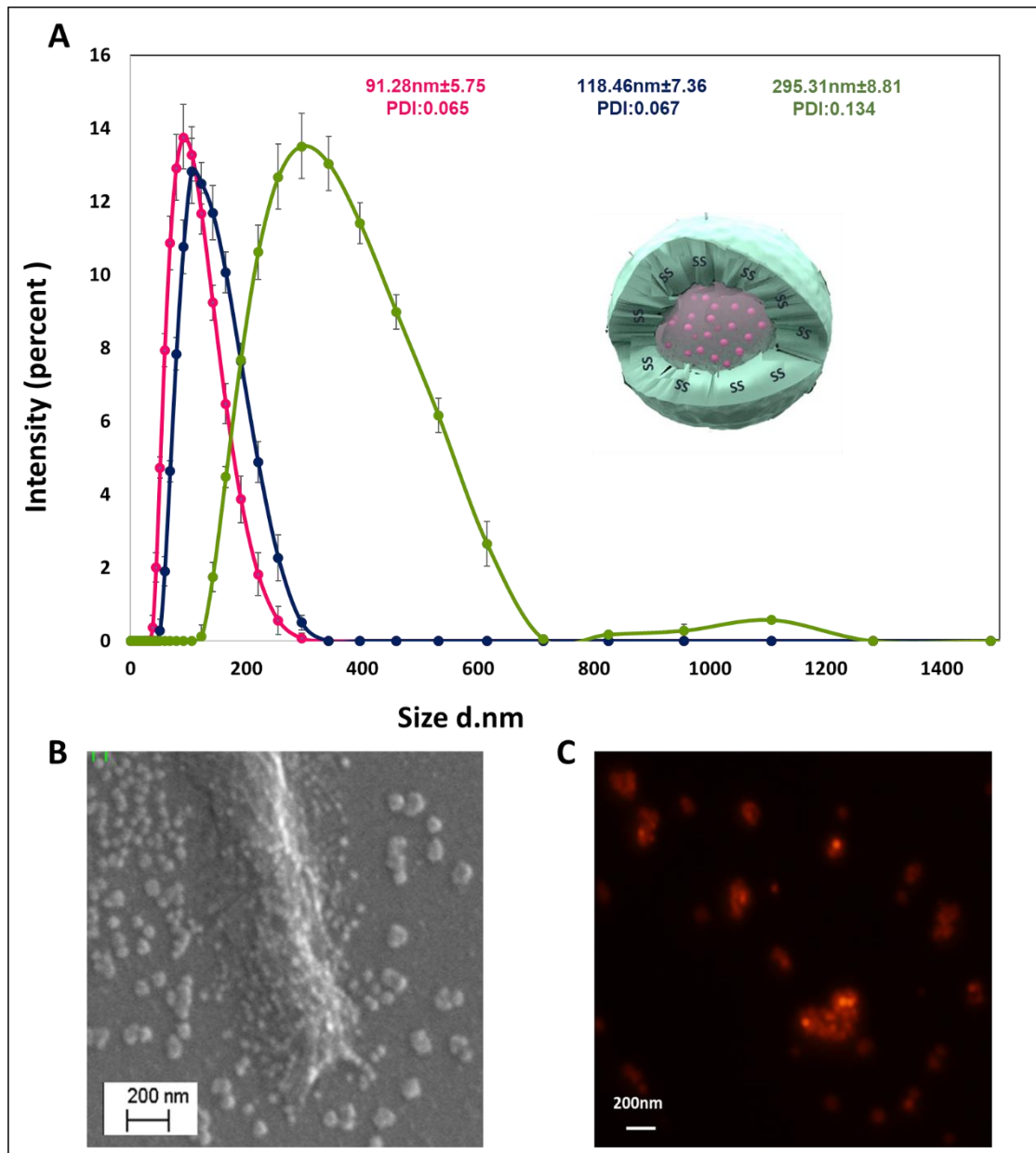


Figure 6-10. Size distribution and morphology studies of PSSG3-Dox. DLS images of at 0h (pink), after 3 months storage (Blue) and in the presence of 10mM DTT for 24hrs (green) (A), SEM images at 0h (B) and fluorescence microscopic images at 0h (C).

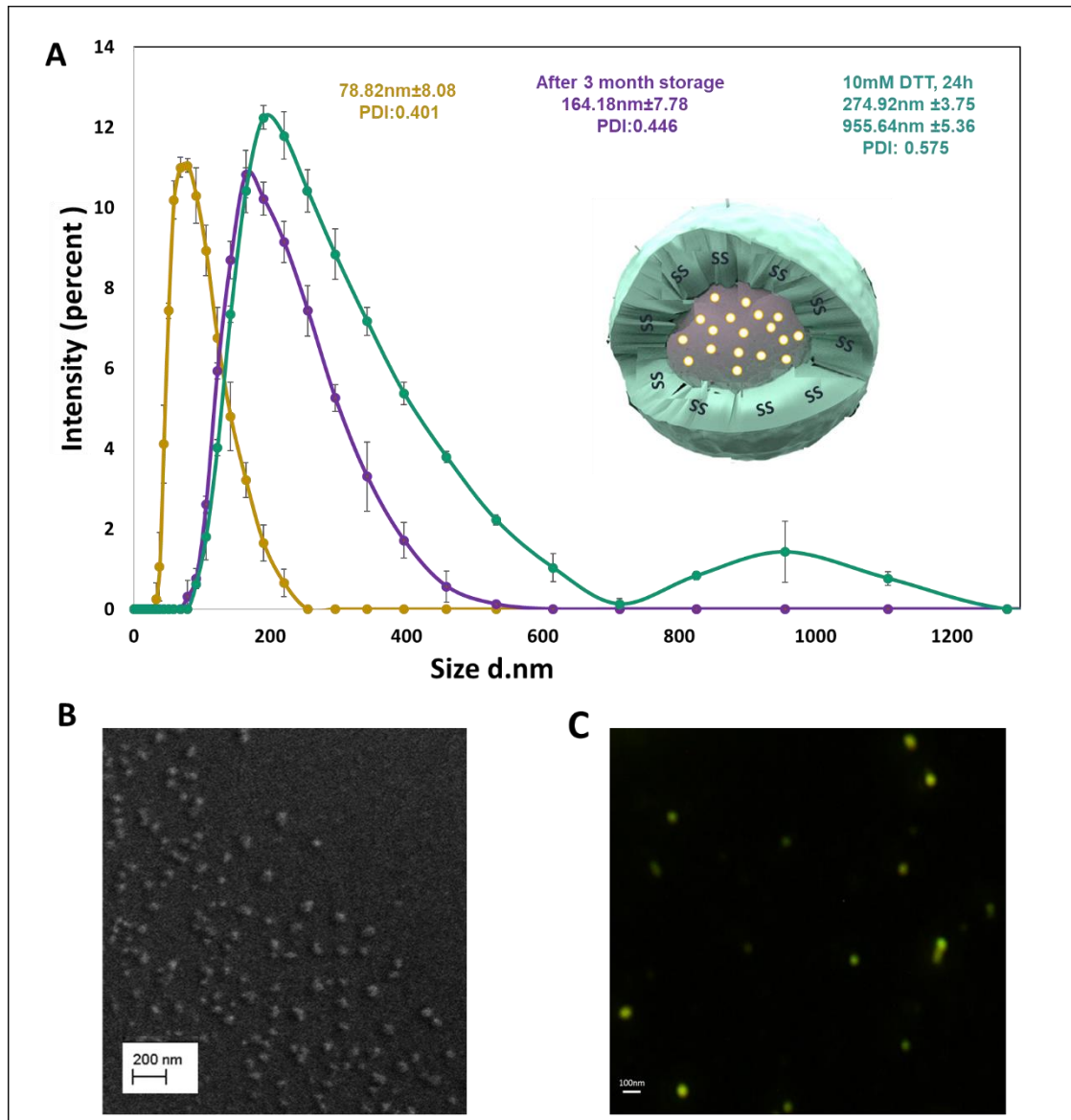


Figure 6-11. Size distribution and morphology studies of PSSG3-Cur. DLS images of at 0h, after 3 months storage and in the presence of 10mM DTT for 24hrs (A), SEM images at 0h (B) and microscopic fluorescence images at 0h(C).

Furthermore, Figure 6-12 shows that the PSSG3-Cur/Dox has a mean size distribution of 112.9nm, which also disassemble in the presence of 10mM DTT to particles of sizes bigger than 624.92nm. The SEM images further confirm the disassembly of the carrier as the PSSG3-Cur/Dox at 0h exhibited spherical morphology (Figure 6-12B) whereas after being exposed to DTT, irregular shapes (Figure 6-12C) corresponding to the disintegrated particles.

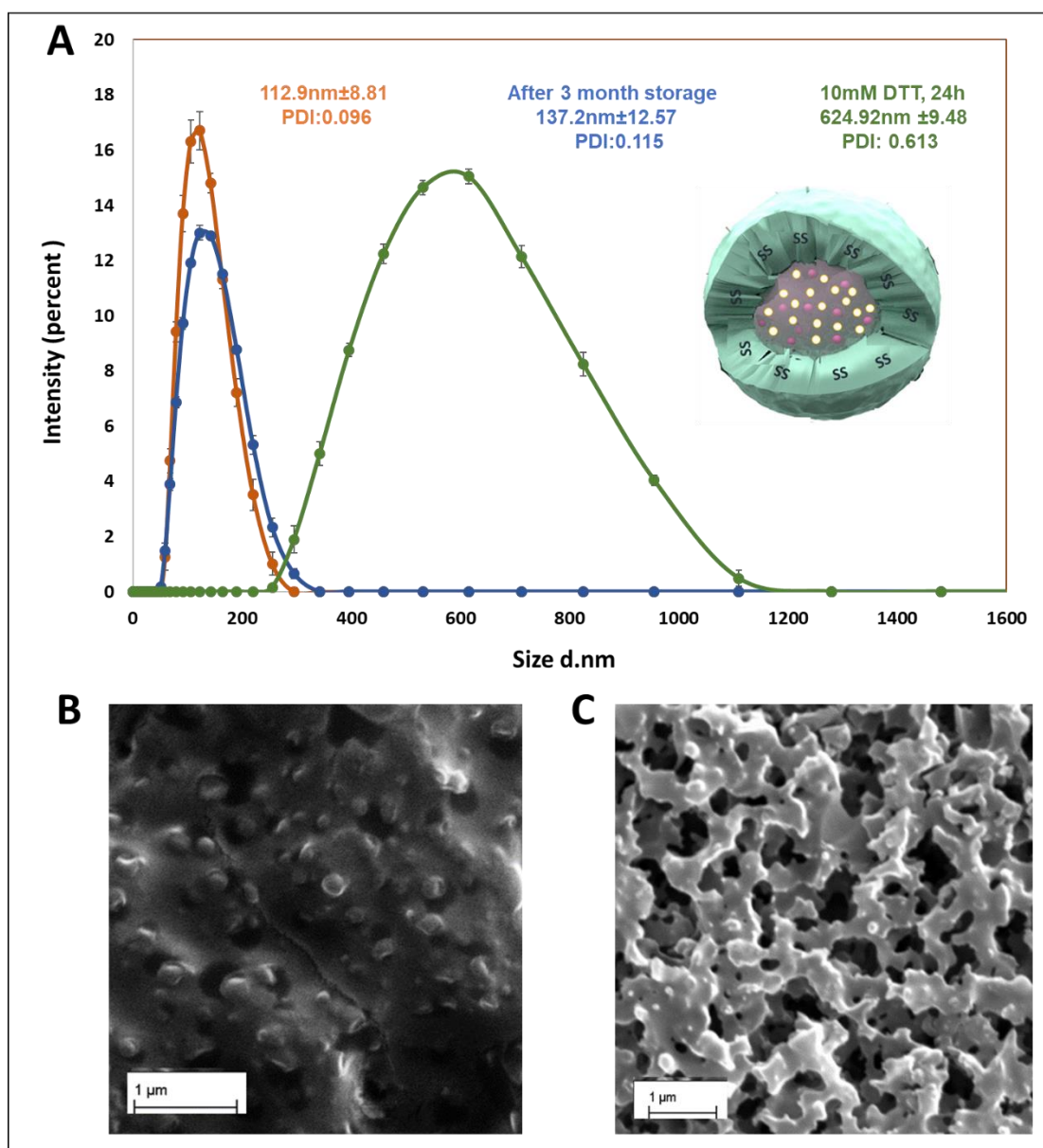


Figure 6-12. Size distribution and morphology studies of PSSG3-Dox/Cur. DLS images at 0h, after 3 months storage and in the presence of 10mM DTT for 24hrs (A), SEM images at 0h (B) and SEM images in the presence of 10mM DTT for 24hrs(C).

6.4.4. In vitro drug Release studies of PSSG3-Dox (or cur or cur/Dox) nanoparticles

The reduction triggered drug release from PSSG3-Dox, PSSG3-Cur and PSSG3-Dox /Cur micelles were evaluated under 10mM DTT condition at pH 7.4 and pH 5.0. Figure 6-13 shows the release curve of Dox from PSSG3-Dox and PSSG3-Dox /Cur in the presence and absence of 10mM DTT. The release of Dox from both carriers shows a significant accelerated release by the addition

of DTT to the release media. Both micelles loaded drugs released nearly 70% of drug Dox in the first 12h under 10mM DTT followed by a sustained release in the subsequent time until 60.5h. Compared to the release at pH 7.4 conditions without DTT, only 13% was released from both carrier formulations. Furthermore, since Dox can protonate under acidic conditions, investigation of Dox release from both formulations was investigated under pH 5.0. A fast release of Dox reached 46% within the first 12 hours also followed by a sustained release reaching 57% of Dox release for a period of 60.5h.

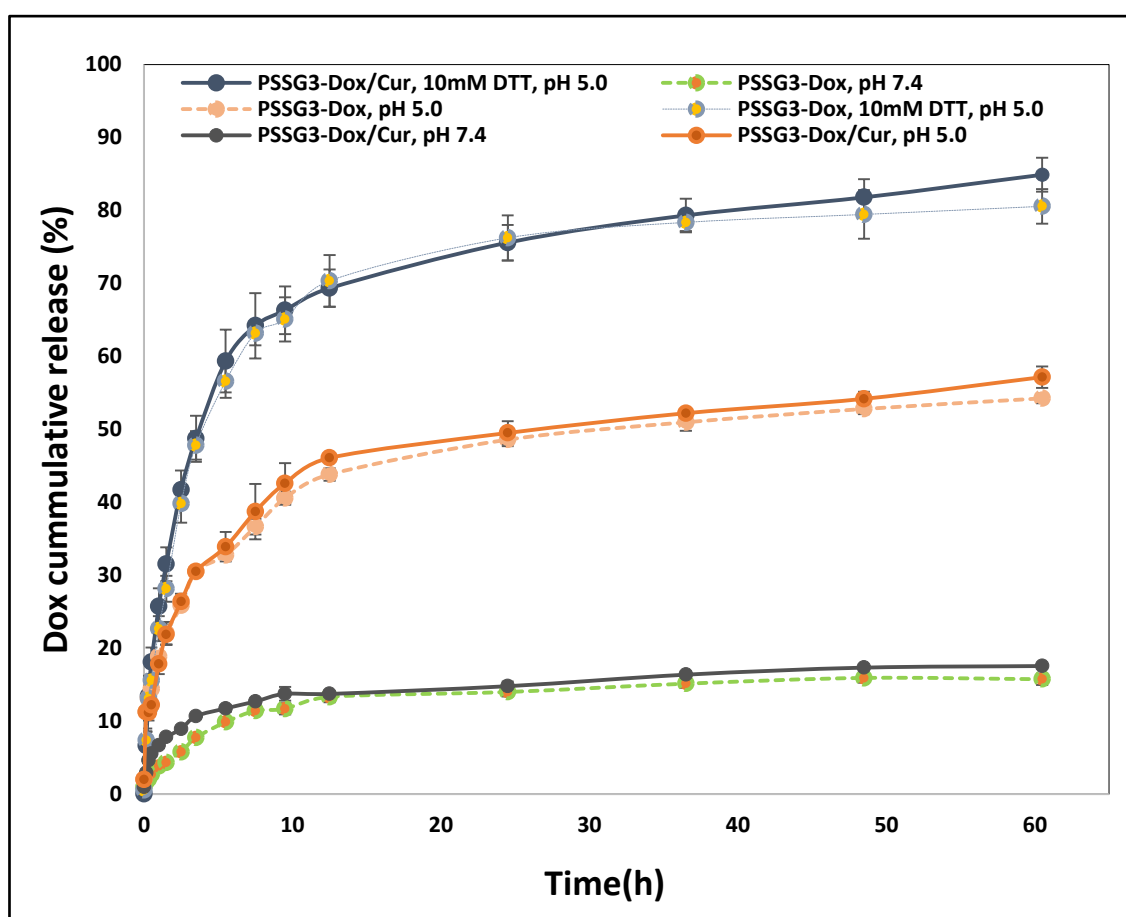


Figure 6-13. Cumulative release profiles of Dox from PSSG3-Dox and PSSG3-Dox/Cur at pH 7.4 (with and without 10mM DTT) and pH 5.0 in a period of 65hours.

The release of Curcumin from PSSG3-Cur and PSSG3-Dox/Cur was also investigated. The curcumin present in PSSG3-Dox/Cur nanoparticles displayed a similar release profile as Dox in the presence of 10mM DTT conditions, nearly

68% of curcumin was released at 12h followed by a sustained release reaching 87% of released curcumin. Also, in acidic conditions, 42% of curcumin from PSSG3-Dox/cur was released at 12h compared to the release of curcumin at pH7.4 where only 25% of curcumin is released for a period of 60.5h.

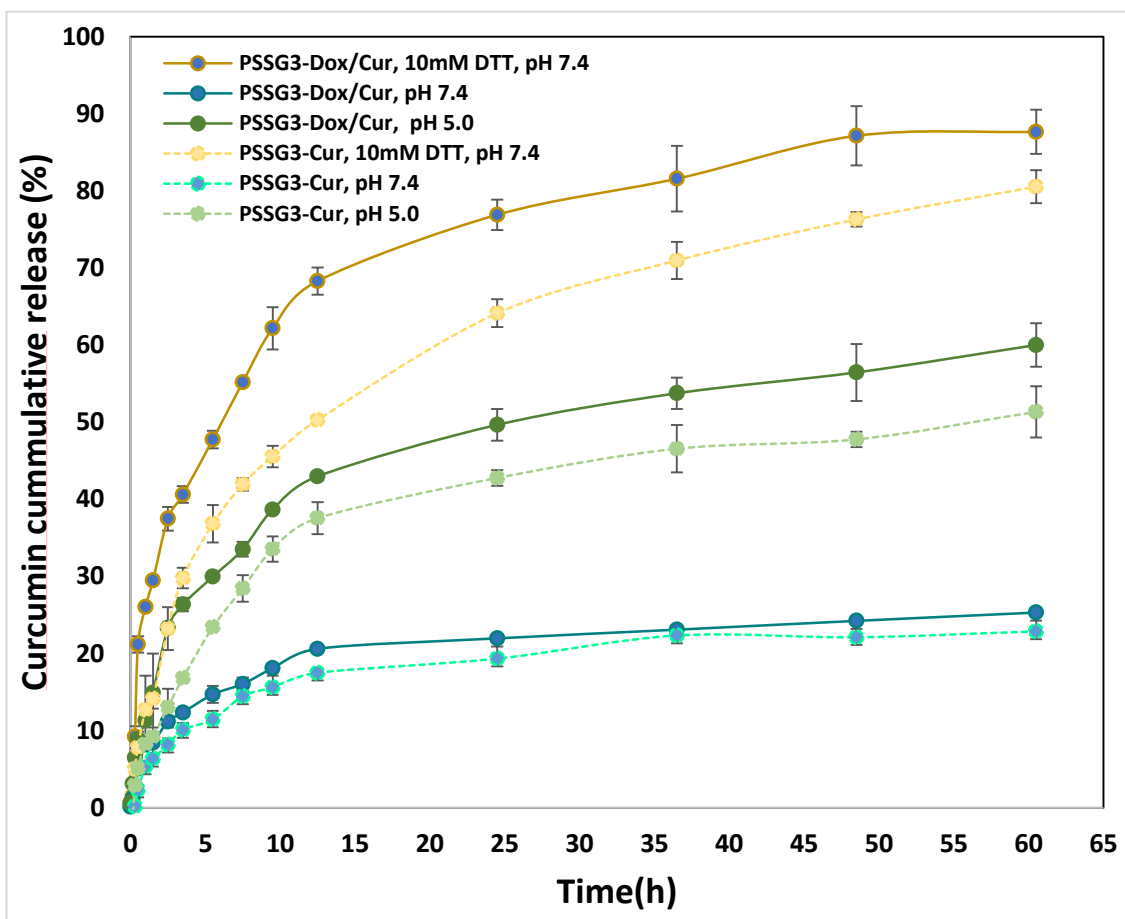


Figure 6-14. Cumulative release profiles of curcumin from PSSG3-Cur and PSSG3-Dox/Cur at pH 7.4 (with and without 10mM DTT) and pH 5.0 in a period of 60.5hour.

In comparison, to the release of curcumin from PSSG3-Dox/Cur, curcumin release from PSSG3-Cur was slower releasing 50% of curcumin at 12h under DTT conditions. Similarly, in acidic conditions (pH 5.0), at 2.5h, the released curcumin from PSSG3Dox/Cur is almost double (23%) than the release in PSSG3-Cur (13%). However, under normal pH condition (7.4) there is no

significant difference between the curcumin percentage released from PSSG3-Dox/Cur (25%) and PSSG3-cur (23%).

6.4.5. Cytotoxicity

The anticancer effect of PSSG3-Dox, PSSG3-Cur and PSSG3-Dox/Cur was tested against HepG2, NIH3T3 and Hek293 cells. Free Dox, free curcumin and blank PSSG3 micelles were used as controls. As seen in Figure 6-15. the blank PSSG3 did not exert any toxicity towards any of the cells tested. On the other hand, all the loaded micelles and free drugs exhibited a strong dose-dependent pattern after 72h of treatment.

Table 6-2. IC₅₀ determined by SRB assay in the HepG2, NIH3T3 and Hek293 cells after 72h of incubation with blank PSSG3, PSSG3-Dox, PSSG3-Cur and PSSG3-Dox/Cur

Drug formulation	IC ₅₀ (µg/mL)		
	HepG2	NIH3T3	Hek293
Dox.HCl	0.049	0.165	3.588
PSSG3-Dox	0.085	2.654	5.764
Curcumin	2.645	6.235	7.355
PSSG3-cur	1.345	10.03	58.641
PSSG3-Dox/Cur	0.013	0.276	0.743

By analysing the IC₅₀ values in table 6-2, The loaded Dox in PSSG3 showed a lower toxic effect on each cell lines compared to free Dox whereas PSSG3-Cur exhibited higher toxicity on HepG2 cells compared to free curcumin. However, in NIH3T3 and Hek293 cells, the toxicity of PSSG3-cur was much lower than free curcumin.

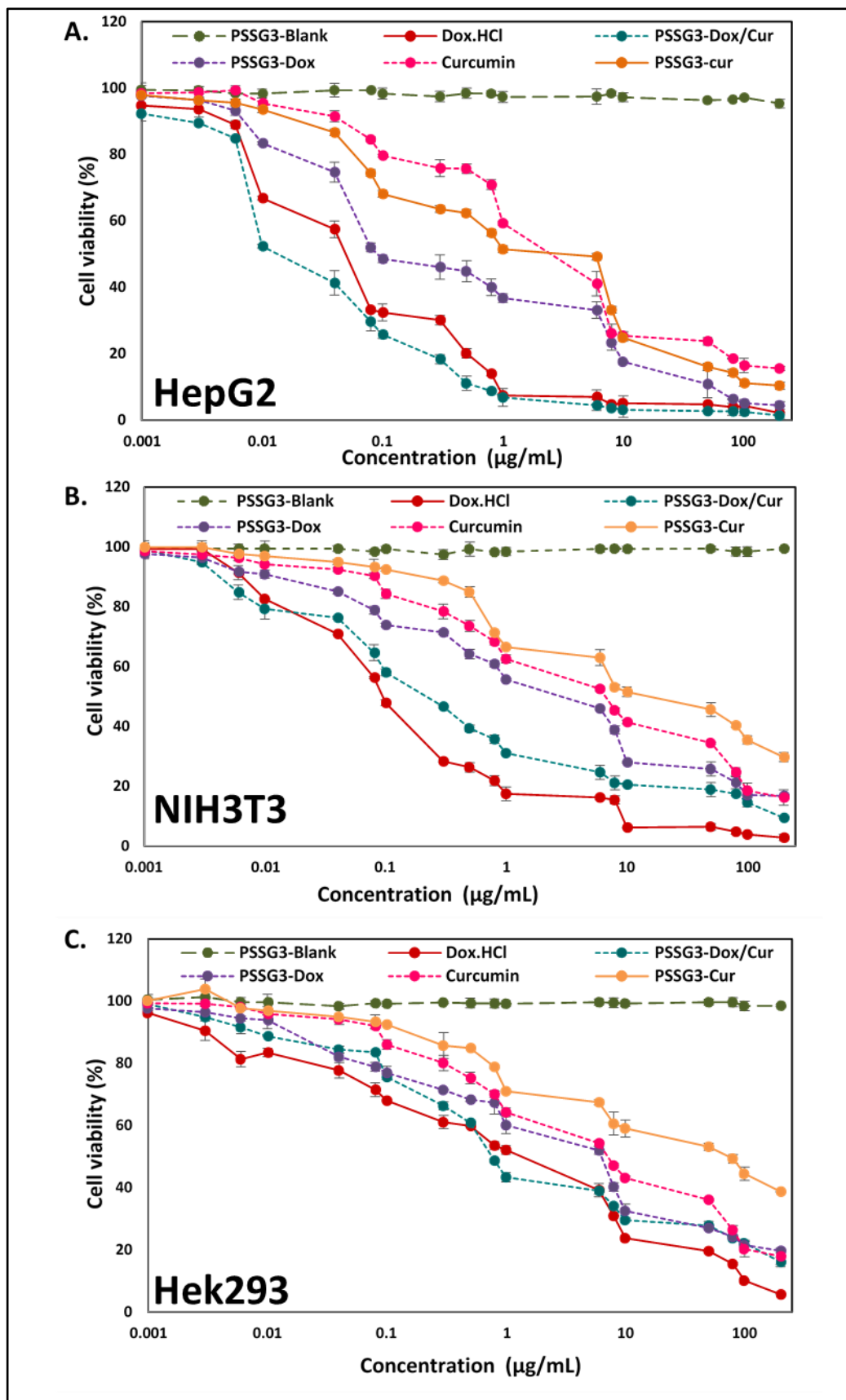


Figure 6-15. Cytotoxicity of blank PSSG3, PSSG3-Dox, PSSG3-Cur and PSSG3-Dox/Cur against A. HepG2 cells, B. NIH3T3 cells and C. Hek293 cells after the 72h incubation period. The concentrations of PSSG3-Dox/Cur corresponds to the concentration of Doxorubicin content.

Moreover, PSSG3-Dox /Cur showed a significant enhancement on the toxicity in HepG2 cells with a very low IC₅₀ value of 0.013 µg/mL compared to PSSG3-Cur, PSSG3-Dox and free Dox and cur.

6.4.6. Cellular uptake by confocal studies

The effect of PSSG3-Dox/Cur, PSSG3-Dox and PSSG3-Cur on the cellular uptake of either or both Dox.HCl and Cur were also evaluated in the HepG2 cells based on the intrinsic red fluorescence of Dox and green fluorescence of Cur. The cells were treated with free Dox.HCl, Curcumin, PSSG3-Dox, PSSG3-Cur and PSSG3- Dox/Cur NPs at Dox concentration of 5.1µg/ML and Cur concentration of 5.1µg/ML for 6hours. As seen in Figure 6-16, free curcumin displayed high green fluorescence in cytoplasm and very little fluorescence in the nucleus compared to free Dox, which was already distributed in the cell nucleus at 6h. This indicates the slow uptake of free curcumin compared to free Dox by the HepG2 cells which are because Dox can easily permeate the nuclear envelope and intercalates DNA (Capranico, Kohn and Pommier, 1990; Gu et al., 2012). All three PSSG3-Dox, PSSG3-Cur and PSSG3-Dox/Cur nanoparticles could be efficiently taken up by hepG2 cells. There was no significant difference in the uptake of single loaded drug nanoparticles PSSG3-Dox and PSSG3-Cur or 2 drugs loaded nanoparticles PSSG3-Dox/Cur. The loaded Dox and curcumin from each nanoparticle were predominately distributed in the cytoplasm after 6 h of incubation. On the other hand, at elevated incubation time, the HepG2 cells treated with PSSG3-Dox/Cur nanoparticles for 10h exhibited higher red and green fluorescence intensity in the nucleus showing that both drugs had been released from PSSG3-Dox/Cur.

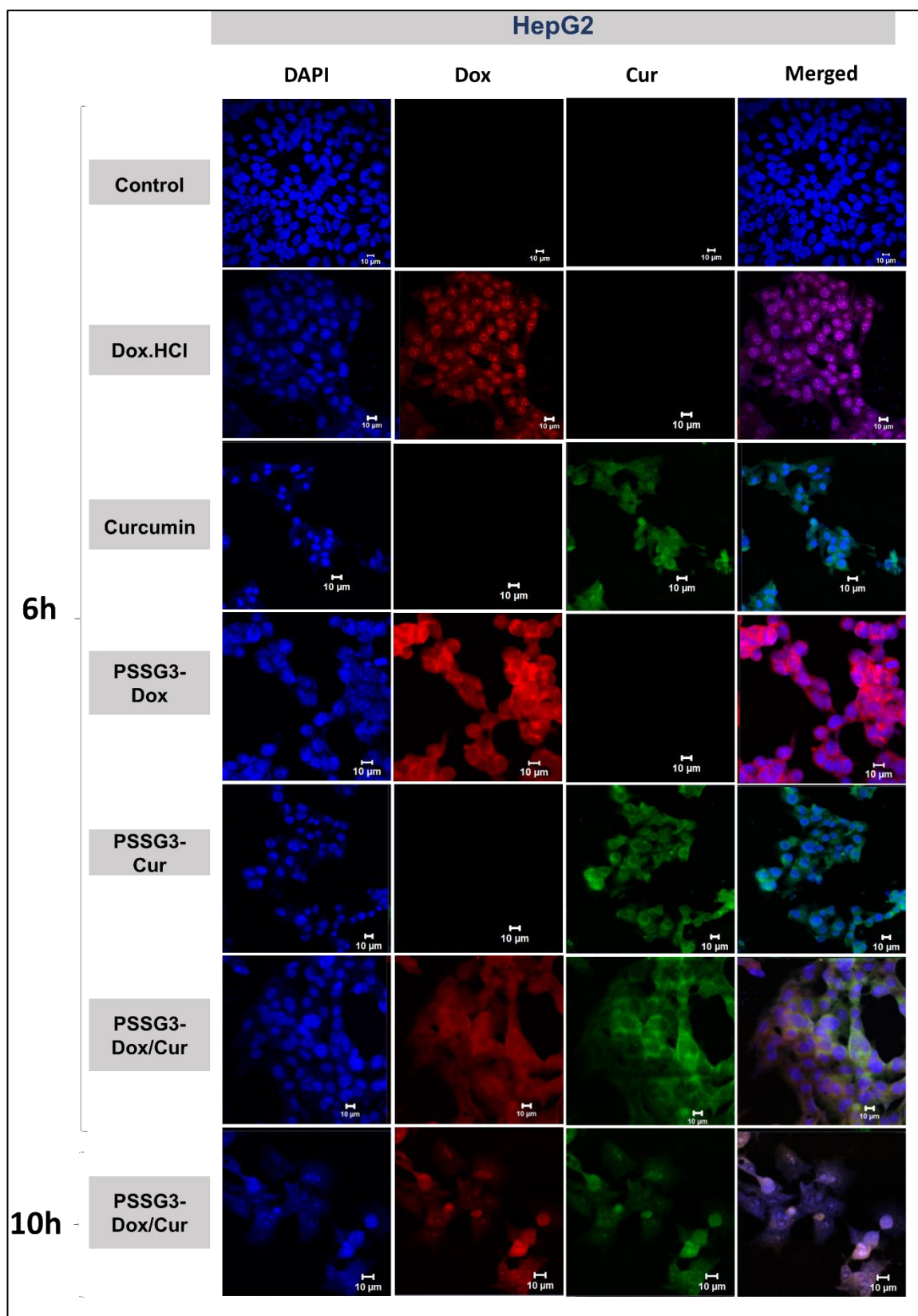


Figure 6-16. Confocal scanning electron micrographs of HepG2 cells after 6h incubation with Dox.HCl, Curcumin, PSSG3-Dox, PSSG3-Cur and after 6 and 10h incubation with PSSG3-Dox/Cur. Cell nuclei were stained with blue (DAPI), cell-associated Dox appeared Red (Dox), and Curcumin appeared green (Cur).

6.5. Discussion

Pullulan has been widely explored in targeted gene, and drug delivery systems, especially, researchers have focussed on redox-sensitive pullulan-based amphiphilic copolymers for Doxorubicin delivery (Wang et al., 2014; Li et al., 2014). Taking advantage of factors such as low pH and high elevated level of GSH in intracellular compartments of the tumour cells, we proposed to modify the previous nanocarrier synthesised PG3 (Chapter 4) by adding a disulphide linkage to improve the drug release rate of hydrophobic drugs. A disulphide linkage has been added in many different amphiphilic systems via esterification or amide formation by either first modifying the polysaccharides acting as backbone then reacting with the hydrophobic group or by either modifying the hydrophobic group first with disulfide linkage and then substitute in the polysaccharide backbone. The disulfide-containing fragments that have been mostly used are cystamine and DTDPA. Cystamine has been conjugated into hydrophobic MSNs via amide formation using EDC/NHS and then linked into deacetylated heparin by Dai et al., 2014, also, Cystamine has been conjugated to carboxylated pullulan to form the amide product Pullulan-SS-NH₂ and then linked with hydrophobic stearic acid using EDC/NHS by Wang et al., 2014. Furthermore, DTDPA has been conjugated into Dextran containing hydrophobic segments PBLG via ester formation using EDC/DMAP and then crosslinked to another molecule of Dextran containing hydrophobic segments PBLG by Zhang et al., 2013. DTDPA has also been conjugated to hydrophobic cholesterol via esterification using DCC/DMAP and then linked into Pullulan via esterification by EDC/DMAP by Li et al., 2014. Based on the published work, we proposed to link our hydrophobic Dendron PLLA into pullulan by adding the disulphide

containing segments DTDPA. Although these published papers showed that the esterification reaction could be done in the presence of DCC/DMAP, successful esterification between DTDPA and Pullulan were only achieved in the presence of EDC/DMAP using DMSO (see appendix section 9-6). Also, to conjugate the hydrophobic Dendron into disulfide modified pullulan via click reaction, azide groups were first successfully added by conjugating PSS-COOH with amine group from 3-azidopropylamine using EDC/NHS. The Dendron of generation 3 PLLA(BOC/PBF) was added in excess, expecting all the azide group to be reacted, therefore reaching 16% of Dendron conjugated via disulphide linkage into pullulan. The amphiphilic PSSG3 system could self-assemble into uniform spherical nanoparticles of 68.1nm with good stability characteristics. PG3 and P(Lac)G3 nanocarriers have been able to load enough Dox, but the loaded carriers have not been able to reach the therapeutic effect that free Dox.HCl can achieve on HepG2 cells. This is maybe due to the slow cumulative release of Dox from the carrier which affects the efficiency of the drug Dox since insufficient intracellular drug release can limit the amount of antitumour drugs that reaches cancer cells which then hinders the efficiency of cancer therapy and induces side effects. We hypothesised here that the disulfide linkage of PSSG3 could improve the drug release of Dox from the carrier and the co-delivery of Cur with Dox would enhance the anticancer effect of Dox since delivering 2 anticancer drugs at the same time would have a higher effect on the cancer cell. Cur and Dox could successfully be encapsulated into the carrier and formed nanoparticles of size ranging 112nm with the loading content of Cur and Dox being 15.59% and 17.01% respectively. It was noted that the encapsulation efficiency of Cur ($88.72\% \pm 2.00$) was higher than that of Dox ($15.59\% \pm 5.30$) and the size of PSSG3-Cur($78.82\text{nm} \pm 8.08$) was smaller than

PSSG3- Dox (91nm \pm 5.75). This is explained by the fact that Dox has a lower logP value 1.3 (Gallois et al., 1996) compared to that of Cur being 3.0, which implicates that molecules of Cur had stronger hydrophobic interaction with hydrophobic groups BOC and PBF from the Dendron G3-PLLA compared to Dox and therefore resulting in smaller core size. Moreover, the release rate of loaded drugs into PSSG3 was enhanced by the breakage of disulphide bonds in the presence of 10mM DTT. Surprisingly, Cur had a higher release rate at pH 5 from PSSG3- Dox/Cur compared to its release from PSSG3-Cur, this suggested that the release of DOX influenced the release of Cur since, in acidic conditions, the Dox protonation triggers its release which also weakens Cur interactions with dendrons. Cur is then released depending on the diffusion of the environmental hydrophilic solutions inside the core of nanoparticles which solubilise the Cur in acidic conditions and therefore releases from the nanoparticles (Shah et al., 2008). Furthermore, it was confirmed that Cur enhanced the toxicity of Dox in HepG2 cells as PSSG3-Dox/cur had higher toxicity effect compared to PSSG3-Dox and free Dox.HCl (Figure 6-18A). Moreover, Cur has shown to have much lower toxicity effect compared to Dox a specially in normal cells suggesting its safety. The fact that disulfide containing Cur was more toxic to HepG2 cells compared to free Cur proves that the nanoparticle influenced the internalisation of Cur and the high content of GSH within the cancerous cells triggered the fast release of Cur, therefore, resulting in higher toxicity. Very interestingly, the loaded carriers were not seen as highly toxic compared to the free drugs toxicity in normal cells NIH3T3 and Hek293 as seen in HepG2 cells. This could be because cancerous cells have higher GSH level than normal cells lines (Jhaveri, Deshpande and Torchilin, 2014) but also it has been reported that NIH3T3 and Hek293 cells can largely be resistant to Cur

treatment and therefore displaying minimal toxicity for which Cur was suggested to have different sensitivity in different cell types (Manson, 2005; Kloesch et al., 2014). Moreover, confocal studies showed the ability of the carrier to be able to deliver Dox and Cur at the same time into HepG2 cells. At 10hours treatment with PSSG3-Dox/Cur, loaded Dox and Cur could already be released in response to the high redox potential in endosome/lysosome and reach the nucleus but also increased fluorescence was still observed in the cytoplasm. Curcumin being in the cytoplasm increases the levels of topoisomerase II-mediated DNA cleavage in the cytoplasm through its natural antioxidant activity (Ketrón et al., 2012) but also generate ROS species which can then cause cell death (Woo et al., 2003; Traverso et al., 2013). Therefore, PSSG3-Curcumin not only can be used for cancer treatment but also in the treatment of other various liver diseases.

Overall, the prodrug PSSG3-Dox/Cur nanoparticles provide a promising approach for combination therapy in cancer therapy.

In summary, the co-delivery system PSSG3-Dox/Cur developed in this study targets HepG2 cells via ASPGR receptors and get internalised inside cells via endocytosis where the loaded Dox protonates at lower pH, weakening the intermolecular hydrophobic interaction of Cur with dendron, therefore, enhancing release rates. In addition to the acidic environment, high level of GSH within endosome and lysosome also improve the release of Dox and Cur by the breakage of disulphide linkage within the PSSG3 carrier. High GSH level decreases the level of ROS within cells, therefore, Cur released would use its antioxidant activity and would not only influence ROS production and increase the levels of topoisomerase II-mediated DNA cleavage (López-Lázaro et al.,

2007) but also would inhibit MDR against Dox resulting in enhanced Dox antitumor efficiency.

CHAPTER 7. GUANIDINYLATED DENDRON GRAFTED PULLULAN TOWARD GENE DELIVERY

7.1. Introduction

Gene therapy has become an immense interest worldwide over the last few decades for the treatment of chronic diseases and tumours. The cationic polymeric vector is one of the most important carriers for the delivery of negative genes among various non-viral gene vectors. Numerous cationic polymers, such as polyethyleneimine (PEI), polyamidoamine (PAMAM), and poly(L-lysine), are known to be efficient non-viral gene carriers (Choi et al., 2004; He et al., 2013; Janiszewska et al., 2016). They form complexes with the negatively charged DNA and still possess a net positive surface charge.

Nevertheless, cationic surface charge mediated toxicity, non-compatibility, and non-specific interactions with blood components limit the use of cationic polymers. Neutralisation of the cationic surface charge is an important strategy to overcome these problems associated with the cationic polymers. For example, shielding of the peripheral cationic groups by PEGylation is demonstrated to reduce the toxicity. However, it may have a negative effect on transfection efficiency (Suk et al., 2016). Therefore, designing a gene vector with a balance of low toxicity and high transfection efficiency is of crucial importance. Previously high transfection efficiency has been achieved using Cellular penetrating peptides (CPPs), which are well-known peptides that can penetrate the plasma membrane of mammalian cells. Among them, human immunodeficiency virus transactivator of transcription (HIV-1 TAT) protein (Vives, Brodin and Lebleu, 1997; Nakase et al., 2008), oligoarginine (Rothbard et al., 2000), penetratin (Dupont, Prochiantz and Joliot, 2011) and virion protein

22 (VP22) (Langel, 2019) are the best-known ones. The most obvious common feature of these CPP structures is undoubtedly the high content of basic amino acid, especially the number of arginine guanidinium residue (Nakase et al., 2008). The guanidinium residues seem to be the essential ingredients of the CPPs to cross the plasma membrane, which has allowed for the design of a range of guanidinium-bearing analogues. Although the exact mechanism of guanidinium-rich polymers improved gene delivery remains unclear, it is suggested that incorporating guanidinium groups to the cationic polymers is a feasible approach to improve transfection efficiency (view chapter 1).

7.2. Aim and Objective

Considering the inherent properties of pullulan and the synthesised lysine dendron of generation 3 (PLLL) (chapter3), we proposed to develop a cationic guanidinylated-based dendronized pullulan for gene delivery. PLLL G3 dendron can be covalently attached into the neutral pullulan through Huisgen azide-alkyne 1,3-dipolar cycloaddition or “click” reaction leading to G3P. The primary amines of the generation 3 lysine dendron periphery could then be converted into guanidine groups resulting in an Octa-guanidine functionalized generation 3 lysine dendrons-graft-pullulan (OGG3P=PLLA+). Herein, we aimed to:

- Synthesise and characterise the conjugation of PLLL into pullulan (G3P),
- Synthesise and characterise the conversion of lysine group into guanidine(OGG3P),
- Investigate the DNA complexation by agarose gel retardation assay of G3P and OGG3P
- Investigate the size, charge and morphology of the DNA complexes

It is important to note that this work was carried out with our colleagues in China, where we aimed to demonstrate that dendrimers structure can be easily manipulated to achieve different purposes. My work presented in this chapter was to demonstrate the ability of Octa-guanidine functionalized generation 3 lysine dendrons-graft-pullulan (OGG3P) to encapsulate a gene, whereas my colleagues in China further carried more studies by investigating the toxicity, gene transfection, and uptake mechanism of OGG3P. Also, the therapeutic plasmid, pKillerRed-mem into the OGG3P carrier was studied. Our colleagues work is not presented here but can be viewed in our published paper (Zhou et al., 2018).

7.3. Methodology

7.3.1. Synthesis of Lysine dendron of generation 3 (PLLL+) and Pullulan azidation

Refer to chapter 3 and 4.

7.3.2. Click reaction between PLL+ dendron and azidated pullulan

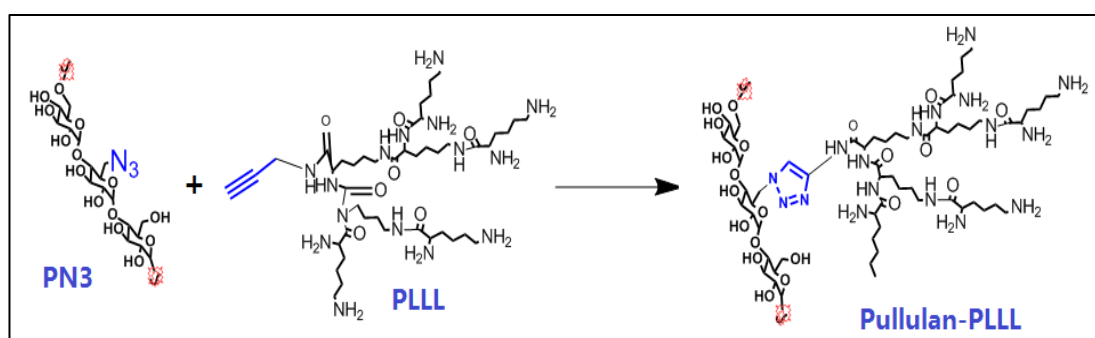


Figure 7-1. Synthesis equation of clicked PLL dendron into pullulan.

Azidated pullulan (0.17g, 0.17 mmol) was dissolved in DMSO under argon atmosphere. PLL (0.33g, 0.34 mmol) and sodium ascorbate (0.05g, 0.23 mmol) were dissolved in the deionised water respectively and added into the

above solution. Then the $\text{CuSO}_4 \cdot 5\text{H}_2\text{O}$ (0.03g, 0.12 mmol) was also dissolved in deionised water and added under a constant flow of argon. Then the reaction mixture was stirred at 45°C for 48 hours in the dark. EDTA-2Na powder (0.04g) was added into the above reaction mixture to chelate the excess copper ion. Finally, the solution was dialysed (MWCO = 3500 Da) with deionised water for 2 days, followed by lyophilisation to get the product pullulan-PLLL(G3P).

7.3.3. Guanidinylation of generation 3 (PLLL) dendrons

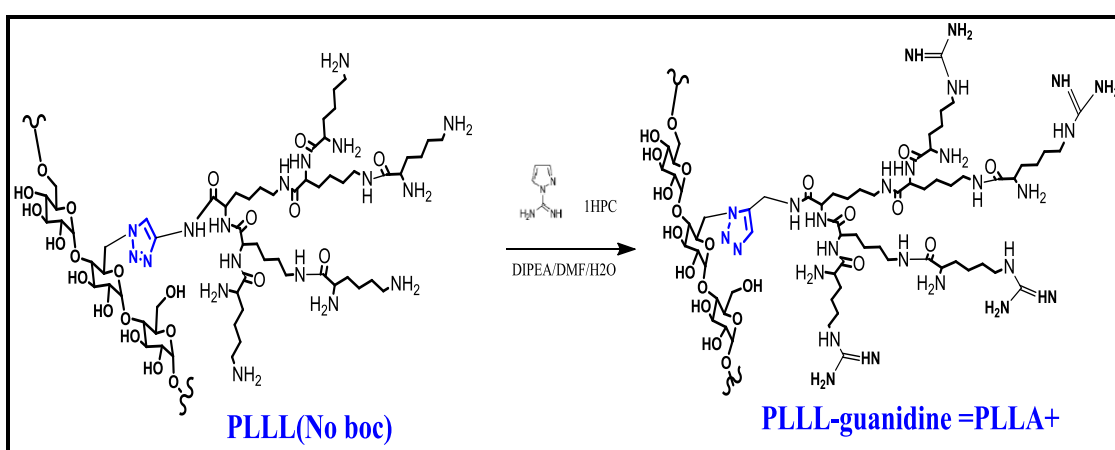


Figure 7-2. Synthesis equation of guanidylated pullulan-PLLL.

Guanidinylation was carried out using 1H-pyrazole-1-carboxamide hydrochloride as the guanidylating reagent. Briefly, the amino groups of Pullulan-PLLL (0.05g, 1mmol) were guanidylated with 5 equivalent moles of 1HPC (0.04g) and DIPEA (1.5ml) in 2ml water/DMF (1/1: V/V) under N_2 atmosphere for 3days at RT to convert the amine groups of lysine to guanidine groups.

The synthesised pullulan-PLLLG was then dialysed (MWCO = 3500 Da) against pure water for 2 days, and the solid white product was obtained by lyophilisation.

7.3.4.Characterisation

The structure of the clicked product Pullulan-PLLL(Boc) and the Octa-guanidine functionalized generation 3 lysine dendrons-graft-pullulan (OGG3P) Characterisation was carried by ¹HNMR and EA, the details of each method is given in chapter 2.

7.3.5.DNA Complexes Assembly

The complexes were prepared by mixing DNA with cationic Pullulan-PLLL(G3P) or OGG3P solution gently at varying weight ratios from 0.2 to 200 (cationic G3P or OGG3P to DNA) in HBG buffer (HEPES 20 mM, pH 7.4, 5% glucose), and incubated at room temperature for 30 min before use.

7.3.6.Agarose Gel Retardation Assay

To study the DNA compaction ability of G3P or OGG3P polymers, gel retardation assay was introduced. The commercially available non-therapeutic pEGFP plasmid-encoded enhanced green fluorescent protein (4731base pair) was used, transformed in Escherichia coli DH5 α and extracted using PureLink[®] HiPure Plasmid Filter Maxiprep Kit. Various G3P/DNA complexes and OGG3P/DNA complexes with different weight ratios (from 0.2 to 200) were mixed and incubated at 37°C for 30 min. 25 kDa PEI/DNA complexes at weight ratio 1.33 and naked DNA were used as positive and negative controls, respectively. The final amount of DNA was adjusted to 200 ng per well. Ten microliters of each different complexes solution were analysed by 1% agarose gel electrophoresis (80 V, 45 min) in standard TAE buffer. After electrophoresis, the gel was stained with ethidium bromide, and the resultant DNA migration behaviours were visualised through the Molecular Imager ChemiDoc XRS+ (Bio-Rad, USA).

7.3.7. Particle Size characterisation

Complexes at varying weight ratios were prepared at a final DNA concentration of 3 µg/mL. Measurements of the particle size distribution and zeta potential were carried out by Malvern Instruments (Zetasizer Nano ZS, Malvern, UK) in physiological conditions (pH 7.4) in deionised water. The morphologies of G3P complexes and OGG3P complexes at the weight ratio of 8 were also observed by transmission electron microscopy (TEM).

7.4. Results

7.4.1. Synthesis and characterisation of clicked Pullulan-PLLL(Boc) (G3P) and OGG3P

The click reaction between pullulan and PLLL(BOC) dendron was confirmed by ¹HNMR. Figure 7-3. shows the ¹HNMR spectra of pure pullulan, pullulan-PLLL(G3P) and OGG3P, as seen, in comparison to pullulan spectra, there were new peaks appeared at 1.0-2.0 ppm and 7.0-8.0 ppm in the G3P and OGG3P spectra which are the designated to the peaks of G3 dendrons.

Additionally, the peak at 7.90 ppm was speculated to be the peak of triazole proton (proton c), which confirmed the successful click reaction. Moreover, the ¹HNMR spectra of G3P showed the heavily diminished intensity of protons' peaks next to primary amines (proton a, δ= 3.02) compared to that of OGG3P spectra were the protons shifted to downfield (proton b, δ = 3.18, protons next to guanidine groups). Therefore, the data from 1H-NMR spectra proved that we have successfully synthesised both G3P and OGG3P. At the same time, the comparison of integration values between the two proton peaks (a and b) also revealed that about 95.90% of primary amines in the G3P polymer were converted to guanidines.

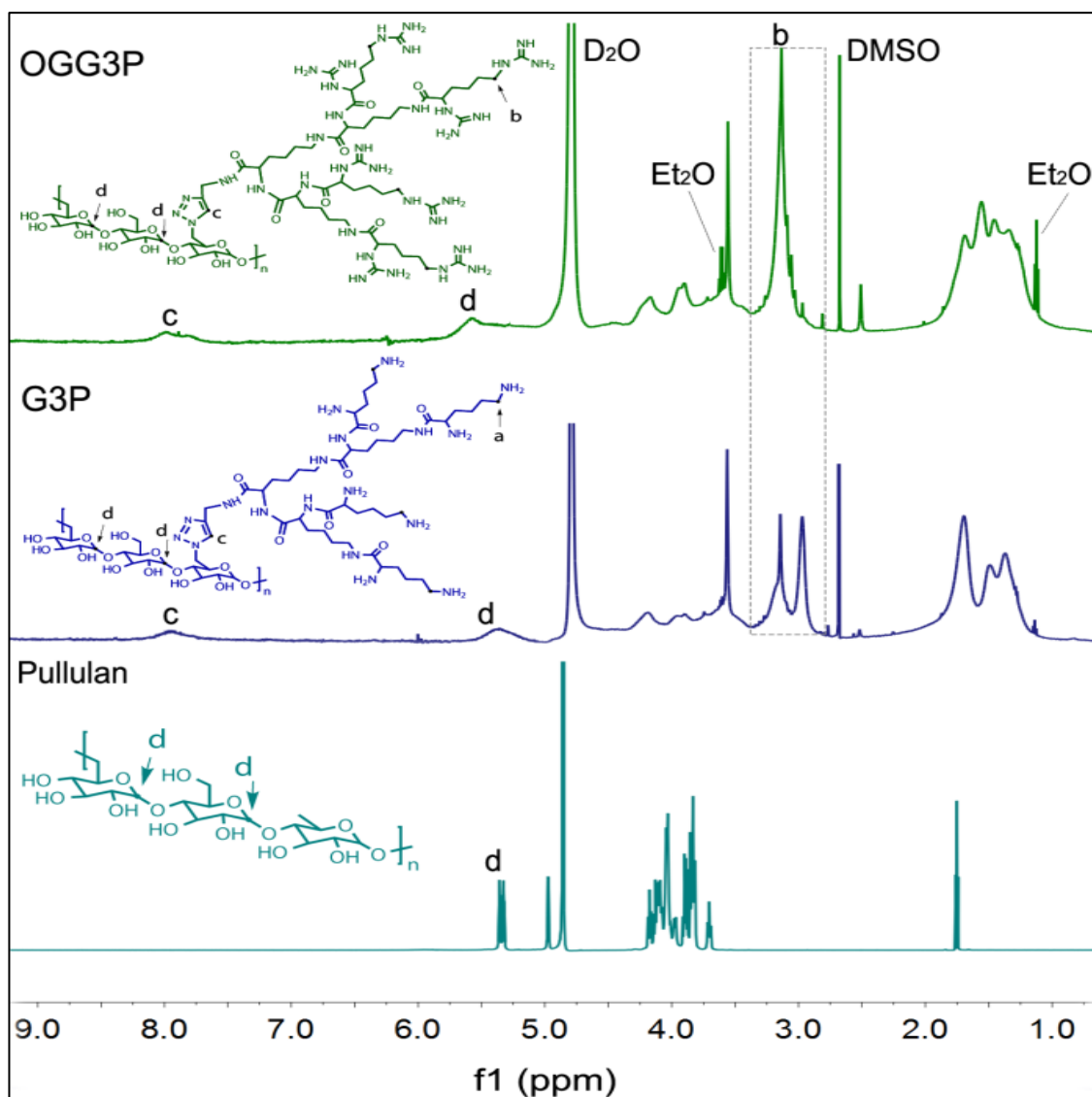


Figure 7-3. The $^1\text{H-NMR}$ spectra of pullulan, pullulan-PLLL(G3P) and the pullulan-octa-guanidine functionalized generation 3 lysine dendrons (OGG3P) in D_2O .

Table 7-1 presented the accurate mass measurements of pure pullulan, azido-pullulan, G3P and OGG3P. The azido content of azidated pullulan was calculated to be 49.02 per 100 anhydrous glucoside units and the PLLL dendrons contents conjugated onto pullulan was determined as 12.62 per 100 anhydrous glucoside units, whereas the contents of guanidines modified PLLL dendrons in OGG3P were 12.52 per 100 anhydrous glucoside units. The elemental analysis further confirmed that the substitution degree of

guanidinylated G3P was established to be 99.21%, which was consistent with the guanidinylation degree result determined from ¹H-NMR.

Table 7-1 Determination of the substitution degree by elemental analysis

	C (%)	N (%)	H (%)	DS (%)
Pullulan	40.33	6.66	/	/
PN3	37.11	6.56	3.74	49.02
G3P	39.24	6.59	11.56	12.62
OGG3P	39.04	6.74	14.77	12.52

7.4.2. Characterisation of DNA Complexes

As the Figure 7-4 shown, OGG3P was able to completely retard the migration of DNA on the gel at the weight ratio less than or equal to 2 and form stable complexes with DNA, whereas G3P could not retard the DNA migration until the weight ratio greater than or equal to 15. These phenomena strongly suggested that the guanidinylated OGG3P cationic polymer had a better DNA compaction ability than natural G3P cationic polymer, which may be the result of specific guanidinium-phosphate interactions.

We also investigated the surface charges of OGG3P complexes as a function of OGG3P cationic polymer to DNA weight ratios by measuring the zeta potential of a suspension using a Malvern Nano ZS equipment. As shown in Figure 7-4B, the zeta potential of OGG3P complexes was 11.73 mV at a weight ratio of 1. Then the zeta potential would increase with the increase of the OGG3P to DNA weight ratios. A zeta potential plateau (~ +23 mV) occurred when the weight ratio reached to 6 despite increasing with the weight ratio up to 40, indicating the OGG3P cationic polymers were able to condense DNA completely and form positively charged nanoparticles.

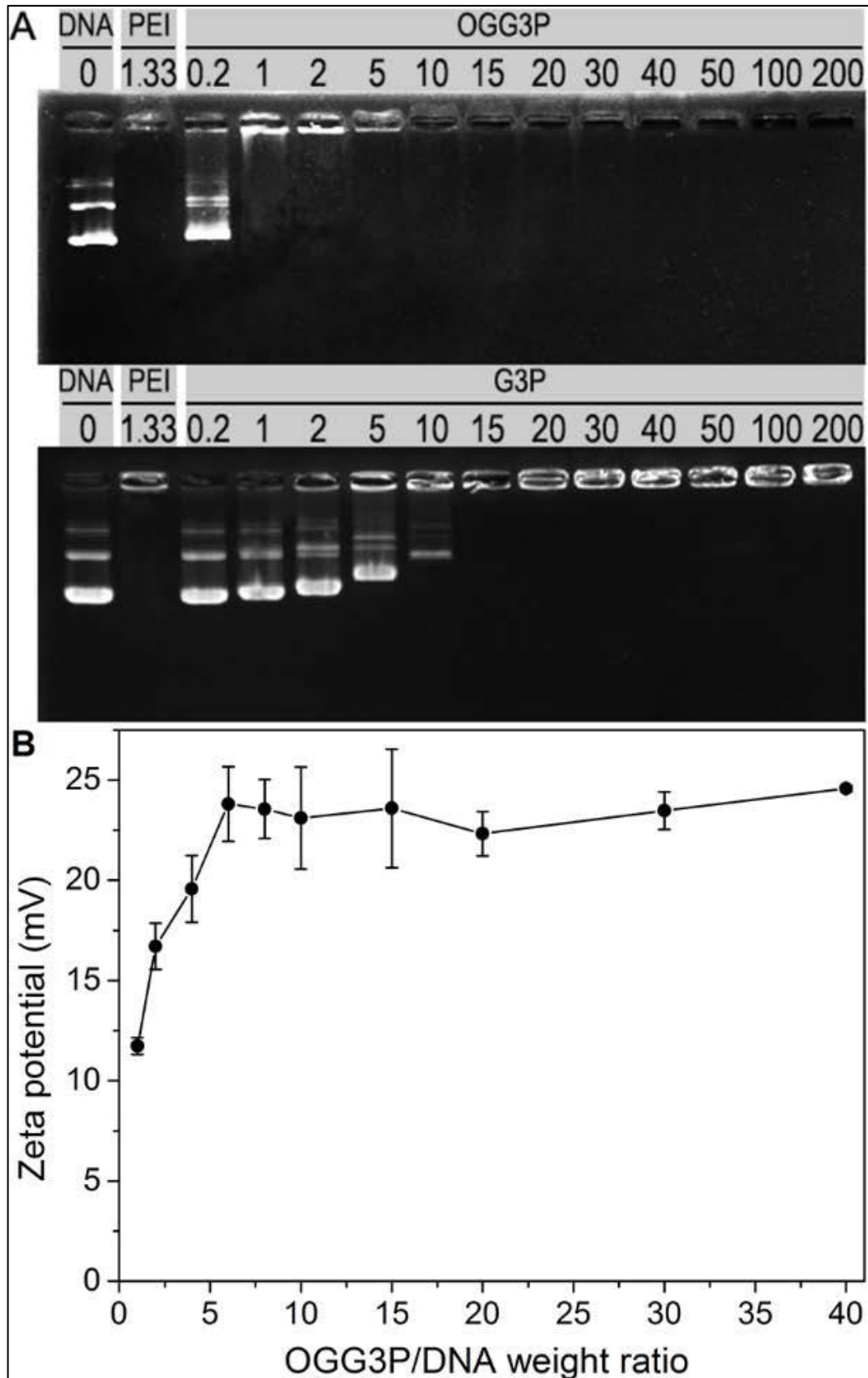


Figure 7-4. A. 2 Gel retardation assays for OGG3P and G3P complexes prepared at varying weight ratios. The different bands present in both gels show the different forms of DNA: nicked, linear, supercoiled, circular or single-stranded form (B) Zeta potential of OGG3P complexes prepared at different OGG3P to DNA weight ratios (Note: DNA made of 4731bp).

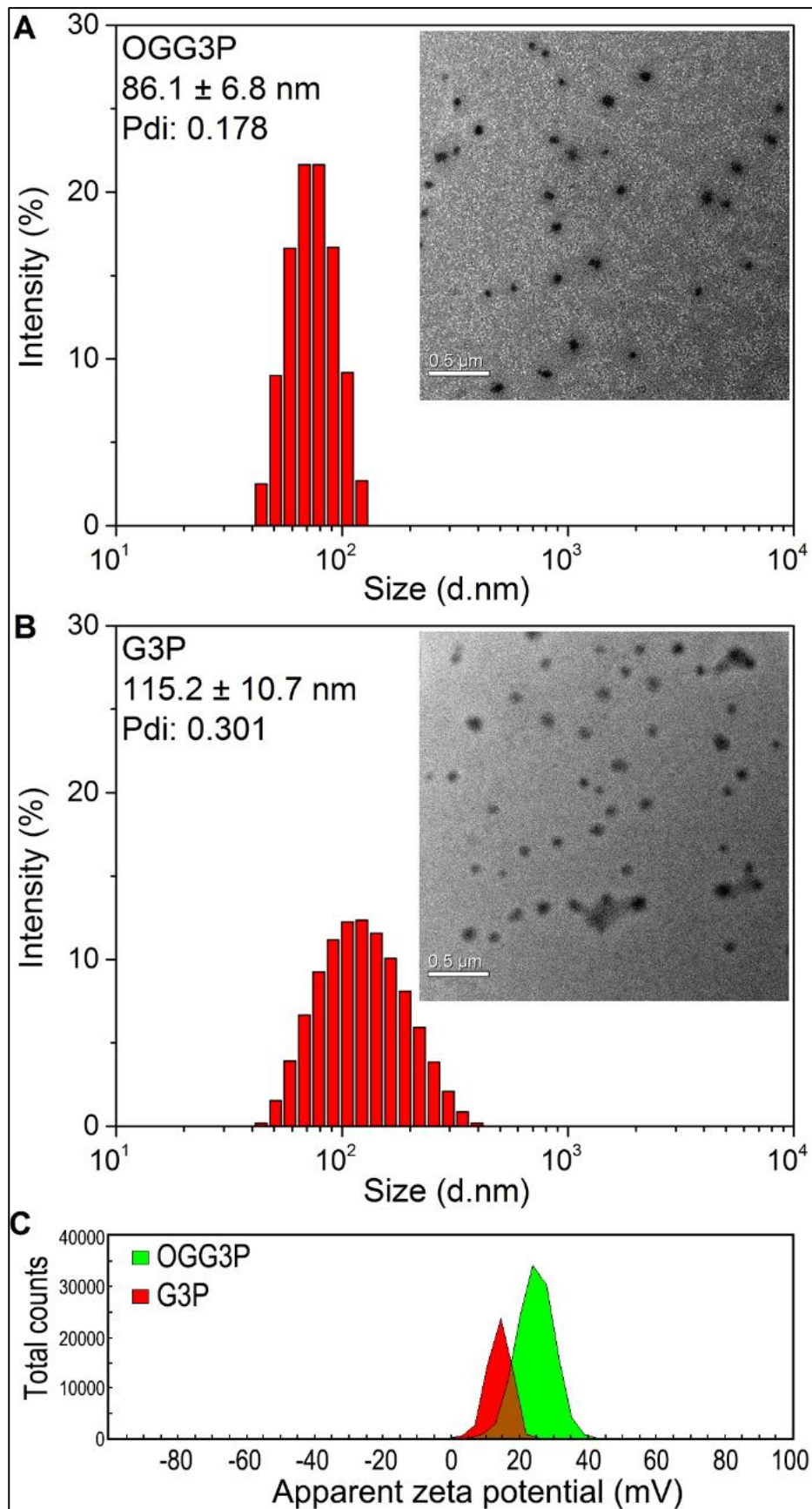


Figure 7-5. Size distribution and TEM images of **A.** OGG3P complexes; **B.** G3P complexes at the weight ratio of 8 and **C.** Zeta potential measurements of OGG3P complexes and G3P complexes at the weight ratio of 8.

The sizes, size distributions and morphologies of OGG3P and G3P complexes were also measured by transmission electron microscopy (TEM) and dynamic light scattering (DLS). As Figure 7-5A&B shown, results from TEM confirmed that both OGG3P and G3P cationic polymers could condense DNA at the weight ratio of 8 and form uniform, compact, and spherical nanoparticles. Samples of OGG3P complexes gave smaller size and narrower size distribution than that of G3P complexes. Additional DLS analyses and zeta-potential measurements also revealed that the resulting OGG3P complexes were well dispersed in the aqueous solution with a size average of 86.1 ± 6.8 nm (polydispersity index (PDI): 0.178) and present a strong zeta potential of 23.6 ± 1.5 mV while G3P complexes were 115.2 ± 10.7 nm with a broad particle size distribution (PDI: 0.301) and showed a zeta potential of 14.1 ± 1.3 mV (Figure 7-5C).

7.5. Discussion

Gene therapy has become a promising strategy for the treatment of cancer. There have been various developed gene carriers including cationic liposomes to linear cationic polymers, and now to topological (branched, dendritic and hyperbranched) cationic polymers. For gene delivery, it is essential that the gene carrier can bind and condense the plasmid DNA into nanoscale complexes and exhibit appropriate positive surface charges. The positively charged nanoscale complexes tend to interact with the negatively charged cell membrane, presumably facilitating their cellular uptake (Albuquerque et al., 2017). With this in mind, we investigated the DNA compaction ability of the cationic polymers (G3P and OGG3P) using gel retardation assay. PEI and naked DNA were used as positive and negative controls, respectively. OGG3P has a high number of amine groups giving a higher positive value of zeta

potential, therefore, can interact more strongly at a lower ratio with the gene via electrostatic attraction resulting in smaller particle sizes compared to G3P. As expected, the general trends in sizes and size distributions found from the TEM observation correlated well with those measured by DLS. The above observations indicated the resulting OGG3P complexes possessed the proper size and narrow size distribution, appropriate positive surface charges and excellent dispersion stability in an aqueous solution, presumably arising from guanidinylated OGG3P had a better DNA compaction ability than natural G3P cationic polymer.

Moreover, the zeta potential of the nanoparticles is most often used as an indicator of dispersion stability. Zeta potential of about ± 25 mV is usually required to achieve a reasonably stable dispersion. Therefore, OGG3P complexes solution could disperse stably when the weight ratio was greater than or equal to 6. Also, the uniform nonionic hydrophilic hydroxyl groups in pullulan probably benefited shielding the excessive harmful cationic charges of the OGG3P cationic carriers. The better DNA compaction ability of OGG3P cationic polymer could protect the enclosed nucleic acids from nucleases and hence maintain their stability and integrity until cellular uptake of complexes taking place.

7.6. Conclusion

In summary, we have successfully developed a tailor-made guanidine-decorated dendronized pullulan, Octa-guanidine functionalized generation 3 lysine dendrons-graft-pullulan (OGG3P) which can act as a vector for gene therapy. The obtained OGG3P could efficiently condense DNA into spherical nanosized complexes with appropriate positive surface charges to enable entry into cells and to assure

successful gene delivery. In conclusion, the guanidine-decorated dendronized pullulan could, therefore, serve as a reliable gene delivery nanopatform to enable the delivery of therapeutic genes.

CHAPTER 8. GENERAL DISCUSSION AND FUTURE STUDIES

8.1. General Discussion

In the past few decades, there have been various anticancer drugs developed most notably taxanes (paclitaxel and docetaxel) and the platinum-based drugs, however, most of these drugs lack aqueous solubility and therefore undergo unwanted interaction within the bloodstream that cause their quick clearance and higher toxicity resulting in lower antitumor efficacy (Narvekar et al., 2014). The use of polymeric-based nanomaterials such amphiphilic micellar system has therefore extensively been studied for the enhancement of anticancer drug solubility, bioavailability and delivery into the tumour site. Nishiyama and Kataoka in 2006 reported the advantages of micelles as delivery systems, including their simple preparation, increased drug solubility, reduced toxicity, increased circulation time, enhanced tissue penetration and targetability.

8.1.1. General chemical structure of the micellar carriers synthesised

Amphiphilic block copolymers consist of hydrophobic segments conjugated with hydrophilic polymers which self-assembles to form regular micelles and have shown to be more promising as micellar carriers especially to minimise micelle disintegration after dilution and to potentially prolong drug delivery (Nishiyama and Kataoka, 2006). In this work, we proposed to develop a new targeting carrier system for the delivery of hydrophobic drugs in a liver tumour. Pullulan was the perfect choice as a polymer because it has a safe history of use in Japan as a food ingredient and as a pharmaceutical bulking agent. Most

importantly, pullulan can target with high affinity to the asialoglycoprotein receptors present in the sinusoidal surface of the hepatocytes of the liver and also can accumulate the liver in higher amounts than other soluble polymers (Rekha and Sharma, 2007). In this work, we have investigated the best experimental parameters to achieve the pullulan azidation (chapter 4) and esterification (section 9.4) in addition to other chemical modification previously achieved by other authors including carboxymethylation, sulfation, etherification, chlorination and oxidation (Prajapati, Jani and Khanda, 2013) which therefore demonstrated that pullulan can easily undergo chemical modification. The chemical modification of pullulan into various derivatives is simplified by its natural chemical structure containing repeating maltotriosyl unit which contains nine hydroxyl groups in a geometrically unique environment, and therefore the introduction of different functional groups into the pullulan extends its potential applications in various fields (Bataille et al., 2011). Furthermore, to develop an amphiphilic micellar system, we proposed to conjugate a hydrophobic segment into the modified pullulan. Recently, a new class of molecules known as dendronized polymers which are linear polymers that bear dendrons at each repeat unit have been developed for drug or gene delivery systems. These systems provide better-enhanced circulation time compared to the linear polymers (Singh and Lillard, 2009) and the dendritic macromolecules form the inner core cavity with a high density of surface functionalities, well-defined structures and molecular weight which is a new model of potential amphiphilic polymer for micelles preparation. We, therefore, developed dendron based on lysine and arginine peptides of third generation (chapter 3). The dendron consisting of amino acids were synthesised to form various peptide bonds in-between generation. Since the amino acids are generally protected by

hydrophobic BOC groups or BOC/PBF groups, we hypothesised that the protecting groups at the terminal surfaces of dendrons could be useful for hydrophobic drug delivery whereas deprotection of the terminal groups would result into cationic amine terminal group for gene delivery. The synthesis was simple and easily repeated until the third generation. However, the purification and deprotection of third generation arginine dendron were difficult (section 9.1). It was therefore decided to stop the synthesis at the third generation. Although the higher generation of dendrons (up to G10 PAMAM dendrimers) have been achieved, it has also been reported that higher generation synthesis and purification is difficult, also, their size increases and become more toxic as the generation increases (Luo et al., 2011). The arginine peptide dendron synthesised consist of appropriately functionalised various terminal functional hydrophobic group (high hydrophobicity of BOC and PBF) at a low generation which should be a great advantage compared to other hydrophobic dendron synthesised previously such as the polylysine dendrons. Firstly, peptide-based dendrons are designed to be biodegradable and have also been reported to be promising as vaccines, antiviral, antibacterial candidates and as new contrast agents for biomedical magnetic resonance imaging (MRI) (Gillies and Frechet, 2005). Secondly, compared to the two types of dendritic polymers commercialised (polyamidoamine (PAMAM) and poly (propylene imine) (PPI)), the synthesised peptide arginine dendron shows higher stability structure because of the peptide bonds, the alkyne core and the terminal protective group of amino acids. Moreover, we have demonstrated that the structure of the dendron could easily be modified, although the removal of BOC/PBF was difficult in the arginine PLLA dendron to achieve cationic dendrons. Another way was therefore developed by synthesising the polylysine PLLL dendron of the

third generation and then converting the guanidine group to achieve terminal arginine containing amine structure OGG3P. The two types of dendrons could, therefore, be conjugated to pullulan to form the block copolymer pullulan based hydrophobic dendron for drug delivery or the pullulan based cationic amine dendron for gene delivery. The azide group in pullulan and alkyne group in dendron makes both molecules extremely stable at standard conditions. Both groups can tolerate oxygen, water, common organic synthesis conditions, biological molecules, a large range of solvents and pH's, and the reaction conditions of living systems (reducing environment, hydrolysis, etc.) and therefore provide the azidated pullulan and alkynated dendron a long period of storage before any further use (Kolb and Sharpless, 2003; Hein, Liu and Wang, 2008). The conjugation of dendron into pullulan is achieved by a simple linking reaction consisting of the cycloaddition between the azide and alkyne group to form a triazole compound, unlike amides and benzenoids, the triazole linkage cannot be cleaved hydrolytically and are almost impossible to oxidise or reduce (Kolb and Sharpless, 2003). The click reaction was carried out many times between dendrons and different pullulan derivatives; the process was simple, fast and high yield was achieved.

8.1.2. The general effect of the hydrophobic/hydrophilic segment in the micellar self-assembly process

The amphiphilic pullulan based hydrophobic dendron could self-assemble into the micellar structure; it is reported that the use of hydrophobic branched segments into a micellar structure induces stability and a tight packing behaviour within the micelle core compared to a simple hydrophobic linear segment (Ree et al., 2017). Moreover, the dendron based pullulan would maintain strongly the micellar structure rather than conventional polymeric

micelles because the hydrophobic dendron is connected via triazole linkage into pullulan derivative (Gillies and Frechet, 2005). It is known that the micellar size, shape, loading efficiency, stability and release rate all depends on the characteristics of the hydrophilic and hydrophobic segments within the system. In this work, three amphiphilic carriers (PG3, P(Lac)G3 and PSSG3) with different chemical characteristics were developed where the hydrophobic dendron was clicked into pullulan, pullulan bearing lactose and to disulphide modified pullulan. The table 8-1 represent all the different chemical and physical characteristics that each carrier possesses. PG3 carrier consists of a simple hydrophilic segment with the highest conjugated hydrophobic segments (20.32%), P(Lac)G3 has a higher hydrophilic segment with 18.51 % of hydrophobic dendrons whereas PSSG3 have a simple hydrophilic segment with the least hydrophobic molecules but elongated. Herein, all carrier system developed in the presence of water showed to be able to self-assemble into a spherical micellar structure which shows that enough hydrophobic dendron was conjugated into pullulan derivatives and that the hydrophilic segment is longer than the core block, therefore, resulting in spherical micelles (Gaucher et al., 2005). The driving force of micelle formation in water usually depends on the hydrophobic effect. By increasing the number of hydrophobic dendron in pullulan, we expect to improve the hydrophobic interaction within the micellar core and therefore reduce their size and CAC value, which would indicate greater stability. For example, Kang and Leroux in 2004 demonstrated by a steady-state pyrene fluorescence technique that increases the PDLLA proportion in PVP-b-PDLLA-b-PVP triblock copolymers from 27 to 55 mol% led to a decrease in CAC values from 19.9 to 5.1 mg/L. Conversely, PG3 containing the higher number of hydrophobic dendron exhibited the highest particle size

(87.07nm) and CAC value (10.47 $\mu\text{g}/\text{mL}$) compared to P(Lac)G3 and PSSG3. P(Lac)G3 presented the smallest particle size of 54nm and CAC value of 8.87 $\mu\text{g}/\text{mL}$, whereas PSSG3 formed micelles of sizes 68.1nm with a CAC value of 9.93 $\mu\text{g}/\text{mL}$. From these observations, we can deduce that the higher number of hydrophobic dendron did not have any significant effect on the size and CAC value compared to when an increase of the hydrophilic segment or the length of the hydrophobic segment was done. For the P(Lac)G3 system, the addition of lactose into pullulan increased the hydrophilicity of the outer layer which imparts steric stability by minimizing the interfacial free energy of the micellar core and by impeding hydrophobic intermicellar attractions (Gaucher et al., 2005), the high hydrophilicity is vital in preventing opsonin when administrated intravenously and for improved circulation. Similarly, to the addition of PEG, the high hydrophilic surface of pullulan and lactose may act as a protective layer around the micelles that can repel the absorption of opsonin proteins via steric repulsion forces, thereby prolonging their blood circulation (OWENSIII and PEPPAS, 2006). For the PSSG3 carrier, the increase in the length of the hydrophobic segment by addition of disulphide linkage influences the micellar stability (Gaucher et al., 2005) but may also influence the size reduction. This is explained by the fact that the hydrophobic segments are far from the hydrophilic segment, making their interaction hard with an aqueous solution and therefore increasing their hydrophobic interaction within the core. Overall, it is known that compared to low molecular weight surfactants, polymeric micelles exhibit significantly lower CAC values, indicating greater thermodynamic stability (Gaucher et al., 2005). It has been reported that the usual size of a pharmaceutical micelle is less than 80 nm, its CMC value is expected to be in a low millimolar region or even lower, and the loading efficacy toward a

hydrophobic drug should be between 5 and 25 wt.% (Rana et al., 2017). Our developed carriers PG3, P(Lac)G3 and PSSG3 all exhibited good spherical particle sizes (50-90nm range), well uniformity and dispersity (relatively low PDI less than 0.25), low CAC values showing great stability of the micelles and no toxicity towards HepG2, U251, Hek293 and NIH3T3 cell lines (Chapter4,5 and 6). All these characteristics show that the micellar systems developed could be beneficial for the delivery of hydrophobic drugs. Therefore, the ability of the carriers to load, release and deliver the hydrophobic drug doxorubicin into cancer cells was investigated, and results are summarised in table 8-1.

8.1.3. The general loading efficiency of hydrophobic drugs into the carriers and their effect on their sizes

Loading content of doxorubicin into the carrier is seen to be enhanced by the number of hydrophobic dendron inside the micellar core and the size, the higher number of dendron and higher particle size showed a higher encapsulation and loading efficiency of doxorubicin in PG3 compared to P(Lac)G3 and PSSG3. The loading efficiency of each carrier was within the (5 and 25 wt.%) pharmaceutical range (Rana et al., 2017). It is also noticeable that the loading of drug exerted some effects on the particle size, all loaded carriers exhibited an increase in sizes which is because of the enlargement of core bulk due to the doxorubicin drug content. However, the contrary effect was seen when loading curcumin into the carrier PSSG3, the loading efficiency was much higher than Doxorubicin, and the size was not increased much like that of loaded Doxorubicin-PSSG3. This show that curcumin being more hydrophobic than doxorubicin had a different effect by improving the compact arrangement among the hydrophobic dendron interactions, therefore, resulting in smaller sizes. These observations agree with the theory reported by Qiu and Bae in

2007 were the author reports that drug encapsulation can exert two contrary effects on particle size, one effect is that the drug may improve the compact arrangement among chains through hydrophobic interactions and the other effect is the enlargement of core bulk due to the drug content.

Moreover, although the sizes of loaded carriers increased, their sizes were not increased to more than 140nm, this indicates that the loaded carriers had right sizes to be able to deliver drugs to their target with prolonged circulation by avoiding recognition via RES and will be able to accumulate in tumours because of the enhanced permeability and retention effect (EPR effect).

8.1.4. The general effect on the release rate of encapsulated drugs

A general drawback on the use of hydrophobic dendrimer core in the micellar system is the difficulty to control the release of molecules (Gillies and Frechet, 2005). The release depends on the strong hydrophobic interactions between drugs and the micellar cores and can be improved by adding cleavable linkage in specific physiological conditions such as pH and redox. The use of Doxorubicin as an example of the hydrophobic drug was an advantage since the drug can protonate in acidic conditions and reduce its interaction with the hydrophobic dendron, therefore, enhancing its release.

This phenomenon was observed in the released studies of Doxorubicin from all carriers where the release at pH 5 showed the highest release rate compared to the release at pH 7.4 and 6.8. Moreover, the release of doxorubicin at pH 5 from each carrier showed a typical biphasic pattern characterised by a fast-initial release during the first 12h followed by a slow sustained release over the next 60 hours.

Table 8-1. Overall physical and chemical characteristics of the PG3, P(Lac)G3 and PSSG3 amphiphilic micellar nanocarriers

Amphiphilic micellar nanocarriers			
	PG3	P(Lac)G3	PSSG3
Chemical composition			
Components	targeting pullulan	<ul style="list-style-type: none"> targeting pullulan & lactose Higher hydrophilic tail (34.45% of lactose) 	<ul style="list-style-type: none"> targeting pullulan disulphide linkage longer hydrophobic tail
G3(PLLA) Dendron (DS)	20.32%	18.51%	16%
Blank micelles characteristics			
Blank size (nm)	87.07nm	54nm	68.1nm
PDI	0.241	0.131	0.098
CAC (µg/mL)	10.47µg/mL	8.87µg/mL	9.93µg/mL
Drug loaded micelles characteristics			
Drug loaded size	138nm (PG3-Dox)	68nm(P(Lac)Dox)	91.28nm (PSSG3-Dox), 78.82nm (PSSG3-Cur) & 112.9nm (PSSG3-Dox/Cur)
Loading content	19.17%	16.89%	18.14% (Dox) & 19.21% (Cur)
Encapsulation efficiency	64.15%	56.34%	59.74% (Dox) & 91.44 % (Cur)
Release Rate (at 60hours)	16 wt% (pH7.4), 23 wt% (pH 6.8) & 53 wt%(pH 5.0)	6 wt% (pH 7.4), 10 wt% (pH 6.8) & 40 wt%(pH 5.0)	<p>Dox</p> <ul style="list-style-type: none"> 16 wt% (pH 7.4), 54 wt%(pH 5.0) and 81wt%(pH 5.0, DTT) from PSSG3-Dox 18 wt% (pH 7.4), 57 wt%(pH 5.0) and 85wt%(pH 5.0, DTT) from PSSG3-Dox/Cur <p>Cur</p> <ul style="list-style-type: none"> 23wt% (pH 7.4), 51 wt%(pH 5.0) and 81wt%(pH 5.0, DTT) from PSSG3-cur 25wt%(pH 7.4), 60 wt%(pH 5.0) and 88wt%(pH 5.0, DTT) from PSSG3-Dox/Cur
Toxicity studies			
IC50 (µg/mL) at 72h			
<ul style="list-style-type: none"> Dox.HCl (0.049 in HepG2, 0.165 in NIH3T3, 3.588 in Hek293 & 0.096in U251) Curcumin (2.645 in HepG2, 6.235in NIH3T3 and 7.355 in Hek293) 	0.276 in HepG2, 5.654 in NIH3T3 , 7.847 in Hek293 and 1.176 in U251 cells	0.317in HepG2, 0.856 in NIH3T3 and 6.358 in Hek293 cells	<ul style="list-style-type: none"> 0.085 in HepG2, 2.654 in NIH3T3 and 5.764 in Hek293 cells from PSSG3-Dox 1.345 in HepG2, 10.03 in NIH3T3 and 58.64 in Hek293 cells from PSSG3-Cur 0.013 in HepG2, 0.276 in NIH3T3 and 0.743 in Hek293 cells from PSSG3-Dox/Cur

The initial fast release of Dox from each nanoparticle could be reasonably explained by the fact that a certain amount of Dox-loaded in the centre of the hydrophobic core may quickly respond to the change of pH value and preferentially diffuse through the pullulan derivative shell, whereas some Dox highly interacting with the hydrophobic dendrons would protonate slowly, causing a sustained release. It is essential to note the higher release rate of doxorubicin from PG3-Dox compared to P(Lac)Dox and PSSG3-Dox, which correlates with the size and loading effect of PG3. PG3 having the higher Dox content enlarges the micellar core and therefore present a higher number of Dox having weak hydrophobic interaction with the hydrophobic dendron which then quickly respond to the pH change and releases from the core. The ability of these carriers releasing the drug in a sustained way makes them beneficial for the treatment of chronic diseases, some infectious diseases and cancers (Trivedi and Kompella, 2010). Although we have demonstrated the excellent stability of the micelles synthesised after 3 months storage, in addition to great CAC values, micelles can still present instability over a long period. A very prolonged sustained release would therefore not be the best option for the use of micelles as not enough drug may be released on the target resulting in limited therapeutic effect. From the PG3 and P(Lac)G3 Dox-loaded carriers, no more than 55% of doxorubicin could be released for a period of 60hours. The presence of the redox stimuli-sensitive disulphide linkage in PSSG3-dox showed some improvement on the release of the drug doxorubicin up to a release rate of 85wt% at a 60h time. Furthermore, the low premature drug release in physiological pH condition (mimicking the blood circulation) confirmed the stability of the drug-loaded PG3-Dox, P(Lac)Dox and PSSDox/Cur/Dox-Cur. This show that the hydrophobic dendrons within micellar core have highly

strong interactions with Dox or Cur, including π - π interactions, hydrogen bonding and hydrophobic interactions.

8.1.5. Effect on the addition of lactose to enhance pullulan targeting on HepG2 cells

In this work, we aimed to actively and passively target the liver cancer cells. All the carriers PG3, P(Lac)G3 and PSSG3 exhibited small enough sizes to be able to target the tumour environment via EPR effect passively. Pullulan chosen as the backbone is reported to be able to target the overexpressed asialoglycoprotein receptor (ASGPR) in hepatoma cells of the liver actively. ASGPR is the most common target site of HCC for targeting drug delivery system because of their high expression on hepatocytes and hepatoma cells (HepG2 expresses 76,000 ASGPRs/cell with a high density on the membrane) but their minimal expression on extrahepatic cells (D'Souza and Devarajan, 2015).

We have investigated the uptake of the carriers into HepG2 cells using confocal laser scanning microscopy; it is important to note the practical advantage of using Doxorubicin and Curcumin as examples of hydrophobic anticancer agents because of their fluorescence properties. Curcumin, for example, has previously been used as a fluorescent probe for directly monitoring in vitro uptake of curcumin combined paclitaxel loaded PLA-TPGS nanoparticles (Nguyen et al., 2016). Therefore, with the use of curcumin and Doxorubicin once treated with cells, was beneficial in indicating their localisation within cells.

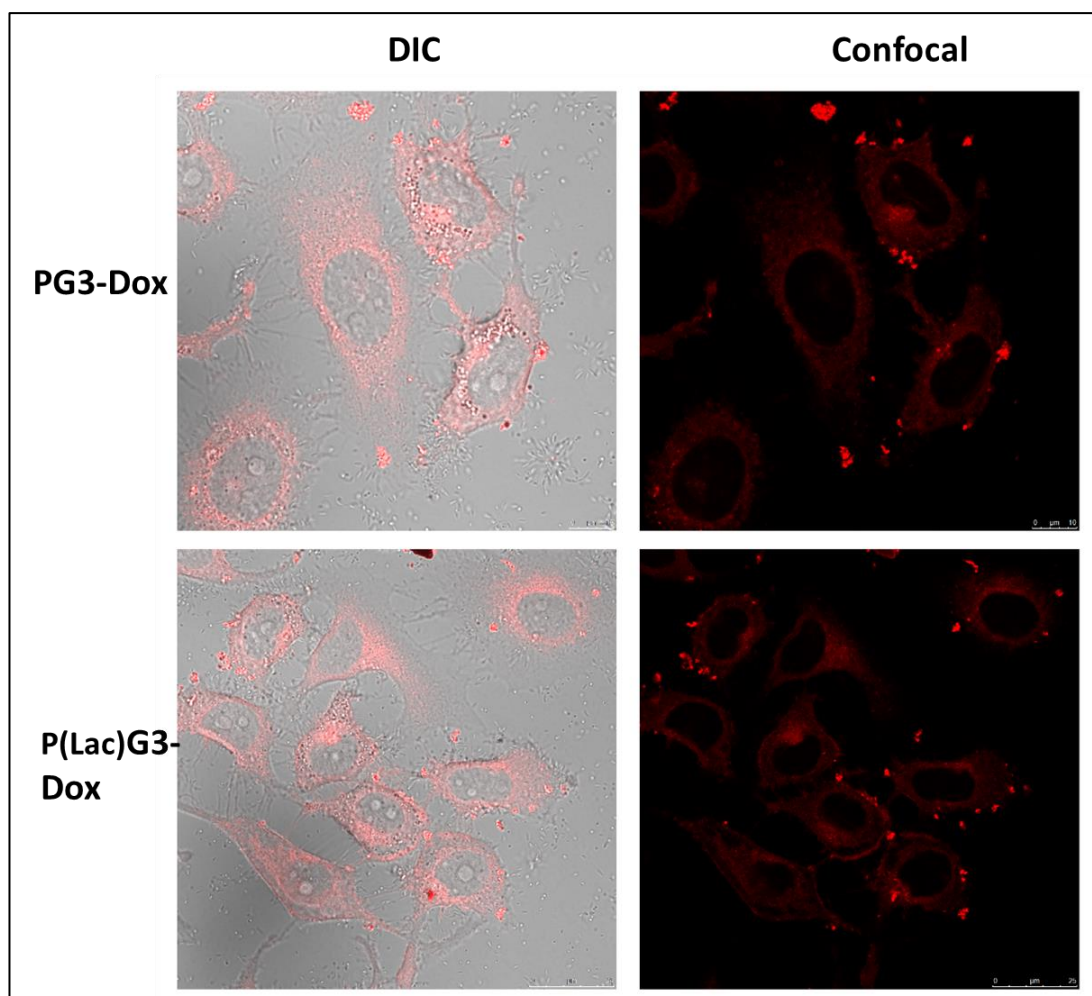


Figure 8-1. The cellular uptake of PG3-Dox and P(Lac)Dox nanoparticles by HepG2 cells after 1h treatment with confocal laser. The left images are DIC images where the fluorescence is overlaid on a bright field image of the cells, whereas the right images are just red fluorescence.

Although we could not demonstrate the targeting effect of pullulan from PG3 into HepG2, there was a difference between the internalisation of Dox.HCl and PG3-Dox or PSSG3-Dox or Cur/Dox in which we deduced that the carriers were internalised via endocytosis into HepG2 cells. We then hypothesised that conjugating the lactobionic acid (a common ligand for hepatoma cells comprising a gluconic acid and Galactose moiety) would enhance the targeting of pullulan into HepG2 cells since pullulan segments in the micellar structure may not expose its chemicals fully on the surface for the receptor-ligand recognition to take place. The ASGPRs can recognise and bind D-galactose (Gal) and N-acetylgalactosamine residues with high specificity and efficiency;

their centre consists of six amino acids in which the H1 subunit forms an active ligand-binding site (D'Souza and Devarajan, 2015). Figure 8-1 and 8-2 show the confocal images and flow cytometry indicating the fluorescence intensity of Dox inside PG3 and P(Lac)G3.

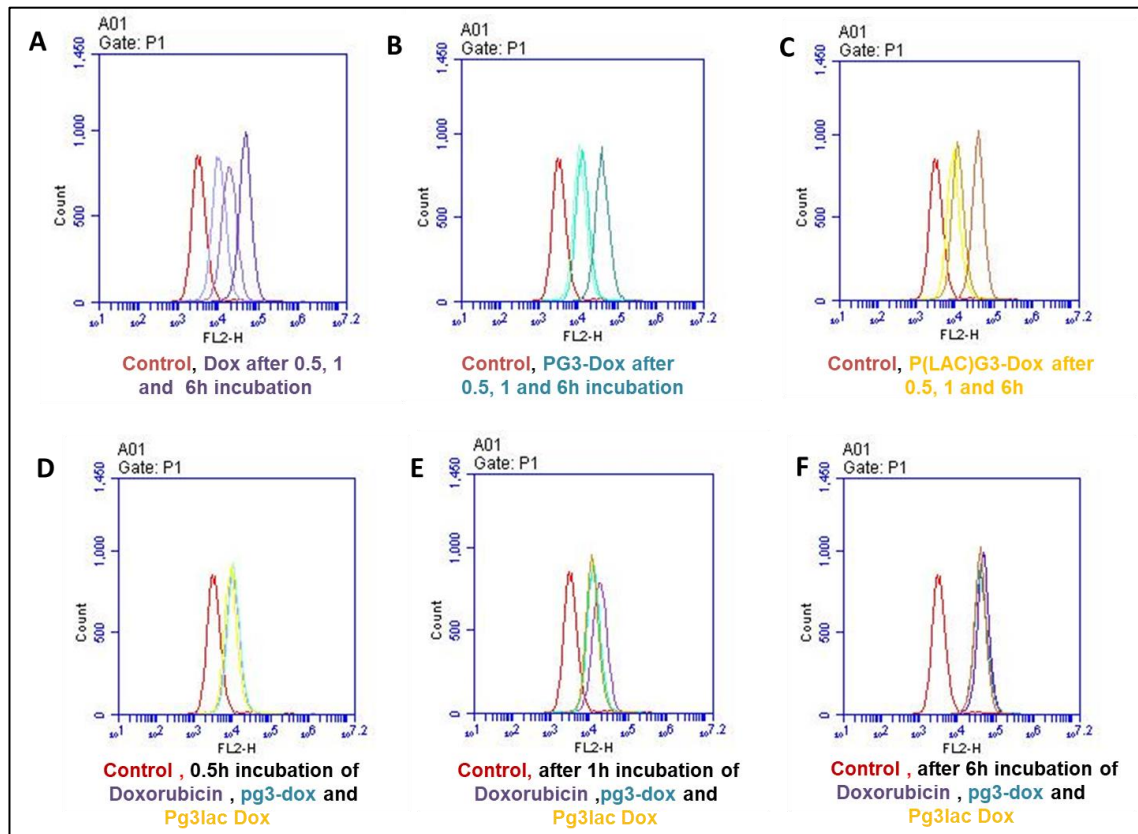


Figure 8-2. The Cellular uptake by Flow Cytometry of Dox.HCl, PG3-Dox and P(Lac)Dox nanoparticles at 0.5,1 and 6h in HepG2 cells. The flow cytometry histograms are represented in 2 ways: The three top plots show the changes in fluorescence intensity over different time for A. Dox.HCl treated HepG2 cells; B. PG3Dox-treated HepG2 and C. P(Lac)Dox-treated HepG2. The three bottom plots compare the fluorescence intensity of Dox.HCl, PG3-Dox and P(Lac)Dox-treated HepG2 cells at different times: D. 0.5h; E. 1h and F. 6h. Untreated HepG2 cells were also used as control (peaks in Red).

Unfortunately, there were no significant changes observed in the uptake of PG3-Dox and P(Lac)G3-Dox by confocal microscopy, and the flow cytometry results indicate that same amount of Dox were internalised at 0.5, 1 and 6h by PG3-Dox and P(Lac)G3-Dox which indicate no difference in the uptake of both

carriers. However, the size and stability of P(LAC)G3 was more convenient for targeted delivery in liver cells.

It is known that the uptake of nanoparticles by cells depends on their size, shape and surface properties. Micrometre-sized rigid spheroids are cleared immediately in the first pass through the microvasculature of various bodily organs and do not enter most cells whereas spherical and short filaments nanoparticles exhibit prolonged circulation and can be taken easily by cells (Geng et al., 2007). Herein, all three micellar formulations were all spherical with a particle size less than 150nm, therefore, facilitated their uptake in cells. Moreover, each formulated micelle was internalised in HepG2 cells via endocytosis followed by their localisation in endosome/lysosome where the drug was then released by the influence of low pH and redox effect. However, the rate of endocytosis was size-independent as seen there was no difference in uptake between all formulated carriers although they exhibited different sizes (Wang et al., 2015). Furthermore, all carriers being internalised by endocytosis could have easily faced hardship in escaping endosomes/lysosomes compartments, but with increased time, confocal and toxicities studies demonstrated the successful release of the drug and their achievement in therapeutic effect towards the cancer cells, especially for PSSG3-Dox. The increased therapeutic effect of PSSG3-Dox emphasises the importance of the addition of disulphide linkage to enhance endosome/lysosome escape of the nanocarriers as in addition to the cytosolic reducing conditions, the endosome and the lysosome also have a redox potential that can be used to promote endosomal and subsequent lysosomal escape (Jhaveri, Deshpande and Torchilin, 2014). In contrast to Dox, Cur is a hydrophobic drug which does not

have similar protonation effect at lower pH. For this reason, the use of disulphide linkage shows its importance to influence the release of curcumin. Moreover, the co-delivery system represents here as another essential future research direction; this is based on the concept of delivering 2 or more therapeutic agents at the same time for combination cancer therapy. In this work, we have demonstrated the ability of PSSG3 to deliver both Dox and Cur at the same time into HepG2 cells with increased therapeutic effect compared to the single drug delivery.

8.2. Conclusions and future studies

In summary, this work not only provides a potential route towards the development of multifunctional pH or redox-sensitive micelles but may also help to enhance the safety of hydrophobic anticancer drugs, increase chemotherapeutic efficacy, overcome chemotherapy resistance and potentially offers an exciting route to inhibit the accumulation of tumours in tissues. Future studies will be to investigate further precisely how the particles get internalised and transported in the cells and how the drugs get unloaded and permeate the intracellular membranous structures. Moreover, Modifying the formulated micelles by conjugating at the same time the amine and BOC/PBF containing dendrons into disulfide-linked pullulan could be used as a potential co-delivery system for drug and gene delivery into tumour cells.

CHAPTER 9. APPENDIX

9.1. The Standard method of Removal of BOC and PBF from PLLA to yield PLLA+

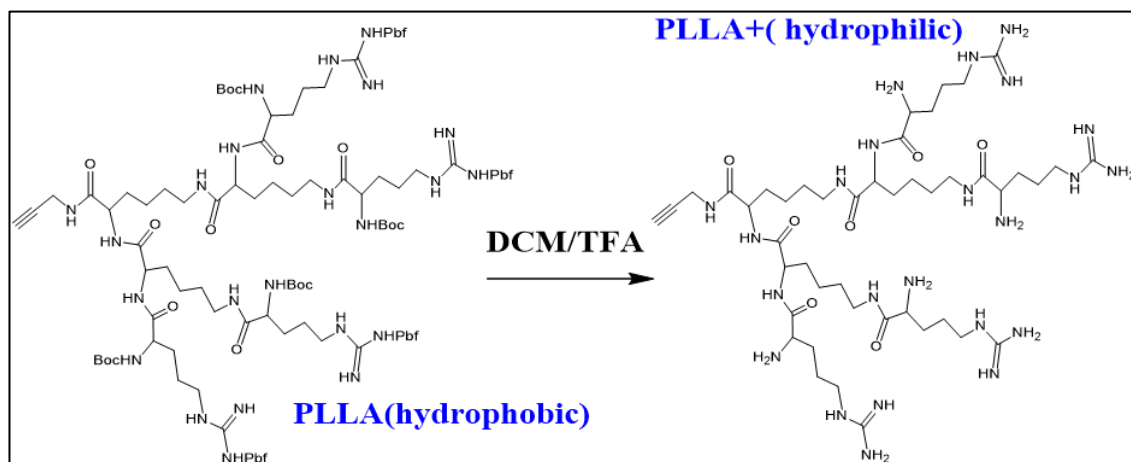


Figure 9.1. Synthesis equation of dendron of generation 3 (PLLA) deprotonation into PLLA+

Like the process used for G1 and G2, the hydrophobic groups of the generation 3 dendrons were removed by treating 3g (1mmol) of PLLA with 5ml of anhydrous CH₂Cl₂ and 8ml of TFA for 24hr at RT under N₂ atmosphere. Then the solvents were removed under vacuum, and the product was precipitated under stirring with anhydrous diethyl ether overnight. The precipitates were collected by centrifugation and then dried under high vacuum. This method was repeated at least 4 times to achieve complete deprotonation. The reaction was carried out for a longer time (36 hours to 48 hours), but an unexpected colour change was observed. In every repeat, the colour change was different; most of the time, the solution would change to a green solution, but sometimes it would be a dark red or dark brown colour.

9.2. Characterisation of deprotected PLLA products (ESI-MS: (calculated 1063.73))

After each deprotection reaction, the products were analysed by MS to verify if the reaction was successful. The Figures 9.2,3,4, and 5 show the MS results of the 4 repeated reaction were no resulted mass values corresponded to the calculated MS value being 1063.73.

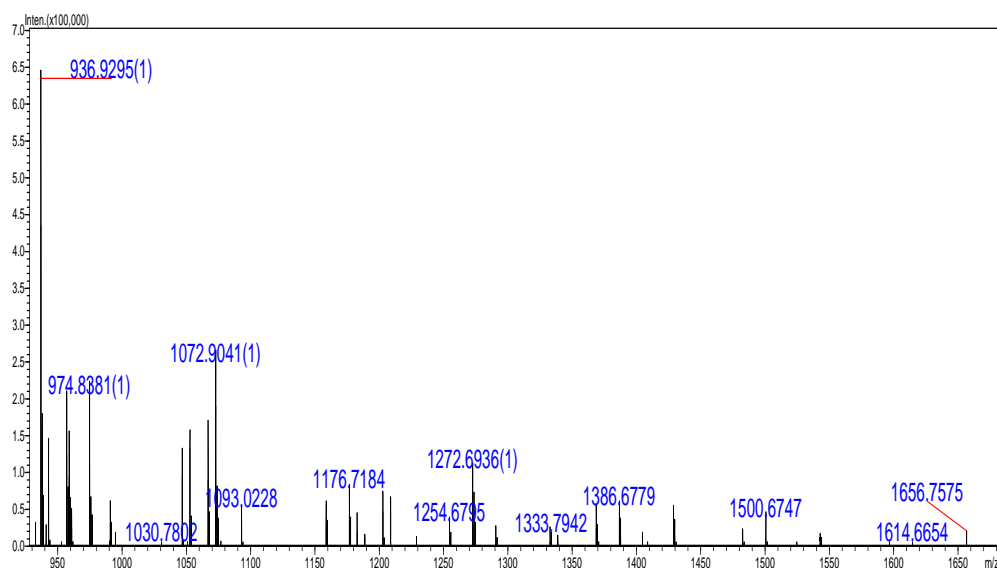


Figure 9.2. ESI-MS of first deprotected PLLA dendron product

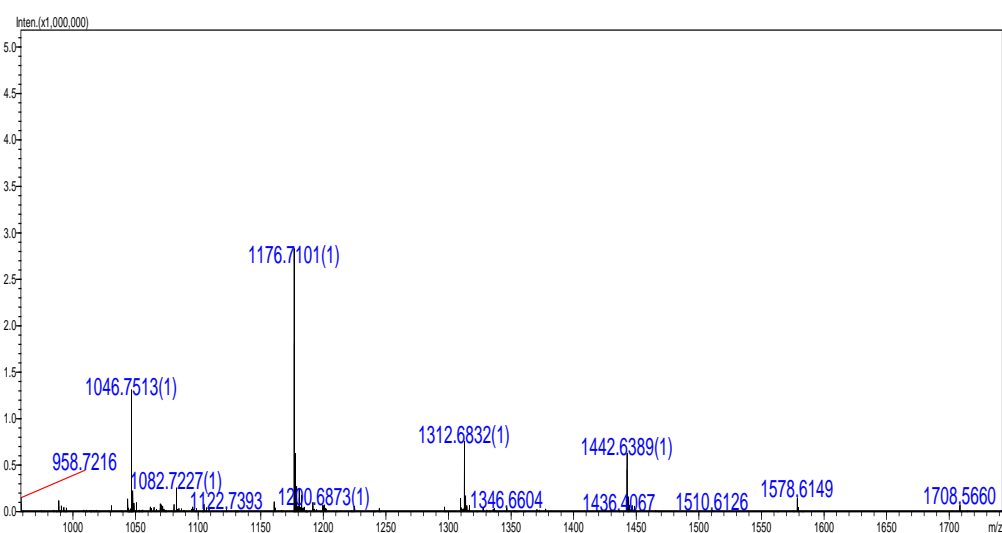


Figure 9.3. ESI-MS of second deprotected PLLA dendron product

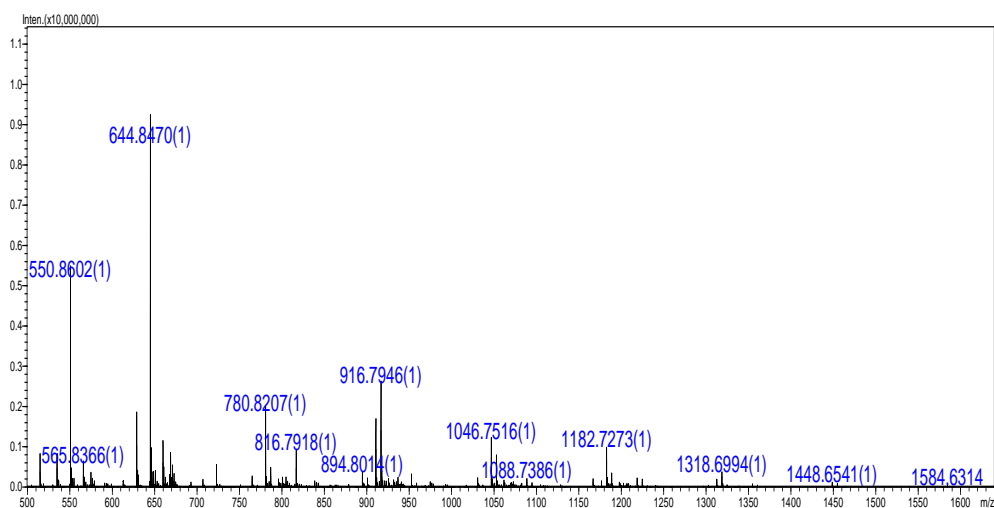


Figure 9.4. ESI-MS of second deprotected PLLA dendron product

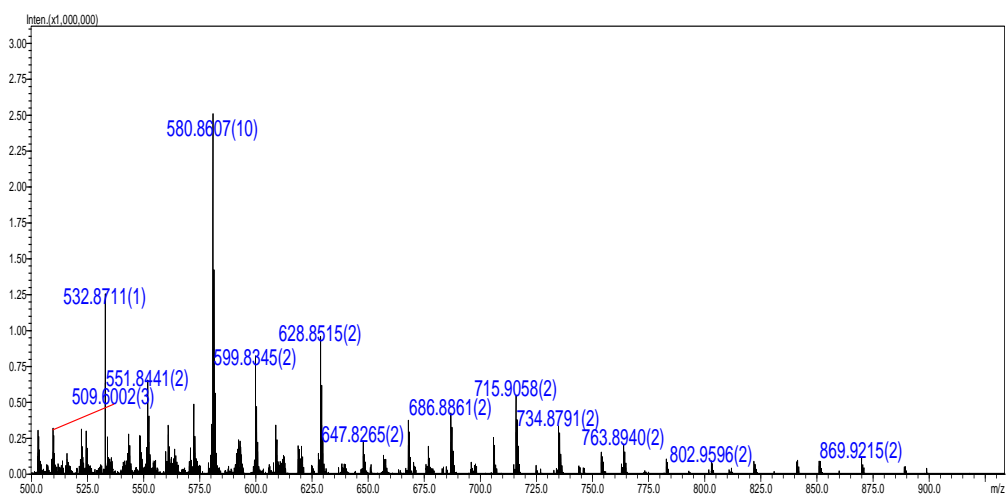


Figure 9.5. ESI-MS of second deprotected PLLA dendron product

Moreover, deprotection of PLLA was expected to present some cationic amine group on the surface that could interact with DNA. Therefore, we investigate if the PLLA deprotection could be achieved after being conjugated to pullulan. PLLA(BOC/PBF) was therefore first conjugated into pullulan and then deprotected. Agarose gel was then carried out to see if the deprotection was successful. However, Figure 9-6 shows that the product was not able to complex with the DNA suggesting the unsuccessful deprotection of PLLA.

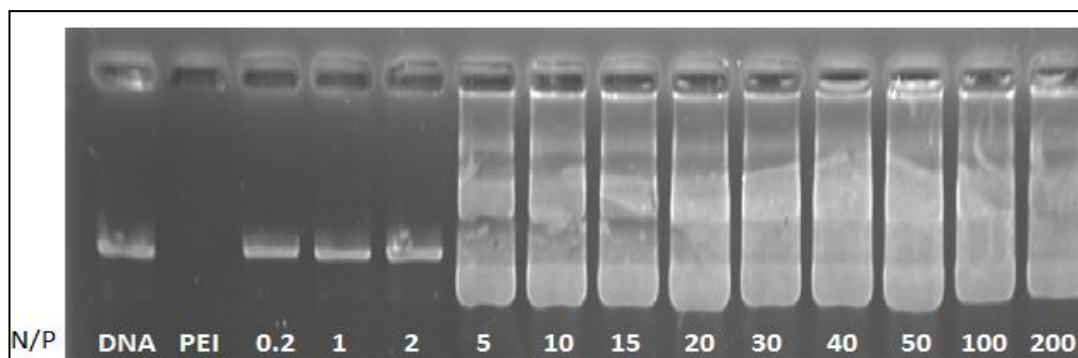


Figure 9.6. Agarose gel electrophoresis retardation assay of PG3/pDNA and PEI/DNA complexes at various N/P ratios.

Finally, we proposed a better way of synthesising the PLLA+ product by synthesising PLLL and then converting the terminal amine groups into guanidine groups. Since G2 was already synthesised, the guanidinylation of G2 dendron was first investigated.

9.3. Guanidinylation of G2 Dendron for gene compaction

Firstly, PLL dendron of generation 2 was clicked into pullulan via the same method as P-PLLA, and the method for the conversion of an amine into guanidine is given in chapter-7.

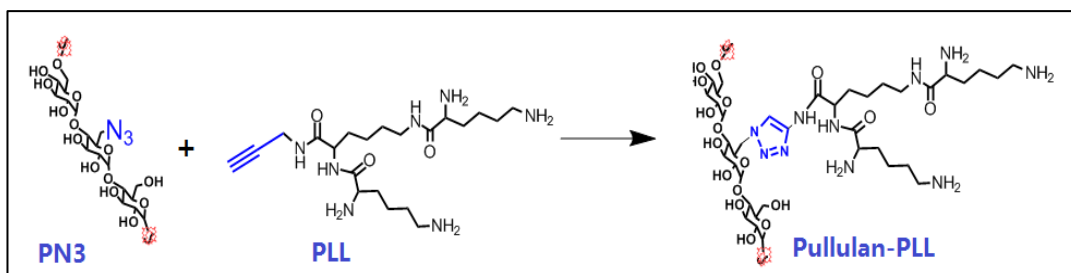


Figure 9.7. Synthesis equation of Pullulan-PLL.

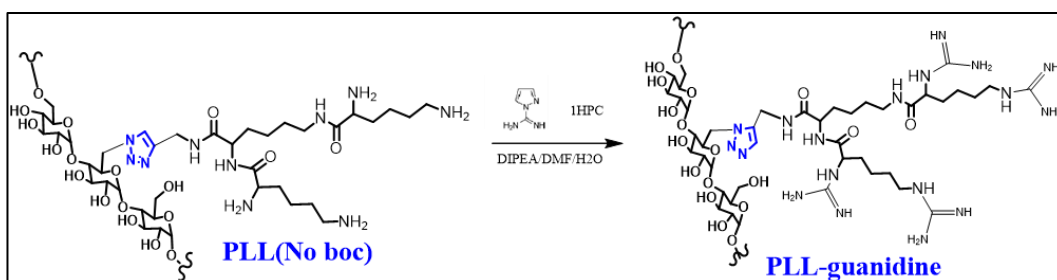


Figure 9.8. Synthesis equation of Pullulan-PLLG.

The FTIR in Figure 9.9 confirms the production of P-PLL.

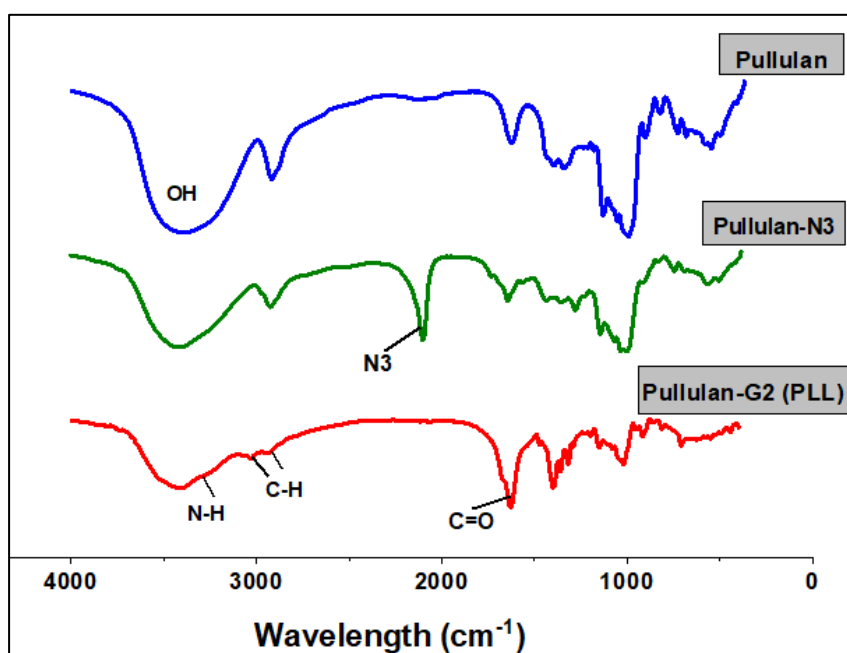


Figure 9.9. FTIR spectrum of Pullulan, PN3 and P-PLL

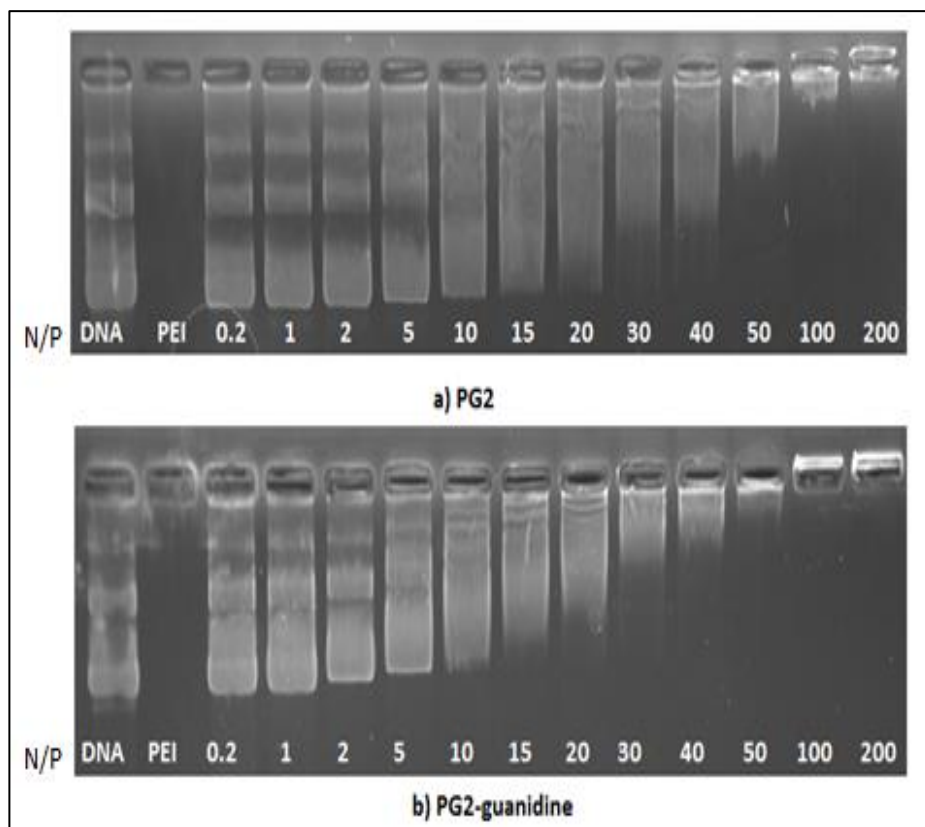


Figure 9.10. Agarose gel electrophoresis retardation assay of PG2/pDNA, PG2G/pDNA and PEI/pDNA complexes at various N/P ratios.

Furthermore, Figure 9.10 shows the Agarose gel electrophoresis retardation assay of PG2/pDNA, PEI/pDNA and PG2G complexes at various N/P ratios showing that the guanidinylation was successful and can improve gene compaction. For this reason, Guanidilation of G3PLLL was then carried out (Chapter-7)

9.4. Method for the Removal of Lysine or arginine from lysine-dendron of generation 2 and Arginine-dendron of generation 3

After purification by column chromatography to remove any traces of lysine or arginine observed by TLC, the dried product was dissolved in chloroform and then washed 3 times with NaHCO_3 (stirred for 3 hours). The product was collected using a separatory funnel and then dehydrated overnight with

Mg₂SO₄. The dried powder was obtained by rotary evaporation and vacuum pump.

9.5. Growth curve of HepG2 and U251 cells

Tumour growth is known to be directly related to cell proliferation. When treating a tumor, the intention is to reverse the growth by killing or removing cancer cells. Determining the growth curve of cells in the subject describes the increases and decreases in the number of cells over time (Dang et al., 2003). Figure 9-11 shows the growth curve of HepG2 and U251 cells, which was cultivated for 237 hours under the same conditions (at 37°C under CO₂).

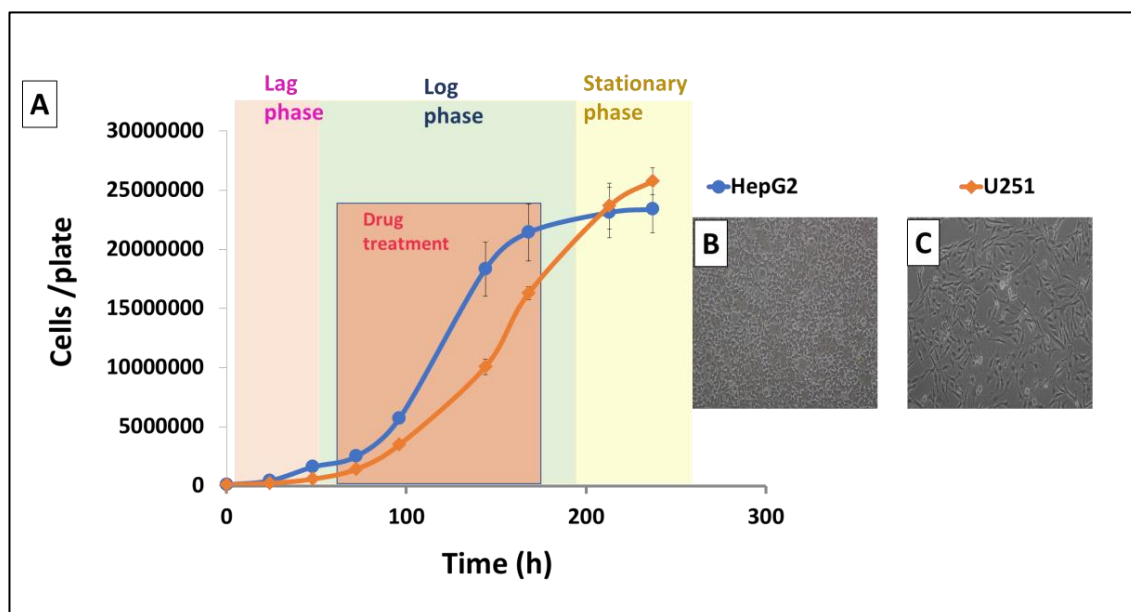


Figure 9-11. A. HepG2 and U251 growth curve (conditions: cells were seeded at 100000 cells B. HepG2 cells visualised and photographed under a light microscope C. U251 cells.

The growth of both cell lines is presented as a semi-logarithmic plot of the cell density versus the time spent in culture. During the lag phase (from 0h to <48h), the cells are seeded, and prolonged growth is observed because the cells are still adapting to the culture environment. Both cells start proliferating

exponentially (doubling time) around 48h and consume the nutrients in the growth medium; this phase is known as the log phase. Treatment of these cells after a period of 48hour growth would, therefore, be more accurate for in vitro cells studies. When all growth medium is spent or when the cells occupy all of the available substrates, the cells enter a phase known as a stationary phase where the proliferation is significantly reduced or ceases entirely (Falgreen et al., 2014). HepG2 cells enter stationary phase around 180 hours, whereas U251 still proliferate until around 213hours.

9.6. Investigation for the best parameters to carry out esterification reaction

Pullulan was reacted with 3,3'-dithiodipropionic acid in the presence of a catalytic amount of DMAP, a best ester-activator intermediate was chosen between DCC and EDC.HCl with a suitable solvent (DMSO or DMF)

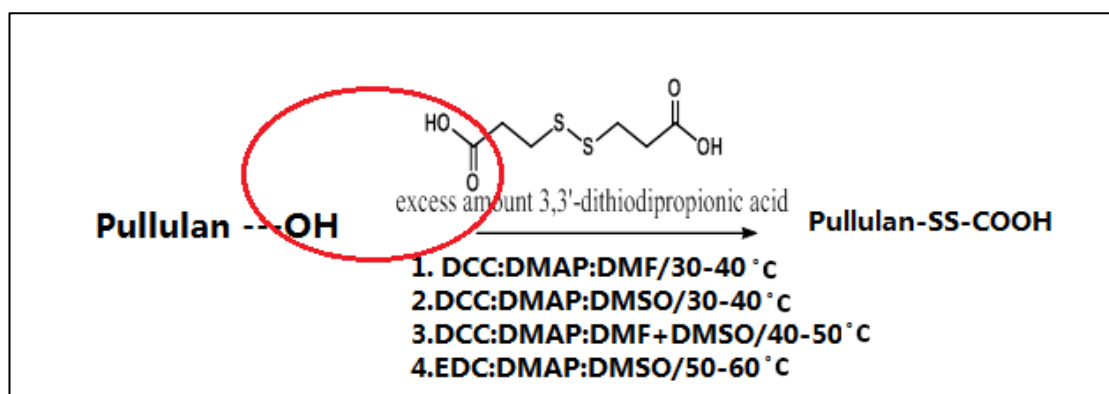


Figure 9-12. Synthesis equation of disulfide-linked pullulan PSS-COOH.

The conversion of pullulan OH into azide group linked by a disulphide bond was first achieved by esterification between OH in pullulan and COOH in DTDA. Different experimental conditions were set up for successful esterification, suitable temperature (30-60°C), catalysts (DCC or EDC.HCl) and solvents (DMSO or DMF) were investigated.

DTDPA (2mmol) and DMAP (0.15mmol) were first dissolved in 50ml of DMSO (or DMF) at 45 °C under N₂ atmosphere. Pullulan (0.5g, 1mmol equivalent of anhydrous glucoside units) and DCC (3mmol) were separately dissolved in 10 ml of DMSO (or DMF or DMSO/DMF: V/V: 1/1) for 30 min at RT. The mixture of pullulan was then added dropwise to the DTDPA mixture solution and stirred for 2 days at 45 °C. Pullulan solids appeared as precipitates into the solution.

Figure 9-13 shows the proton NMR of each product obtained after the reaction with different conditions.

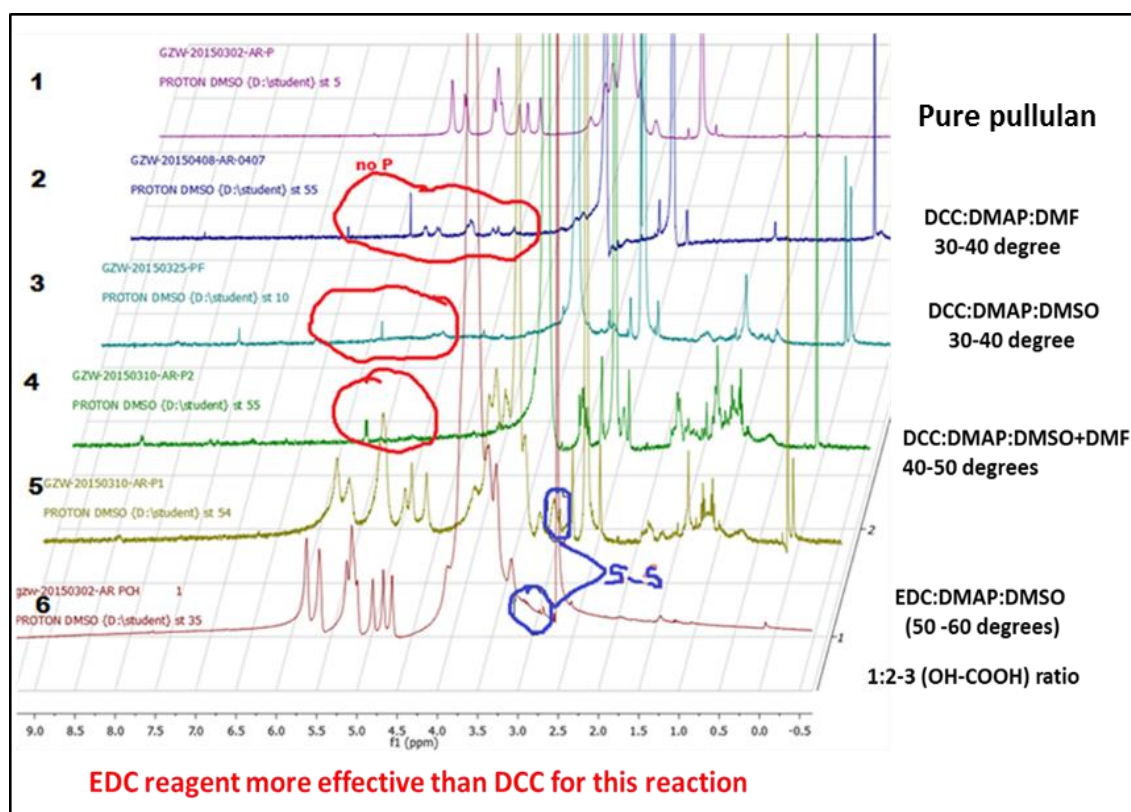


Figure 9-13. ¹H NMR (400 MHz, DMSO-d₆) of each pullulan derivatives obtained after different experimental condition.

As seen, the products 2,3 and 4 obtained after reaction using DCC as the coupling agents did not give any characteristic peaks in ¹H NMR of the pullulan whereas product obtained when using EDC.HCl gave both pullulan and DTPA

peaks characteristics. It was therefore deduced that the best parameters for successful esterification are using EDC.HCl and DMAP which are all dissolved in DMSO and the reaction are carried between 50-60°C.

References

- Abbott, N. (2005) Dynamics of CNS Barriers: Evolution, Differentiation, and Modulation. *Cellular and Molecular Neurobiology*, 25(1), pp. 5-23.
- Ahles, T.A. and Saykin, A.J. (2007) Candidate mechanisms for chemotherapy-induced cognitive changes. *Nature Reviews Cancer*, 7(3), p.192.
- Aina, O., Sroka, T., Chen, M. and Lam, K. (2002) Therapeutic cancer targeting peptides. *Biopolymers*, 66(3), pp. 184-199.
- Aizawa, K., Liu, C., Tang, S., Veeramachaneni, S., Hu, K., Smith, D. and Wang, X. (2016) Tobacco carcinogen induces both lung cancer and non-alcoholic steatohepatitis and hepatocellular carcinomas in ferrets which can be attenuated by lycopene supplementation. *International Journal of Cancer*, 139(5), pp.1171-1181.
- Akhlaghi, S.P., Peng, B., Yao, Z., Tam, K.C. (2013) Sustainable nanomaterials derived from polysaccharides and amphiphilic compounds. *Soft Matter*, (9), 7905-7918.
- Akiyoshi, K., Deguchi, S., Moriguchi, N., Yamaguchi, S. and Sunamoto, J. (1993) Self-aggregates of hydrophobized polysaccharides in water. Formation and characteristics of nanoparticles. *Macromolecules*, 26(12), pp. 3062-3068.
- Albuquerque, L., de Castro, C., Riske, K., da Silva, M., Muraro, P., Schmidt, V., Giacomelli, C. and Giacomelli, F. (2017) Gene Transfection Mediated by Cationic Polymers Requires Free Highly Charged Polymer Chains to Overcome Intracellular Barriers. *Biomacromolecules*, 18(6), pp. 1918-1927.
- Alexis, F., Pridgen, E., Molnar, L. and Farokhzad, O. (2008) Factors Affecting the Clearance and Biodistribution of Polymeric Nanoparticles. *Molecular Pharmaceutics*, 5(4), pp. 505-515.
- Allen, C., Maysinger, D. and Eisenberg, A. (1999) Nano-engineering block copolymer aggregates for drug delivery. *Colloids and Surfaces B: Biointerfaces*, 16(1-4), pp. 3-27.
- Allen, T., Hansen, C., Martin, F., Redemann, C. and Yau-Young, A. (1991) Liposomes containing synthetic lipid derivatives of poly(ethylene glycol) show prolonged circulation half-lives in vivo. *Biochimica et Biophysica Acta (BBA) - Biomembranes*, 1066(1), pp. 29-36.
- Allen, T.M. and Cullis, P.R. (2004) Drug delivery systems: entering the mainstream. *Science*, 303(5665), pp.1818-1822.
- Allison, R. (2014) Photodynamic therapy: oncologic horizons. *Future Oncology*, 10(1), pp. 123-124.
- Allison, R., Downie, G., Cuenca, R., Hu, X., Childs, C. and Sibata, C. (2004) Photosensitizers in clinical PDT. *Photodiagnosis and Photodynamic Therapy*, 1(1), pp. 27-42.

Ambattu, L. and Rekha, M. (2015) Betaine conjugated cationic pullulan as effective gene carrier. *International Journal of Biological Macromolecules*, 72, pp. 819-826.

Amselem, S., Cohen, R. and Barenholz, Y. (1993) In vitro tests to predict in vivo performance of liposomal dosage forms. *Chemistry and Physics of Lipids*, 64(1-3), pp. 219-237.

Anderson, R. (1998) the caveolae membrane system. *Annual Review of Biochemistry*, 67(1), pp. 199-225.

Andreadis, A. (1987) Generation of Protein Isoform Diversity by Alternative Splicing: Mechanistic and Biological Implications. *Annual Review of Cell and Developmental Biology*, 3(1), pp. 207-242.

Aniento, F. (1993) Cytoplasmic dynein-dependent vesicular transport from early to late endosomes [published erratum appears in *J Cell Biol* 1994 Feb;124(3):397]. *The Journal of Cell Biology*, 123(6), pp. 1373-1387.

Ansari, L., Shiehzadeh, F., Taherzadeh, Z., Nikoofal-Sahlabadi, S., Momtaziborojeni, A., Sahebkar, A. and Eslami, S. (2017) The most prevalent side effects of pegylated liposomal doxorubicin monotherapy in women with metastatic breast cancer: a systematic review of clinical trials. *Cancer Gene Therapy*, 24(5), pp. 189-193.

Antwi, S., Eckert, E., Sabaque, C., Leof, E., Hawthorne, K., Bamlet, W., Chaffee, K., Oberg, A. and Petersen, G. (2015) Exposure to environmental chemicals and heavy metals, and risk of pancreatic cancer. *Cancer Causes & Control*, 26(11), pp.1583-1591.

Araújo, R., Santos, S., Igne Ferreira, E. and Giarolla, J. (2018) New Advances in General Biomedical Applications of PAMAM Dendrimers. *Molecules*, 23(11), p. 2849.

Arcamone, F., Cassinelli, G., Franceschi, G., Penco, S., Pol, C., Redaelli, S. and Selva, A., 1972. Structure and physicochemical properties of adriamycin (doxorubicin). In *International symposium on adriamycin* (pp. 9-22). Springer, Berlin, Heidelberg.

Armulik, A., Genové, G. and Betsholtz, C. (2011) Pericytes: developmental, physiological, and pathological perspectives, problems, and promises. *Developmental cell*, 21(2), pp.193-215.

Arruebo, M., Vilaboa, N., Sáez-Gutierrez, B., Lambea, J., Tres, A., Valladares, M. and González-Fernández, Á. (2011) Assessment of the Evolution of Cancer Treatment Therapies. *Cancers*, 3(3), pp. 3279-3330.

Arshady, R. (1989) Preparation of microspheres and microcapsules by interfacial polycondensation techniques. *Journal of Microencapsulation*, 6(1), pp. 13-28.

Aschenbrenner, E., Bley, K., Koynov, K., Makowski, M., Kappl, M., Landfester, K., Weiss, C.K. (2013) Using the polymeric ouzo effect for the preparation of polysaccharide-based nanoparticles. *Langmuir*, (29), 8845-8855.

- Attarwala, H. (2010) Role of antibodies in cancer targeting. *Journal of Natural Science, Biology and Medicine*, 1(1), p. 53.
- Azzam, E., Jay-Gerin, J. and Pain, D. (2012) Ionizing radiation-induced metabolic oxidative stress and prolonged cell injury. *Cancer Letters*, 327(1-2), pp. 48-60.
- Bachem(2018) Documents.bachem.com, [online]. [Accessed 28 August 2018]. Available at: <http://documents.bachem.com/coupling_reagents.pdf>.
- Bae, B.C. and Na, K. (2010) Self-quenching polysaccharide-based nanogels of pullulan/folate-photosensitizer conjugates for photodynamic therapy. *Biomaterials*, 31(24), pp.6325-6335.
- Bagwell, C., Collon, P., Anderson, T., Clark, A., Nelson, A., Skulski, M. and Troyer, L. (2017) Accelerator Mass Spectrometry Radiocarbon Dating: Refining the Procedure at the University of Notre Dame. *STUDENT RESEARCH PAPERS*, p.21.
- Balogh, L., Swanson, D., Tomalia, D., Hagnauer, G. and McManus, A. (2001) Dendrimer–Silver Complexes and Nanocomposites as Antimicrobial Agents. *Nano Letters*, 1(1), pp. 18-21.
- Bareford, L. and Swaan, P. (2007) Endocytic mechanisms for targeted drug delivery. *Advanced Drug Delivery Reviews*, 59(8), pp. 748-758.
- Barenholz, Y. (2012) Doxil® — The first FDA-approved nano-drug: Lessons learned. *Journal of Controlled Release*, 160(2), pp. 117-134.
- Barnett, G., West, C., Dunning, A., Elliott, R., Coles, C., Pharoah, P. and Burnet, N. (2009) Normal tissue reactions to radiotherapy: towards tailoring treatment dose by genotype. *Nature Reviews Cancer*, 9(2), pp. 134-142.
- Barua, S. and Mitragotri, S. (2014) Challenges associated with penetration of nanoparticles across cell and tissue barriers: A review of current status and future prospects. *Nano Today*, 9(2), pp. 223-243.
- Bar-Zeev, M., Livney, Y. and Assaraf, Y. (2017) Targeted nanomedicine for cancer therapeutics: Towards precision medicine overcoming drug resistance. *Drug Resistance Updates*, 31, pp. 15-30.
- Basakran, N. (2015) CD44 as a potential diagnostic tumor marker. *Saudi Medical Journal*, 36(4), pp. 273-279.
- Basniwal, R., Khosla, R. and Jain, N. (2014) Improving the Anticancer Activity of Curcumin Using Nanocurcumin Dispersion in Water. *Nutrition and Cancer*, 66(6), pp. 1015-1022.
- Bataille, I., Meddahi-Pellé, A., Le Visage, C., Letourneur, D. and Chaubet, F. (2011) Pullulan for biomedical uses. *Polysaccharides in medicinal and pharmaceutical applications*, pp.145-182.
- Becker, E. (1993) A brief history of nuclear magnetic resonance. *Analytical Chemistry*, 65(6), pp. 295a-302a.

- Belbekhouche, S., Ali, G., Dulong, V., Picton, L. and Le Cerf, D. (2011) 'Synthesis and characterization of thermosensitive and pH-sensitive block copolymers based on polyetheramine and pullulan with different length', *Carbohydrate Polymers*, 86(1), pp. 304–312.
- Bhadra, D., Bhadra, S., Jain, S. and Jain, N. (2003) A PEGylated dendritic nanoparticulate carrier of fluorouracil. *International Journal of Pharmaceutics*, 257(1-2), pp. 111-124.
- Bhokare, S.G., Dongaonkar, C.C., Lahane, S.V., Salunke, P.B., Sawale, V.S. and Thombare, M.S. (2016) Herbal Novel Drug Deliver: A Review. *World Journal of Pharmacy and Pharmaceutical Sciences*, 5(8), pp.593-611.
- Bhuvaneshwari, R., Gan, Y., Soo, K. and Olivo, M. (2009) The effect of photodynamic therapy on tumor angiogenesis. *Cellular and Molecular Life Sciences*, 66(14), pp. 2275-2283.
- Bisht, S. and Maitra, A. (2009) Dextran-doxorubicin/chitosan nanoparticles for solid tumor therapy. *Wiley Interdisciplinary Reviews: Nanomedicine and Nanobiotechnology*, 1(4), pp. 415-425.
- Bitko, V., Musiyenko, A., Shulyayeva, O. and Barik, S. (2004) Inhibition of respiratory viruses by nasally administered siRNA. *Nature Medicine*, 11(1), pp. 50-55.
- Blaese, R.M., Culver, K.W., Miller, A.D., Carter, C.S., Fleisher, T., Clerici, M., Shearer, G., Chang, L., Chiang, Y., Tolstoshev, P. and Greenblatt, J.J. (1995) T lymphocyte-directed gene therapy for ADA- SCID: initial trial results after 4 years. *Science*, 270(5235), pp.475-480.
- Blouin, A. (1977) Distribution of organelles and membranes between hepatocytes and nonhepatocytes in the rat liver parenchyma. A stereological study. *The Journal of Cell Biology*, 72(2), pp. 441-455.
- Bobo, D., Robinson, K., Islam, J., Thurecht, K. and Corrie, S. (2016) Nanoparticle-Based Medicines: A Review of FDA-Approved Materials and Clinical Trials to Date. *Pharmaceutical Research*, 33(10), pp. 2373-2387.
- Bogner, A., Jouneau, P., Thollet, G., Basset, D. and Gauthier, C. (2007) A history of scanning electron microscopy developments: Towards "wet-STEM" imaging. *Micron*, 38(4), pp. 390-401.
- Bordignon, C., Notarangelo, L.D., Nobili, N., Ferrari, G., Casorati, G., Panina, P., Mazzolari, E., Maggioni, D., Rossi, C., Servida, P. and Ugazio, A.G., (1995) Gene therapy in peripheral blood lymphocytes and bone marrow for ADA-immunodeficient patients. *Science*, 270 (5235), pp. 470-475.
- Boris, D. and Rubinstein, M. (1996). A Self-Consistent Mean Field Model of a Starburst Dendrimer: Dense Core vs Dense Shell. *Macromolecules*, 29(22), pp.7251-726
- Bottino, C., Moretta, L., & Moretta, A. (2006). NK cell activating receptors and tumor recognition in humans. In *Immunobiology of Natural Killer Cell Receptors* (pp. 175-182). Springer, Berlin, Heidelberg.

Bourquin, J., Milosevic, A., Hauser, D., Lehner, R., Blank, F., Petri-Fink, A. and Rothen-Rutishauser, B. (2018) Biodistribution, Clearance, and Long-Term Fate of Clinically Relevant Nanomaterials. *Advanced Materials*, 30(19), p. 1704307.

Boyd, R., Pichaimuthu, S. and Cuenat, A. (2011) New approach to inter-technique comparisons for nanoparticle size measurements; using atomic force microscopy, nanoparticle tracking analysis and dynamic light scattering. *Colloids and Surfaces A: Physicochemical and Engineering Aspects*, 387(1-3), pp. 35-42.

Bozzuto, G. and Molinari, A. (2015) Liposomes as nanomedical devices. *International Journal of Nanomedicine*, p. 975.

Brannon-Peppas, L. and Blanchette, J. (2012) Nanoparticle and targeted systems for cancer therapy. *Advanced Drug Delivery Reviews*, 64, pp. 206-212.

Bravo-Osuna, I., Vauthier, C., Farabollini, A., Palmieri, G.F., Ponchel, G. (2007). Mucoadhesion mechanism of chitosan and thiolated chitosan-poly (isobutyl cyanoacrylate) core-shell nanoparticles. *Biomaterials*, (28), 2233-2243.

Brighton, D. (2005) *The Royal Marsden hospital handbook of cancer chemotherapy*. Edinburgh: Elsevier Churchill Livingstone.

Bulbake, U., Doppalapudi, S., Kommineni, N. and Khan, W. (2017) Liposomal Formulations in Clinical Use: An Updated Review. *Pharmaceutics*, 9(4), p. 12.

Buschauer, S., Koch, A., Wiggermann, P., Muller, M. and Hellerbrand, C. (2018) Hepatocellular carcinoma cells surviving doxorubicin treatment exhibit increased migratory potential and resistance to doxorubicin re-treatment in vitro. *Oncology Letters*.

Byrne, J., Betancourt, T. and Brannon-Peppas, L. (2008) Active targeting schemes for nanoparticle systems in cancer therapeutics. *Advanced Drug Delivery Reviews*, 60(15), pp. 1615-1626.

Cai, H., Ni, C. and Zhang, L. (2012) Preparation of complex nano-particles based on alginic acid/poly[(2-dimethylamino) ethyl methacrylate] and a drug vehicle for doxorubicin release controlled by ionic strength. *European Journal of Pharmaceutical Sciences*, 45(1-2), pp. 43-49.

Caley, A. and Jones, R. (2012) The principles of cancer treatment by chemotherapy. *Surgery (Oxford)*, 30(4), pp. 186-190.

Callaghan, P. (1993) Principles of nuclear magnetic resonance microscopy: Oxford University Press.

Cancer.org. (2017) Early History of Cancer | American Cancer Society. [online]. Available at: <https://www.cancer.org/cancer/cancer-basics/history-of-cancer/what-is-cancer.html> [Accessed 3 Jul. 2015].

Cao, Y., Gu, Y., Ma, H., Bai, J., Liu, L., Zhao, P., He, H. (2010) Self-assembled nanoparticle drug delivery systems from galactosylated polysaccharide-doxorubicin conjugate loaded doxorubicin. *Int. J. Biol. Macromol*, (46), pp. 245-249.

Capranico, G., Kohn, K. and Pommier, Y. (1990) Local sequence requirements for DNA cleavage by mammalian topoisomerase II in the presence of doxorubicin. *Nucleic Acids Research*, 18(22), pp. 6611-6619.

Carvalho, A., Fernandes, A.R. and Baptista, P.V. (2019) Nanoparticles as Delivery Systems in Cancer Therapy: Focus on Gold Nanoparticles and Drugs. In *Applications of Targeted Nano Drugs and Delivery Systems* (pp. 257-295). Elsevier.

Carvalho, C., Santos, R., Cardoso, S., Correia, S., Oliveira, P., Santos, M. and Moreira, P. (2009) Doxorubicin: The Good, the Bad and the Ugly Effect. *Current Medicinal Chemistry*, 16(25), pp. 3267-3285.

Castano, A., Mroz, P. and Hamblin, M. (2006) Photodynamic therapy and anti-tumour immunity. *Nature Reviews Cancer*, 6(7), pp. 535-545.

Castro, B., Dormoy, J., Evin, G. and Selve, C. (1975) Reactifs de couplage peptidique I (1) - l'hexafluorophosphate de benzotriazolyl N-oxytrisdiméthylamino phosphonium (B.O.P.). *Tetrahedron Letters*, 16(14), pp. 1219-1222.

Chandel, A.K.S., Bera, A., Nutan, B., Jewrajka, S.K. (2016) Reactive compatibilizer mediated precise synthesis and application of stimuli responsive polysaccharides-polycaprolactone amphiphilic co-network gels. *Polymer*, (99), 470-479

Chang, P., Peng, S., Lee, C., LU, C., Tsal, S., Shieh, T., Wu, T., Tu, M., Chen, M. and Yang, J. (2013) Curcumin-loaded nanoparticles induce apoptotic cell death through regulation of the function of MDR1 and reactive oxygen species in cisplatin-resistant CAR human oral cancer cells. *International Journal of Oncology*, 43(4), pp. 1141-1150.

Charles, N., Holland, E., Gilbertson, R., Glass, R. and Kettenmann, H. (2011) The brain tumor microenvironment. *Glia*, 59(8), pp. 1169-1180.

Chen, W., Meng, F., Cheng, R. and Zhong, Z. (2010) pH-Sensitive degradable polymersomes for triggered release of anticancer drugs: A comparative study with micelles. *Journal of Controlled Release*, 142(1), pp. 40-46.

Chen, W., Zhong, P., Meng, F., Cheng, R., Deng, C., Feijen, J. and Zhong, Z. (2013) 'Redox and pH-responsive degradable micelles for dually activated intracellular anticancer drug release', *Journal of Controlled Release*, 169(3), pp. 171-179.

Chen, W., Zhong, P., Meng, F., Cheng, R., Deng, C., Feijen, J. and Zhong, Z. (2013) Redox and pH-responsive degradable micelles for dually activated intracellular anticancer drug release. *Journal of Controlled Release*, 169(3), pp. 171-179.

Chen, Y., Wang, X., Yan, Z., Wang, J., Luo, J. and Liu, Q., 2012. Hepatic arterial infusion with irinotecan, oxaliplatin, and floxuridine plus systemic chemotherapy as first-line treatment of unresectable liver metastases from colorectal cancer. *Oncology Research and Treatment*, 35(9), pp.480-484.

Cheng, H.N. and Neiss, T.G. (2012) Solution NMR spectroscopy of food polysaccharides. *Polymer reviews*, 52(2), pp.81-114.

Cheng, R., Feng, F., Meng, F., Deng, C., Feijen, J. and Zhong, Z. (2011) Glutathione-responsive nano-vehicles as a promising platform for targeted intracellular drug and gene delivery. *Journal of Controlled Release*, 152(1), pp. 2-12.

Cheek, C.F. (2012) Protecting normal cells from the cytotoxicity of chemotherapy. *Cell Cycle*, 11(12), pp.2227-2227.

Cho, H., Yoon, I., Yoon, H., Koo, H., Jin, Y., Ko, S., Shim, J., Kim, K., Kwon, I. and Kim, D. (2012) Polyethylene glycol-conjugated hyaluronic acid-ceramide self-assembled nanoparticles for targeted delivery of doxorubicin. *Biomaterials*, 33(4), pp. 1190-1200.

Choi, J., Nam, K., Park, J., Kim, J., Lee, J. and Park, J. (2004) Enhanced transfection efficiency of PAMAM dendrimer by surface modification with L-arginine. *Journal of Controlled Release*, 99(3), pp. 445-456.

Choi, J.Y., Ryu, K., Lee, G.J., Kim, K. and Kim, T.I. (2015) Agmatine-containing bioreducible polymer for gene delivery systems and its dual degradation behavior. *Biomacromolecules*, 16(9), pp.2715-2725.

Chou, W.Y., Marky, L.A., Zaunzowski, D. and Breslauer, K.J. (1987) The thermodynamics of drug-DNA interactions: Ethidium bromide and propidium iodide. *J Biomol Struct Dyn*, 5(2), pp. 345-359.

Choudhary, S., Gupta, L., Rani, S., Dave, K. and Gupta, U. (2017) Impact of Dendrimers on Solubility of Hydrophobic Drug Molecules. *Frontiers in Pharmacology*, 8.

Chowdhary, R.K., Shariff, I. and Dolphin, D. (2003) Drug release characteristics of lipid-based benzoporphyrin derivative. *J Pharm Pharm Sci*, 6(1), pp.13-9.

Cimecioglu, A. L., Ball, D. H., Huang, S. H., & Kaplan, D. L. (1997). A direct regioselective route to 6-azido-6-deoxy polysaccharides under mild and homogeneous conditions. *Macromolecules*, 30, 155–156.

Cohen, I.R., Quintana, F.J., Carmi, P. and Mor, F., Alma Bio Therapeutics, 2018. *DNA Vaccines Encoding Heat Shock Proteins*. U.S. Patent Application 15/957,625.

Collett, B.M., 2007. Scanning electron microscopy: A review and report of research in wood science. *Wood and Fiber Science*, 2(2), pp.113-133.

Dai, L., Li, J., Zhang, B., Liu, J., Luo, Z. and Cai, K. (2014) Redox-Responsive Nanocarrier Based on Heparin End-Capped Mesoporous Silica Nanoparticles for Targeted Tumor Therapy in Vitro and in Vivo. *Langmuir*, 30(26), pp. 7867-7877.

Dai, W., Jin, W., Zhang, J., Wang, X., Wang, J., Zhang, X., Wan, Y. and Zhang, Q. (2012) Spatiotemporally controlled co-delivery of anti-vasculature agent and

cytotoxic drug by octreotide-modified stealth liposomes. *Pharmaceutical research*, 29(10), pp.2902-2911.

Danaei, M., Dehghankhold, M., Ataei, S., Hasanzadeh Davarani, F., Javanmard, R., Dokhani, A., Khorasani, S. and Mozafari, M. (2018) Impact of Particle Size and Polydispersity Index on the Clinical Applications of Lipidic Nanocarrier Systems. *Pharmaceutics*, 10(2), p. 57.

Dang, C., Gilewski, T.A., Surbone, A. and Norton, L., 2003. Growth curve analysis.

Danhier, F., Feron, O. and Pr eat, V. (2010) To exploit the tumor microenvironment: Passive and active tumor targeting of nanocarriers for anti-cancer drug delivery. *Journal of Controlled Release*, 148(2), pp. 135-146.

Daniel, D., Chiu, C., Giraudo, E., Inoue, M., Mizzen, L., Chu, N. and Hanahan, D. (2005) CD4+T Cell-Mediated Antigen-Specific Immunotherapy in a Mouse Model of Cervical Cancer. *Cancer Research*, 65(5), pp. 2018-2025.

Daniel, D., Meyer-Morse, N., Bergsland, E., Dehne, K., Coussens, L. and Hanahan, D. (2003) Immune Enhancement of Skin Carcinogenesis by CD4+T Cells. *The Journal of Experimental Medicine*, 197(8), pp. 1017-1028.

Danquah, M., Zhang, X. and Mahato, R. (2011) Extravasation of polymeric nanomedicines across tumor vasculature. *Advanced Drug Delivery Reviews*, 63(8), pp. 623-639.

Dawson, M., Krauland, E., Wirtz, D. and Hanes, J. (2004) Transport of Polymeric Nanoparticle Gene Carriers in Gastric Mucus. *Biotechnology Progress*, 20(3), pp. 851-857.

De Visser, K., Korets, L. and Coussens, L. (2005) De novo carcinogenesis promoted by chronic inflammation is B lymphocyte dependent. *Cancer Cell*, 7(5), pp. 411-423.

Delaney, G., Jacob, S., Featherstone, C. and Barton, M. (2005) The role of radiotherapy in cancer treatment. *Cancer*, 104(6), pp. 1129-1137.

D'Emanuele, A., Jevprasesphant, R., Penny, J. and Attwood, D. (2004) The use of a dendrimer-propranolol prodrug to bypass efflux transporters and enhance oral bioavailability. *Journal of Controlled Release*, 95(3), pp. 447-453.

Detampel, P., Witzigmann, D., Kr ahenb uhl, S. and Huwyler, J. (2013) Hepatocyte targeting using pegylated asialofetuin-conjugated liposomes. *Journal of Drug Targeting*, 22(3), pp. 232-241.

Di Sabatino, A., Lenti, M., Corazza, G. and Gianfrani, C. (2018) Vaccine Immunotherapy for Celiac Disease. *Frontiers in Medicine*, 5.

Dimitrios P. Bogdanos, Bin Gao, M. Eric Gershwin. (2013) Liver Immunology. *Compr Physiol*, 3, pp 567-598.

Do, H., Healey, J., Waller, E. and Lollar, P. (1999) Expression of Factor VIII by Murine Liver Sinusoidal Endothelial Cells. *Journal of Biological Chemistry*, 274(28), pp. 19587-19592.

Dojindo Laboratories (2018) Cell Counting Kit-8 | Dojindo. Dojindo.eu.com, [online]. [Accessed 4 June 2018]. Available at: <<http://www.dojindo.eu.com/store/p/456-Cell-Counting-Kit-8.aspx>>.

Dolmans, D. E., Fukumura, D., & Jain, R. K. (2003). Photodynamic therapy for cancer. *Nature reviews cancer*, 3(5), pp. 380.

Dougherty, T., Cooper, M. and Mang, T. (1990) Cutaneous phototoxic occurrences in patients receiving Photofrin®. *Lasers in Surgery and Medicine*, 10(5), pp. 485-488.

D'Souza, A. and Devarajan, P. (2015) Asialoglycoprotein receptor mediated hepatocyte targeting — Strategies and applications. *Journal of Controlled Release*, 203, pp. 126-139.

Dubois, L., Campanati, L., Righy, C., Dâ Andrea-Meira, I., Spohr, T., Porto-Carreiro, I., Pereira, C., BalÃ§a-Silva, J., Kahn, S., DosSantos, M., Oliveira, M., Ximenes-da-Silva, A., Lopes, M., Faveret, E., Gasparetto, E. and Moura-Neto, V. (2014) Gliomas and the vascular fragility of the blood brain barrier. *Frontiers in Cellular Neuroscience*, 8.

Dupayage, L., Nouvel, C., Six, J.L. (2011) Protected versus unprotected dextran macroinitiators for atp synthesis of dex-g-pmma. *J. Polym. Sci., Part A: Polym. Chem*, (49), 35-46.

Dupayage, L., Save, M., Dellacherie, E., Nouvel, C., Six, J.-L. (2008) Pmma-grafted dextran glycopolymers by atom transfer radical polymerization. *J. Polym. Sci., Part A: Polym. Chem*, (46), 7606-7620.

Dupont, E., Prochiantz, A. and Joliot, A. (2011) Penetratin story: an overview. In *Cell-Penetrating Peptides* (pp. 21-29). Humana Press.

Eisenbrey, J., Burstein, O., Kambhampati, R., Forsberg, F., Liu, J. and Wheatley, M. (2010) Development and optimization of a doxorubicin loaded poly(lactic acid) contrast agent for ultrasound directed drug delivery. *Journal of Controlled Release*, 143(1), pp. 38-44.

El-Aneed, A. (2004) an overview of current delivery systems in cancer gene therapy. *Journal of Controlled Release*, 94(1), pp. 1-14.

Eliaz, R., Nir, S., Marty, C. and Szoka, F. (2004) Determination and Modeling of Kinetics of Cancer Cell Killing by Doxorubicin and Doxorubicin Encapsulated in Targeted Liposomes. *Cancer Research*, 64(2), pp. 711-718.

El-Serag, H. (2004) Hepatocellular carcinoma: Recent trends in the United States. *Gastroenterology*, 127(5), pp. S27-S34.

Elzoghby, A., Samy, W. and Elgindy, N. (2018) *Albumin-based nanoparticles as potential controlled release drug delivery systems. Journal of controlled release*, 157(2), pp.168-182.

Espinosa-Diez, C., Miguel, V., Mennerich, D., Kietzmann, T., Sánchez-Pérez, P., Cadenas, S. and Lamas, S. (2015) Antioxidant responses and cellular adjustments to oxidative stress. *Redox Biology*, 6, pp. 183-197.

Falgreen, S., Laursen, M., Bødker, J., Kjeldsen, M., Schmitz, A., Nyegaard, M., Johnsen, H., Dybkær, K. and Bøgsted, M. (2014) Exposure time independent summary statistics for assessment of drug dependent cell line growth inhibition. *BMC Bioinformatics*, 15(1), p. 168.

Fan, D., Yu, J., Yan, R., Xu, X., Wang, Y., Xie, X., Liu, C., Liu, Y. and Huang, H. (2018) Preparation and Evaluation of Doxorubicin-Loaded Micelles Based on Glycyrrhetic Acid Modified Gelatin Conjugates for Targeting Hepatocellular Carcinoma. *Journal of Nanomaterials*, 2018, pp. 1-13.

Fang, J., Nakamura, H. and Maeda, H. (2011) The EPR effect: Unique features of tumor blood vessels for drug delivery, factors involved, and limitations and augmentation of the effect. *Advanced Drug Delivery Reviews*, 63(3), pp. 136-151.

Fang, S., Niu, Y., Zhang, W., Zhang, Y., Yu, L., Zhang, Y. and Li, X. (2015) Liposome-like nanocapsules of dual drug-tailed betaine for cancer therapy. *International Journal of Pharmaceutics*, 493(1-2), pp. 460-465.

Farber, S., Diamond, L., Mercer, R., Sylvester, R. and Wolff, J. (1948) Temporary Remissions in Acute Leukemia in Children Produced by Folic Acid Antagonist, 4-Aminopteroyl-Glutamic Acid (Aminopterin). *New England Journal of Medicine*, 238(23), pp. 787-793.

Farkona, S., Diamandis, E. and Blasutig, I. (2016) Cancer immunotherapy: the beginning of the end of cancer?. *BMC Medicine*, 14(1).

Farris, S., Unalan, I.U., Introzzi, L., Fuentes-Alventosa, J.M. and Cozzolino, C.A. (2014) 'Pullulan-based films and coatings for food packaging: Present applications, emerging opportunities, and future challenges', *Journal of Applied Polymer Science*, 131(13), p. n/a–n/a. doi: 10.1002/app.40539.

Fassoulaki, A., Triga, A., Melemini, A. and Sarantopoulos, C. (2005) Multimodal Analgesia with Gabapentin and Local Anesthetics Prevents Acute and Chronic Pain After Breast Surgery for Cancer. *Anesthesia & Analgesia*, 101(5), pp. 1427-1432.

Fisher, P. (2005) Ismda-7/IL-24a "Magic Bullet" for Cancer?. *Cancer Research*, 65(22), pp. 10128-10138.

Folkman, J. (1996) Fighting Cancer by Attacking its Blood Supply. *Scientific American*, 275(3), pp. 150-154.

Fosgerau, K. and Hoffmann, T. (2015) Peptide therapeutics: current status and future directions. *Drug Discovery Today*, 20(1), pp. 122-128.

Fowers, K.D. and Kopeček, J. (2012) Targeting of Multidrug-Resistant Human Ovarian Carcinoma Cells With Anti-P-Glycoprotein Antibody Conjugates. *Macromolecular bioscience*, 12(4), pp.502-514.

Frey, H. (2003). Book Review: Dendrimers and other Dendritic Polymers By Jean M. J. Fréchet and Donald A. Tomalia. *Angewandte Chemie International Edition*, 42(20), pp.2215-2216.

Friedmann, T. (1992) A brief history of gene therapy. *Nature genetics*, 2(2), pp.93.

Fumagalli, G., Marucci, C., Christodoulou, M., Stella, B., Dosio, F. and Passarella, D. (2016) Self-assembly drug conjugates for anticancer treatment. *Drug Discovery Today*, 21(8), pp. 1321-1329.

Fumagalli, S., Ortolano, F. and De Simoni, M. (2014) A close look at brain dynamics: Cells and vessels seen by in vivo two-photon microscopy. *Progress in Neurobiology*, 121, pp. 36-54.

Furuse, K., Fukuoka, M., Kato, H., Horai, T., Kubota, K., Kodama, N., Kusunoki, Y., Takifuji, N., Okunaka, T. and Konaka, C. (1993) A prospective phase II study on photodynamic therapy with photofrin II for centrally located early-stage lung cancer. The Japan Lung Cancer Photodynamic Therapy Study Group. *Journal of Clinical Oncology*, 11(10), pp. 1852-1857.

Gasser, M. and Waaga-Gasser, A.M., 2016. Therapeutic antibodies in cancer therapy. In *Protein Targeting Compounds* (pp. 95-120). Springer, Cham.

Gabizon, A., Chisin, R., Amselem, S., Druckmann, S., Cohen, R., Goren, D., Fromer, I., Peretz, T., Sulkes, A. and Barenholz, Y. (1991) Pharmacokinetic and imaging studies in patients receiving a formulation of liposome-associated adriamycin. *British Journal of Cancer*, 64(6), pp. 1125-1132.

Gallois, L., Fiallo, M., Laigle, A., Priebe, W. and Garnier-Suillerot, A. (1996) The Overall Partitioning of Anthracyclines into Phosphatidyl-Containing Model Membranes Depends Neither on the Drug Charge Nor the Presence of Anionic Phospholipids. *European Journal of Biochemistry*, 241(3), pp. 879-887.

Gaucher, G., Dufresne, M., Sant, V., Kang, N., Maysinger, D. and Leroux, J. (2005) Block copolymer micelles: preparation, characterization and application in drug delivery. *Journal of Controlled Release*, 109(1-3), pp. 169-188.

Ge, J., Neofytou, E., Cahill, T., Beygui, R. and Zare, R. (2011) Drug Release from Electric-Field-Responsive Nanoparticles. *ACS Nano*, 6(1), pp. 227-233.

Geisberg, C. and Sawyer, D. (2010) Mechanisms of Anthracycline Cardiotoxicity and Strategies to Decrease Cardiac Damage. *Current Hypertension Reports*, 12(6), pp. 404-410.

Geng, Y., Dalhaimer, P., Cai, S., Tsai, R., Tewari, M., Minko, T., & Discher, D. E. (2007). Shape effects of filaments versus spherical particles in flow and drug delivery. *Nature Nanotechnology*, 2(4), 249–255.

Gewirtz, D. (1999) A critical evaluation of the mechanisms of action proposed for the antitumor effects of the anthracycline antibiotics adriamycin and daunorubicin. *Biochemical Pharmacology*, 57(7), pp. 727-741.

Ghaghada, K., Saul, J., Natarajan, J., Bellamkonda, R. and Annapragada, A. (2005) Folate targeting of drug carriers: A mathematical model. *Journal of Controlled Release*, 104(1), pp. 113-128.

- Gillies, E. and Frechet, J. (2005) Dendrimers and dendritic polymers in drug delivery. *Drug Discovery Today*, 10(1), pp. 35-43.
- Gilman, A. (1946) Therapeutic applications of chemical warfare agents. In *Federation proceedings*, 5, pp. 285).
- Godsey, M.E., Suryaprakash, S. and Leong, K.W. (2013) Materials innovation for co-delivery of diverse therapeutic cargos. *RSC advances*, 3(47), pp.24794-24811.
- Goel, S., Duda, D., Xu, L., Munn, L., Boucher, Y., Fukumura, D. and Jain, R. (2011) Normalization of the Vasculature for Treatment of Cancer and Other Diseases. *Physiological Reviews*, 91(3), pp. 1071-1121.
- Gollnick, S. and Brackett, C. (2009) Enhancement of anti-tumor immunity by photodynamic therapy. *Immunologic Research*, 46(1-3), pp. 216-226.
- Goodarzi, N., Varshochian, R., Kamalinia, G., Atyabi, F. and Dinarvand, R. (2013) A review of polysaccharide cytotoxic drug conjugates for cancer therapy. *Carbohydrate Polymers*, 92(2), pp. 1280-1293.
- Goodman, L. (1946) nitrogen mustard therapy. *Journal of the American Medical Association*, 132(3), pp. 126.
- Gorad, R.S., Mandlik, S.K. and Gujar, K.N. (2013) Liver specific drug targeting strategies: a review. *Int. J. Pharm. Sci. Res.*, 11, pp.4145-4157.
- Gottesman, M., Fojo, T. and Bates, S. (2002) Multidrug resistance in cancer: role of ATP-dependent transporters. *Nature Reviews Cancer*, 2(1), pp. 48-58.
- Griffith, T., Stokes, B., Kucaba, T., Earel Jr., J., VanOosten, R., Brincks, E. and Norian, L. (2009) TRAIL Gene Therapy: From Preclinical Development to Clinical Application. *Current Gene Therapy*, 9(1), pp. 9-19.
- Gu, C., Le, V., Lang, M., Liu, J. (2014) Preparation of polysaccharide derivatives chitosan-graftpoly(varepsilon-caprolactone) amphiphilic copolymer micelles for 5-fluorouracil drug delivery. *Colloids Surf., B*, (116), 745-750.
- Gu, F.X., Karnik, R., Wang, A.Z., Alexis, F., Levy-Nissenbaum, E., Hong, S., Langer, R.S. and Farokhzad, O.C. (2007) Targeted nanoparticles for cancer therapy. *Nano today*, 2(3), pp.14-21.
- Gu, H., Liu, Zhang, Sun, Xie and Xia (2012) Delivering hydrophilic and hydrophobic chemotherapeutics simultaneously by magnetic mesoporous silica nanoparticles to inhibit cancer cells. *International Journal of Nanomedicine*, p. 999.
- Guhagarkar, S., Majee, S., Samad, A. and Devarajan, P. (2011) Evaluation of pullulan-functionalized doxorubicin nanoparticles for asialoglycoprotein receptor-mediated uptake in Hep G2 cell line. *Cancer Nanotechnology*, 2(1-6), pp. 49-55.
- Hanahan, D. and Weinberg, R. (2011) Hallmarks of Cancer: The Next Generation. *Cell*, 144(5), pp. 646-674.

Hauenschild, T. and Hinderberger, D. (2019) A Platform of Phenol-Based Nitroxide Radicals as an “EPR Toolbox” in Supramolecular and Click Chemistry. *ChemPlusChem*, 84(1), pp.43-51.

Harashima, H., Ochi, Y. and Kiwada, H. (1994) Kinetic modelling of liposome degradation in serum: Effect of size and concentration of liposomes in vitro. *Biopharmaceutics & Drug Disposition*, 15(3), pp. 217-225.

Harashima, H., Sakata, K., Funato, K. and Kiwada, H. (1994) Enhanced hepatic uptake of liposomes through complement activation depending on the size of liposomes. *Pharmaceutical research*, 11(3), pp.402-406.

Harris, P. (2018) Transmission electron microscopy of carbon: a brief history. *C*, 4(1), p.4.

Hassani, L.N., Hendra, F., Bouchemal, K. (2012) Auto-associative amphiphilic polysaccharides as drug delivery systems. *Drug Discovery Today* (17), 608-614.

Hawker, C. and Frechet, J. (1990) Preparation of polymers with controlled molecular architecture. A new convergent approach to dendritic macromolecules. *Journal of the American Chemical Society*, 112(21), pp. 7638-7647.

Hayashida, K., Bartlett, A., Chen, Y. and Park, P. (2010) Molecular and Cellular Mechanisms of Ectodomain Shedding. *The Anatomical Record: Advances in Integrative Anatomy and Evolutionary Biology*, 293(6), pp. spc1-spc1.

He, C., Chen, F., Li, B. and Hu, Z. (2014) Neurophysiology of HCN channels: from cellular functions to multiple regulations. *Progress in neurobiology* [online], 112, pp. 1-23.

He, Y., Cheng, G., Xie, L., Nie, Y., He, B. and Gu, Z. (2013) Polyethyleneimine/DNA polyplexes with reduction-sensitive hyaluronic acid derivatives shielding for targeted gene delivery. *Biomaterials*, 34(4), pp. 1235-1245.

Hein, C., Liu, X. and Wang, D. (2008) Click Chemistry, A Powerful Tool for Pharmaceutical Sciences. *Pharmaceutical Research*, 25(10), pp. 2216-2230.

Hemming, P.E.C. (2007) C, H, N Micro-analysis: a comparative review of the effects of instrument design on analytical performance.

Herzog, R.W., Cao, O. and Srivastava, A. (2010) Two decades of clinical gene therapy—success is finally mounting. *Discovery medicine*, 9(45), p.105.

Hidalgo-Alvarez, R., 2009. *Structure and functional properties of colloidal systems*. CRC Press.

Hillaireau, H. and Couvreur, P. (2009) Nanocarriers' entry into the cell: relevance to drug delivery. *Cellular and Molecular Life Sciences*, 66(17), pp. 2873-2896.

- Hiroi, T. and Shibayama, M. (2017) Measurement of Particle Size Distribution in Turbid Solutions by Dynamic Light Scattering Microscopy. *Journal of Visualized Experiments*, (119).
- Hortobagyi, G.N. (1997) Anthracyclines in the treatment of cancer. *Drugs*, 54(4), pp.1-7.
- Hua, S. and Wu, S. (2013) The use of lipid-based nanocarriers for targeted pain therapies. *Frontiers in Pharmacology*, 4.
- Huang, C.Y., Ju, D.T., Chang, C.F., Reddy, P.M. and Velmurugan, B.K. (2017) A review on the effects of current chemotherapy drugs and natural agents in treating non-small cell lung cancer. *Biomedicine*, 7(4).
- Hulla, J. E., Sahu, S. C., & Hayes, A. W. (2015). Nanotechnology: History and future. *Human & experimental toxicology*, 34(12), pp. 1318-1321.
- Huseynov, E., Garibov, A. and Mehdiyeva, R. (2016) TEM and SEM study of nano SiO₂ particles exposed to influence of neutron flux. *Journal of Materials Research and Technology*, 5(3), pp. 213-218.
- Hussain, M., Shahwar, D., Hassan, M., Tahir, M., Iqbal, M. and Sher, M. (2010) An efficient esterification of pullulan using carboxylic acid anhydrides activated with iodine. *Collection of Czechoslovak Chemical Communications*, 75(1), pp. 133-143.
- IARC.FR-Globocan.(2019) *Global Cancer Observatory*. *Gco.iarc.fr*, [online]. [Accessed 6 May 2017]. Available at: <<https://gco.iarc.fr/>>.
- IARC.FR-WHO.(2017) *Cancer mortality database (IARC)*. *Www-dep.iarc.fr*, [online]. [Accessed 6 May 2017]. Available at: <<http://www-dep.iarc.fr/WHODb/WHODb.htm>>.
- Iijima, S. (1991). Helical microtubules of graphitic carbon. *nature*, 354(6348), pp. 56.
- Ilium, L., Davis, S., Wilson, C., Thomas, N., Frier, M. and Hardy, J. (1982) Blood clearance and organ deposition of intravenously administered colloidal particles. The effects of particle size, nature and shape. *International Journal of Pharmaceutics*, 12(2-3), pp. 135-146.
- Immordino, M.L., Dosio, F. and Cattell, L. (2006) Stealth liposomes: review of the basic science, rationale, and clinical applications, existing and potential. *International journal of nanomedicine*, 1(3), pp.297
- Ishida, T., Shiraga, E. and Kiwada, H. (2009) Synergistic antitumor activity of metronomic dosing of cyclophosphamide in combination with doxorubicin-containing PEGylated liposomes in a murine solid tumor model. *Journal of Controlled Release*, 134(3), pp.194-200.
- Iyer, A., Khaled, G., Fang, J. and Maeda, H. (2006) Exploiting the enhanced permeability and retention effect for tumor targeting. *Drug Discovery Today*, 11(17-18), pp. 812-818.

Jackson, S. and Bartek, J. (2009) The DNA-damage response in human biology and disease. *Nature*, 461(7267), pp. 1071-1078.

Jacobetz, M., Chan, D., Neesse, A., Bapiro, T., Cook, N., Frese, K., Feig, C., Nakagawa, T., Caldwell, M., Zecchini, H., Lolkema, M., Jiang, P., Kultti, A., Thompson, C., Maneval, D., Jodrell, D., Frost, G., Shepard, H., Skepper, J. and Tuveson, D. (2012) Hyaluronan impairs vascular function and drug delivery in a mouse model of pancreatic cancer. *Gut*, 62(1), pp. 112-120.

Jacobs, F., Gordts, S., Muthuramu, I. and De Geest, B. (2012) The Liver as a Target Organ for Gene Therapy: State of the Art, Challenges, and Future Perspectives. *Pharmaceuticals*, 5(12), pp. 1372-1392.

Jain, R. (1987) Transport of molecules across tumor vasculature. *CANCER AND METASTASIS REVIEW*, 6(4), pp. 559-593.

Jain, R. (2005) Normalization of Tumor Vasculature: An Emerging Concept in Antiangiogenic Therapy. *Science*, 307(5706), pp. 58-62.

Jang, K., Seol, D., Ding, L., Heo, D., Lee, S., Martin, J. and Kwon, I. (2018) Ultrasound-triggered PLGA microparticle destruction and degradation for controlled delivery of local cytotoxicity and drug release. *International Journal of Biological Macromolecules*, 106, pp. 1211-1217.

Janiszewska, J., Posadas, I., Játiva, P., Bugaj-Zarebska, M., Urbanczyk-Lipkowska, Z. and Ceña, V. (2016) Second Generation Amphiphilic Poly-Lysine Dendrons Inhibit Glioblastoma Cell Proliferation without Toxicity for Neurons or Astrocytes. *PLOS ONE*, 11(11), p. e0165704.

Jenssen, H., Hamill, P. and Hancock, R.E. (2006) Peptide antimicrobial agents. *Clinical microbiology reviews*, 19(3), pp.491-511.

Jevprasesphant, R., Penny, J., Attwood, D. and D'Emanuele, A. (2004) Transport of dendrimer nanocarriers through epithelial cells via the transcellular route. *Journal of Controlled Release*, 97(2), pp. 259-267.

Jhaveri, A., Deshpande, P. and Torchilin, V. (2014) Stimuli-sensitive nanopreparations for combination cancer therapy. *Journal of controlled release*, 190, pp.352-370.

Jo, H.Y., Kim, Y., Park, H.W., Moon, H.E., Bae, S., Kim, J., Kim, D.G. and Paek, S.H., 2015. The unreliability of MTT assay in the cytotoxic test of primary cultured glioblastoma cells. *Experimental neurobiology*, 24(3), pp.235-245.

Jones, S. and Merkel, O. (2016) Tackling breast cancer chemoresistance with nano-formulated siRNA. *Gene Therapy*, 23(12), pp.821-828.

Joshi, P., Vishwakarma, R. and Bharate, S. (2017) Natural alkaloids as P-gp inhibitors for multidrug resistance reversal in cancer. *European Journal of Medicinal Chemistry*, 138, pp. 273-292.

Julka, P., Chacko, R., Nag, S., Parshad, R., Nair, A., Oh, D., Hu, Z., Koppiker, C., Nair, S., Dawar, R., Dhindsa, N., Miller, I., Ma, D., Lin, B., Awasthy, B. and Perou, C. (2008) A phase II study of sequential neoadjuvant gemcitabine plus

doxorubicin followed by gemcitabine plus cisplatin in patients with operable breast cancer: prediction of response using molecular profiling. *British Journal of Cancer*, 98(8), pp. 1327-1335.

Jung, K. and Reszka, R. (2001) Mitochondria as subcellular targets for clinically useful anthracyclines. *Advanced Drug Delivery Reviews*, 49(1-2), pp. 87-105.

Kadish, K., Smith, K. and Guilard, R. (2010) *Handbook of porphyrin science*. Singapore: World Scientific.

Kalepu, S. and Nekkanti, V. (2015) Insoluble drug delivery strategies: review of recent advances and business prospects. *Acta Pharmaceutica Sinica B*, 5(5), pp. 442-453.

Kalka, K., Merk, H., & Mukhtar, H. (2000). Photodynamic therapy in dermatology. *Journal of the American Academy of Dermatology*, 42(3), pp. 389-413.

Kaneo, Y., Tanaka, T., Nakano, T. and Yamaguchi, Y. (2001) 'Evidence for receptor-mediated hepatic uptake of pullulan in rats', *Journal of Controlled Release*, 70(3), pp. 365–373. doi: 10.1016/s0168-3659(00)00368-0.

Kang, N. and Leroux, J. (2004) Triblock and star-block copolymers of N-(2-hydroxypropyl) methacrylamide or N-vinyl-2-pyrrolidone and d,l-lactide: synthesis and self-assembling properties in water. *Polymer*, 45(26), pp. 8967-8980.

Kanwal, U., Irfan Bukhari, N., Ovais, M., Abass, N., Hussain, K. and Raza, A.(2018) Advances in nano-delivery systems for doxorubicin: an updated insight. *Journal of drug targeting*, 26(4), pp.296-310.

Kapur, B. (2014) The fruits of long endeavors – 200 years of oncology. *Medical Journal Armed Forces India*, 70(2), pp. 95-97.

Kardos, N. and Luche, J. (2001) Sonochemistry of carbohydrate compounds. *Carbohydrate Research*, 332(2), pp. 115-131.

Kauffman, M., Kauffman, M., Zhu, H., Jia, Z. and Li, Y. (2016) Fluorescence-Based Assays for Measuring Doxorubicin in Biological Systems. *Reactive Oxygen Species*.

Kawasaki, R., Sasaki, Y., Katagiri, K., Mukai, S.-a., Sawada, S.-i., Akiyoshi, K. (2016) Magnetically guided protein transduction by hybrid nanogel chaperones with iron oxide nanoparticles. *Angew. Chem. Int. Ed.* (55), 11377-11381.

Ketron, A., Gordon, O., Schneider, C. and Osheroff, N. (2012) Oxidative Metabolites of Curcumin Poison Human Type II Topoisomerases. *Biochemistry*, 52(1), pp. 221-227.

Khalil, N., Nascimento, T., Casa, D., Dalmolin, L., Mattos, A., Hoss, I., Romano, M. and Mainardes, R. (2013) Pharmacokinetics of curcumin-loaded PLGA and PLGA–PEG blend nanoparticles after oral administration in rats. *Colloids and Surfaces B: Biointerfaces*, 101, pp. 353-360.

- Khodabandehloo, H., Zahednasab, H. and Ashrafi Hafez, A. (2016) Nanocarriers Usage for Drug Delivery in Cancer Therapy. *Iranian Journal of Cancer Prevention*, 9(2), e3966
- Kiessling, L. L., Gestwicki, J. E., & Strong, L. E. (2000). Synthetic multivalent ligands in the exploration of cell-surface interactions. *Current opinion in chemical biology*, 4(6), 696-703.
- Kim, J., Choi, J., Nam, K., Lee, M., Park, J. and Lee, J. (2006) Enhanced transfection of primary cortical cultures using arginine-grafted PAMAM dendrimer, PAMAM-Arg. *Journal of Controlled Release*, 114(1), pp. 110-117.
- Kipnis, J. (2016) multifaceted interactions between adaptive immunity and the central nervous system. *Science*, 353(6301), pp. 766-771.
- Kitazawa, H., Sato, H., Adachi, I., Masuko, Y. and Horikoshi, I. (1997) Microdialysis Assessment of Fibrin Glue Containing Sodium Alginate for Local Delivery of Doxorubicin in Tumor-Bearing Rats. *Biological & Pharmaceutical Bulletin*, 20(3), pp. 278-281.
- Kiyomiya, K.I., Matsuo, S. and Kurebe, M. (2001) Differences in intracellular sites of action of Adriamycin in neoplastic and normal differentiated cells. *Cancer chemotherapy and pharmacology*, 47(1), pp.51-56.
- Kloesch, B., Dietersdorfer, E., Loeblich, S. and Steiner, G.(2014)Anti-Inflammatory and Pro-apoptotic Effects of Curcumin and Resveratrol on the Human Lung Fibroblast Cell Line MRC-5. *Alternative & Integrative Medicine*, pp.1-11.
- Knook, D. and Sleyster, E. (1980) Isolated parenchymal, Kupffer and endothelial rat liver cells characterized by their lysosomal enzyme content. *Biochemical and Biophysical Research Communications*, 96(1), pp. 250-257.
- Kolb, H. and Sharpless, K. (2003) The growing impact of click chemistry on drug discovery. *Drug Discovery Today*, 8(24), pp. 1128-1137.
- Kobayashi, H., Turkbey, B., Watanabe, R. and Choyke, P. (2014) Cancer Drug Delivery: Considerations in the Rational Design of Nanosized Bioconjugates. *Bioconjugate Chemistry*, 25(12), pp. 2093-2100.
- König W, Geiger R. (1970) A new method for synthesis of peptides: activation of the carboxyl group with dicyclohexylcarbodiimide using 1-hydroxybenzotriazoles as additives. *Chem Ber*, 103(3), pp. 788-98.
- Kosmidou, C., Efstathiou, N., Hoang, M., Notomi, S., Konstantinou, E., Hirano, M., Takahashi, K., Maidana, D., Tsoka, P., Young, L., Gragoudas, E., Olsen, T., Morizane, Y., Miller, J. and Vavvas, D. (2018) Issues with the Specificity of Immunological Reagents for NLRP3: Implications for Age-related Macular Degeneration. *Scientific Reports*, 8(1).
- Krishan, A. and Hamelik, R.M. (2005) Flow cytometric monitoring of fluorescent drug retention and efflux. In *Chemosensitivity: Volume II* (pp. 149-166). Humana Press, Totowa, NJ.

Kulthe, S., Choudhari, Y., Inamdar, N. and Mourya, V. (2012) Polymeric micelles: authoritative aspects for drug delivery. *Designed Monomers and Polymers*, 15(5), pp. 465-521.

Kumar, A., Gautam, B., Dubey, C. and Tripathi, P.K. (2014) A review: role of doxorubicin in treatment of cancer. *International Journal of Pharmaceutical Sciences and Research*, 5(10), p.4105.

Kumar, D., Saini, N., Pandit, V. and Ali, S. (2012) An Insight to Pullulan: A Biopolymer in Pharmaceutical Approaches. *International Journal of Basic and Applied Sciences*, 1(3).

Kumareswaran, R., Gupta, A. and Vankar, Y. (1997) Chlorotrimethylsilane Catalysed Acylation of Alcohols¹. *Synthetic Communications*, 27(2), pp. 277-282.

Kumari, M., Ray, L., Purohit, M., Patnaik, S., Pant, A., Shukla, Y., Kumar, P. and Gupta, K. (2017) Curcumin loading potentiates the chemotherapeutic efficacy of selenium nanoparticles in HCT116 cells and Ehrlich's ascites carcinoma bearing mice. *European Journal of Pharmaceutics and Biopharmaceutics*, 117, pp. 346-362.

Kurz, T., Eaton, J. and Brunk, U. (2010) Redox Activity Within the Lysosomal Compartment: Implications for Aging and Apoptosis. *Antioxidants & Redox Signaling*, 13(4), pp. 511-523.

Kratz, F., Warnecke, A., Scheuermann, K., Stockmar, C., Schwab, J., Lazar, P., Drückes, P., Esser, N., Drevs, J., Rognan, D. and Bissantz, C. (2002) Probing the cysteine-34 position of endogenous serum albumin with thiol-binding doxorubicin derivatives. Improved efficacy of an acid-sensitive doxorubicin derivative with specific albumin-binding properties compared to that of the parent compound. *Journal of medicinal chemistry*, 45(25), pp.5523-5533.

Langel, Ü. (2019) Protein Delivery and Mimicry. In *CPP, Cell-Penetrating Peptides* (pp. 157-193). Springer, Singapore.

Larenas-Linnemann, D., Antolín-Amérigo, D., Parisi, C., Nakonechna, A., Luna-Pech, J., Wedi, B., Davila, I., Gómez, M., Levin, M., Ortega Martell, J., Klimek, L., Rosario, N., Muraro, A., Agache, I., Bousquet, J., Sheikh, A. and Pfaar, O. (2017) National clinical practice guidelines for allergen immunotherapy: An international assessment applying AGREE-II. *Allergy*, 73(3), pp. 664-672.

Larkin P. (2011) *Infrared and Raman spectroscopy; principles and spectral interpretation*: Elsevier

Lei, Y., Han, H., Yuan, F., Javeed, A. and Zhao, Y. (2017) The brain interstitial system: Anatomy, modeling, in vivo measurement, and applications. *Progress in neurobiology* [online], 157, pp. 230-246.

Lejbkowicz, F. and Salzberg, S. (1997) Distinct Sensitivity of Normal and Malignant Cells to Ultrasound in Vitro. *Environmental Health Perspectives*, 105, pp. 1575.

- Li, H., Cui, Y., Liu, J., Bian, S., Liang, J., Fan, Y. and Zhang, X. (2014) Reduction breakable cholesteryl pullulan nanoparticles for targeted hepatocellular carcinoma chemotherapy. *J. Mater. Chem. B*, 2(22), pp. 3500-3510.
- Li, H., Xu, X., Li, Y., Geng, Y., He, B. and Gu, Z. (2013) Design and self-assembly of amphiphilic peptide dendron-jacketed polysaccharide polymers into available nanomaterials. *Polymer Chemistry*, 4(7), pp.2235-2238.
- Li, J., Huo, M., Wang, J., Zhou, J., Mohammad, J.M., Zhang, Y., Zhu, Q., Waddad, A.Y., Zhang, Q. (2012) Redox-sensitive micelles self-assembled from amphiphilic hyaluronic aciddeoxycholic acid conjugates for targeted intracellular delivery of paclitaxel. *Biomaterials*, (33), 2310-2320.
- Li, M., Zhang, W., Wang, B., Gao, Y., Song, Z. and Zheng, Q.C. (2016) Ligand-based targeted therapy: a novel strategy for hepatocellular carcinoma. *International journal of nanomedicine*, 11, p.5645.
- Li, N., Li, N., Yi, Q., Luo, K., Guo, C., Pan, D. and Gu, Z. (2014) Amphiphilic peptide dendritic copolymer-doxorubicin nanoscale conjugate self-assembled to enzyme-responsive anti-cancer agent. *Biomaterials*, 35(35), pp. 9529-9545.
- Li, S. and Huang, L. (2008) Pharmacokinetics and Biodistribution of Nanoparticles. *Molecular Pharmaceutics*, 5(4), pp. 496-504.
- Liebeskind, D., Bases, R., Elequin, F., Neubort, S., Leifer, R., Goldberg, R. and Koenigsberg, M. (1979) Diagnostic Ultrasound: Effects on the DNA and Growth Patterns of Animal Cells. *Radiology*, 131(1), pp. 177-184.
- Liebeskind, D., Bases, R., Mendez, F., Elequin, F. and Koenigsberg, M. (1979) Sister chromatid exchanges in human lymphocytes after exposure to diagnostic ultrasound. *Science*, 205(4412), pp. 1273-1275.
- Liu, J., Li, M., Luo, Z., Dai, L., Guo, X. and Cai, K. (2017) Design of nanocarriers based on complex biological barriers in vivo for tumor therapy. *Nano Today*, 15, pp. 56-90.
- López-Lázaro, M., Willmore, E., Jobson, A., Gilroy, K.L., Curtis, H., Padget, K. and Austin, C.A. (2007) Curcumin induces high levels of topoisomerase I- and II- DNA complexes in K562 leukemia cells. *Journal of natural products*, 70(12), pp.1884-1888.
- Lu, D., Wen, X., Liang, J., Gu, Z., Zhang, X. and Fan, Y. (2009) A pH -sensitive nano drug delivery system derived from pullulan/doxorubicin conjugate. *Journal of Biomedical Materials Research Part B: Applied Biomaterials*, 89B (1), pp. 177-183.
- Luo, K., Li, C., Li, L., She, W., Wang, G., Gu, Z. (2012) Arginine functionalized peptide dendrimers as potential gene delivery vehicles. *Biomaterials* 33, 4917–4927.
- Luo, K., Li, C., Wang, G., Nie, Y., He, B., Wu, Y. and Gu, Z. (2011) Peptide dendrimers as efficient and biocompatible gene delivery vectors: synthesis and in vitro characterization. *Journal of controlled release*, 155(1), pp.77-87.

Lyon, J., Mokarram, N., Saxena, T., Carroll, S. and Bellamkonda, R. (2017) Engineering challenges for brain tumor immunotherapy. *Advanced Drug Delivery Reviews*, 114, pp.19-32.

Ma, D., Zhang, H., Chen, Y., Lin, J. and Zhang, L. (2013) New cyclodextrin derivative containing poly(L-lysine) dendrons for gene and drug co-delivery. *Journal of Colloid and Interface Science*, 405, pp. 305-311.

Ma, S., Zhou, J., Wali, A., He, Y., Xu, X., Tang, J. and Gu, Z. (2015) Self-assembly of pH-sensitive fluorinated peptide dendron functionalized dextran nanoparticles for on-demand intracellular drug delivery. *Journal of Materials Science: Materials in Medicine*, 26(8).

Ma, Y., Wang, J., Tao, W., Sun, C., Wang, Y., Li, D., Fan, F., Qian, H. and Yang, X. (2015) Redox-Responsive Polyphosphoester-Based Micellar Nanomedicines for Overriding Chemoresistance in Breast Cancer Cells. *ACS Applied Materials & Interfaces*, 7(47), pp. 26315-26325.

Maas, H., Lemmens, V., Nijhuis, P., de Hingh, I., Koning, C. and Janssen-Heijnen, M. (2013) Benefits and drawbacks of short-course preoperative radiotherapy in rectal cancer patients aged 75 years and older. *European Journal of Surgical Oncology (EJSO)*, 39(10), pp. 1087-1093.

Macintosh, I. and Davey, D. (1970) Chromosome Aberrations Induced by an Ultrasonic Fetal Pulse Detector. *BMJ*, 4(5727), pp. 92-93.

Maeda, H. and Konno, T. (1997) Metamorphosis of neocarzinostatin to SMANCS: Chemistry, biology, pharmacology, and clinical effect of the first prototype anticancer polymer therapeutic. In *Neocarzinostatin* (pp. 227-267). Springer, Tokyo.

Mahajan, S.D., Law, W.C., Aalinkeel, R., Reynolds, J., Nair, B.B., Yong, K.T., Roy, I., Prasad, P.N. and Schwartz, S.A. (2012) Nanoparticle-mediated targeted delivery of antiretrovirals to the brain. In *Methods in enzymology* (Vol. 509, pp. 41-60). Academic Press.

Mai, K., Zhang, S., Liang, B., Gao, C., Du, W. and Zhang, L.M. (2015) Water soluble cationic dextran derivatives containing poly (amidoamine) dendrons for efficient gene delivery. *Carbohydrate polymers*, 123, pp.237-245.

Malam, Y., Loizidou, M. and Seifalian, A. (2009) Liposomes and nanoparticles: nanosized vehicles for drug delivery in cancer. *Trends in Pharmacological Sciences*, 30(11), pp. 592-599.

Malik, N., Evagorou, E. and Duncan, R. (1999) Dendrimer-platinate. *Anti-Cancer Drugs*, 10(8), pp. 767-776.

Malik, N., Wiwattanapatapee, R., Klopsch, R., Lorenz, K., Frey, H., Weener, J.W., Meijer, E.W., Paulus, W. and Duncan, R. (2000) Dendrimers: Relationship between structure and biocompatibility in vitro, and preliminary studies on the biodistribution of ¹²⁵I-labelled polyamidoamine dendrimers in vivo. *Journal of Controlled Release*, 65(1-2), pp.133-148.

- Maluccio, M. and Covey, A. (2012) 'Recent progress in understanding, diagnosing, and treating hepatocellular carcinoma', *CA: A Cancer Journal for Clinicians*, 62(6), pp. 394–399. doi: 10.3322/caac.21161.
- Maluf, F. and Spriggs, D. (2002) Anthracyclines in the Treatment of Gynecologic Malignancies. *Gynecologic Oncology*, 85(1), pp. 18-31.
- Mansoori, B., Mohammadi, A., Davudian, S., Shirjang, S. and Baradaran, B. (2017) The Different Mechanisms of Cancer Drug Resistance: A Brief Review. *Advanced Pharmaceutical Bulletin*, 7(3), pp. 339-348.
- Manson, M. (2005) Inhibition of survival signalling by dietary polyphenols and indole-3-carbinol. *European Journal of Cancer*, 41(13), pp. 1842-1853.
- Margarida Cardoso, M., Peça, I., Raposo, C., Petrova, K., Teresa Barros, M., Gardner, R. and Bicho, A. (2016) Doxorubicin-loaded galactose-conjugated poly(d,l-lactide-co-glycolide) nanoparticles as hepatocyte-targeting drug carrier. *Journal of Microencapsulation*, 33(4), pp. 315-322.
- Marshall, E. (1999) CLINICAL TRIALS:Gene Therapy Death Prompts Review of Adenovirus Vector. *Science*, 286(5448), pp. 2244-2245.
- Meng, H., Liong, M., Xia, T., Li, Z., Ji, Z., Zink, J.I. and Nel, A.E. (2010) Engineered design of mesoporous silica nanoparticles to deliver doxorubicin and P-glycoprotein siRNA to overcome drug resistance in a cancer cell line. *ACS nano*, 4(8), pp.4539-4550.
- Mescher AL. Junqueira's Basic Pathology: Text & Atlas. 12 ed: McGraw-Hill Education 2010.pp. 289.
- Miller, D., Smith, N., Bailey, M., Czarnota, G., Hynynen, K. and Makin, I. (2012) Overview of Therapeutic Ultrasound Applications and Safety Considerations. *Journal of Ultrasound in Medicine*, 31(4), pp. 623-634.
- Minotti, G., Menna, P., Salvatorelli, E., Cairo, G. and Gianni, L. (2004) Anthracyclines: molecular advances and pharmacologic developments in antitumor activity and cardiotoxicity. *Pharmacological reviews*, 56(2), pp.185-229.
- Mishra, N., Yadav, N., Rai, V., Sinha, P., Yadav, K., Jain, S. and Arora, S. (2013) Efficient Hepatic Delivery of Drugs: Novel Strategies and Their Significance. *BioMed Research International*, 2013, pp. 1-20.
- Misono, T., 2019. Dynamic Light Scattering (DLS). In *Measurement Techniques and Practices of Colloid and Interface Phenomena* (pp. 65-69). Springer, Singapore.
- Mita, M.M., Natale, R.B., Wolin, E.M., Dinh, H., Wieland, S., Levitt, D.J. and Mita, A.C., 2014. Pharmacokinetic study of doxorubicin in solid tumor patients.
- Miyata, K., Nishiyama, N., & Kataoka, K. (2012). *Rational design of smart supramolecular assemblies for gene delivery: chemical challenges in the creation of artificial viruses*. *Chem. Soc. Rev.*, 41(7), 2562–2574.

Mohanty, C. and Sahoo, S. (2010) The in vitro stability and in vivo pharmacokinetics of curcumin prepared as an aqueous nanoparticulate formulation. *Biomaterials*, 31(25), pp. 6597-6611.

Mohar, I., Brempele, K.J., Murray, S.A., Ebrahimkhani, M.R. and Crispe, I.N. (2015) Isolation of non-parenchymal cells from the mouse liver. In *Malaria Vaccines* (pp. 3-17). Humana Press, New York, NY.

Mokhtari, R., Homayouni, T., Baluch, N., Morgatskaya, E., Kumar, S., Das, B. and Yeger, H. (2017) Combination therapy in combating cancer. *Oncotarget*, 8(23).

Montalbetti, C. and Falque, V. (2005) Amide bond formation and peptide coupling. *Tetrahedron*, 61(46), pp. 10827-10852.

Mura, S., Nicolas, J. and Couvreur, P. (2013) Stimuli-responsive nanocarriers for drug delivery. *Nature Materials*, 12(11), pp. 991-1003.

Murphy, T. and Yee, K.W. (2017) Cytarabine and daunorubicin for the treatment of acute myeloid leukemia. *Expert opinion on pharmacotherapy*, 18(16), pp.1765-1780.

Muscariello, L., Rosso, F., Marino, G., Giordano, A., Barbarisi, M., Cafiero, G. and Barbarisi, A. (2005) A critical overview of ESEM applications in the biological field. *Journal of Cellular Physiology*, 205(3), pp. 328-334.

Myers, R., Lau, B., Kunihiro, D., Torrey, R., Woolley, J. and Tosk, J. (1989) Modulation of hematoporphyrin derivative-sensitized phototherapy with corynebacterium parvum in murine transitional cell carcinoma. *Urology*, 33(3), pp. 230-235.

Na, M., Yiyun, C., Tongwen, X., Yang, D., Xiaomin, W., Zhenwei, L., Zhichao, C., Guanyi, H., Yunyu, S. and Longping, W. (2006) Dendrimers as potential drug carriers. Part II. Prolonged delivery of ketoprofen by in vitro and in vivo studies. *European Journal of Medicinal Chemistry*, 41(5), pp. 670-674.

Nakamura, Y., Mochida, A., Choyke, P. and Kobayashi, H. (2016) Nanodrug Delivery: Is the Enhanced Permeability and Retention Effect Sufficient for Curing Cancer. *Bioconjugate Chemistry*, 27(10), pp. 2225-2238.

Nakase, I., Takeuchi, T., Tanaka, G. and Futaki, S. (2008) Methodological and cellular aspects that govern the internalization mechanisms of arginine-rich cell-penetrating peptides. *Advanced Drug Delivery Reviews*, 60(4-5), pp. 598-607.

Nanjwade, B., Bechra, H., Derkar, G., Manvi, F. and Nanjwade, V. (2009) Dendrimers: Emerging polymers for drug-delivery systems. *European Journal of Pharmaceutical Sciences*, 38(3), pp. 185-196.

Naran, K., Nundalall, T., Chetty, S. and Barth, S. (2018) Principles of Immunotherapy: Implications for Treatment Strategies in Cancer and Infectious Diseases. *Frontiers in Microbiology*, 9.

Narvekar, M., Xue, H., Eoh, J. and Wong, H. (2014) Nanocarrier for Poorly Water-Soluble Anticancer Drugs—Barriers of Translation and Solutions. *AAPS PharmSciTech*, 15(4), pp. 822-833.

National Nanotechnology Initiative (NNI). (2018) *What is Nanotechnology? | Nano*. *Nano.gov*, [online]. [Accessed 5 July 2018]. Available at: <<https://www.nano.gov/nanotech-101/what/definition>>.

Nayak, S. and Herzog, R. (2009) Progress and prospects: immune responses to viral vectors. *Gene Therapy*, 17(3), pp. 295-304.

Nguyen, H., Ha, P., Nguyen, A., Nguyen, D., Do, H., Thi, Q. and Thi, M. (2016) Curcumin as fluorescent probe for directly monitoring in vitro uptake of curcumin combined paclitaxel loaded PLA-TPGS nanoparticles. *Advances in Natural Sciences: Nanoscience and Nanotechnology*, 7(2), p. 025001.

Nichifor, M., Mocanu, G., Stanciu, M.C. (2014) Micelle-like association of polysaccharides with hydrophobic end groups. *Carbohydr. Polym.*, (110), 209-218.

Nishiyama, N. and Kataoka, K. (2006) Current state, achievements, and future prospects of polymeric micelles as nanocarriers for drug and gene delivery. *Pharmacology & Therapeutics*, 112(3), pp. 630-648.

Nishiyama, N., Arnida, Jang, W., Date, K., Miyata, K. and Kataoka, K. (2006) Photochemical enhancement of transgene expression by polymeric micelles incorporating plasmid DNA and dendrimer-based photosensitizer. *Journal of Drug Targeting*, 14(6), pp. 413-424.

Noriega-Luna, B., Godínez, L.A., Rodríguez, F.J., Rodríguez, A., Larrea, G., Sosa-Ferreira, C.F., Mercado-Curiel, R.F., Manríquez, J. and Bustos, E. (2014) Applications of dendrimers in drug delivery agents, diagnosis, therapy, and detection. *Journal of Nanomaterials*, 2014, p.39.

Oerlemans, C., Bult, W., Bos, M., Storm, G., Nijsen, J.F.W. and Hennink, W.E. (2010) Polymeric micelles in anticancer therapy: targeting, imaging and triggered release. *Pharmaceutical research*, 27(12), pp.2569-2589.

Ogawara, K., Yoshida, M., Higaki, K., Toshikuro Kimura, Shiraishi, K., Nishikawa, M., Takakura, Y. and Hashida, M. (1999) Hepatic uptake of polystyrene microspheres in rats: Effect of particle size on intrahepatic distribution. *Journal of Controlled Release*, 59(1), pp. 15-22.

Orellana, E. and Kasinski, A. (2016) Sulforhodamine B (SRB) Assay in Cell Culture to Investigate Cell Proliferation. *BIO-PROTOCOL*, 6(21).

Ostroff, G.R. and Ernesto, S.O.T.O., University of Massachusetts (UMass), 2016. *Yeast cell wall particles for receptor-targeted nanoparticle delivery*. U.S. Patent 9,242,857.

OWENSIII, D. and PEPPAS, N. (2006) Opsonization, biodistribution, and pharmacokinetics of polymeric nanoparticles. *International Journal of Pharmaceutics*, 307(1), pp. 93-102.

Padilla De Jesús, O., Ihre, H., Gagne, L., Fréchet, J. and Szoka, F. (2002) Polyester Dendritic Systems for Drug Delivery Applications: In Vitro and In Vivo Evaluation. *Bioconjugate Chemistry*, 13(3), pp. 453-461.

Panchbhai, A. (2015) Wilhelm Conrad Röntgen and the discovery of X-rays: Revisited after centennial. *Journal of Indian Academy of Oral Medicine and Radiology*, 27(1), p. 90.

Pang, J.D., Zhuang, B.X., Mai, K., Chen, R.F., Wang, J. and Zhang, L.M. (2015) Click modification of helical amylose by poly (l-lysine) dendrons for non-viral gene delivery. *Materials Science and Engineering: C*, 49, pp.485-492.

Pakunlu, R.I., Wang, Y., Tsao, W., Pozharov, V., Cook, T.J. and Minko, T., 2004. Enhancement of the efficacy of chemotherapy for lung cancer by simultaneous suppression of multidrug resistance and antiapoptotic cellular defense: novel multicomponent delivery system. *Cancer research*, 64(17), pp.6214-6224.

Parkin, D. (2006) The global health burden of infection-associated cancers in the year 2002. *International Journal of Cancer*, 118(12), pp.3030-3044.

Parkin, D., Bray, F., Ferlay, J. and Pisani, P. (2005) Global Cancer Statistics, 2002. *CA: A Cancer Journal for Clinicians*, 55(2), pp. 74-108.

Peer, D., Karp, J., Hong, S., Farokhzad, O., Margalit, R. and Langer, R. (2007) Nanocarriers as an emerging platform for cancer therapy. *Nature Nanotechnology*, 2(12), pp. 751-760.

Pelissari, F. M., Neri-Numa, I. A., Molina, G., Ferreira, D. C., & Pastore, G. (2018). Potential of nanoparticles as drug delivery system for cancer treatment. In *Applications of Nanocomposite Materials in Drug Delivery* (pp. 431-468). Woodhead Publishing.

Pérez-Arnaiz, C., Busto, N., Leal, J.M. and García, B. (2014) New insights into the mechanism of the DNA/doxorubicin interaction. *The Journal of Physical Chemistry B*, 118(5), pp.1288-1295.

Pillai, G. (2014) Nanomedicines for Cancer Therapy: An Update of FDA Approved and Those under Various Stages of Development. *SOJ Pharmacy & Pharmaceutical Sciences*, 1(2).

Pino, P., Pelaz, B., Zhang, Q., Maffre, P., Nienhaus, G. and Parak, W. (2014) Protein corona formation around nanoparticles – from the past to the future. *Mater. Horiz.*, 1(3), pp. 301-313.

Poon, S., McPherson, J., Tan, P., Teh, B. and Rozen, S. (2014) Mutation signatures of carcinogen exposure: genome-wide detection and new opportunities for cancer prevention. *Genome Medicine*, 6(3), pp. 24.

Prajapati, V., Jani, G. and Khanda, S. (2013) Pullulan: An exopolysaccharide and its various applications. *Carbohydrate Polymers*, 95(1), pp. 540-549.

Pramod, P.S., Takamura, K., Chaphekar, S., Balasubramanian, N., Jayakannan, M. (2012) Dextran vesicular carriers for dual encapsulation of

hydrophilic and hydrophobic molecules and delivery into cells. *Biomacromolecules*, (13), 3627-3640.

Prasad, P. N. (2003) Bioimaging: principles and techniques. *Introduction to Biophotonics*, pp. 203-254.

Priyadarsini, K. (2014) The Chemistry of Curcumin: From Extraction to Therapeutic Agent. *Molecules*, 19(12), pp. 20091-20112.

Qi, S.S., Sun, J.H., Yu, H.H. and Yu, S.Q. (2017) Co-delivery nanoparticles of anti-cancer drugs for improving chemotherapy efficacy. *Drug delivery*, 24(1), pp.1909-1926.

Qin, J., Asempah, I., Laurent, S., Fornara, A., Muller, R. and Muhammed, M. (2009) Injectable Superparamagnetic Ferrogels for Controlled Release of Hydrophobic Drugs. *Advanced Materials*, 21(13), pp. 1354-1357.

Qin, S. Y., Zhang, A. Q., Cheng, S. X., Rong, L., & Zhang, X. Z. (2017) Drug self-delivery systems for cancer therapy. *Biomaterials*, 112, pp. 234-247.

Qiu, L. and Bae, Y. (2007) Self-assembled polyethylenimine-graft-poly(ϵ -caprolactone) micelles as potential dual carriers of genes and anticancer drugs. *Biomaterials*, 28(28), pp. 4132-4142.

Quader, S., Cabral, H., Mochida, Y., Ishii, T., Liu, X., Toh, K., Kinoh, H., Miura, Y., Nishiyama, N. and Kataoka, K. (2014) 'Selective intracellular delivery of proteasome inhibitors through pH-sensitive polymeric micelles directed to efficient antitumor therapy', *Journal of Controlled Release*, 188, pp. 67–77. doi: 10.1016/j.jconrel.2014.05.048.

Rahman, A.M., Yusuf, S.W. and Ewer, M.S. (2007) Anthracycline-induced cardiotoxicity and the cardiac-sparing effect of liposomal formulation. *International journal of nanomedicine*, 2(4), p.567.

Ran, C., Zhang, Z., Hooker, J. and Moore, A. (2011) In Vivo Photoactivation Without "Light": Use of Cherenkov Radiation to Overcome the Penetration Limit of Light. *Molecular Imaging and Biology*, 14(2), pp. 156-162.

Rana, S., Bhattacharjee, J., Barick, K.C., Verma, G., Hassan, P.A. and Yakhmi, J.V. (2017) Interfacial engineering of nanoparticles for cancer therapeutics. In *Nanostructures for Cancer Therapy* (pp. 177-209).

Rangasamy, L., Chelvam, V., Kanduluru, A., Srinivasarao, M., Bandara, N., You, F., Orellana, E., Kasinski, A. and Low, P. (2018) New Mechanism for Release of Endosomal Contents: Osmotic Lysis via Nigericin-Mediated K⁺/H⁺ Exchange. *Bioconjugate Chemistry*, 29(4), pp. 1047-1059.

Ratain MJ, Plunkett WK Jr. (2003) General Mechanisms of Drug Action. *Holland-Frei Cancer Medicine*. 6th edition.

Ree, B., Satoh, Y., Sik Jin, K., Isono, T., Jong Kim, W., Kakuchi, T., Satoh, T. and Ree, M. (2017) Well-defined and stable nanomicelles self-assembled from brush cyclic and tadpole copolymer amphiphiles: a versatile smart carrier platform. *NPG Asia Materials*, 9(12), p. e453.

Rekha, M.R. and Sharma, C.P. (2007) Pullulan as a promising biomaterial for biomedical applications: a perspective. *Trends in Biomaterials and Artificial Organs*, 20(2), pp.116-121.

Rescigno, M., Avogadri, F. and Curigliano, G. (2007) Challenges and prospects of immunotherapy as cancer treatment. *Biochimica et Biophysica Acta (BBA) - Reviews on Cancer*, 1776(1), pp. 108-123.

Reza, M., Kontturi, E., Jääskeläinen, A.S., Vuorinen, T. and Ruokolainen, J. (2015) Transmission electron microscopy for wood and fiber analysis– A review. *BioResources*, 10(3), pp.6230-6261.

Richard P. (1960) Feynman There's plenty of room at the bottom. *Eng.Sci*, 22, pp.22-36

Rivankar, S. (2014) An overview of doxorubicin formulations in cancer therapy. *Journal of cancer research and therapeutics*, 10(4), p.853.

Rivera-Espinoza, Y. and Muriel, P. (2009) Pharmacological actions of curcumin in liver diseases or damage. *Liver International*, 29(10), pp. 1457-1466.

Rosen, M., Cohen, A., Dahanayake, M. and Hua, X. (1982) Relationship of structure to properties in surfactants. 10. Surface and thermodynamic properties of 2-dodecyloxypoly(ethenoxyethanol)s, $C_{12}H_{25}(OC_2H_4)_x OH$, in aqueous solution. *The Journal of Physical Chemistry*, 86(4), pp. 541-545.

Rosenthal, I. (1991) phthalocyanines as photodynamic sensitizers. *Photochemistry and Photobiology*, 53(6), pp. 859-870.

Rosenthal, I. (2004) Sonodynamic therapy: a review of the synergistic effects of drugs and ultrasound. *Ultrasonics Sonochemistry*.

Rothbard, J.B., Garlington, S., Lin, Q., Kirschberg, T., Kreider, E., McGrane, P.L., Wender, P.A. and Khavari, P.A. (2000) Conjugation of arginine oligomers to cyclosporin A facilitates topical delivery and inhibition of inflammation. *Nature medicine*, 6(11), p.1253.

RSC.org. (2019) *CHNS elemental analysers*. [online]. [accessed 28 May 2019]. Available at: https://www.rsc.org/images/chns-elemental-analysers-technical-brief-29_tcm18-214833.pdf.

Ryken, T., Kalkanis, S., Buatti, J. and Olson, J. (2014) The role of cytoreductive surgery in the management of progressive glioblastoma. *Journal of Neuro-Oncology*, 118(3), pp. 479-488.

Saber-Samandari, S., Gulcan, H., Saber-Samandari, S. and Gazi, M. (2014) Efficient Removal of Anionic and Cationic Dyes from an Aqueous Solution Using Pullulan-graft-Polyacrylamide Porous Hydrogel. *Water, Air, & Soil Pollution*, 225(11).

Saltzstein, H., Levin, P. and Sharp, J. (1957) The possibilities and limitations of surgery in cancer. *The American Journal of Surgery*, 93(3), pp. 338-355.

Samad, A., Sultana, Y. and Aqil, M. (2007) Liposomal Drug Delivery Systems: An Update Review. *Current Drug Delivery*, 4(4), pp. 297-305.

Sanoj Rejinold, N., Muthunarayanan, M., Divyarani, V., Sreerekha, P., Chennazhi, K., Nair, S., Tamura, H. and Jayakumar, R. (2011) Curcumin-loaded biocompatible thermoresponsive polymeric nanoparticles for cancer drug delivery. *Journal of Colloid and Interface Science*, 360(1), pp. 39-51.

Sasaki, Y., Tsuchido, Y., Sawada, S.I. and Akiyoshi, K. (2011) Construction of protein-crosslinked nanogels with vitamin B6 bearing polysaccharide. *Polymer Chemistry*, 2(6), pp.1267-1270.

Sasse, D., Spornitz, U. and Piotr Maly, I. (1992) Liver Architecture. *Enzyme*, 46(1-3), pp. 8-32.

Schafer, F. and Buettner, G. (2001) Redox environment of the cell as viewed through the redox state of the glutathione disulfide/glutathione couple. *Free Radical Biology and Medicine*, 30(11), pp. 1191-1212.

Schmidt-Wolf, G. D., & Schmidt-Wolf, I. G. (2003) Non-viral and hybrid vectors in human gene therapy: an update. *Trends in molecular medicine*, 9(2), pp. 67-72.

Sercombe, L., Veerati, T., Moheimani, F., Wu, S.Y., Sood, A.K. and Hua, S. (2015) Advances and challenges of liposome assisted drug delivery. *Frontiers in pharmacology*, 6, p.286.

Shah, C.P., Mishra, B., Kumar, M., Priyadarsini, K.I. and Bajaj, P.N.(2008) Binding studies of curcumin to polyvinyl alcohol/polyvinyl alcohol hydrogel and its delivery to liposomes. *Current Science*, pp.1426-1432.

Shakir, D. (2009) Chemotherapy Induced Cardiomyopathy: Pathogenesis, Monitoring and Management. *Journal of Clinical Medicine Research*.

Shanker, M., Jin, J., Branch, C., Miyamoto, S., Grimm, E., Roth, J. and Ramesh, R. (2011) Tumor Suppressor Gene-Based Nanotherapy: From Test Tube to the Clinic. *Journal of Drug Delivery*, 2011, pp. 1-10.

Sharma, P. and Allison, J. (2015) Immune Checkpoint Targeting in Cancer Therapy: Toward Combination Strategies with Curative Potential. *Cell*, 161(2), pp. 205-214.

She, W., Li, N., Luo, K., Guo, C., Wang, G., Geng, Y. and Gu, Z. (2013) Dendronized heparin-doxorubicin conjugate-based nanoparticle as pH-responsive drug delivery system for cancer therapy. *Biomaterials*, 34(9), pp. 2252-2264.

Shen, S., Liu, M., Li, T., Lin, S. and Mo, R. (2017) Recent progress in nanomedicine-based combination cancer therapy using a site-specific co-delivery strategy. *Biomaterials Science*, 5(8), pp. 1367-1381.

Shey, J., Holtman, K.M., Wong, R.Y., Gregorski, K.S., Klamczynski, A.P., Orts, W.J., Glenn, G.M. and Imam, S.H. (2006) The azidation of starch. *Carbohydrate polymers*, 65(4), pp.529-534.

- Shiratori, Y., Tananka, M., Kawase, T., Shiina, S., Komatsu, Y. and Omata, M. (1993) Quantification of Sinusoidal Cell Function in Vivo. *Seminars in Liver Disease*, 13(01), pp. 39-49.
- Shupe, T., Williams, M., Brown, A., Willenberg, B. and Petersen, B. (2010) Method for the decellularization of intact rat liver. *Organogenesis*, 6(2), pp. 134-136.
- Singh, R. and Lillard, J. (2009) Nanoparticle-based targeted drug delivery. *Experimental and Molecular Pathology*, 86(3), pp. 215-223.
- Sivakumar, P. and Panduranga Rao, K. (2003) The use of cholesteryl pullulan for the preparation of stable vincristine liposomes. *Carbohydrate Polymers*, 51(3), pp. 327-332.
- Skehan, P., Storeng, R., Scudiero, D., Monks, A., McMahon, J., Vistica, D., Warren, J., Bokesch, H., Kenney, S. and Boyd, M. (1990) New Colorimetric Cytotoxicity Assay for Anticancer-Drug Screening. *JNCI Journal of the National Cancer Institute*, 82(13), pp. 1107-1112.
- Smith, B. (2011) Fundamentals of Fourier transform infrared spectroscopy. Boca Raton: CRC Press.
- Smith, S. (2017) War! What is it good for? Mustard gas medicine. *Canadian Medical Association Journal*, 189(8), pp. E321-E322.
- Söderberg, A., Sahaf, B. and Rosén, A. (2000) Thioredoxin reductase, a redox-active selenoprotein, is secreted by normal and neoplastic cells: presence in human plasma. *Cancer research*, 60(8), pp.2281-2289.
- Sudhakar, A. (2009) History of cancer, ancient and modern treatment methods. *Journal of cancer science & therapy*, 1(2), pp. 1.
- Sudhakar, A. (2009) History of Cancer, Ancient and Modern Treatment Methods. *Journal of Cancer Science & Therapy*, 01(02), p. i-iv.
- Sugumaran, K., Gowthami, E., Swathi, B., Elakkiya, S., Srivastava, S., Ravikumar, R., Gowdhaman, D. and Ponnusami, V. (2013) Production of pullulan by *Aureobasidium pullulans* from Asian palm kernel: A novel substrate. *Carbohydrate Polymers*, 92(1), pp. 697-703.
- Suk, J., Xu, Q., Kim, N., Hanes, J. and Ensign, L. (2016) PEGylation as a strategy for improving nanoparticle-based drug and gene delivery. *Advanced Drug Delivery Reviews*, 99, pp. 28-51.
- Sun, W., Hu, Q., Ji, W., Wright, G. and Gu, Z. (2017) Leveraging Physiology for Precision Drug Delivery. *Physiological Reviews*, 97(1), pp. 189-225.
- Svenson, S. and Tomalia, D. (2012) Dendrimers in biomedical applications—reflections on the field. *Advanced Drug Delivery Reviews*, 64, pp. 102-115.
- Swierczewska, M., Lee, K. and Lee, S. (2015) What is the future of PEGylated therapies? *Expert Opinion on Emerging Drugs*, 20(4), pp. 531-536.

Syková, E. and Nicholson, C. (2008) Diffusion in Brain Extracellular Space. *Physiological Reviews*, 88(4), pp. 1277-1340.

Takahashi, H., Sawada, S.-i., Akiyoshi, K. (2011) Amphiphilic polysaccharide nanoballs: A new building block for nanogel biomedical engineering and artificial chaperones. *ACS Nano*, (5), 337-345.

Talekar, M., Kendall, J., Denny, W. and Garg, S. (2011) Targeting of nanoparticles in cancer. *Anti-Cancer Drugs*, 22(10), pp. 949-962.

Taniguchi, N., Arakawa, C., & KOBAYASHI, T. (1974) On the basic concept of 'nano-technology'. In *Proceedings of the International Conference on Production Engineering, 1974-8*(Vol. 2, pp. 18-23).

Teramoto, N. and Shibata, M. (2006) Synthesis and properties of pullulan acetate. Thermal properties, biodegradability, and a semi-clear gel formation in organic solvents. *Carbohydrate Polymers*, 63(4), pp. 476-481.

Tewes, F., Munnier, E., Antoon, B., Ngaboni Okassa, L., Cohen-Jonathan, S., Marchais, H., Douziech-Eyrolles, L., Soucé, M., Dubois, P. and Chourpa, I. (2007) Comparative study of doxorubicin-loaded poly(lactide-co-glycolide) nanoparticles prepared by single and double emulsion methods. *European Journal of Pharmaceutics and Biopharmaceutics*, 66(3), pp. 488-492.

Thao, L., Lee, C., Kim, B., Lee, S., Kim, T., Kim, J., Lee, E., Oh, K., Choi, H., Yoo, S. and Youn, Y. (2017) Doxorubicin and paclitaxel co-bound lactosylated albumin nanoparticles having targetability to hepatocellular carcinoma. *Colloids and Surfaces B: Biointerfaces*, 152, pp. 183-191.

Thomas, C., Ehrhardt, A. and Kay, M. (2003) Progress and problems with the use of viral vectors for gene therapy. *Nature Reviews Genetics*, 4(5), pp. 346-358.

Thorley, J., McKeating, J. and Rappoport, J. (2010) Mechanisms of viral entry: sneaking in the front door. *Protoplasma*, 244(1-4), pp. 15-24.

Thorn, C., Oshiro, C., Marsh, S., Hernandez-Boussard, T., McLeod, H., Klein, T. and Altman, R. (2011) Doxorubicin pathways. *Pharmacogenetics and Genomics*, 21(7), pp. 440-446.

Tokarska-Schlattner, M., Dolder, M., Gerber, I., Speer, O., Wallimann, T. and Schlattner, U. (2007) Reduced creatine-stimulated respiration in doxorubicin challenged mitochondria: Particular sensitivity of the heart. *Biochimica et Biophysica Acta (BBA) - Bioenergetics*, 1767(11), pp. 1276-1284.

Tomalia, D. (1996) Starburst dendrimers - Nanoscopic supermolecules according to dendritic rules and principles. *Macromolecular Symposia*, 101(1), pp. 243-255.

Tomalia, D., Baker, H., Dewald, J., Hall, M., Kallos, G., Martin, S., Roeck, J., Ryder, J. and Smith, P. (1985) A New Class of Polymers: Starburst-Dendritic Macromolecules. *Polymer Journal*, 17(1), pp. 117-132.

Touchstone, J.C. (1992) *Practice of Thin Layer Chromatography*. 3rd ed. New York: John Wiley and Sons, Inc., pp. 1-2, 11.

Traverso, N., Ricciarelli, R., Nitti, M., Marengo, B., Furfaro, A., Pronzato, M., Marinari, U. and Domenicotti, C. (2013) Role of Glutathione in Cancer Progression and Chemoresistance. *Oxidative Medicine and Cellular Longevity*, 2013, pp. 1-10.

Trivedi, R. and Kompella, U. (2010) Nanomicellar formulations for sustained drug delivery: strategies and underlying principles. *Nanomedicine*, 5(3), pp. 485-505.

Türker-Kaya, S. and Huck, C. (2017) A review of mid-infrared and near-infrared imaging: principles, concepts and applications in plant tissue analysis. *Molecules*, 22(1), p.168.

Uramoto, H., & Tanaka, F. (2014) Recurrence after surgery in patients with NSCLC. *Translational lung cancer research*, 3(4), pp. 242.

Usmani, S., Bedi, G., Samuel, J., Singh, S., Kalra, S., Kumar, P., Ahuja, A., Sharma, M., Gautam, A. and Raghava, G. (2017) THPdb: Database of FDA-approved peptide and protein therapeutics. *PLOS ONE*, 12(7), p. e0181748.

Utsunomiya, S. and Ewing, R.C. (2003) Application of high-angle annular dark field scanning transmission electron microscopy, scanning transmission electron microscopy-energy dispersive X-ray spectrometry, and energy-filtered transmission electron microscopy to the characterization of nanoparticles in the environment. *Environmental science & technology*, 37(4), pp.786-791.

Valeur, E. and Bradley, M. (2009) Amide bond formation: beyond the myth of coupling reagents. *Chem. Soc. Rev.*, 38(2), pp. 606-631.

Van Tellingen, O., Yetkin-Arik, B., de Gooijer, M., Wesseling, P., Wurdinger, T. and de Vries, H. (2015) Overcoming the blood–brain tumor barrier for effective glioblastoma treatment. *Drug Resistance Updates*, 19, pp. 1-12.

Varde, N.K. and Pack, D.W. (2004) Microspheres for controlled release drug delivery. *Expert Opinion on Biological Therapy*, 4(1), pp.35-51.

Varkouhi, A., Scholte, M., Storm, G. and Haisma, H. (2011) Endosomal escape pathways for delivery of biologicals. *Journal of Controlled Release*, 151(3), pp. 220-228.

Vermes, I., Haanen, C., Steffens-Nakken, H. and Reutelingsperger, C. (1995) A novel assay for apoptosis. Flow cytometric detection of phosphatidylserine expression on early apoptotic cells using fluorescein labelled annexin v. *J Immunol Methods*, 184(1), pp. 39-51.

Vichai, V. and Kirtikara, K. (2006) Sulforhodamine B colorimetric assay for cytotoxicity screening. *Nature Protocols*, 1(3), pp. 1112-1116.

Vinothini, K., Rajendran, N.K., Munusamy, M.A., Alarfaj, A.A. and Rajan, M. (2019) Development of biotin molecule targeted cancer cell drug delivery of

doxorubicin loaded κ-carrageenan grafted graphene oxide nanocarrier. *Materials Science and Engineering*: 100, pp. 676-687.

Vives, E., Brodin, P. and Lebleu, B. (1997) A truncated HIV-1 Tat protein basic domain rapidly translocates through the plasma membrane and accumulates in the cell nucleus. *Journal of Biological Chemistry*, 272(25), pp.16010-16017.

Von Maltzahn, G., Park, J., Lin, K., Singh, N., Schwöppe, C., Mesters, R., Berdel, W., Ruoslahti, E., Sailor, M. and Bhatia, S. (2011) Nanoparticles that communicate in vivo to amplify tumour targeting. *Nature Materials*, 10(7), pp. 545-552.

Vonarbourg, A., Passirani, C., Saulnier, P. and Benoit, J. (2006) Parameters influencing the stealthiness of colloidal drug delivery systems. *Biomaterials*, 27(24), pp. 4356-4373.

Wang, C., Wang, Z., Zhang, X. (2012) Amphiphilic building blocks for self-assembly: From amphiphiles to supra-amphiphiles. *Acc. Chem. Res.* (45), 608-618.

Wang, H., Zhao, Y., Wu, Y., Hu, Y.L., Nan, K., Nie, G. and Chen, H. (2011) Enhanced anti-tumor efficacy by co-delivery of doxorubicin and paclitaxel with amphiphilic methoxy PEG-PLGA copolymer nanoparticles. *Biomaterials*, 32(32), pp.8281-8290.

Wang, J., Mao, W., Lock, L.L., Tang, J., Sui, M., Sun, W., Cui, H., Xu, D. and Shen, Y. (2015) The role of micelle size in tumor accumulation, penetration, and treatment. *ACS nano*, 9(7), pp.7195-7206.

Wang, L., Yang, W., Read, P., Larner, J. and Sheng, K. (2010) Tumor cell apoptosis induced by nanoparticle conjugate in combination with radiation therapy. *Nanotechnology*, 21(47), p. 475103.

Wang, T., Upponi, J. and Torchilin, V. (2012) Design of multifunctional non-viral gene vectors to overcome physiological barriers: Dilemmas and strategies. *International Journal of Pharmaceutics*, 427(1), pp. 3-20.

Wang, X., Wang, J., Bao, Y., Wang, B., Wang, X. and Chen, L.(2014) Novel reduction-sensitive pullulan-based micelles with good hemocompatibility for efficient intracellular doxorubicin delivery. *RSC Advances*, 4(104), pp.60064-60074.

Watanabe, Y., Liu, X., Shibuya, I. and Akaike, T. (2000) Functional evaluation of poly-(N-p-vinylbenzyl-O-β-Dgalactopyranosyl-[1-4]-D-gluconamide)(PVLA) as a liver specific carrier. *Journal of Biomaterials Science, Polymer Edition*, 11(8), pp. 833-848.

Watson, D.G. (2005) *Pharmaceutical Analysis: A Textbook for Pharmacy Students and Pharmaceutical Chemists*. 2nd ed. London: Elsevier Churchill Livingstone, pp. 315-321.

Webb, A. (2014) Cavity-and waveguide-resonators in electron paramagnetic resonance, nuclear magnetic resonance, and magnetic resonance imaging. *Progress in nuclear magnetic resonance spectroscopy*, 83, pp.1-20.

- Weil, C. M., Gibson, M., Spear, P. G., & Scolnick, E. M. (1981). Construction and isolation of a transmissible retrovirus containing the src gene of Harvey murine sarcoma virus and the thymidine kinase gene of herpes simplex virus type 1. *Journal of virology*, 39(3), pp. 935-944.
- Wells, P. N. T. (1977) Ultrasonics in medicine and biology. *Physics in Medicine & Biology*, 22(4), pp. 629.
- Wiley, D. and Skehel, J. (1987) The Structure and Function of the Hemagglutinin Membrane Glycoprotein of Influenza Virus. *Annual Review of Biochemistry*, 56(1), pp. 365-394.
- Wiman, K. G. (1993) The retinoblastoma gene: role in cell cycle control and cell differentiation. *The FASEB journal*, 7(10), pp. 841-845.
- Witkowski, H. and Koniorczyk, M. (2018) New sampling method to improve the reliability of FTIR analysis for Self-Compacting Concrete. *Construction and Building Materials*, 172, pp. 196-203.
- Wlodkowic, D., Telford, W., Skommer, J. and Darzynkiewicz, Z. (2011) Apoptosis and beyond: Cytometry in studies of programmed cell death. *Methods Cell Biol*, 103, pp. 55-98.
- Wong, M., Jiang, J., Goggins, W., Liang, M., Fang, Y., Fung, F., Leung, C., Wang, H., Wong, G., Wong, V. and Chan, H. (2017) International incidence and mortality trends of liver cancer: a global profile. *Scientific Reports*, 7(1).
- Woo, J., Kim, Y., Choi, Y., Kim, D., Lee, K., Bae, J., Min, D., Chang, J., Jeong, Y., Lee, Y., Park, J. and Kwon, T. (2003) Molecular mechanisms of curcumin-induced cytotoxicity: induction of apoptosis through generation of reactive oxygen species, down-regulation of Bcl-XL and IAP, the release of cytochrome c and inhibition of Akt. *Carcinogenesis*, 24(7), pp. 1199-1208.
- Wragg, S. and Drickamer, K. (1999) Identification of Amino Acid Residues That Determine pH Dependence of Ligand Binding to the Asialoglycoprotein Receptor during Endocytosis. *Journal of Biological Chemistry*, 274(50), pp. 35400-35406.
- Wu, J. (2002) 'Targeting hepatocytes for drug and gene delivery: Emerging novel approaches and applications', *Frontiers in Bioscience*, 7(1-3), p. d717. doi: 10.2741/wu2.
- Wu, J., Lu, Y., Lee, A., Pan, X., Yang, X., Zhao, X. and Lee, R.J. (2007) Reversal of multidrug resistance by transferrin-conjugated liposomes co-encapsulating doxorubicin and verapamil. *J Pharm Pharm Sci*, 10(3), pp.350-357.
- Wyld, L., Audisio, R. and Poston, G. (2014) The evolution of cancer surgery and future perspectives. *Nature Reviews Clinical Oncology*, 12(2), pp. 115-124.
- Xia, Y., Ding, S., Liu, Y. and Qi, Z. (2017) Facile Synthesis and Self-Assembly of Amphiphilic Polyether-Octafunctionalized Polyhedral Oligomeric Silsesquioxane via Thiol-Ene Click Reaction. *Polymers*, 9(12), p. 251.

- Xiao, W., Chen, X., Yang, L., Mao, Y., Wei, Y. and Chen, L. (2010) Co-delivery of doxorubicin and plasmid by a novel FGFR-mediated cationic liposome. *International journal of pharmaceutics*, 393(1-2), pp.120-127.
- Xu, W., Ding, J., Xiao, C., Li, L., Zhuang, X., Chen, X. (2015) Versatile preparation of intracellular-acidity-sensitive oxime-linked polysaccharide-doxorubicin conjugate for malignancy therapeutic. *Biomaterials*, (54), 72-86.
- Xu, Y., Guo, X., Tu, L., Zou, Q., Li, Q., Tang, C., Chen, B., Wu, C. and Wei, M. (2015) Lactoferrin-modified PEGylated liposomes loaded with doxorubicin for targeting delivery to hepatocellular carcinoma. *International Journal of Nanomedicine*, p. 5123.
- Yallapu, M., Jaggi, M. and Chauhan, S. (2012) Curcumin nanoformulations: a future nanomedicine for cancer. *Drug Discovery Today*, 17(1-2), pp. 71-80.
- Yamaoka, T., Tabata, Y. and Ikada, Y. (1993) 'Body distribution profile of polysaccharides after intravenous administration', *Drug Delivery*, 1(1), pp. 75–82. doi: 10.3109/10717549309031345
- YAMAOKA, T., TABATA, Y. and IKADA, Y. (1995) 'Comparison of body distribution of Poly(vinyl alcohol) with other water-soluble polymers after intravenous administration', *Journal of Pharmacy and Pharmacology*, 47(6), pp. 479–486. doi: 10.1111/j.2042-7158.1995.tb05835.x.
- Yan, G., Wang, J., Hu, L., Wang, X., Yang, G., Fu, S., Cheng, X., Zhang, P. and Tang, R. (2017) Stepwise targeted drug delivery to liver cancer cells for enhanced therapeutic efficacy by galactose-grafted, ultra-pH-sensitive micelles. *Acta Biomaterialia*, 51, pp. 363-373.
- Yang, W., Wang, M., Ma, L., Li, H. and Huang, L. (2014) Synthesis and characterization of biotin modified cholesteryl pullulan as a novel anticancer drug carrier. *Carbohydrate Polymers*, 99, pp. 720-727.
- Yang, Z., Gao, D., Cao, Z., Zhang, C., Cheng, D., Liu, J., & Shuai, X. (2015) Drug and gene co-delivery systems for cancer treatment. *Biomaterials Science*, 3(7), 1035–1049.
- Yiu, W. K., Basco, M. T., Aruny, J. E., Cheng, S. W., & Sumpio, B. E. (2007) Cryosurgery: a review. *The International journal of angiology: official publication of the International College of Angiology, Inc*, 16(1), pp. 1.
- Yoo, H. and Park, T. (2004) Folate receptor targeted biodegradable polymeric doxorubicin micelles. *Journal of Controlled Release*, 96(2), pp. 273-283.
- Yu, B., Tai, H., Xue, W., Lee, L. and Lee, R. (2010) Receptor-targeted nanocarriers for therapeutic delivery to cancer. *Molecular Membrane Biology*, 27(7), pp. 286-298.
- Yu, M. and Zheng, J. (2015) Clearance Pathways and Tumor Targeting of Imaging Nanoparticles. *ACS Nano*, 9(7), pp. 6655-6674.
- Yu, T. (2004) A review of research into the uses of low level ultrasound in cancer therapy. *Ultrasonics Sonochemistry*, 11(2), pp. 95-103.

Yu, X., Trase, I., Ren, M., Duval, K., Guo, X. and Chen, Z. (2016) Design of nanoparticle-based carriers for targeted drug delivery. *Journal of nanomaterials*, 2016.

Zangger, K. (2015) Pure shift NMR. *Progress in nuclear magnetic resonance spectroscopy*, 86, pp.1-20.

Zhan, Y., Gonçalves, M., Yi, P., Capelo, D., Zhang, Y., Rodrigues, J., Liu, C., Tomás, H., Li, Y. and He, P. (2015) Thermo/redox/pH-triple sensitive poly(N-isopropylacrylamide-co-acrylic acid) nanogels for anticancer drug delivery. *Journal of Materials Chemistry B*, 3(20), pp. 4221-4230.

Zhang, A., Zhang, Z., Shi, F., Xiao, C., Ding, J., Zhuang, X., He, C., Chen, L. and Chen, X. (2013) Redox-Sensitive Shell-Crosslinked Polypeptide-block-Polysaccharide Micelles for Efficient Intracellular Anticancer Drug Delivery. *Macromolecular Bioscience*, 13(9), pp. 1249-1258.

Zhang, H., Li, X., Gao, F., Liu, L., Zhou, Z. and Zhang, Q. (2009) Preparation of folate-modified pullulan acetate nanoparticles for tumor-targeted drug delivery. *Drug Delivery*, 17(1), pp. 48-57.

Zhang, Y., Yu, J., Bomba, H.N., Zhu, Y. and Gu, Z. (2016) Mechanical force-triggered drug delivery. *Chemical reviews*, 116(19), pp.12536-12563.

Zhao, D., Liu, C.J., Zhuo, R.X. and Cheng, S.X. (2012) Alginate/CaCO₃ hybrid nanoparticles for efficient codelivery of antitumor gene and drug. *Molecular pharmaceuticals*, 9(10), pp.2887-2893.

Zhou, J., Mohamed Wali, A., Ma, S., He, Y., Yue, D., Tang, J. and Gu, Z. (2018) Tailoring the Supramolecular Structure of Guanidinylated Pullulan toward Enhanced Genetic Photodynamic Therapy. *Biomacromolecules*, 19(6), pp. 2214-2226.

Zhou, J., Patel, T., Sirianni, R., Strohbahn, G., Zheng, M., Duong, N., Schafbauer, T., Huttner, A., Huang, Y., Carson, R., Zhang, Y., Sullivan, D., Piepmeyer, J. and Saltzman, W. (2013) Highly penetrative, drug-loaded nanocarriers improve treatment of glioblastoma. *Proceedings of the National Academy of Sciences*, 110(29), pp. 11751-11756.

Zhou, Y., Yu, J., Feng, X., Li, W., Wang, Y., Jin, H., Huang, H., Liu, Y. and Fan, D. (2016) Reduction-responsive core-crosslinked micelles based on a glycol chitosan–lipoic acid conjugate for triggered release of doxorubicin. *RSC Adv.*, 6(37), pp. 31391-31400.

Ziello, J. E., Huang, Y., & Jovin, I. S. (2010) Cellular endocytosis and gene delivery. *Molecular Medicine*, 16(5-6), pp. 222.

Zitvogel, L., Tesniere, A., & Kroemer, G. (2006) Cancer despite immunosurveillance: immunoselection and immunosubversion. *Nature Reviews Immunology*, 6(10), pp. 715.

